NASA Contractor Report 195435

Advanced Small Rocket Chambers Option 3–110 lbf Ir-Re Rocket

Volume II

Donald M. Jassowski and Leonard Schoenman
Gen Corp Aerojet
Sacramento, California

February 1995

Prepared for
Lewis Research Center
Under Contract NAS3–25646

National Aeronautics and
Space Administration

APPENDIX A

NOZZLE CONTOUR OPTIMIZATION

Memo

22 March 1991
RAB:rab:5246:0159g

To: Don Jassowski

From Randy Bell

Subject: 100 lbf Engine
1) Area Ratio Analysis
2) Test Article Pc/MR Survey

Distribution: L. Schoenman, S. Rosenberg, R. Hewitt, C. Cotter, J. Salmon

A performance analysis has been performed on the 100 lb_f engine as requested by Don Jassowski of the Research and Technology group. This memo lists the assumptions, parameters, etc. used in the analysis. JANNAF simplified performance prediction techniques per CPIA 246 were used with an assumed energy release efficiency (ERE) of 98% for a single stream tube model, based on test data from a 40:1 nozzle which yielded Isp_{vac} = 309.4 s.

TASK I.

It was requested that performance be calculated for the 100 lb_f engine varying area ratio and nozzle length. The following describe the assumptions and other parameters used in the analysis. Results are shown in enclosures 1 - 6.

1. Physical Characteristics
   Throat Radius = 0.4035
   Chamber Radius = 0.850
   Chamber Length = 4.4"
   Normalized Dnstrm Throat Radius of Curvature = 2.0
   Length Upstream of Throat = 8.6" (Jassowski)
   Nozzle Attachment Half Angle = 30^o
   Nozzle Exit Half Angle = 7^o

2. Operating Point
   N_2O_4 / MMH
   Pc = 110 psia
   MR = 1.65
   $T_o = T_f = 70^o$ F
   Area Ratio = 100 - 300
   % Bell Nozzle = 80, 90, 100

3. Wall Temperature
The chamber wall is regeneratively cooled to 1.8" from the injector face. The remaining 2.6" is radiation cooled. Therefore, the regen part of the chamber was treated as an adiabatic wall (5000° F) since the energy removed returns as heated fuel. Everything downstream of the 1.8" station was input according to the temperature profile (enclosure 7) provided by D.B. Makel.

TASK II.

An analysis has been performed on the 100 lb_f test article (low area ratio) engine as requested by Don Jassowski of the Research and Technology group. Below are the assumptions, parameters, etc. used in the analysis.

It was requested that performance be calculated for the 100 lb_f engine varying mixture ratio and Pc. Results are shown on enclosures 8 and 9.

1. Physical Characteristics
Throat Radius = 0.423
Chamber Radius = 0.853
Chamber Length = 4.4"
Normalized Dnstrm Throat Radius of Curvature = 0.5
15° Conical Nozzle - Area Ratio = 1.600

2. Operating Point
N_2O_4 / MMH
$T_o = T_f = 70°$ F
Mixture Ratio = 1.2 - 2.0
Pc = 80 - 130 psia

3. Wall Temperature
The chamber wall is regeneratively cooled to 1.8" from the injector face. The remaining 2.6" is radiation cooled. Therefore, the regen part of the chamber was treated as an adiabatic wall (5000° F) since the energy removed returns as heated fuel. The wall downstream of the 1.8" station was input as a constant temperature of 1500° F.

Randy A. Bell
Combustion and
Fluid Dynamics Analysis

Reviewed By:

R E Walker

R. E. Walker
Combustion and
Fluid Dynamics Analysis

Approved By:

Jeff Phipps

Jeff Phipps, Manager
Combustion and
Fluid Dynamics Analysis

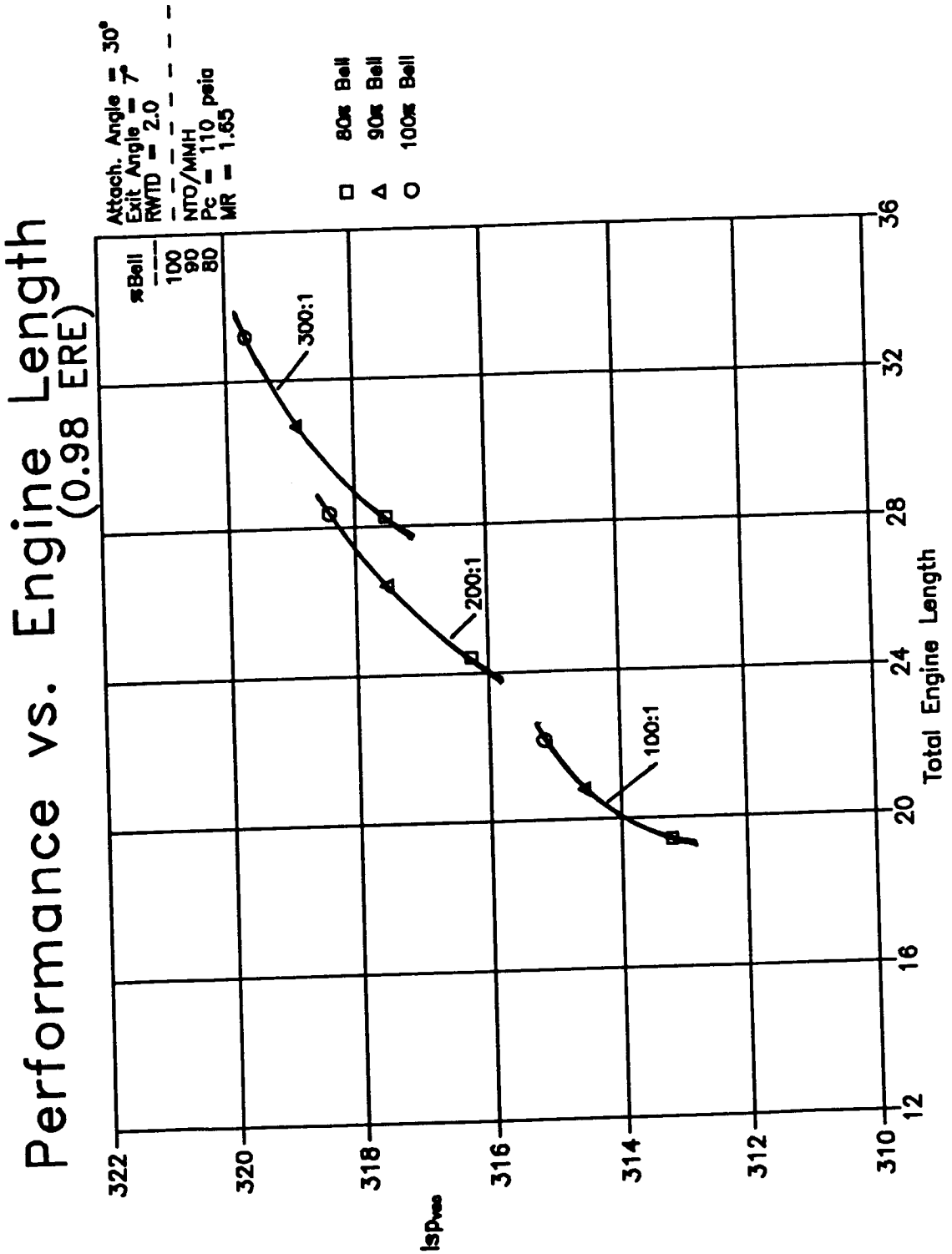
Performance vs. Engine Length
(0.98 ERE)
Attach. Angle = 30°
Exit Angle = 7°
RWTD = 2.0
NTO/MMH
Pc = 110 psia
MR = 1.65
εBell
100
90
80
80% Bell
90% Bell
100% Bell
300:1
200:1
100:1
322
320
318
316
314
312
310
Isp vac
12
16
20
24
28
32
36
Total Engine Length

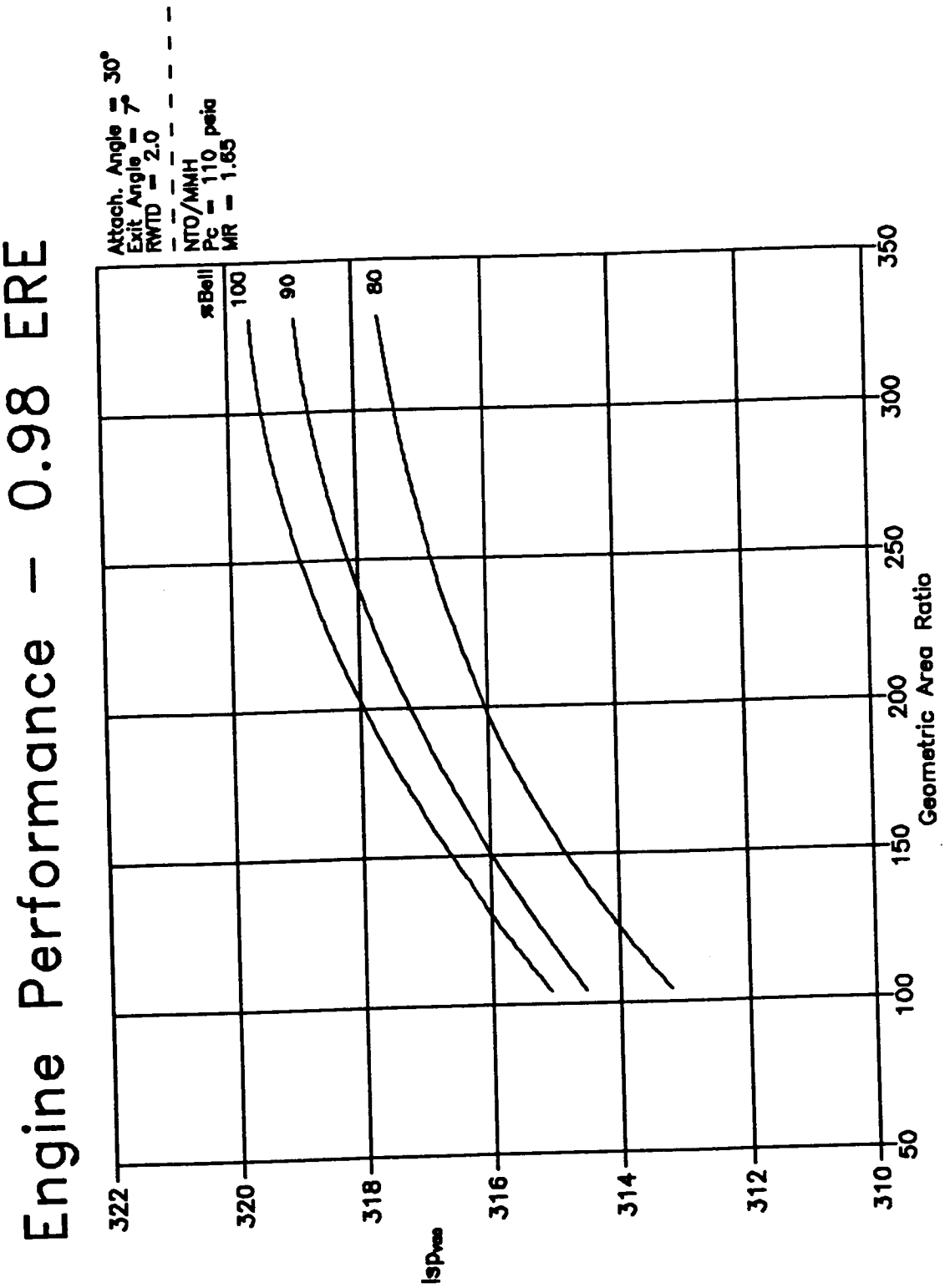
Engine Performance – 0.98 ERE
Attach. Angle = 30°
Exit Angle = 7°
RWTD = 2.0
NTO/MMH
Pc = 110 psia
MR = 1.85
%Bell
100
90
80
322
320
318
316
314
312
310
Isp vac
50
100
150
200
250
300
350
Geometric Area Ratio

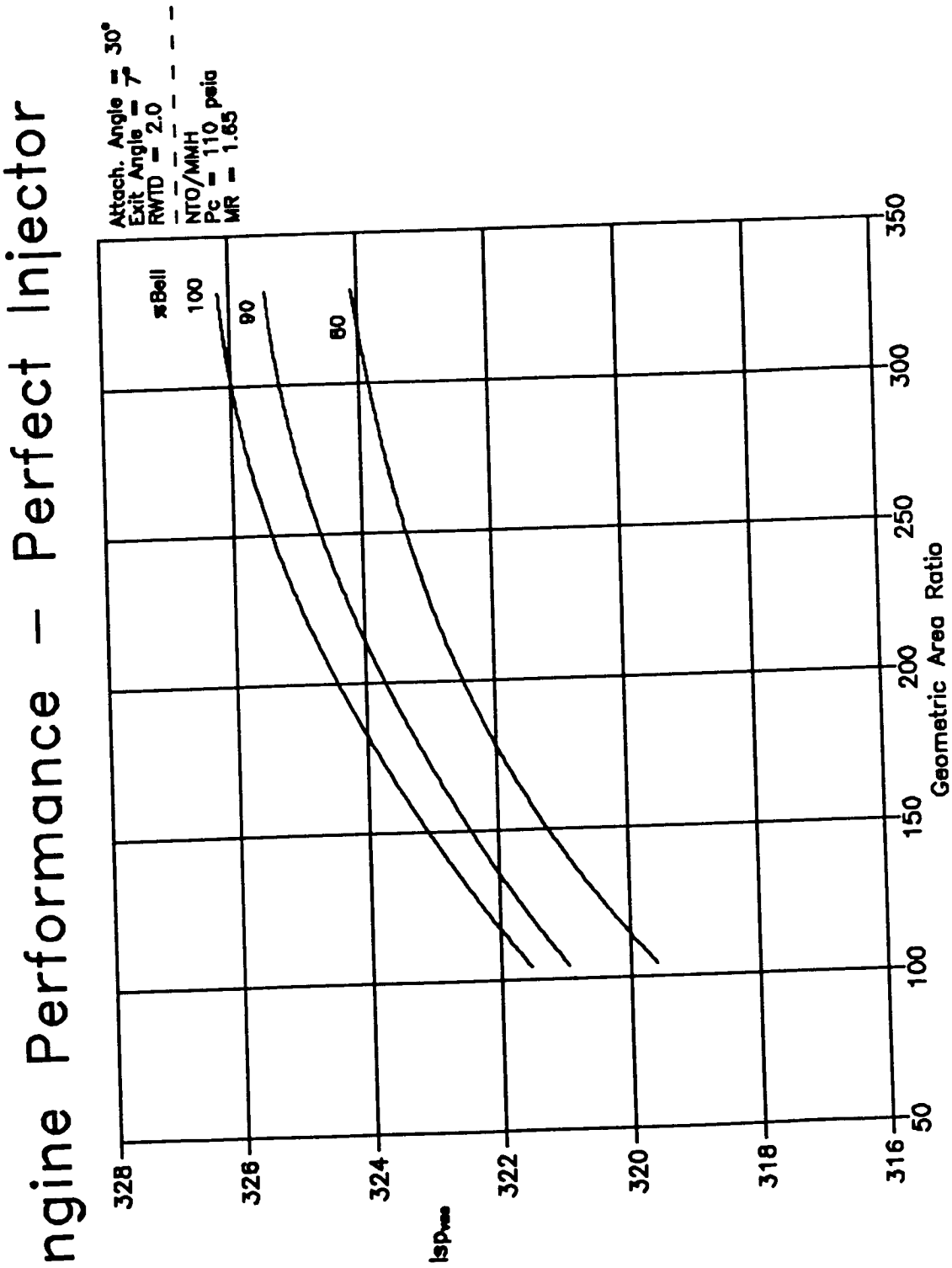
Engine Performance – Perfect Injector
Attach. Angle = 30°
Exit Angle = 7°
RWTD = 2.0
NTO/MMH
Pc = 110 psia
MR = 1.65
%Bell
100
90
80
328
326
324
322
320
318
316
50
100
150
200
250
300
350
Geometric Area Ratio

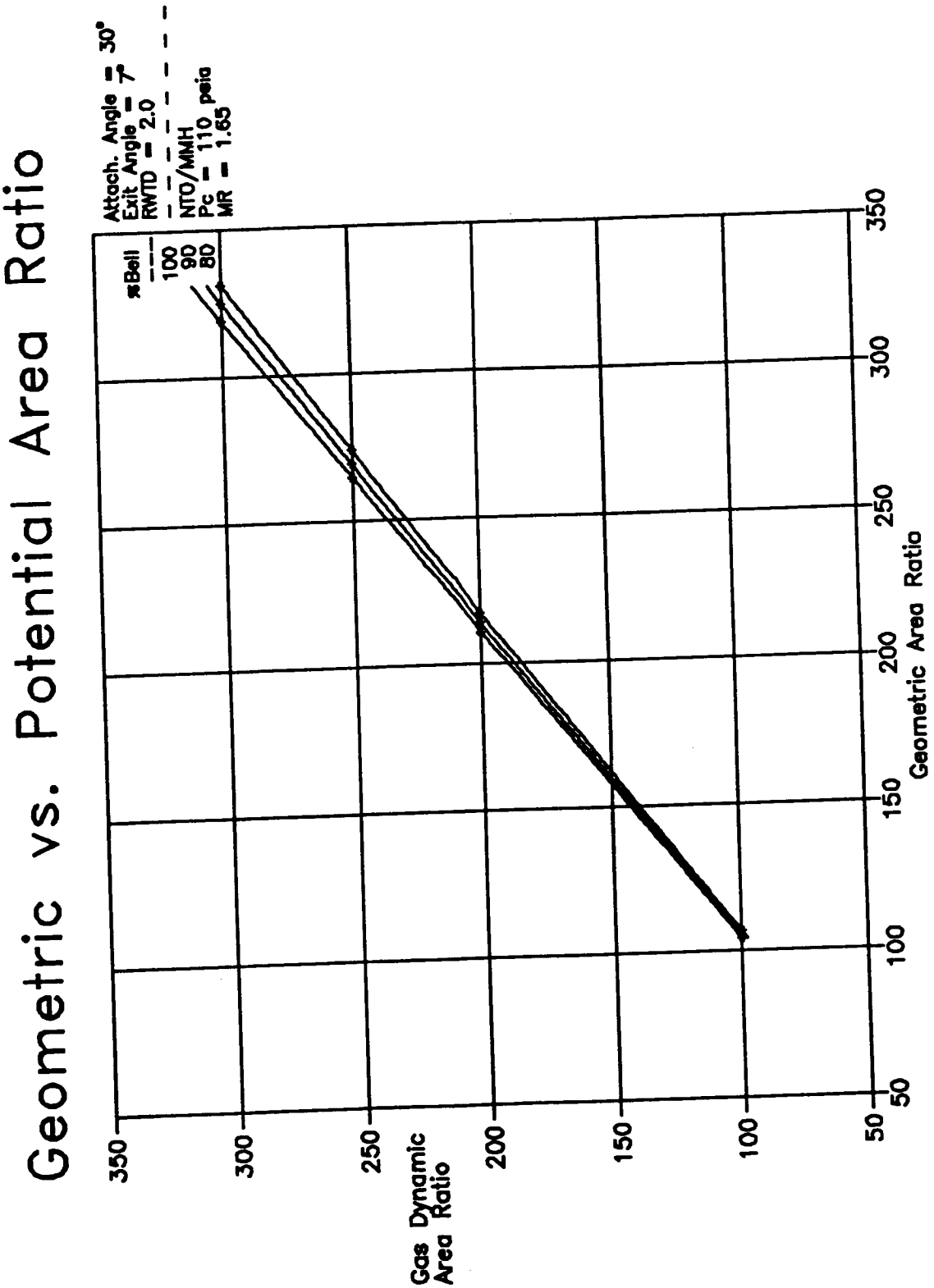
Geometric vs. Potential Area Ratio
Attach. Angle = 30°
Exit Angle = 7°
RWTD = 2.0
NTO/MMH
Pc = 110 psia
MR = 1.65
%Bell
100
90
80
Gas Dynamic Area Ratio
Geometric Area Ratio
350
300
250
200
150
100
50

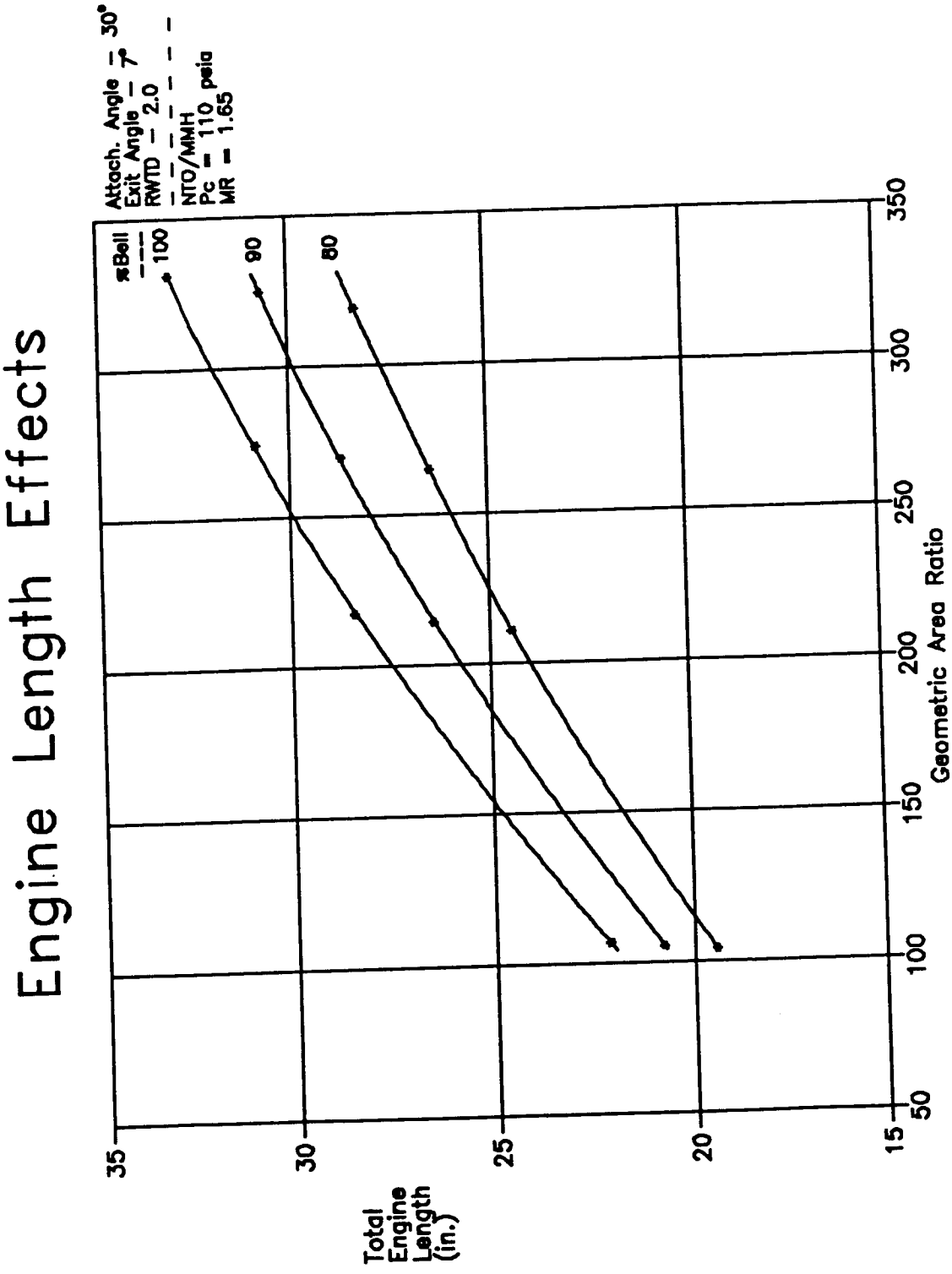
Engine Length Effects
Attach. Angle = 30°
Exit Angle = 7°
RWTD = 2.0
NTO/MMH
Pc = 110 psia
MR = 1.65
%Bell
100
90
80
Total Engine Length (in.)
Geometric Area Ratio
35
30
25
20
15
50
100
150
200
250
300
350

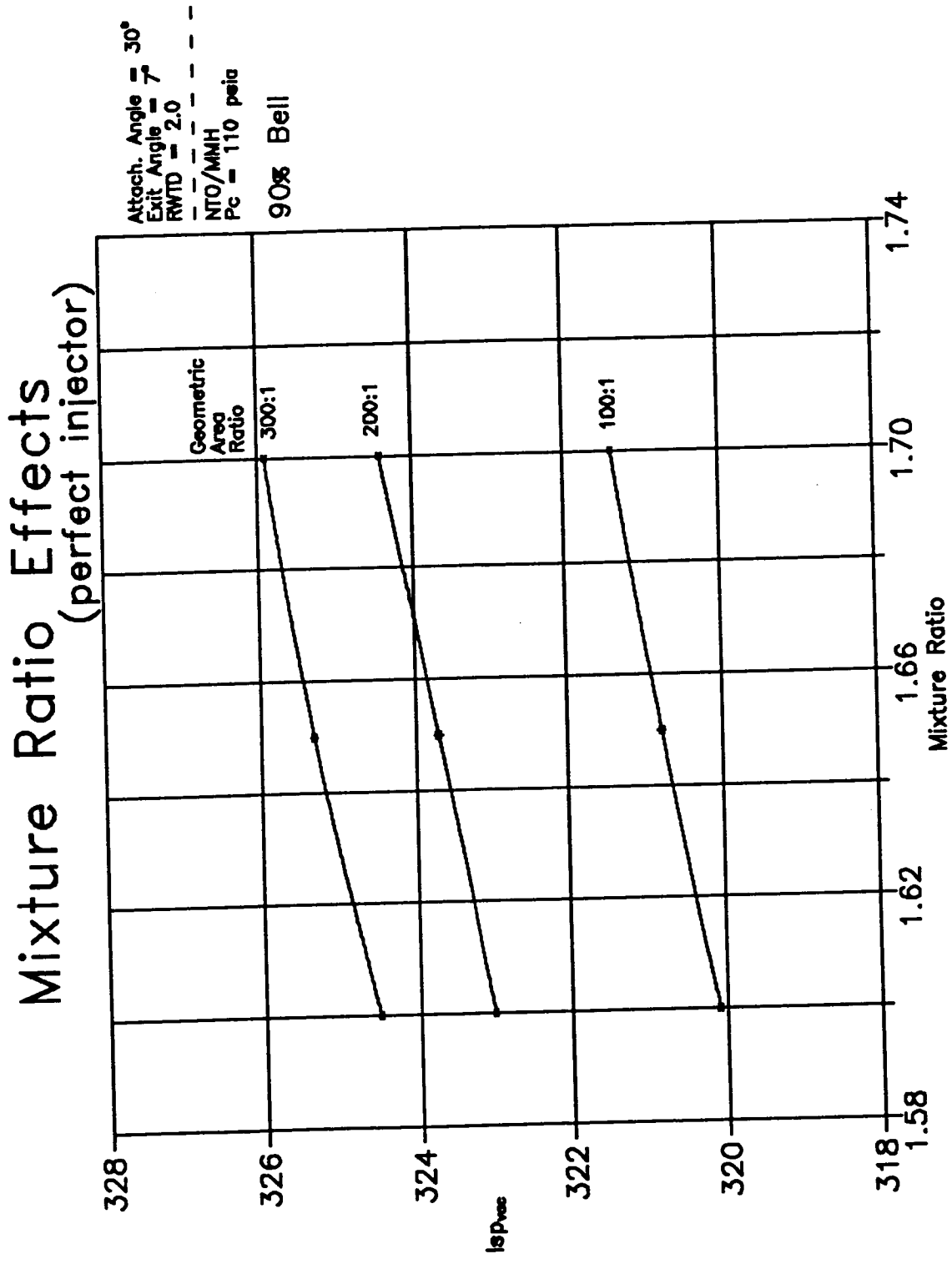
Mixture Ratio Effects
(perfect injector)
Attach. Angle = 30°
Exit Angle = 7°
RWTD = 2.0
NTO/MMH
Pc = 110 psia
90% Bell
Geometric Area Ratio
300:1
200:1
100:1
328
326
324
322
320
318
Isp vac
1.58
1.62
1.66
1.70
1.74
Mixture Ratio

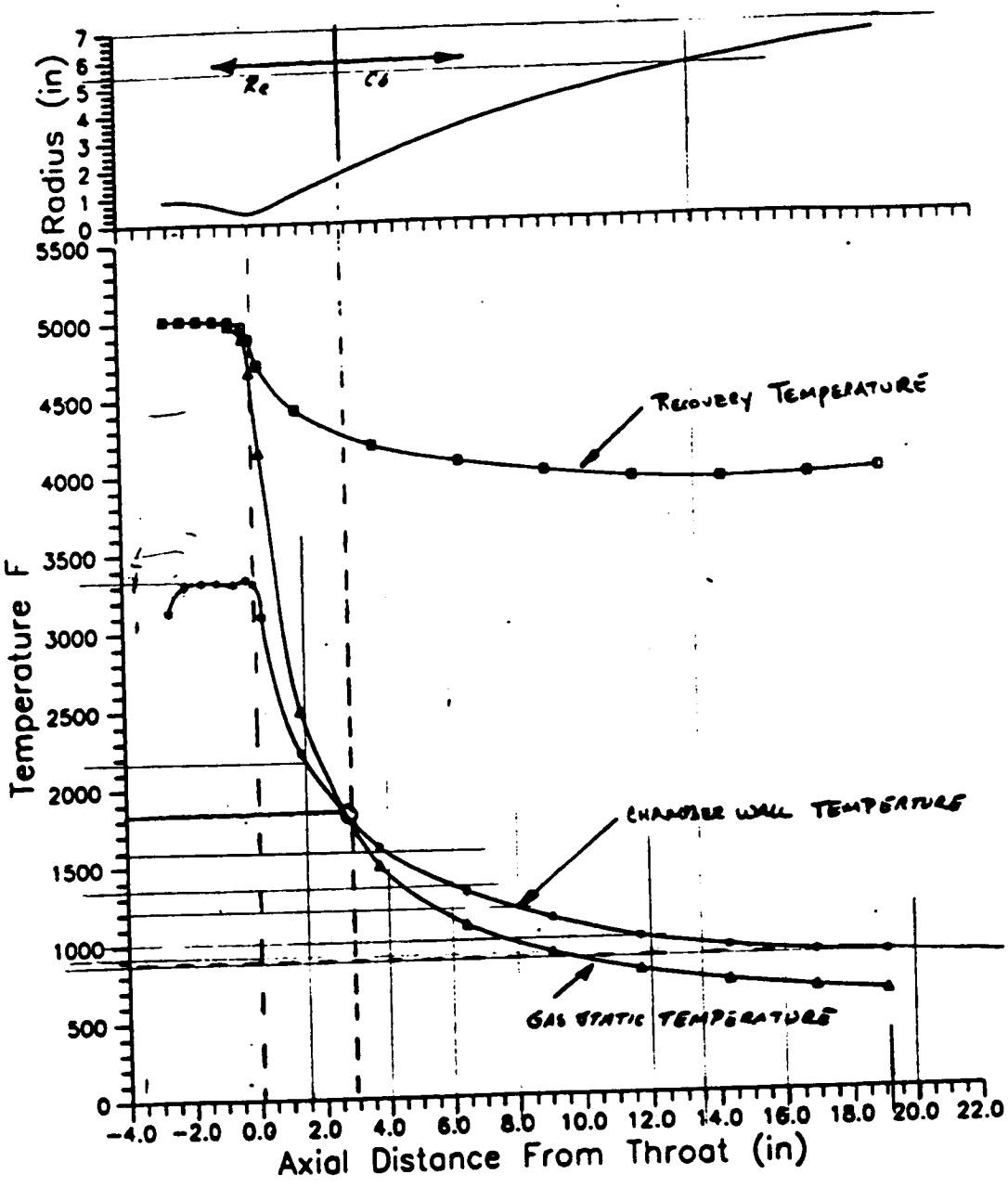

Figure 4. Steady State Axial Chamber and Gas Temperature Profile (No Radiation Shield).

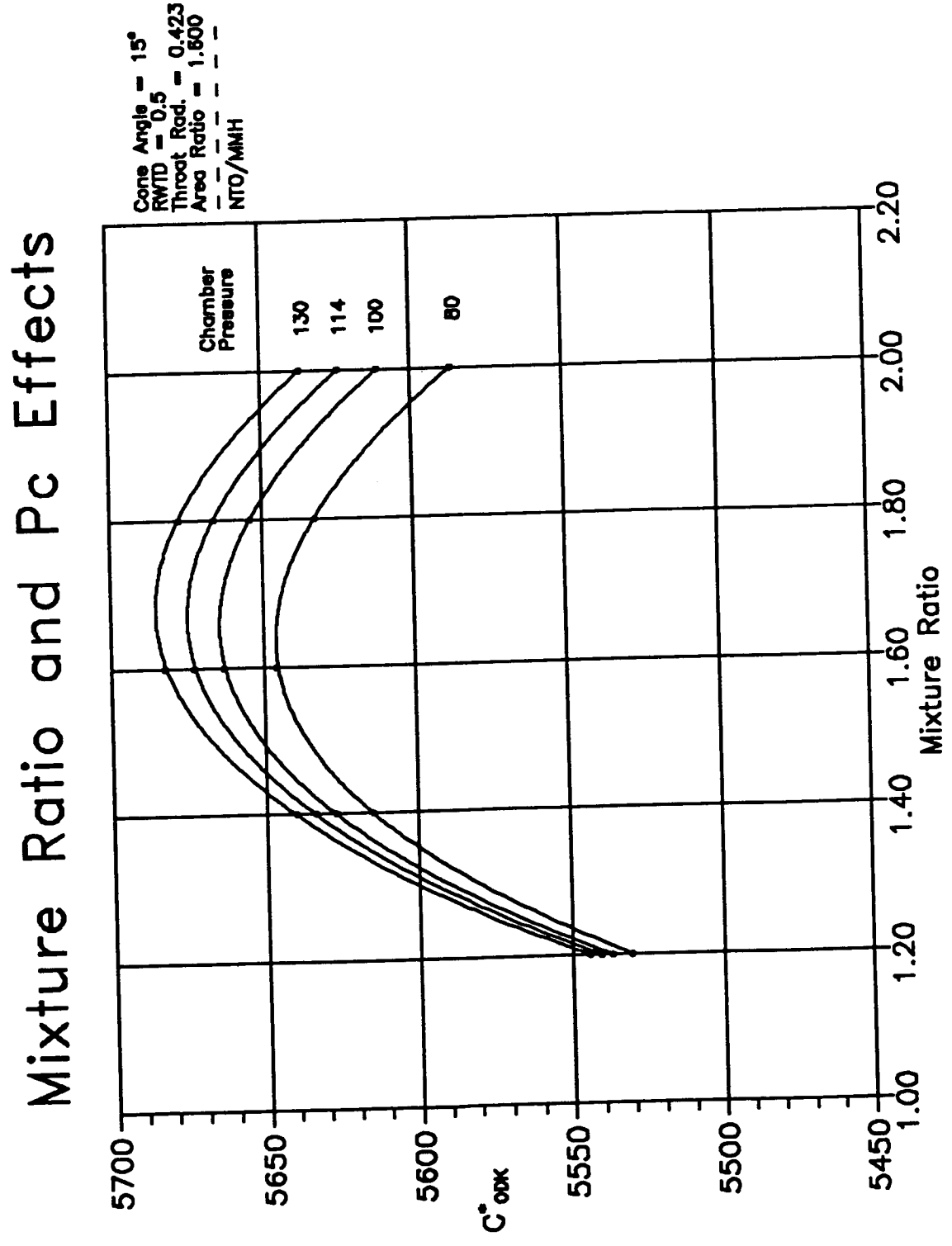
Mixture Ratio and Pc Effects
Cone Angle = 15°
RWTD = 0.5
Throat Rad. = 0.423
Area Ratio = 1.800
NTO/MMH
Chamber Pressure
130
114
100
80
C* ODK
5700
5650
5600
5550
5500
5450
1.00
1.20
1.40
1.60
1.80
2.00
2.20
Mixture Ratio

ERE 98%

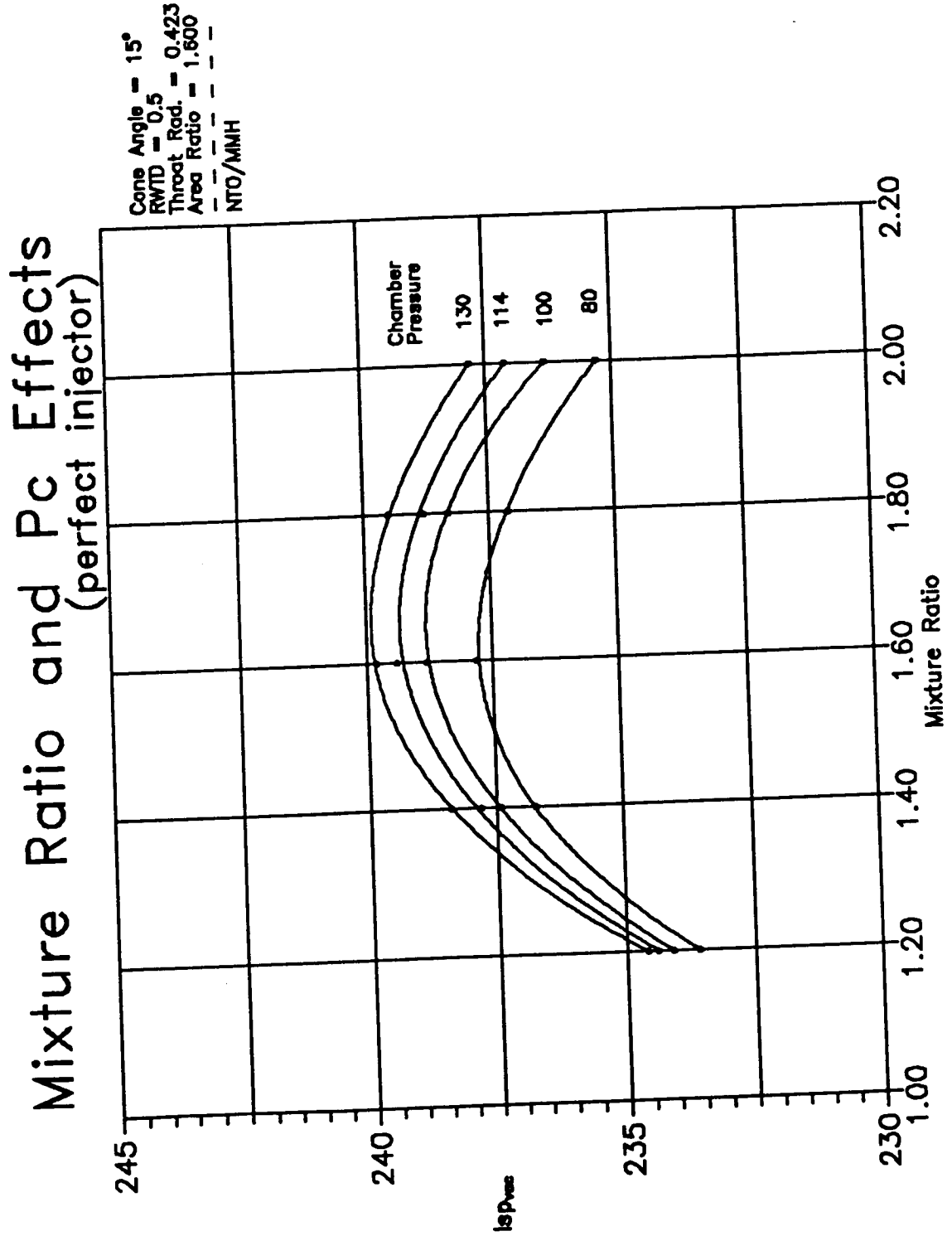
Mixture Ratio and Pc Effects
(perfect injector)
Cone Angle = 15°
RWTD = 0.5
Throat Rad. = 0.423
Area Ratio = 1.800
NTO/MMH
Chamber Pressure
130
114
100
80
245
240
235
230
1.00
1.20
1.40
1.60
1.80
2.00
2.20
Mixture Ratio
Isp

APPENDIX B

THERMAL ANALYSIS

Memo

8 January 1991

TO: L. Schoenman

FROM: D. B. Makel

SUBJECT: 100 lbf Ir/Re Chamber Thermal Analysis

COPIES: D. M. Jassowski, S. D. Rosenberg, R&T:5220 File

1.0 Executive Summary

A thermal analysis has been conducted of the 100 lbf Ir/Re chamber. A SINDA thermal model of the thruster was used for the analysis. The analysis consisted of;

(1) Prediction of the steady state chamber and nozzle temperature profile at nominal O/F=1.65, Pc=110 psi conditions.

(2) Analysis of the thermal soak to the regeneratively cooled baseline and modified front end adaptor designs.

(3) Estimation of the effect of CRAF satellite radiation shielding on the maximum chamber temperature.

The major conclusions from the analysis are:

(1) Maximum temperature of the columbium skirt is 1820 F with no radiation shielding, 1880 F with shielding, and 2010 F unshielded with a low emissivity coating (ε=0.45).

(2) Maximum chamber temperature is 3350 F assuming no radiation shield and 3650 F assuming worst-case effect of spacecraft radiation shield.

(3) Approximate times to reach 95% of steady state temperature were:

Chamber Barrel:	10 sec
Columbium Nozzle Attachment:	30 sec
End of Nozzle Skirt:	60 sec
Re Chamber Head End Attachment point:	200 sec

(4) The maximum temperature of the front end adaptor/Re interface is less than 500 F and occurs during the thermal soak back.

(5) The maximum coolant side wall temperature during the thermal soak back is predicted to be 404 F for the modified front end adaptor design with no radiation shielding and 408 F with the radiation shield. These temperatures are below the initial exothermic temperature of MMH (450 F). This prediction requires that the coolant channel lands achieve at least 80% of prefect thermal contact with the backside of the adaptor. This requirement means that the gas side wall part must be brazed to the adaptor body.

2.0 SINDA Model

A 2-D axisymmetric SINDA model of the chamber and front end adaptor has been constructed. Temperature dependent thermal conductivities and capacitances were used and are listed in Appendix A. Features of the design which are smeared or lost by the model are:

1) Coolant inlet and exit tubes are ignored.

2) Channels from the inlet manifold to the regen channel entrance are ignored.

3) Spiral regen channels are modeled as alternating fins and cooling channels.

4) Triangular thrust take out flange is smeared as a circular flange of equivalent mass.

3.0 Thermal Boundary Conditions

Gas Side Boundary Conditions

The thermal boundary conditions assumed for the analysis are shown in Figure 1. The nominal operating point analyzed was O/F=1.65 and Pc=110 psi. A uniform heat flux of 3 Btu/in^2-sec to the gas side surface of the CRES front adaptor was directly input the model. The input flux was based on a 100 F coolant temperature rise with a fuel mass flow rate of 0.13 lbm/sec was assumed as the worst case based on previous test data [1] summarized in Table 1. In the barrel section of chamber, a heat transfer coefficient of 0.000425 Btu/in^2-sec-F derived from previous test data (Figure 2) was used. The recovery temperatures were calculated assuming equilibrium conditions from TRANS72. The heat transfer coefficient in the throat was calculated using a laminarized throat Stanton number correlation from reference [2] (see Figure 3).

$$St=0.318\ Re^{-0.5}Pr^{-0.6} \qquad (1)$$

In the nozzle the heat transfer coefficient was calculated using

$$St=0.322\ Re_x^{-0.5}Pr^{-0.67} \qquad (2)$$

The start length x_o was calculated by assuming continuity of the heat transfer coefficient at the throat and setting equations (1) and (2) equal at that point. Table 2 summarizes the node locations, properties, and calculated heat transfer coefficients input to the model.

Coolant Side Boundary Conditions

A fuel inlet temperature of 120 F (worst case) and a bulk temperature rise of 100 F were assumed. The coolant side heat transfer coefficient was calculated using equation (3).

$$Nu=0.023\ Re^{0.8}Pr^{0.6} \qquad (3)$$

The coefficient on the channel walls in the regen channel inlet was increased by 1.5 to account for increased cooling due to jet impingement and swirl in the flow. The bulk temperature rise was assumed to vary linearly and a bulk coolant temperature ranging from 120 F (at the inlet regen channel) to 220 F (at the exit regen channel) was assigned as the boundary condition for each of the channels.

Radiation Boundary Conditions

Three different external radiation conditions were analyzed for the final design. Internal radiation exchange between nozzle surfaces and the exit plane was included in the model and was not changed. The four cases analyzed are:

(1) Baseline Test Configuration

No spacecraft heat shield, all exterior view factors equal one, ε_{Re}=1.0, ε_{Cb}=0.9.

(2) Baseline Test Configuration With Low Emissivity Nozzle

No spacecraft heat shield, all exterior view factors equal one, ε_{Re}=1.0, ε_{Cb}=0.45.

(3) Baseline Spacecraft Configuration

Spacecraft heat shield in place, exterior view factors on Re chamber equal 0.6, ε_{Re}=1.0, ε_{Cb}=0.9.

4.0 Steady State Temperature Profiles

The steady state temperature profile of the Re chamber and nozzle skirt extension were calculated using a sixteen node model. The temperature profile in the front end adaptor was modeled using a 90 node model to account for the complex shape and cooling channels. Figure 4 shows the axial temperature profile for the case of no heat shielding (radiation case #1). The maximum temperature in the chamber is approximately 3350 F and occurs just upstream of the throat. Previous test data show the same temperature distributions. This serves as a check on the model boundary conditions and node connectivity since the chamber heat transfer coefficients were derived previous test data. The joint of the chamber and skirt is indicated on the figure. The maximum temperature of this interface is 1820 F. The end of the skirt at area ratio 250:1 is predicted to reach only 918 F.

Figure 5 shows the steady state axial temperature profiles for the three radiation cases. When the chamber is assumed to be shielded the barrel and throat temperatures are increased by 300 F Reducing the emissivity of the nozzle skirt from 0.9 to 0.45 increases the nozzle exit temperature 200 F. In addition, the temperature of chamber/skirt interface is approximately 1820 F for the unshielded case, 1880 F for the shielded case, and 2010 F for the unshielded low emissivity skirt case.

The steady state temperature profile in the front end adaptor with no radiation shielding is shown in Figure 6. The maximum temperature is 1393 F and occurs at the

tip of the trip. The temperature at the front tip of the adaptor is predicted to be 1256 F. This temperature is approximately 150 F lower than test data measured from the baseline design (which was thicker in the tip region) is shown in Figure 7. When the chamber is shielded the maximum temperature is 1409 F and occurs at the front end tip of the adaptor. This increased temperature is due to additional radiation off the chamber region directly adjacent to the tip. The bulk backside temperature distribution is approximately 210 F and is primarily a function of the coolant inlet and exit temperatures and the temperature of the transition joint from the chamber to the adaptor is 463 at 200 seconds and is nearly level (this temperature is not expected to exceed 500 F). The temperature drop along the thinned Re "thermal resistor" is approximately 1100 F. The steady state heat flow is .2 Btu/sec which would result in only a 2 F temperature rise in the incoming fuel. The thrust take out ring which is cooled by the annular fuel manifold during a test reaches only 160 F when the inlet temperature is 120 F.

5.0 Thermal Soak Analysis And Front End Adaptor Redesign

Several analyses of the thermal soak back to the front end adaptor were conducted concurrent with the detailed mechanical design. At shutdown, the fuel valve is closed and MMH is trapped in the coolant channels, inlet and exit manifolds. In order to prevent exothermic decomposition of this fuel, which can cause "popping" and potentially serious engine damage, the fuel must be kept below its decomposition temperature of 450 F. A design goal of not exceeding 400 F on any wetted surface was set. Analysis of the baseline design, based on the previous 100 lbf thruster program, is shown in Figure 8. In this design the cooling channel lands are assumed to be in perfect thermal contact with the adaptor body. The coolant channel wall temperature was exceeded at three locations with the highest at the side wall nearest the trip reaching 620 F. The final design arrived at has a maximum coolant side wall temperature of 404 F without radiation shielding and 408 F with radiation shielding. These temperatures reflect a worst case analysis. The parametric cases run are summarized in Table 3 and Figures 9 through 19. All the parametric cases were calculated assuming no radiation shield.

The first parametric case (Figure 9) was to double the thermal mass of the thrust take-out flange to reduce the effect of heat soaking back from the chamber. This produced a 40 F reduction in the maximum temperature to 580 F. The final soak out temperature of the part was decreased 25 degrees from approximately 300 F to 275 F. The second case (Figure 10) was to reduce the thermal mass of the tip of the adaptor by a factor of 2 (with the flange reduced to its original mass). This resulted in a 140 F reduction in the maximum temperature to 480 F. In order to reduce the temperature further, the conductance from the tip region to the cooled backside region was increased by a factor 1.25 (case 3, Figure 11) consistent with space available. This resulted in a temperature reduction to 460 F.

Based on the results above, the tip region was redesigned to minimize the thermal mass of tip and increase conduction towards the backside. The model was adjusted to reflect these changes and the maximum temperature was reduced to 407 F as shown in Figure 12. This interim design assumed 100% thermal contact of cooling channel lands and the adaptor backside. The next case (5) was with the this same design except with no contact of the lands and the backside. For this case the maximum temperature reached 632 F in the region of the cooling channels near the trip (see Figure 13). The analysis was repeated for 1% and 50% contact (Figures 14 and 15) and yielded maximum temperatures of 620 and 428 respectively. The 1% thermal contact corresponds to approximate contact afforded by thermal growth of the inner part when assembled with no interference. The 50% thermal contact is representative of the contact which might be achieved with a shrink fit with a temperature difference of 300 F.

The cooling channel geometry was redesigned as shown in Figure 16 to minimize the thermal mass in the gas side wall and increase the mass of the lands without adding pressure drop to the system. This new design resulted in an increase in the ratio of land mass to gas side wall mass of 1.3. The soak was analyzed for the case of the redesigned gas side wall and the lands disconnected (case 8, Figure 17). For this case the coolant side wall temperature in the area of the trip reaches 554 F. With this same design and assuming a thermal contact of 50% the maximum coolant wall temperature during soak was reduced to 422 F (at the tip) and the temperature in the trip region channel walls was reduced to 328 F (case 9, Figure 18). Based on the result of case 9, it was recommended that the cooling channel lands be brazed to the adaptor body to ensure good thermal contact. An 80% thermal contact has been assumed to approximate the effect of brazing the parts together. For this case (case 10, Figure 19) the maximum temperature on the wetted surface nearest the side wall in the tip region was 404 F.

The thermal soak back analysis of the final design is shown in Figure 20. The analyses indicate that the maximum coolant side wall temperature occuring during soak back is very sensitive to the thermal contact between the lands and the adaptor body. The analyses further indicate that a high quality metallic bond such as brazing is required to provide the good thermal contact (80% of theoretical) needed to prevent MMH decomposition during the soak.

References

1. Schoenman, L., Franklin, J., and P. T. Lansaw, Feasibility Demonstration of a High-Preformance 100 lbf Rocket Engine: Final Report, JPL Contract 957882, January 1989.

2. Schoenman, L. and P Block, "Laminar Boundary-Layer Heat Transfer in Low Thrust Rocket Nozzles," J. Spacecraft, Vol. 5, No. 9, 1967.

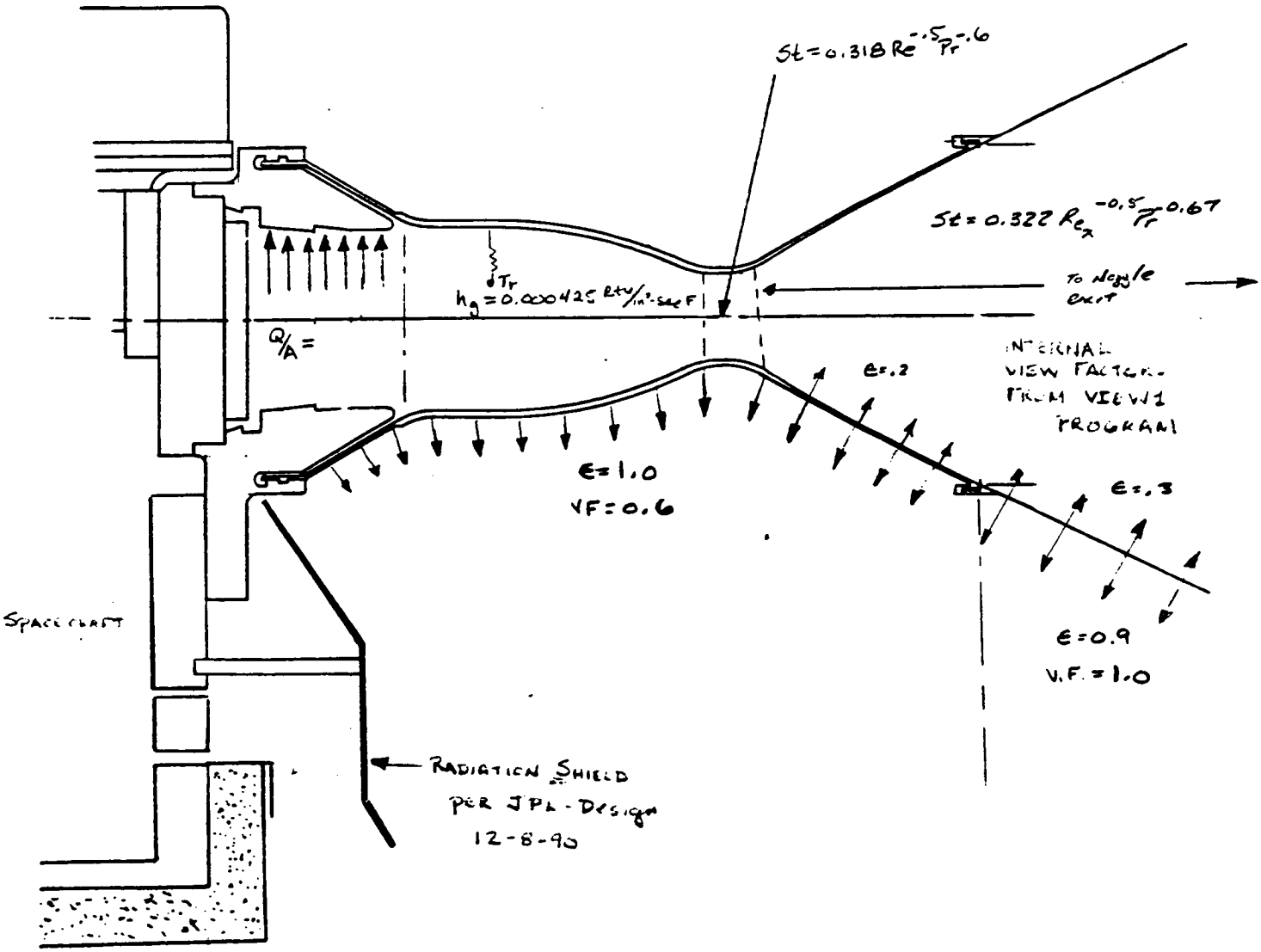

Figure 1. 100 lbf Ir/Re Chamber Layout With SINDA Model Thermal Boundary Conditions.

Table 1. Regen Fuel Temperature Rise At O/F=1.65 (From Ref. 1)

TEST	Pc	Delta T	% FFC
194	99	88	10
201	99	91	6
217	109	81	5
247	114	78	5
242	99	61	5

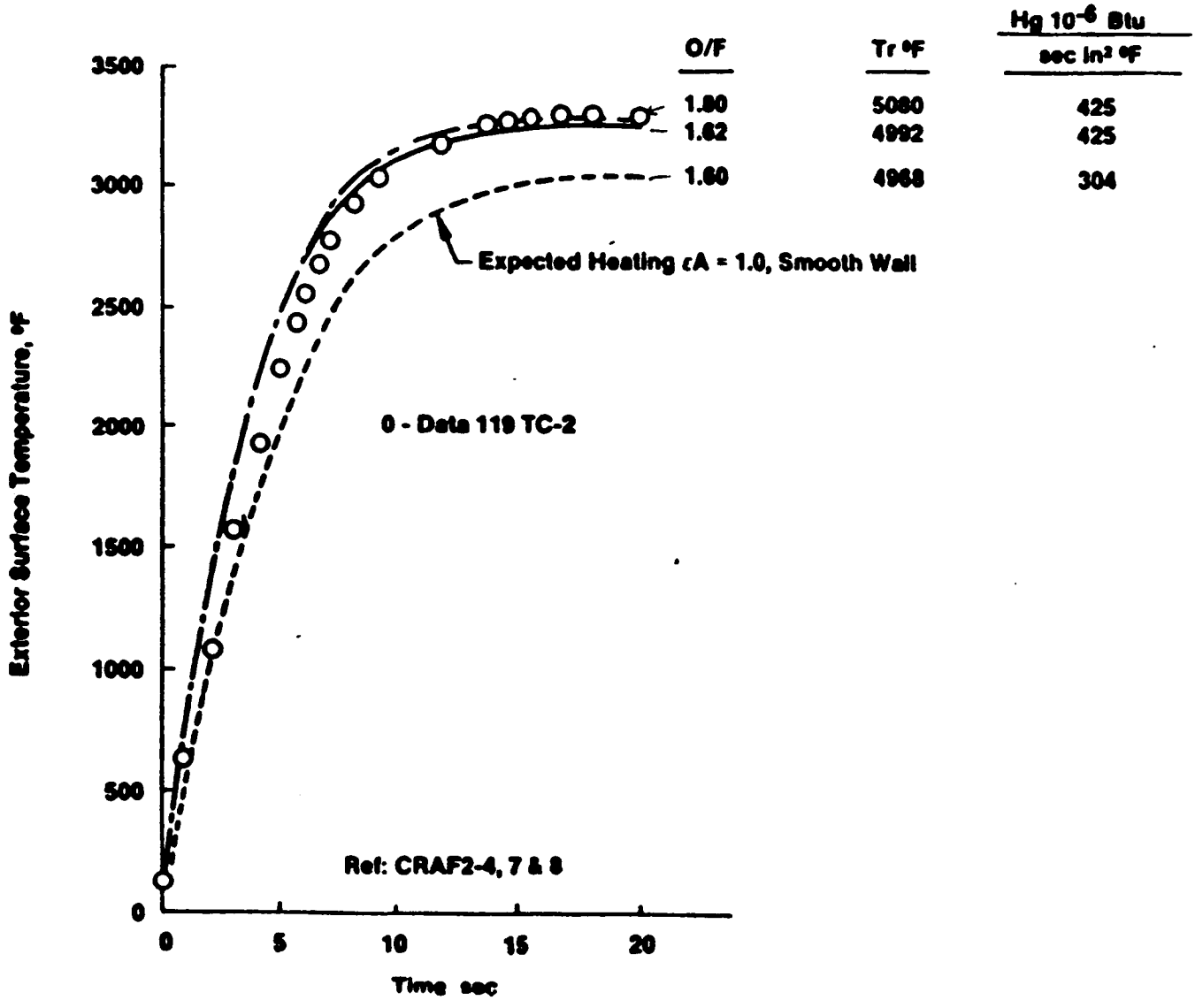

Figure 2. Test Data Used to Derive Chamber Heat Transfer Coefficient From Reference [1].

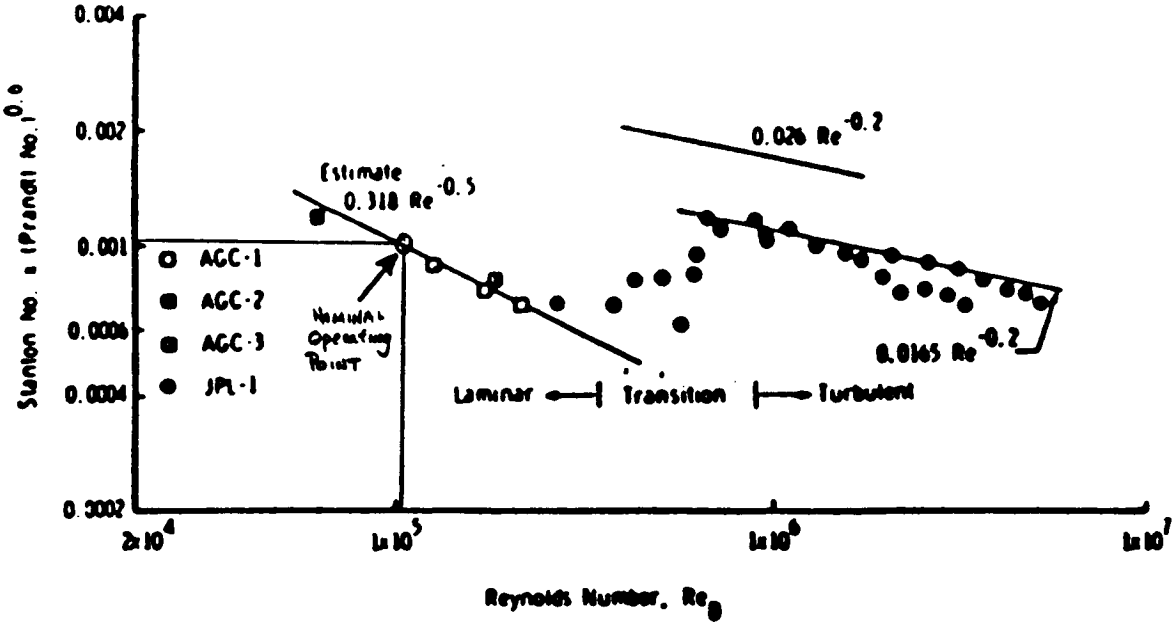

THROAT STANTON NUMBER DATA SUMMARY

Figure 3. Throat Stanton Number Correlation Used From Reference [2].

Table 2. Summary of Gas Side Boundary Conditions

Node	Bulk Temp R	Mn	Sonic Velocity	Density den lbm/in3	Viscosity amu lbm/in-s-zc	Thermal Conductivity Btu/in-sec-F	Pr	Specific Heat Btu/lbm-F	ReD	Heat Coeff. Btu/in2-sec-R	Recovery Temp F	Static Temp F	Axial Distance (in)	Radial Distance (in)
1	5472	0.1	3921	0.0378	4.96E-06	1.39E-05	0.4	1.12	4.74E+04	4.250E-04	5013	5012	-2.625	0.853
2	5472	0.1	3921	0.0378	4.96E-06	1.39E-05	0.4	1.12	4.74E+04	4.250E-04	5013	5012	-2.125	0.853
3	5470	0.	3920	0.0377	4.96E-06	1.39E-05	0.4	1.12	4.72E+04	4.250E-04	5013	5010	-1.625	0.804
4	5463	0.2	3918	0.0374	4.96E-06	1.38E-05	0.4	1.11	5.33E+04	4.250E-04	5010	5003	-1.125	0.6975
5	5437	0.3	3908	0.0361	4.94E-06	1.36E-05	0.4	1.1	6.19E+04	4.250E-04	5000	4977	-0.625	0.5545
6	5349	0.6	3874	0.0319	4.88E-06	1.28E-05	0.4	1.05	8.55E+04	5.000E-04	4968	4889	-0.25	0.4365
7	5128	1.0	3792	0.0235	4.73E-06	1.1E-05	0.4	0.94	1.06E+05	5.689E-04	4887	4668	0	0.404
8	4609	1.6	3613	0.0012	4.37E-06	7.28E-06	0.43	0.71	1.09E+04	3.568E-04	4716	4149	0.25	0.452
9	2952	3.0	2953	0.00156	3.13E-06	2.56E-06	0.585	0.48	9.52E+04	7.950E-05	4421	2492	1.385	1.0315
10	1947	4.2	2405	0.000298	2.29E-06	1.84E-06	0.585	0.47	5.16E+04	2.098E-05	4185	1487	3.7565	2.202
11	1555	4.9	2149	0.000123	1.93E-06	1.59E-06	0.575	0.47	3.61E+04	1.032E-05	4067	1095	6.447	3.362
12	1366	5.3	2017	7.31E-05	1.75E-06	1.44E-06	0.566	0.47	2.95E+04	6.669E-06	3997	906	9.0675	4.3115
13	1247	5.6	1933	5.17E-05	1.63E-06	1.34E-06	0.559	0.46	2.61E+04	4.790E-06	3947	787	11.713	5.099
14	1170	5.8	1871	4.02E-05	1.55E-06	1.29E-06	0.559	0.48	2.38E+04	3.932E-06	3928	710	14.343	5.756
15	1116	6.0	1817	3.34E-05	1.49E-06	1.35E-06	0.569	0.52	2.24E+04	3.492E-06	3943	656	16.9755	6.3
16	1085	6.2	1777	2.96E-05	1.46E-06	1.48E-06	0.581	0.59	2.12E+04	3.488E-06	3970	625	19.1715	6.685

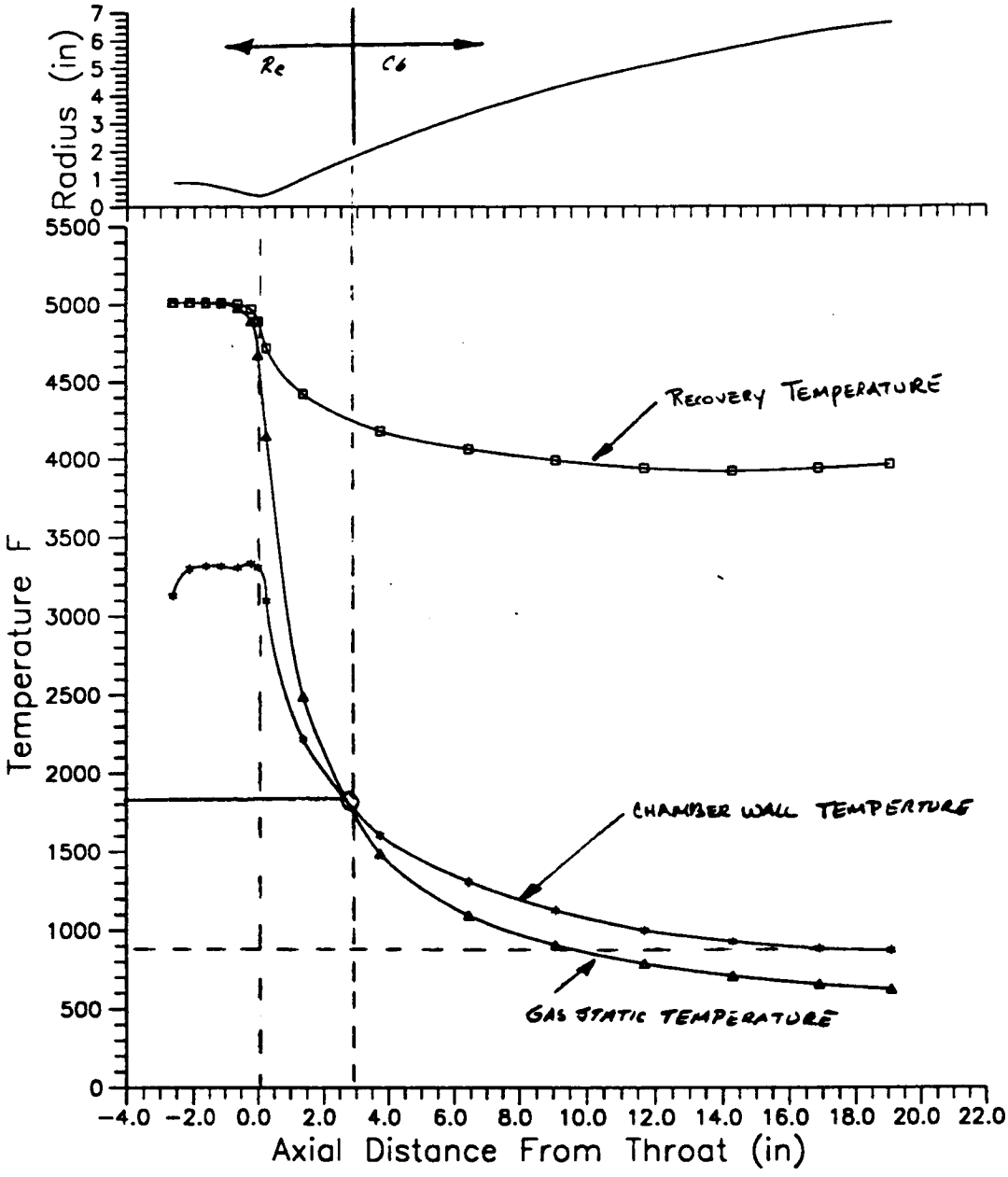

Figure 4. Steady State Axial Chamber and Gas Temperature Profile (No Radiation Shield).

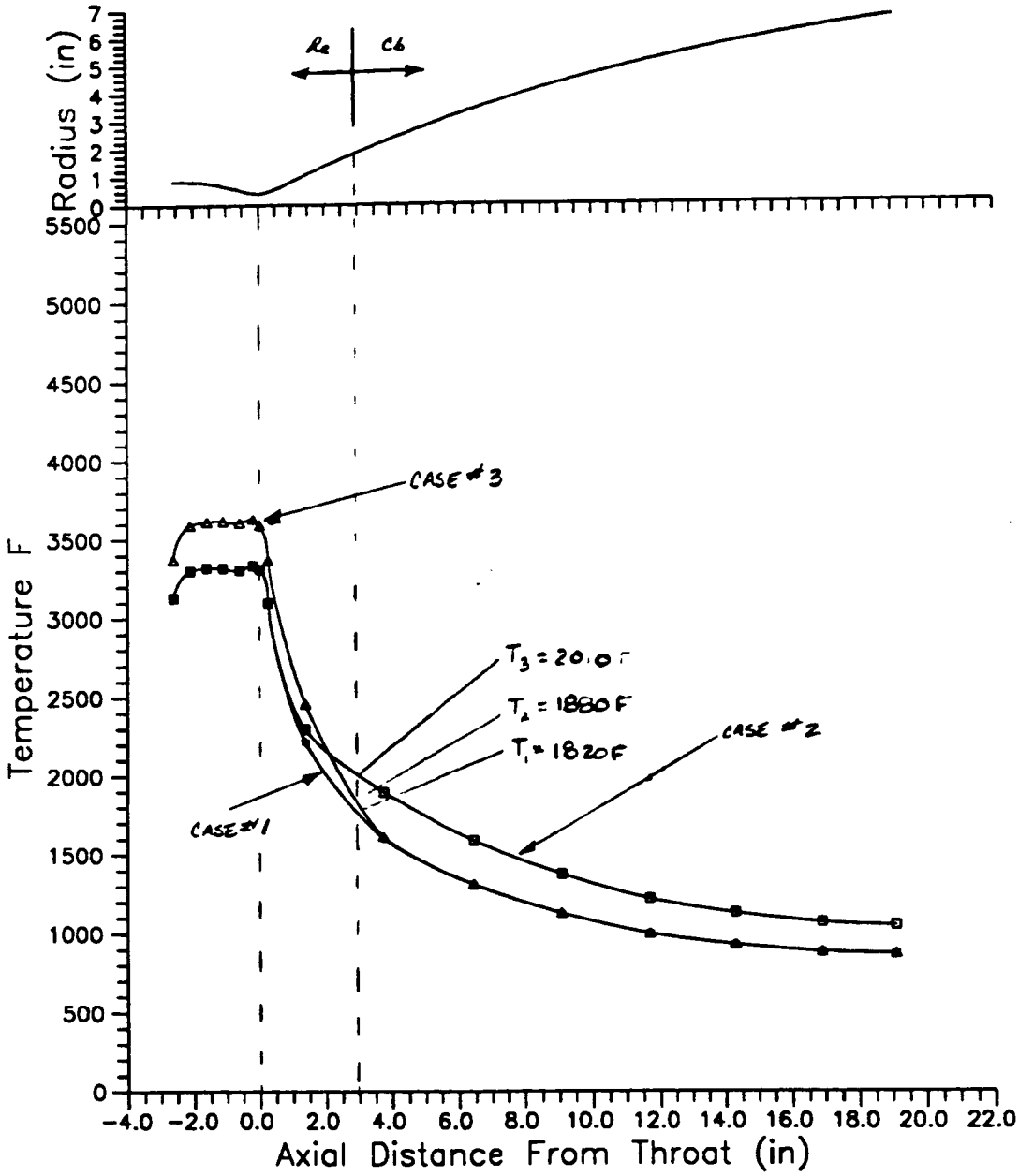

Figure 5. Axial Chamber Temperature Profiles for Radiation Cases #1, #2, and #3.

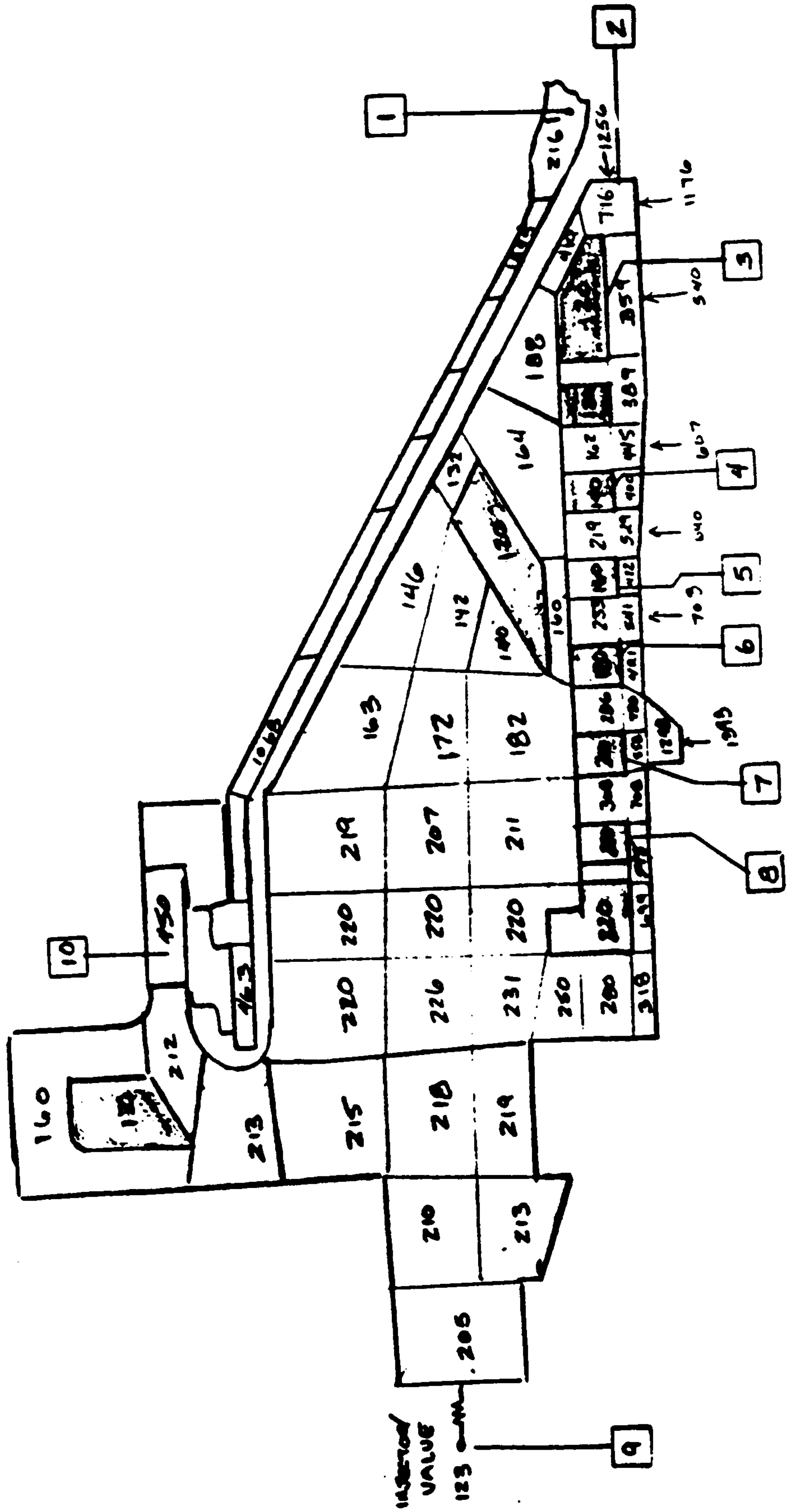

Figure 6. Steady State Front End Temperature Distribution.

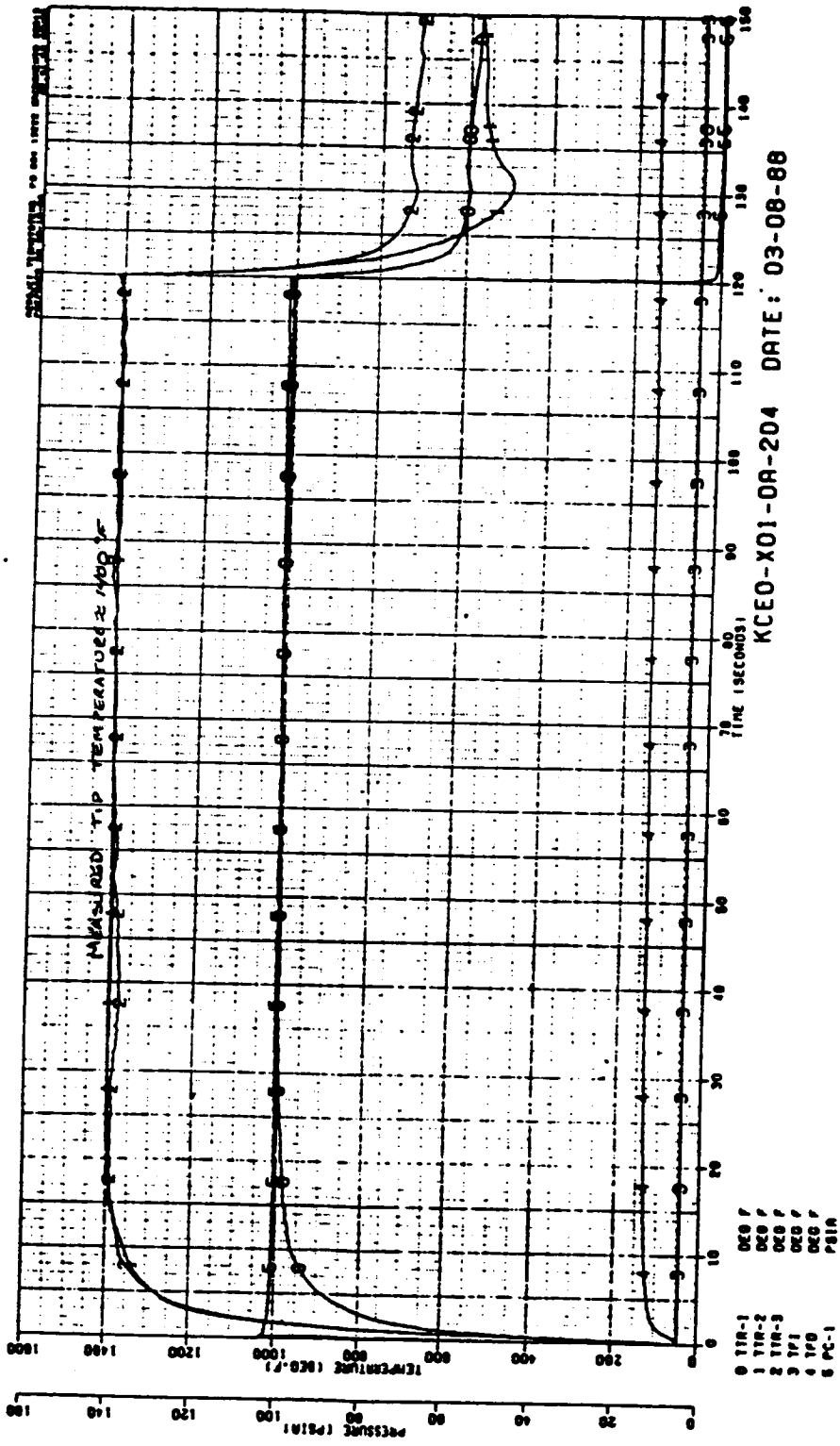

Figure 7. Front End Adaptor Tip Temperature From Reference [1].

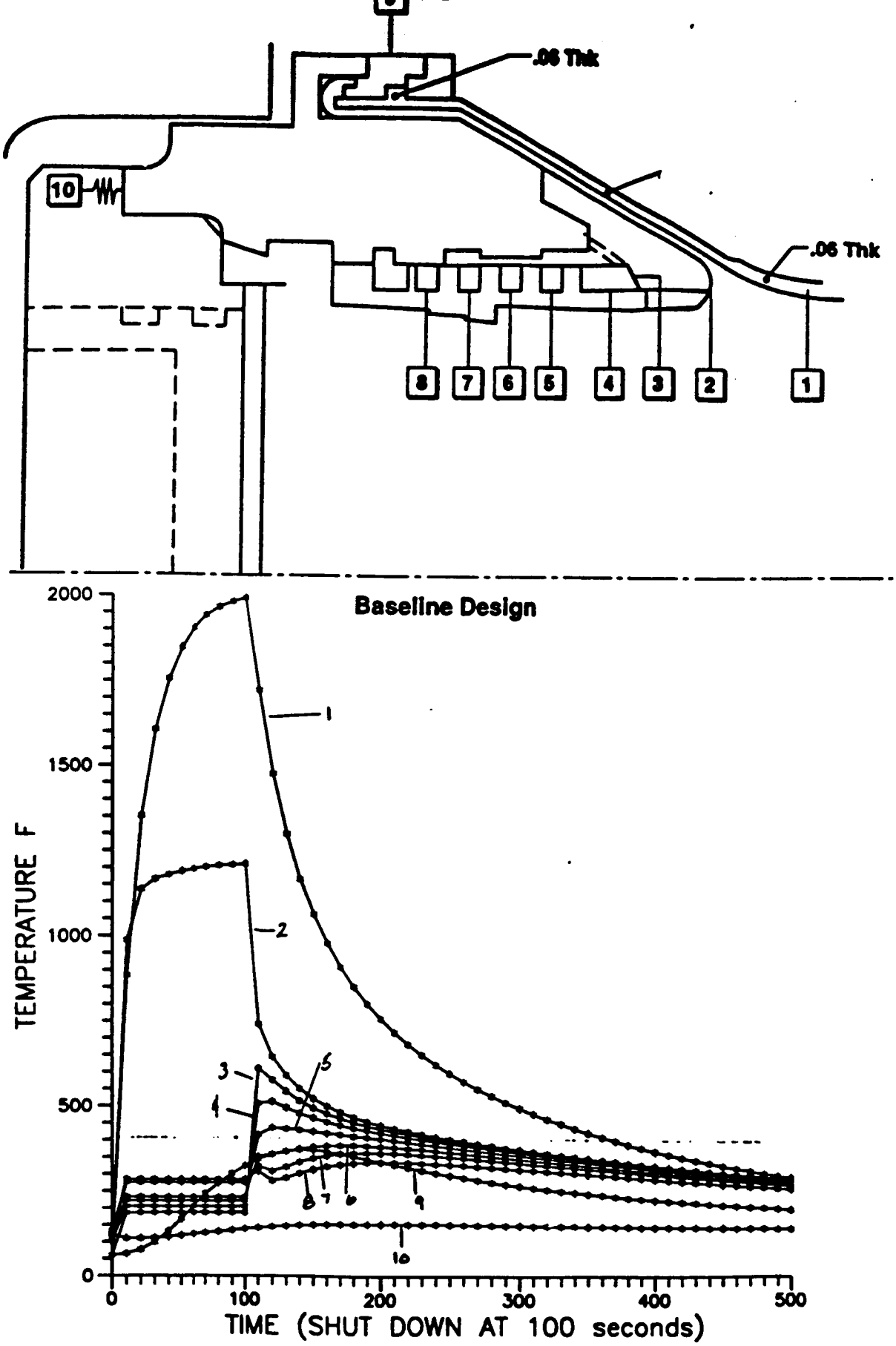

Figure 8. Thermal Soak For Baseline Design.

Table 3. Design Parametric Cases

Parameteric Case No.	Change Made To Model	Objective Of Change	Max 3 F	Max B F	Conclusion	Fig No.
Baseline	Baseline	Baseline	620	310	Decomposition of MMH very likely in channel near tip of adaptor.	8
1	Doubled mass of flangle portion of front end adaptor from 0.6 lbm to 1.2 lbm.	To determine sensitivity to thermal soak from chamber and nozzle.	580	305	Additional flange mass reduces final soak temp. by 25 F. Little effect on coolant overheat.	9
2	Reduced mass of front end tip by factor of 0.5.	To verify that channel overheating was due to heat soak from tip.	480	370	Redesign of front end required	10
3	Same as (2) and increased conductance from tip to backside of adaptor by factor of 1.25.	Try to reduce overheat by soaking to cool back region of adaptor.	460	370	Increased conductance to cool backside.	11
4	Version 1 of modified design	Adjusted model to reflect design changes.	407	385	New tip design adequately reduces overheating with lands connected.	12
5	Same as (4) except with lands disconnected.	Effect of no contact between gas-side wall and backside of adaptor.	475	632	Worst overheating shifts to region near trip.	13
6	Same as (4) except with 1% contact of of channel lands.	Case approximating contact due to thermal expansion.	480	620	Minor benefit from CTE effect.	14
7	Same as (4) except with 50% contact of of channel lands.	Case approximating shrink fit of parts.	428	385	Shrink fit with delta temp 300 F	15
8	Reduced mass of trip by 80% and disconnected channel lands.	To evaluate if overheat with lands disconnected is prevented by reducing mass of trip.	470	554	Reduction in trip mass alone does not solve overheating.	17
9	Same trip as (8) with 50% contact, redesigned cooling channel, and reduced thickness gas side wall.	Redesigned gas side wall which increases land to wall volume by 1.3, and assume a shrink fit.	422	328	Redesigned gas side wall reduces temperature near trip and has little effect on wall near trip.	18
10	Same as (9) except with 80% contact to simulate brazed part.	Try to reduce max channel temp to 400 F body	404	300	Final design meets requirements.	19

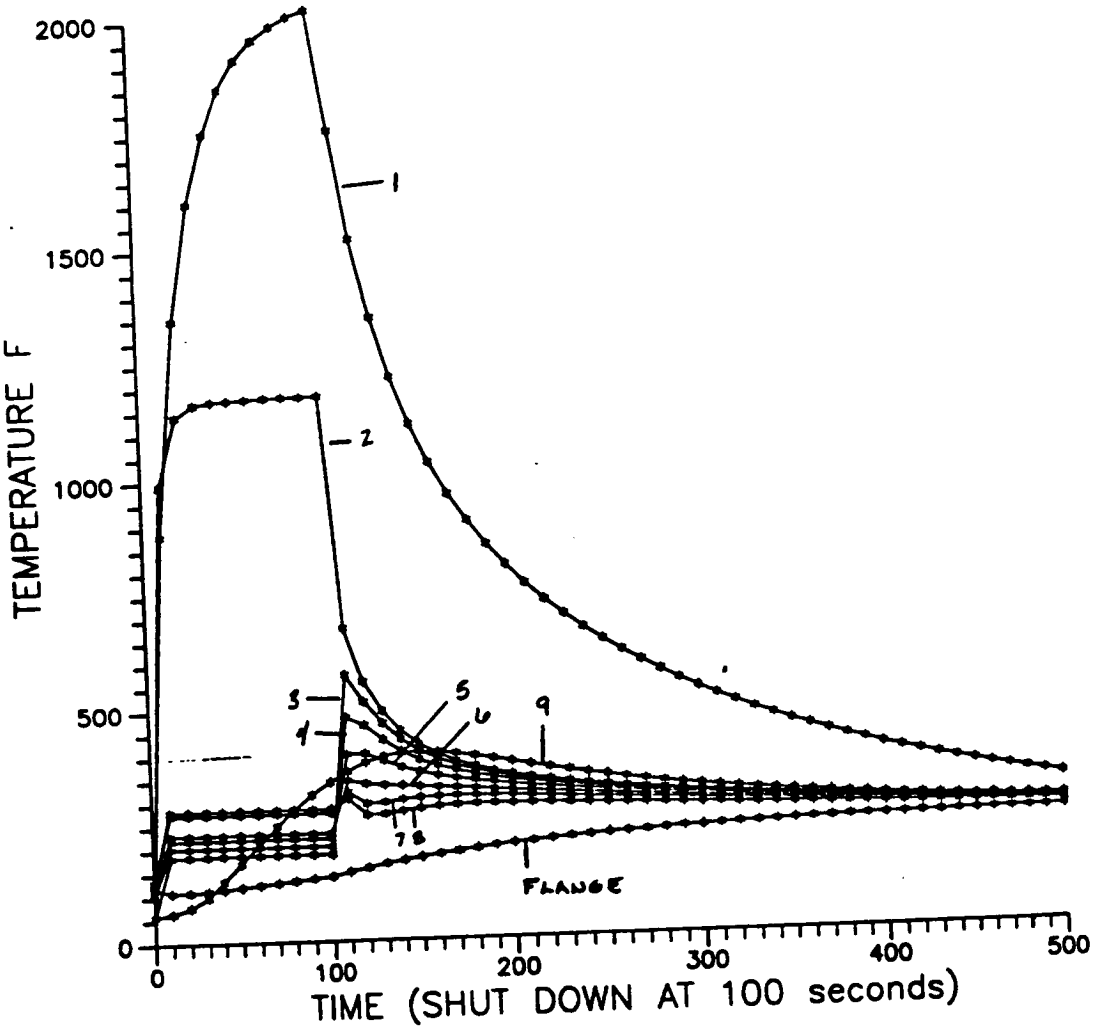

Figure 9. Parametric Case No. 1.

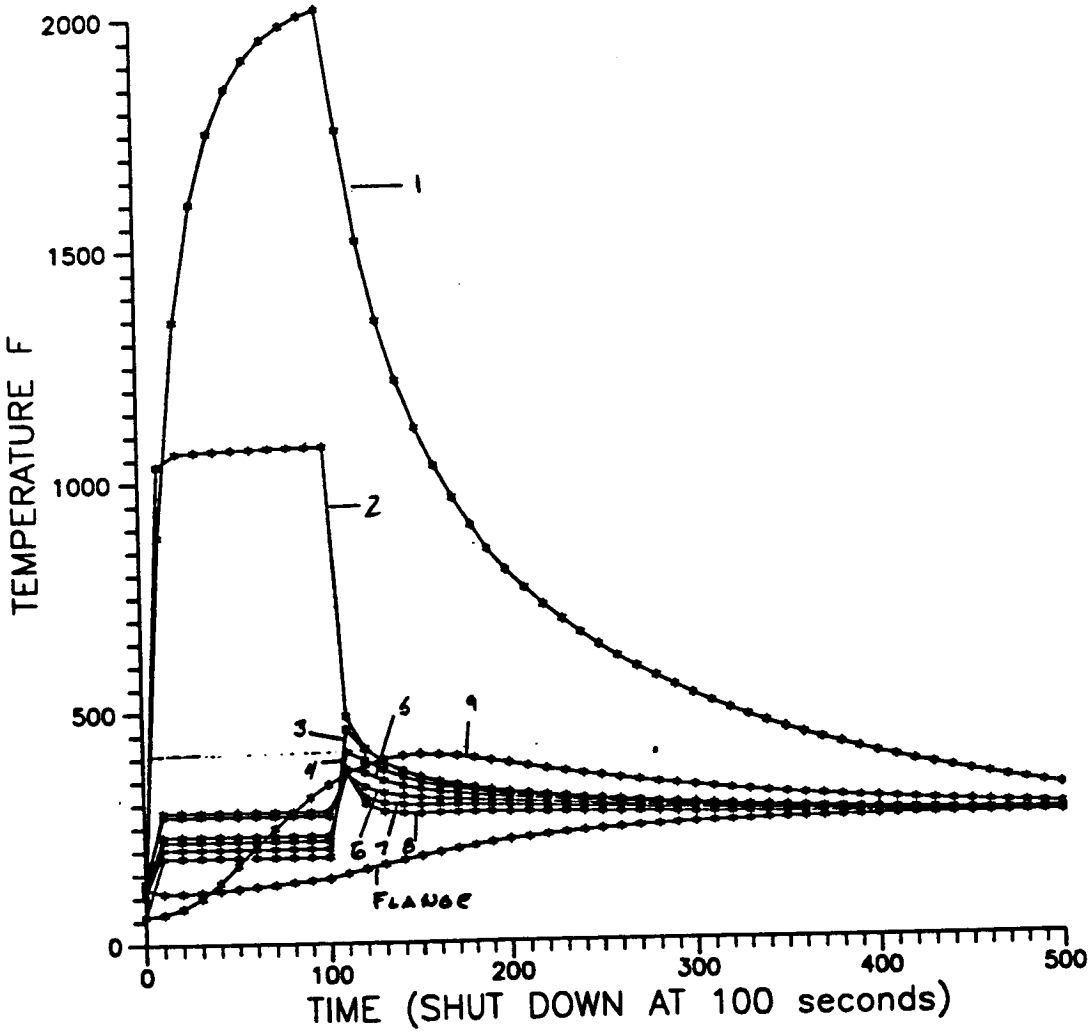

Figure 10. Parametric Case No. 2.

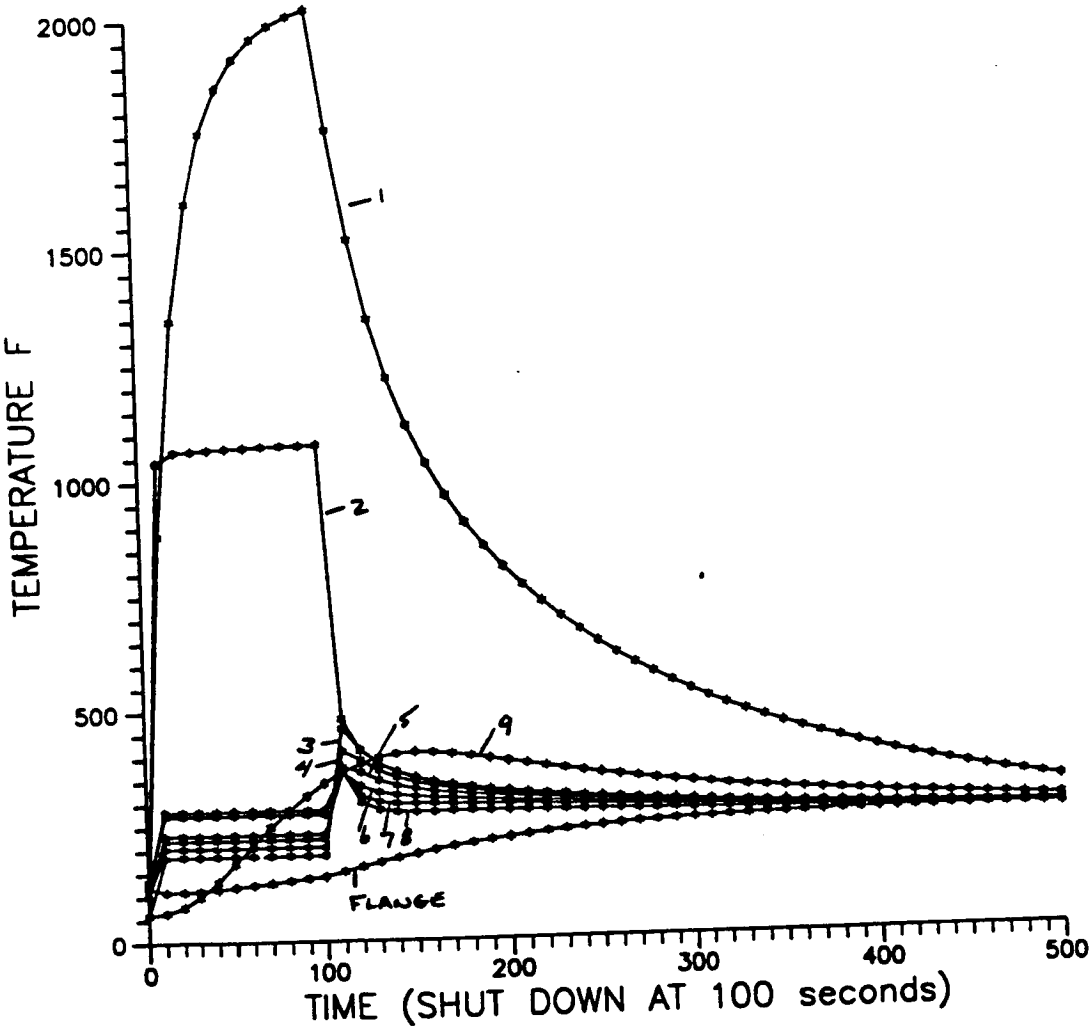

Figure 11. Parametric Case No. 3.

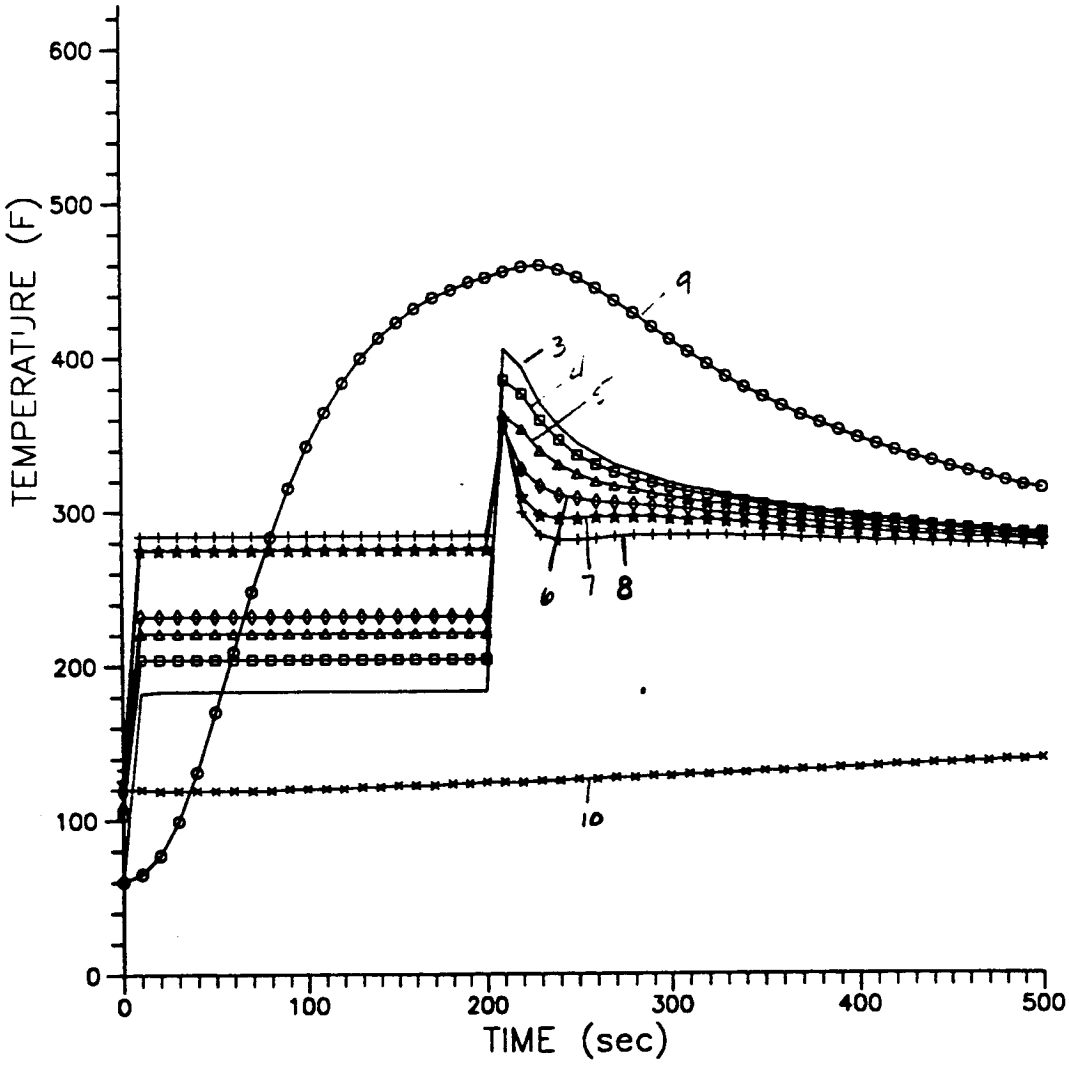

Figure 12. Parametric Case No. 4.

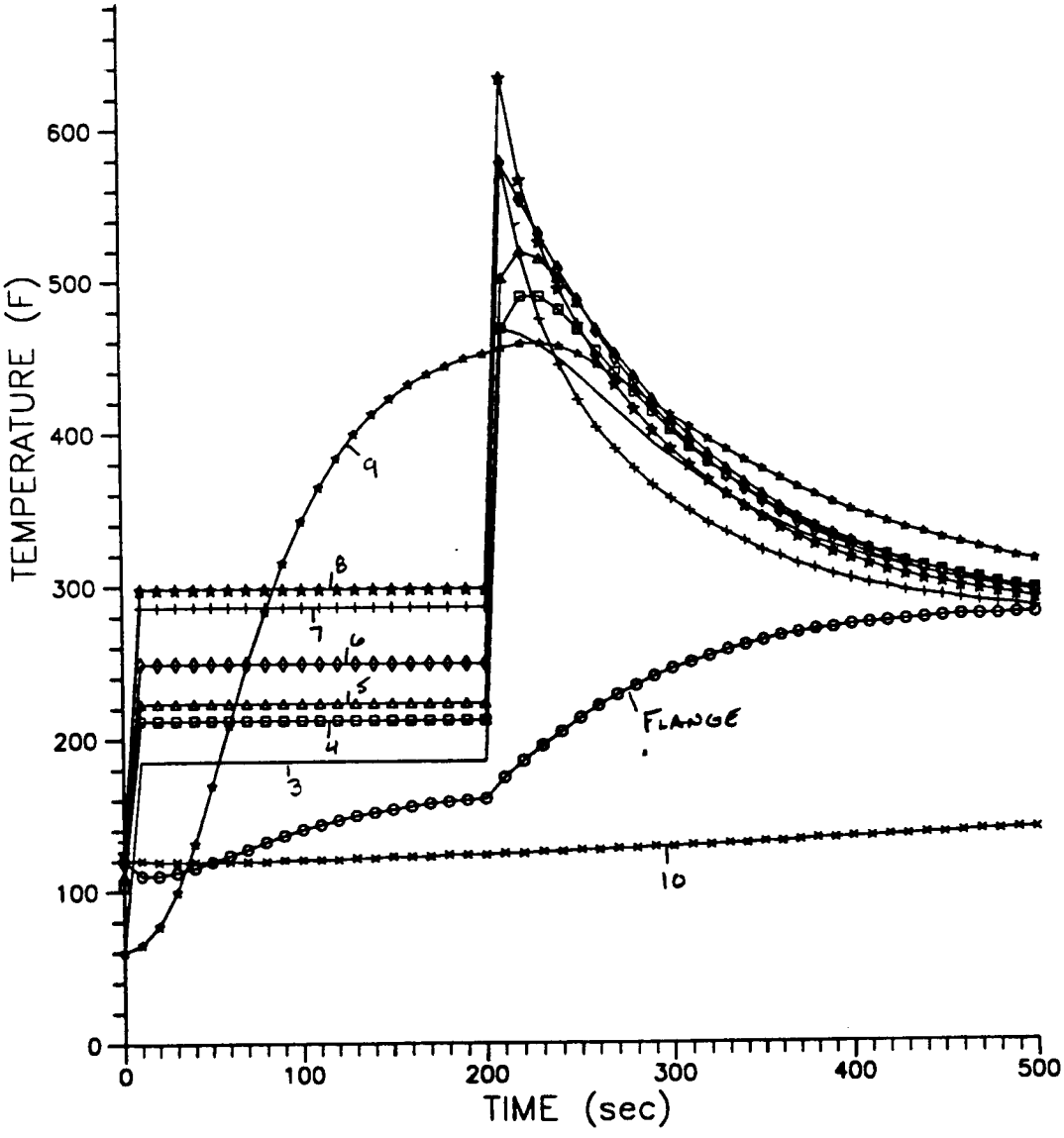

Figure 13. Parametric Case No. 5.

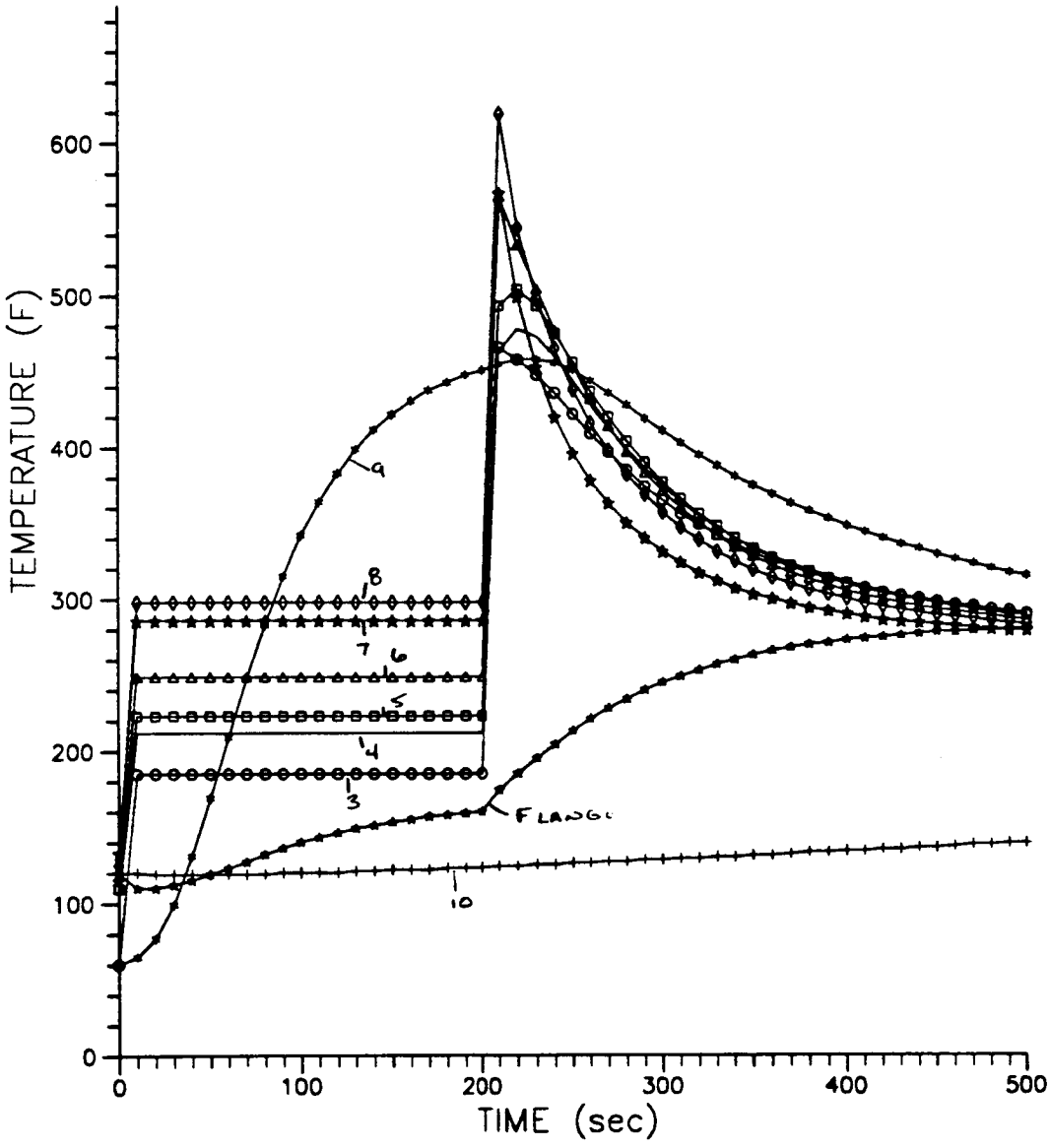

Figure 14. Parametric Case No. 6.

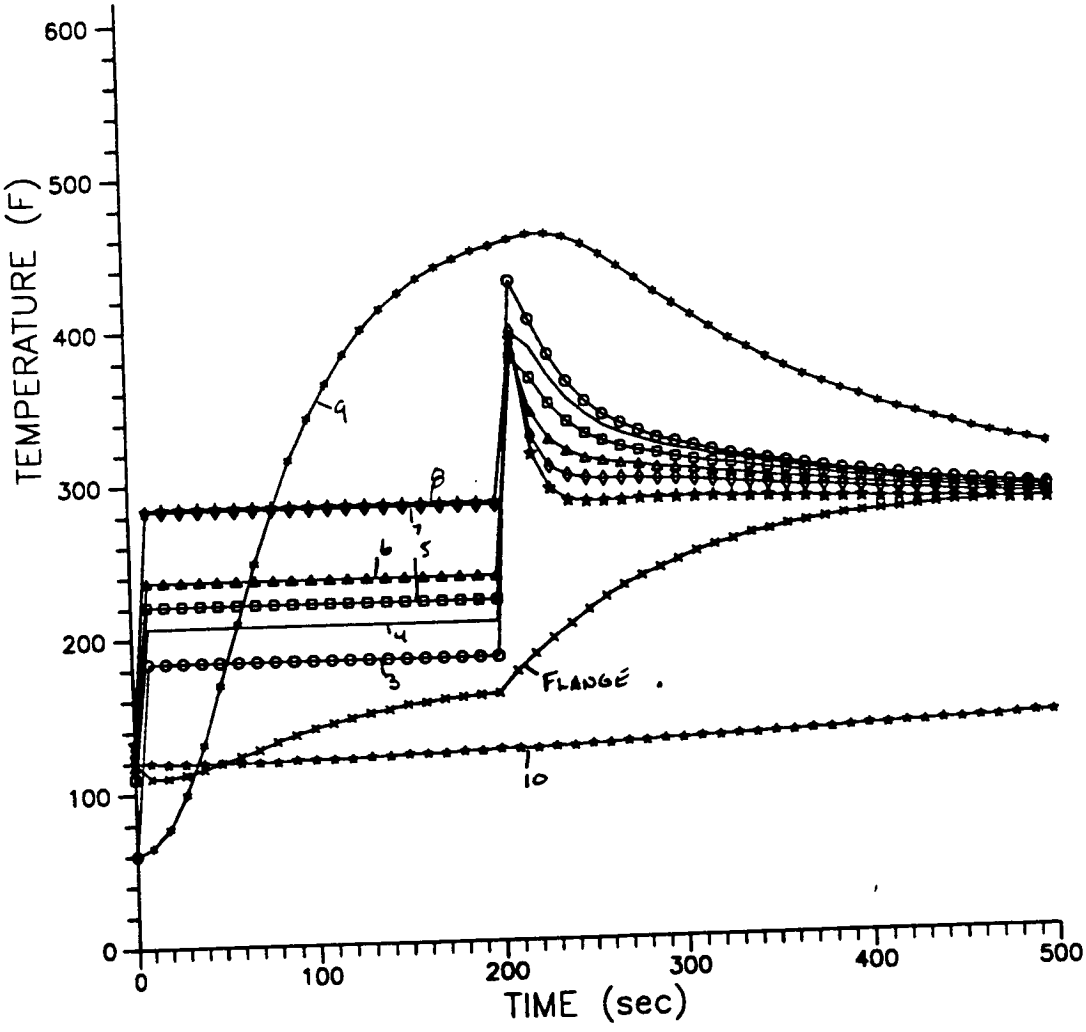

Figure 15. Parametric Case No. 7.

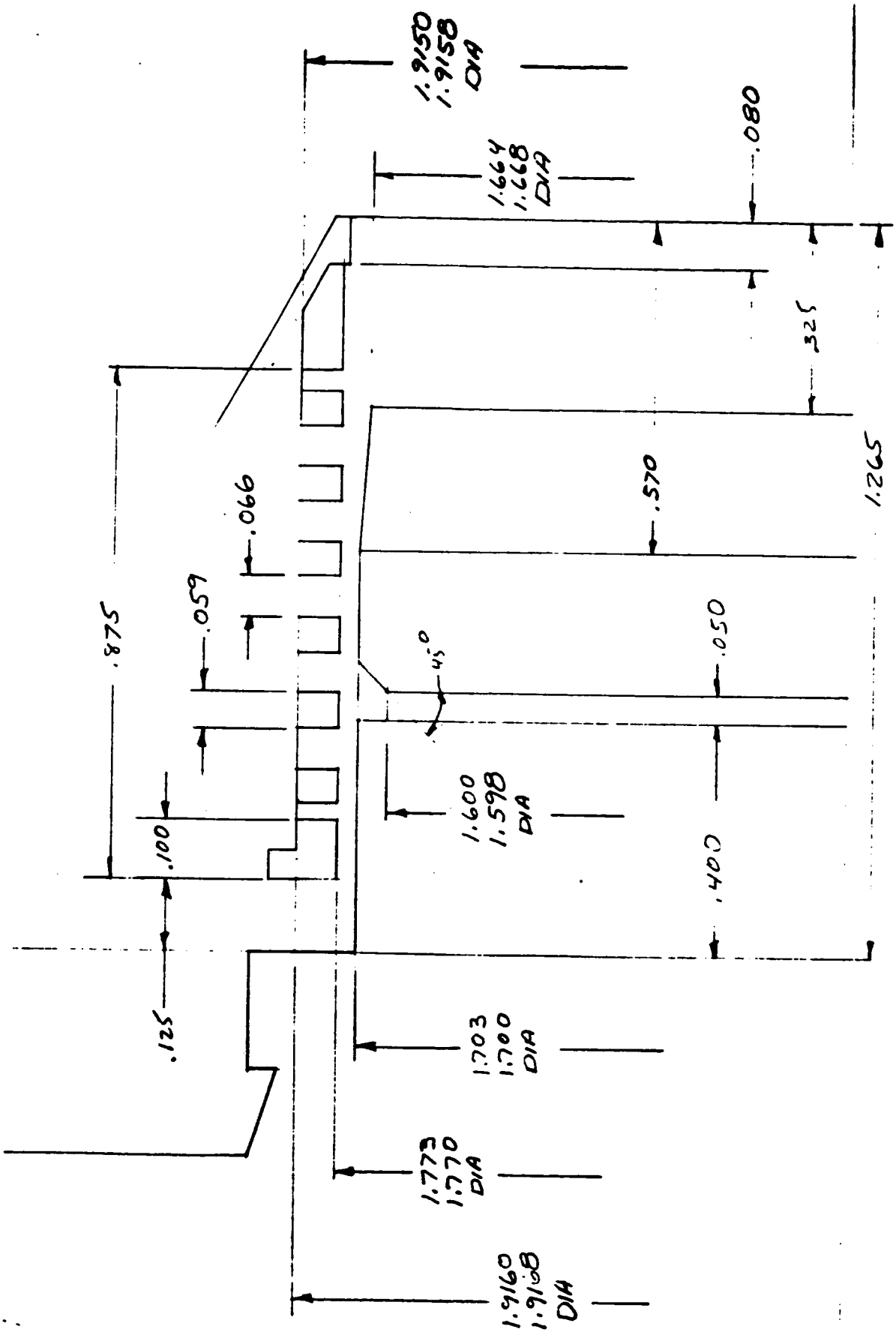

Figure 16. Modified Cooling Channel Design.

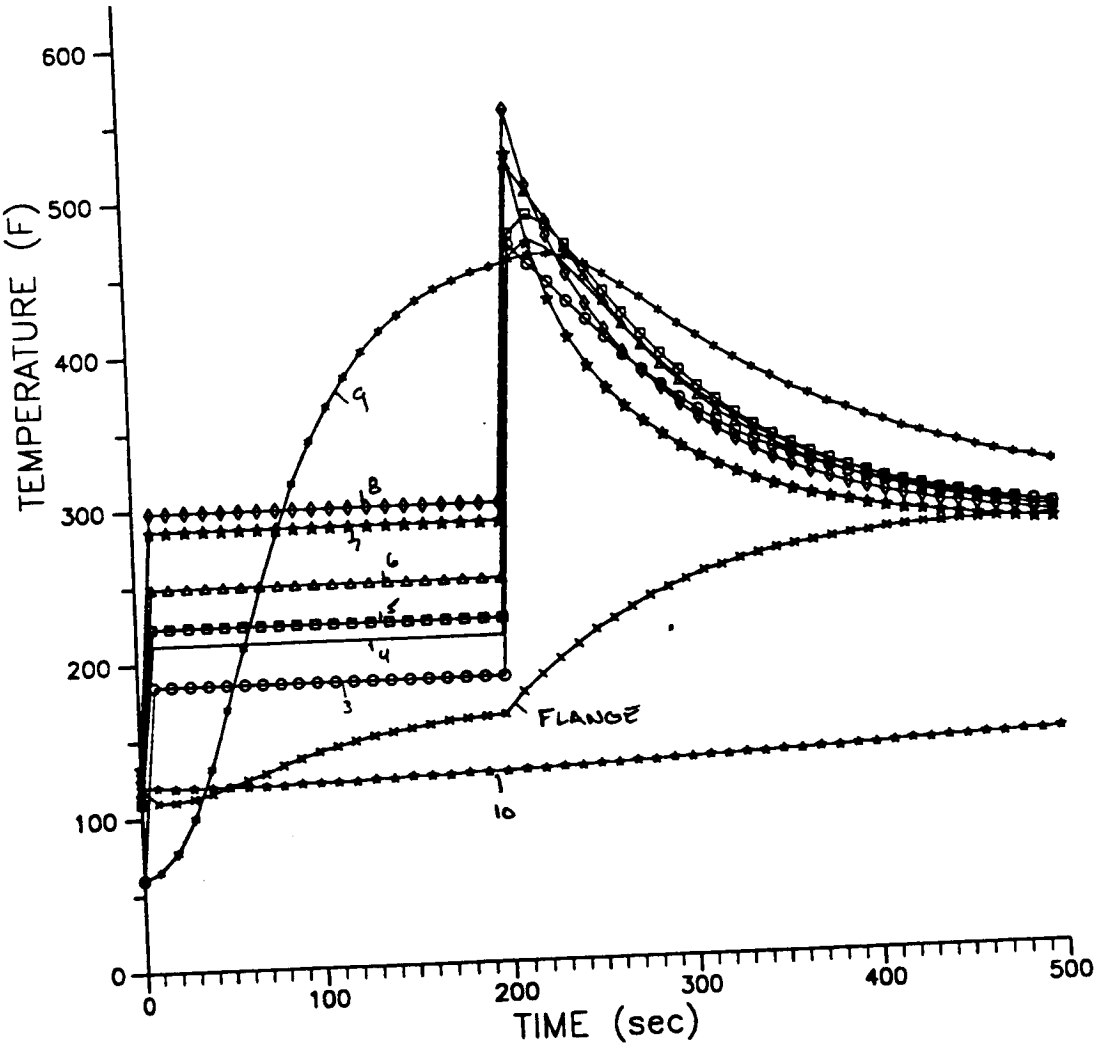

Figure 17. Parametric Case No. 8.

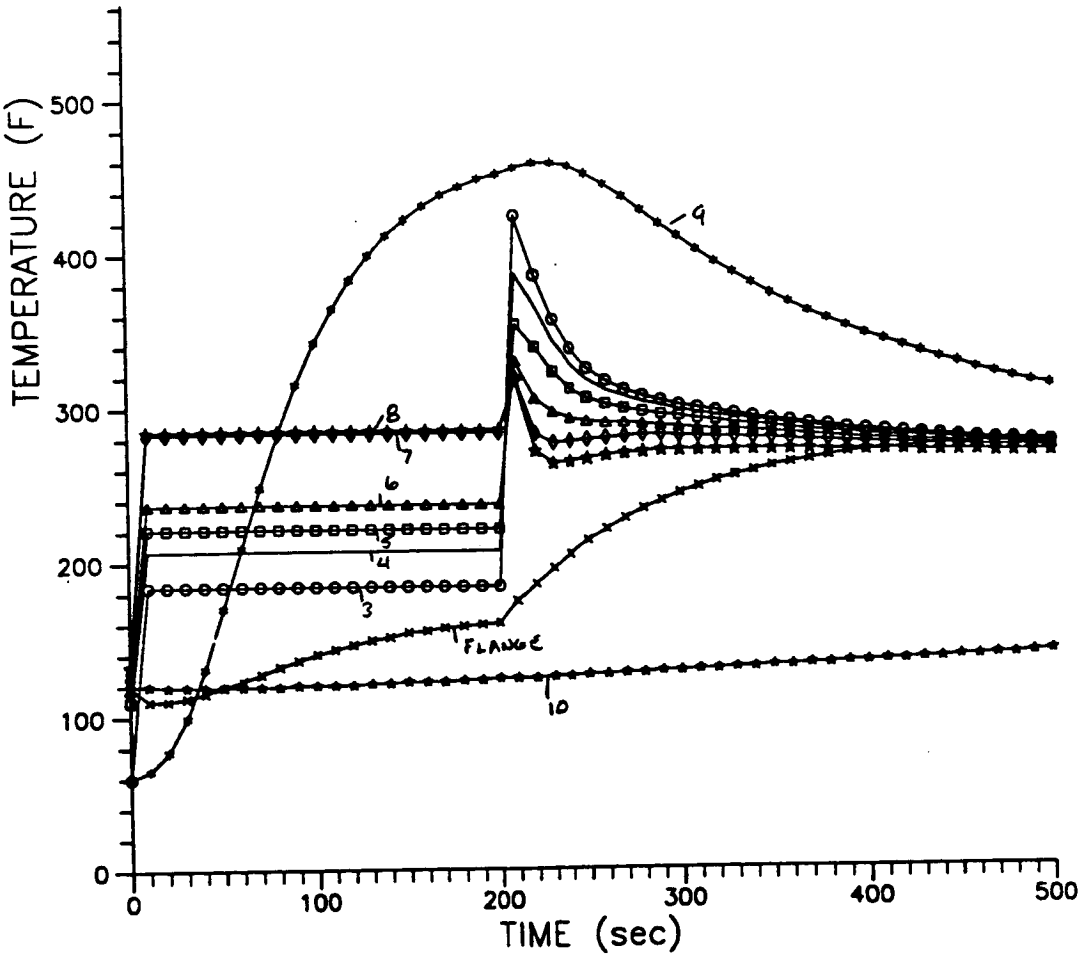

Figure 18. Parametric Case No. 9.

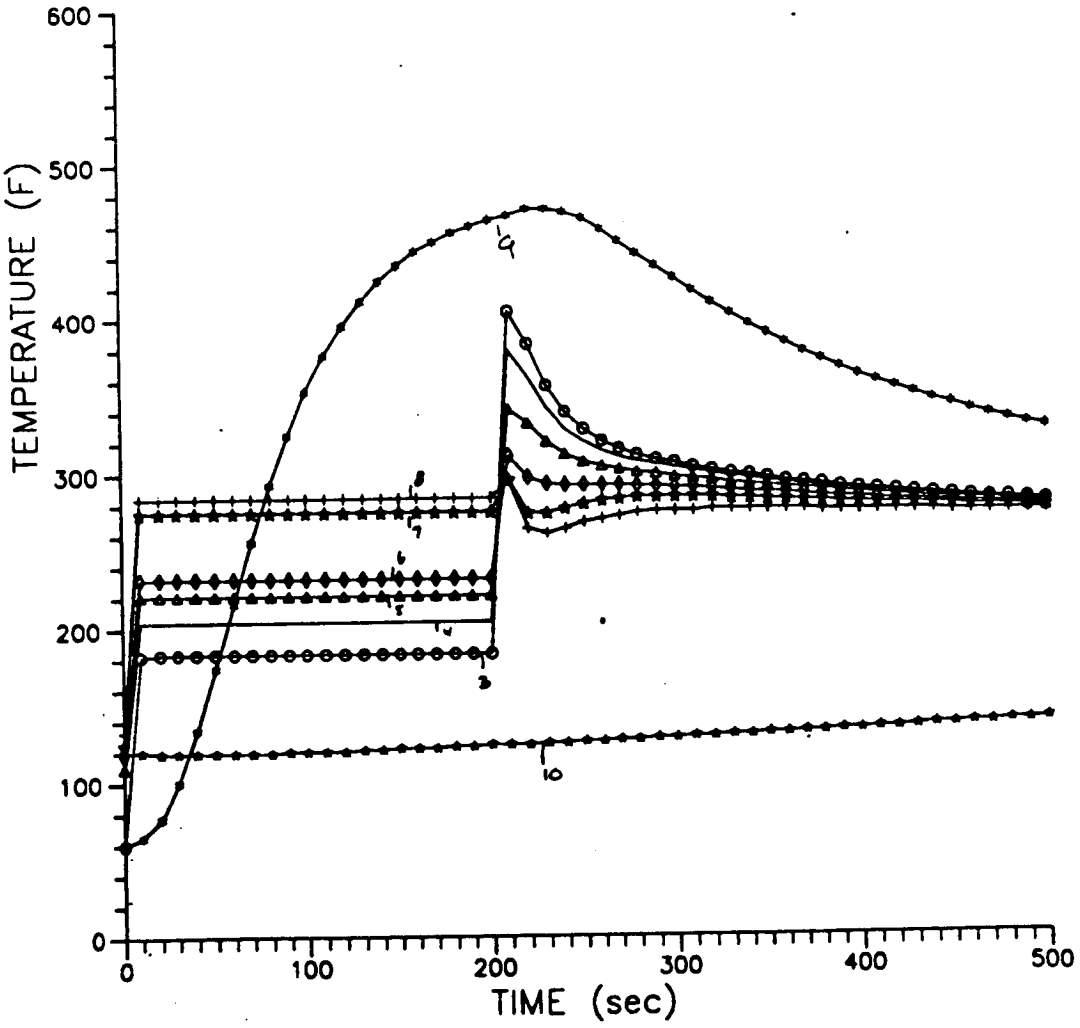

Figure 19. Final Design Soak Temperatures.

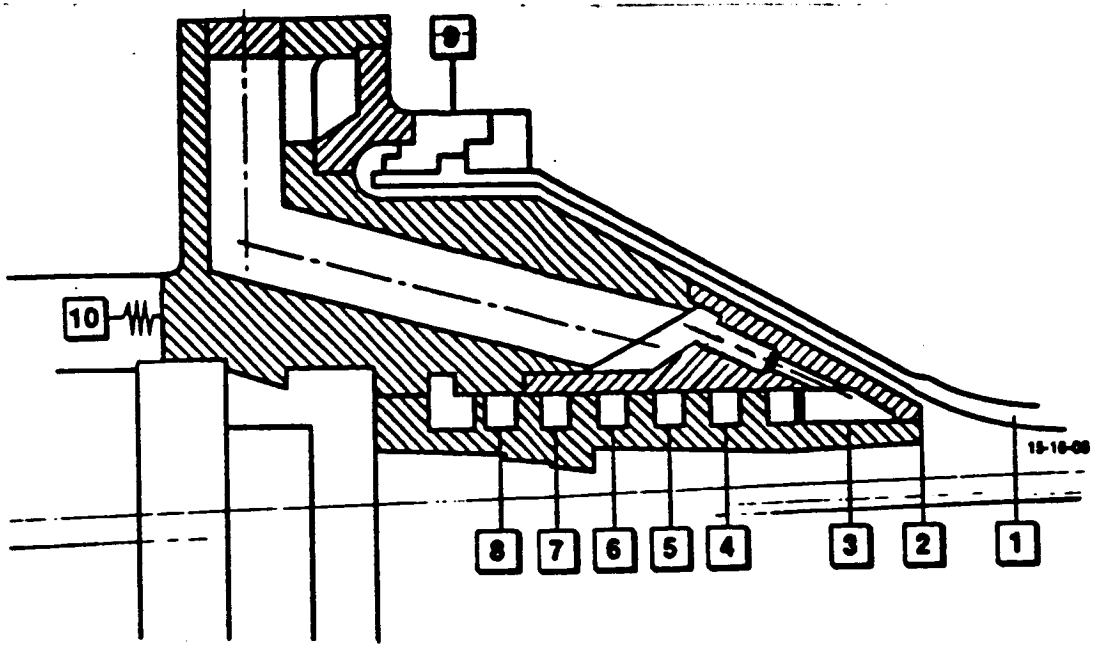

Modified Design

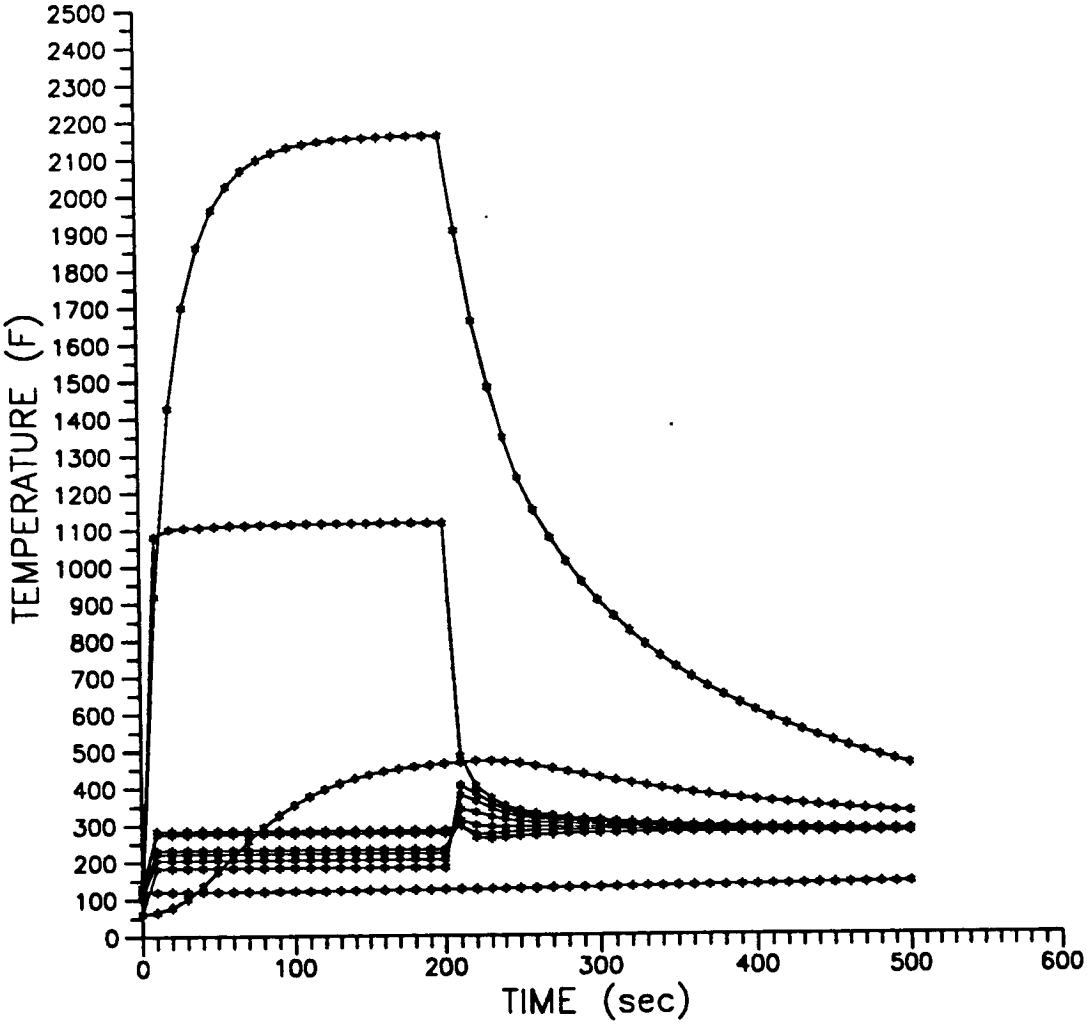

Figure 20. Thermal Soak Temperature For Modified Design

Appendix A

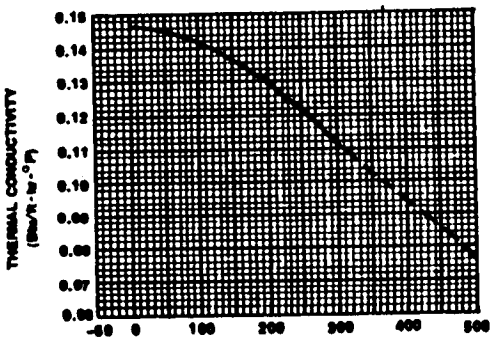

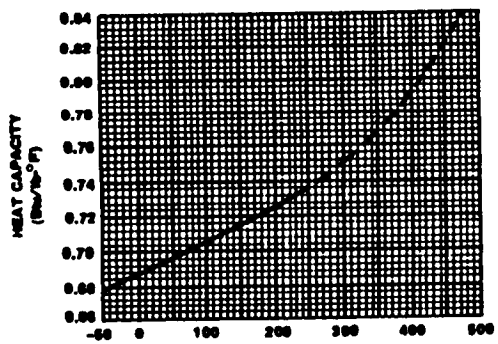

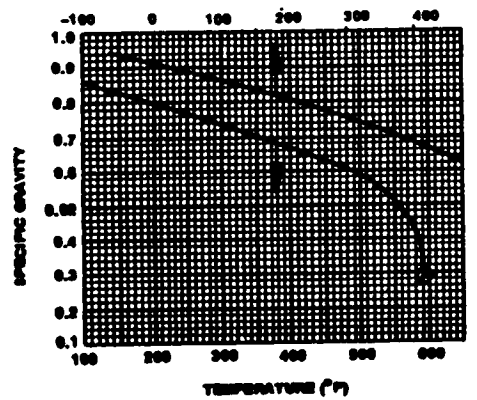

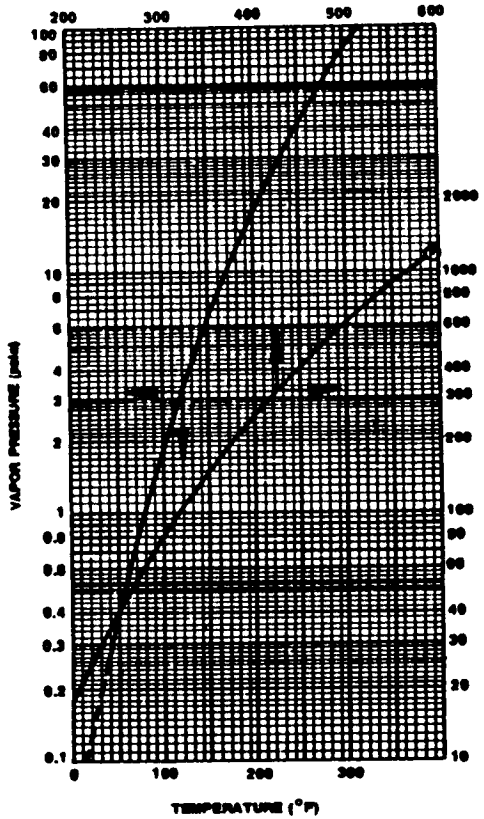

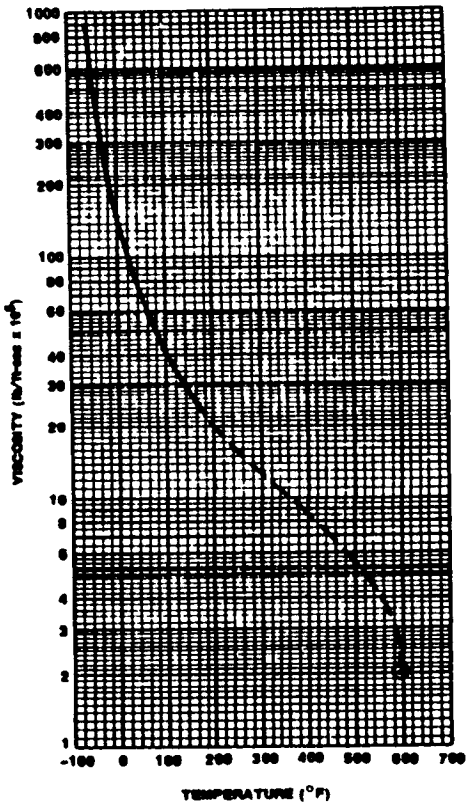

PHYSICAL PROPERTIES OF MONOMETHYL HYDRAZINE: $CH_3N_2H_3$

MOLECULAR WEIGHT	46.0724
FREEZING TEMPERATURE (°F)	-62.3
NORMAL BOILING POINT (°F)	189.8
CRITICAL TEMPERATURE (°F)	594
CRITICAL PRESSURE (psia)	1195
HEAT OF FORMATION (cal/mole liq. @ 298.16°K)	13,100
HEAT OF VAPORIZATION (Btu/lb @ 298.16°K)	377

REFERENCE DATA ——
EXTRAPOLATED DATA – – –
CRITICAL POINT ⊙

REVISED NOV. 1974

TABLE I

SENSITIVITY OF HYDRAZINE FUELS TO COMPRESSION, SHOCK AND HEATING

Material	Threshold Temperature Limits for Sensitivity to External Stimuli, °F: Adiabatic Compression[1] N_2H_4	Adiabatic Compression[1] N_2H_4/MMH[3]	Adiabatic Compression[1] MMH	Hydrodynamic Shock[2] N_2H_4[1]	Hydrodynamic Shock[2] MMH[1]	Thermal Stability of N_2H_4 and MMH at Liquid-Vapor Equilibrium: Temperature at Initial Exotherm, °F N_2H_4	Temperature at Initial Exotherm, °F MMH	Temperature at Bursting Point of Rupture Disc, °F N_2H_4	Temperature at Bursting Point of Rupture Disc, °F MMH
304L S.S.	195-215	~400	>512	>425		450-460[4]	450-455[5]	520-530[6]	525-530[7]
316 S.S.	205		>450	>400	>442	400-420	435-445	570-580	540-570
321 S.S.	210		>512			485-495	435-460	530-560	525-545
347 S.S.	~200	>425	>504	>423		460	450-455	530-535	530-540
17-7 PH S.S.	~130	240-350	>486			465-475	455	535-540	540-545
Inconel-X	~130		>481	>403	>403	490-495	430-445	535-540	500
Haynes-25	205		>512	>406		485	435	530-535	520-525
Hastelloy-X	210		>473	>400	>485	385-420	475-495	510-545	525-565
2014-T6 Al	>90		>300			440	390	525-550	530
6061-T6 Al	<63		>155			410	385	502	460

*Bursting pressure, 5300 psi; corresponds closely to the spontaneous ignition temperature.

(1) Liquid/vapor samples blanketed with N_2 and adiabatically compressed in a U-tube apparatus with N_2 to 200-300 psig

(2) Totally liquid samples contained in 1-in. O.D. tubes and hydrodynamically shocked by detonation of a blasting cap and 50-gm Pentolite booster charge (Liquid Propellant Test Methods, Test No. 8, "Critical Diameter and Detonation Velocity Test", May 1964)

(3) 2.5 to 10% wt MMH

(4) 395-455°F for N_2H_4 vapor only

(5) 390-455°F for MMH vapor only

(6) 442-455°F for N_2H_4 vapor only

(7) 434-454°F for MMH vapor only

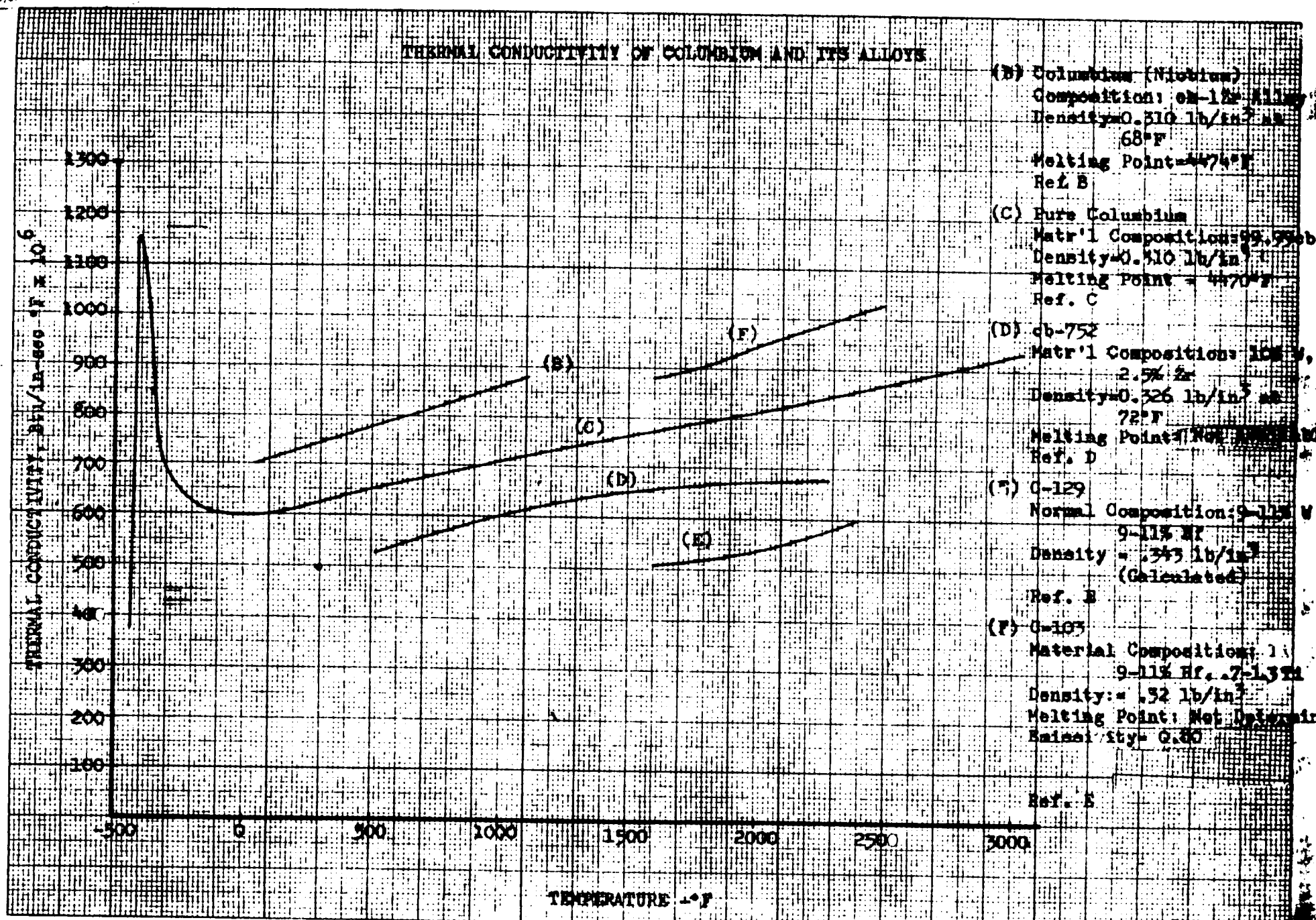
THERMAL CONDUCTIVITY OF COLUMBIUM AND ITS ALLOYS
THERMAL CONDUCTIVITY - BTU/HR-FT-°F
TEMPERATURE - °F
1300
1200
1100
1000
900
800
700
600
500
400
300
200
100
-500
0
500
1000
1500
2000
2500
3000
(B)
(C)
(D)
(E)
(F)
(B) Columbium (Niobium)
Composition: cb-1Zr Alloy
Density=0.310 lb/in³ at 68°F
Melting Point=4474°F
Ref. B
(C) Pure Columbium
Matr'l Composition=99.9%cb
Density=0.310 lb/in³
Melting Point = 4470°F
Ref. C
(D) cb-752
Matr'l Composition: 10% W, 2.5% Zr
Density=0.326 lb/in³ at 72°F
Melting Point: Not Determinable
Ref. D
(E) C-129
Normal Composition: 9-11% W
9-11% Hf
Density = .345 lb/in³ (Calculated)
Ref. E
(F) C-103
Material Composition: 10% Hf, 1% Ti
9-11% Hf, .7-1.3% Ti
Density: = .32 lb/in³
Melting Point: Not Determined
Emissivity= 0.80
Ref. E

ENCLOSURE (1)

FIG SHOWS ONLY 11 OF THE CURVES REPORTED IN TABLE

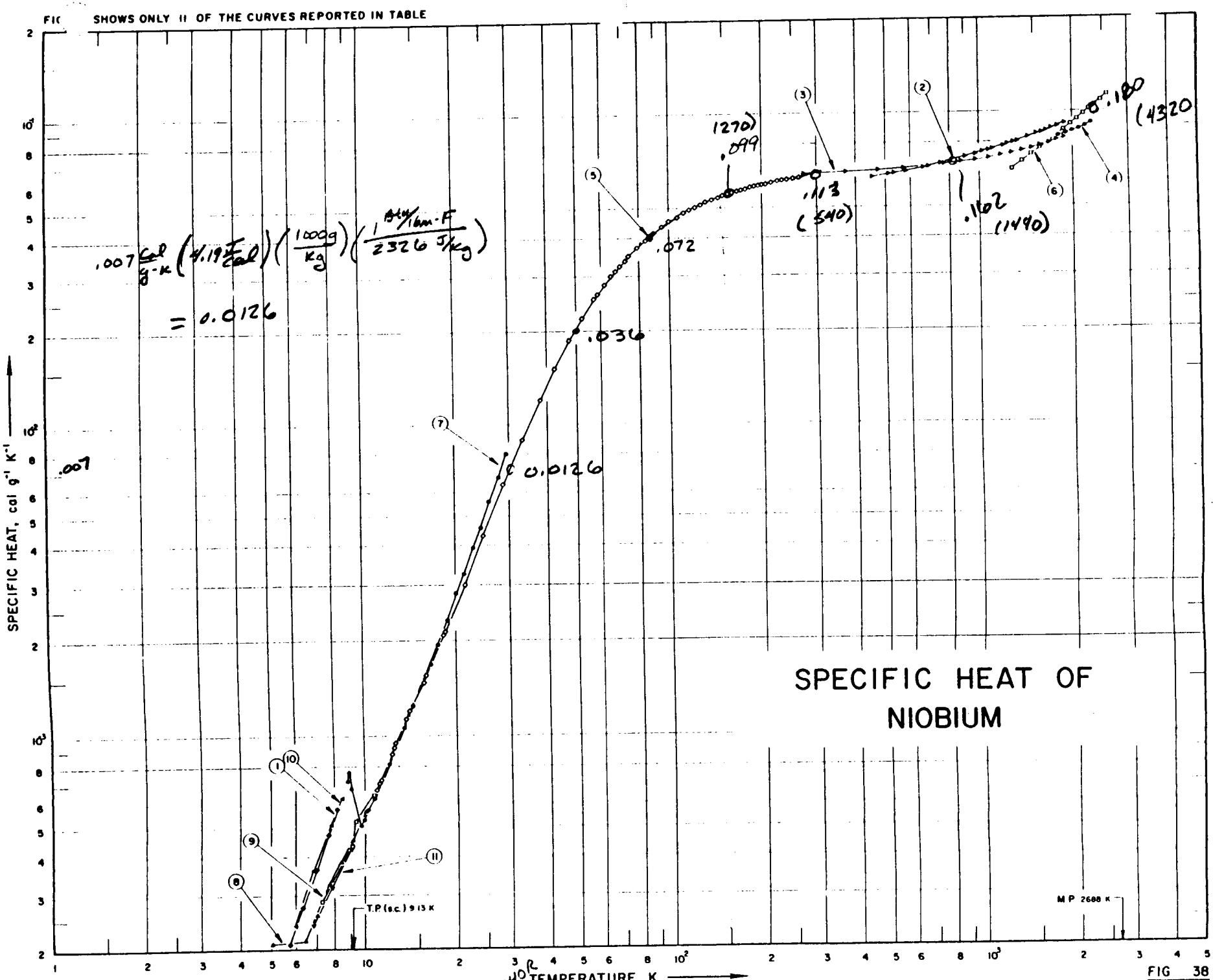

FIG 38

APPENDIX C

DYNAMIC ANALYSIS

GENCORP
AEROJET

Propulsion Division

20 January 1992

Memo

TO: L. Schoenman

FROM: J. H. Beuttler

SUBJECT: 100 lbF Thrust Engine Structural Dynamics Analysis

COPIES TO: G. Nelson, N. R. Shimp, File

ENCLOSURE: (1) 100 lbF Engine Structural Dynamics Analysis

This memo presents results of the evaluation of the 100 lb engine design. In response to a request from the Research & Technology group, preliminary dynamic response analyses were performed on the engine assembly. An area of particular concern was the chamber forward joint and throat when subjected to the random and sinusoidal base excitation requirements specified by the customer, NASA/Lewis and JPL.

Analyses results indicate limitations with this design. Some possible changes are suggested along with an assessment of the potential for improvement.

J. H. Beuttler

J. H. Beuttler
Metallic Structures & Dynamics
Engineering Analysis Department

APPROVED BY:

E. Lueders

E. Lueders, Manager
Metallic Structures & Dynamics
Engineering Analysis Department

ENCLOSURE (1)

100 LB. ENGINE
STRUCTURAL DYNAMICS ANALYSIS

PREPARED BY:

J.H. Beuttler
Metallic Structures & Dynamics
Engineering Analysis Department

APPROVED BY:

E. Lueders, Manager
Metallic Structures & Dynamics
Engineering Analysis Department

REVIEWED BY:

L. M. Greenhill
Metallic Structures & Dynamics
Engineering Analysis Department

INTRODUCTION

In response to a request from the Research & Technology group to evaluate the 286:1 area ratio 100 lbF engine design, preliminary dynamic response analyses were performed on the engine assembly. An area of particular concern was the chamber forward joint and throat when subjected to the random and sinusoidal base excitation requirements specified by the customer, NASA/Lewis and JPL. For the purpose of this analysis, it was assumed that the gimbal at the head end of the engine is fully rigid and has no influence on the load transmission from the propulsion system interface.

SUMMARY

A three-dimensional finite element model (FEM) was constructed using the ANSYS computer code and a harmonic response analysis was performed. Plate elements were used to define the injector and nozzle, and beam elements were used to resolve loads at the forward joint.

Thirty natural modes were calculated in the frequency range of interest, 20 Hz to 2000 Hz, however, two of these modes were found to provide the majority of response. These were calculated to have natural frequencies at 75 Hz and 910 Hz.

Harmonic response analyses were performed using excitation at a base seismic mass. An amplification factor of Q = 50 was assumed, which corresponds to a damping ratio of $\zeta = 0.01$.

Base random response analyses predict a maximum 3-sigma principle equivalent plate stress of 150 ksi in the throat region. Sinusoidal excitation results, which specifies a 15 G base input in the 25-100 Hz frequency range, predict a maximum principle equivalent plate stress of 857 ksi, also in the throat region. The chamber is to be constructed of rhenium which is assumed to have an allowable stress (ultimate) of 170 ksi.

Maximum loads at the injector forward joint were calculated to be 2500 lbs due to the sinusoidal excitation. The resultant bending stresses in the rhenium material was calculated to be 18 ksi, and lower stresses were calculated for the stainless steel. However, this joint is of a complex design, and precise resolution of its load carrying capability was beyond the scope of this effort.

CONCLUSIONS AND RECOMMENDATIONS

Option 1

Redesign of the throat area. It is recommended that additional support be provided through the throat to not only provide better load carrying capability, but to also raise the fundamental mode natural frequency of 75 Hz out of the critical excitation range. The specified base input drops to 5 G's in the 100-200 Hz frequency range, and to zero above that.

It is estimated that by adding a ring having an outside diameter of 1.8", spanning the length of the throat, with a thickness of 0.1", the resultant increased stiffness may raise the fundamental mode above 200 Hz. This estimation is supported by

preliminary hand calculations, but in order to confirm the overall improvement in stresses, this analysis should be repeated.

Option 2

Another possible design improvement may be to provide ribs across the throat area. As mentioned above, any design change should be verified through analysis.

Option 3

Reducing the columbium skirt mass by wall thinning and/or length reduction would also help raise the natural frequency above the 100 Hz level where the input load is reduced from 15 to 5 g's.

Due to its complexity and critical nature, a more detailed analysis of the chamber forward joint should be performed before fabrication.

In the event a subsequent analysis is performed, further recommendations are made as listed below:

(1) An overall finer finite element model resolution should be used with the STIF93 8-node isoparametric shell element. This particular element is more ideally suited to the modelling of curved shells than the simpler, though less expensive, STIF63 elastic quadrilateral shell element used in this analysis.

(2) No account was made in this analysis for the silicide coating on the nozzle. This is predicted to increase the thickness by up to 0.004" with a corresponding increase in mass and should be incorporated in subsequent analyses.

(3) It should be noted that the existence of a pyro shock environment was stated, however no data defining a spectra was supplied. An environment of this nature can usually be quite severe depending on its type and location of origin. It is recommended that this issue be addressed prior to fabrication.

ANALYSIS

GEOMETRY

A three-dimensional finite element model (FEM) was constructed using the ANSYS computer code. Figure 1 depicts the component layout. The origin of the global coordinate system is located at the top of the nozzle, aft of the throat. The global Z axis is the axis of rotation and is positive in the direction towards the exit plane. The X and Y axes form a plane perpendicular to the Z axis in accordance with the right hand rule (Fig. 2).

The chamber/skirt assembly was described with the STIF63 elastic quadrilateral shell element, however, due to the complex curvature, it was degenerated to a triangular element in order to avoid warpage.

The skirt FEM followed the geometry description of the -1 configuration with a constant element thickness of 0.014 inches (Fig. 3).

The skirt elements were assigned the properties of columbium as shown:

E (modulus of elasticity) = 13,100,000 psi
c (weight density) = 0.3188 lbs/in^3

S_y (allowable yield stress) = 34,000 psi
S_u (allowable ultimate stress) = 50,000 psi

Maximum thickness was applied, instead of the 0.011" nominal value, for a worst-case evaluation resulting from increased mass effects. However, no account was made for the silicide coating which is predicted to increase the thickness by 0.004" with a corresponding increase in mass.

The chamber FEM followed the geometry description of the -1 configuration (Fig. 4). Element thickness of 0.035" was used at the aft section just forward of the nozzle, and 0.062" was used through the throat and main body. A thickness of 0.035" was used at the conical forward section.

The chamber elements were assigned the properties of rhenium as shown:

E (modulus of elasticity) = 65,500,000 psi
c (weight density) = 0.7728 lbs/in^3

S_u (allowable ultimate stress) = 170,000 psi

Beam elements were utilized in the chamber forward joint area for load resolution. The STIF4 three dimensional elastic beam element was employed using properties calculated to provide high stiffness, but without causing complications with the numerical calculations.

A complete listing of the ANSYS FILE18 input commands used to generate the model are shown in Appendix A.

The skirt weight was calculated to be approximately 2.3 lbs and the chamber was 1.4 lbs accounting for a total model weight of 3.7 lbs.

A relatively coarse mesh was selected in order to keep computing costs to a minimum (Fig. 2). 544 elements and 292 nodes were defined accounting for 1752 degrees-of-freedom (DOF) overall. The coarse overall mesh was refined in the throat region to obtain better resolution.

In the event a more detailed analysis is desired in the future, it is recommended that an overall finer resolution be used with the STIF93 8-node isoparametric shell element. This particular element is more ideally suited to the modelling of curved shells.

METHOD OF ANALYSIS

Natural frequencies were calculated using the Householder reduced modal extraction procedure (KAN,2) of the ANSYS computer code. In order to conserve computing costs, the Guyan reduction technique was employed to reduce the total degrees of freedom.

The reduced harmonic response analysis technique (KAN,6) of the ANSYS computer code was employed using the mode superposition method.

Resultant accelerations and stresses due to the specified random environment (Fig. 5) input were then calculated using the ANSYS POST26 processor. Similar results due to the specified sine environment were calculated through direct multiplication (Appendix B).

Appendix C contains a flow chart of the analysis method and a listing of the computer files utilized for the development of the FEM, subsequent response analyses, and results. These files have been archived and are located in the VAX archive directory [E24595.REA100.TESTE].

DETAILED ANALYSIS

Modal analysis was performed with matrices reduced to 200 DOF from the full model size of 1752 DOF. This value was initially chosen in the interest of conserving computing costs, however, practical experience dictates a 10:1 ratio between number of DOF and number of modes used in the analysis. Thirty modes (Table I) were extracted in the frequency range of interest, 20-2000 Hz, as dictated by the input environments (Appendix B). In this case, the ratio of DOF to modes of 7:1 was considered adequate.

Base excitation was supplied at a seismic mass, which was coupled to the FEM at the beam ends of the injector forward joint, and was assigned a value 1E8 greater than the model weight. Response due to unit gravity harmonic acceleration of the seismic mass was determined. An amplification factor of Q = 50 was assumed, which corresponds to a damping ratio of $\zeta = 0.01$. Modal extraction results, which are utilized in this analysis, are determined by restricting motion of the seismic mass to the direction of excitation only.

Modal analyses results indicated high participation from the fundamental mode of vibration, which is described as cantilever motion of the nozzle about the throat (Fig. 6). This response is most likely to produce maximum loads and stresses from lateral base vibration. Therefore, in order to conserve budget, only base random and sinusoidal vibration analyses were performed; the specified acoustic spectra was not applied. In addition, only lateral (X-axis) excitation response analysis was performed.

It should be noted that the existence of a pyro shock environment was stated, however no data defining a spectra was supplied. An environment of this nature can usually be quite severe depending on its type and location of origin. It is recommended that this issue be addressed prior to fabrication.

DETAILED RESULTS

A listing of the first 30 modes is presented in Table I. The majority of response was found to occur at 75 Hz which is described as cantilever motion of the nozzle (skirt) about the throat (Fig. 6). High response was also calculated at 910 Hz which indicates bending in the nozzle and at the injector body (Fig. 7).

A sample power spectral density (PSD) acceleration response function taken at the engine exit plane is shown in Fig. 8.

The table below lists the maximum stresses and loads by environment and region.

PRINCIPLE EQUIVALENT PLATE STRESSES (SIGE)		
	Random Analysis PSD Accel Environment, 13.3 G_{rms} Composite 3r, PSI	Sinusoidal Analysis Sine Environment, 15 G's @ 75 Hz PSI
Chamber Fwd Section Element #499	56037	318150
Chamber Throat Element #312	149646	856980
Chamber Aft Section Element #168	135138	773745
Skirt Element #17	31458	179790
BEAM AXIAL LOADS		
		Sinusoidal Analysis Sine Environment, 15 G's @ 75 Hz LBS
Chamber Fwd Joint Element #529		2490

The resultant bending stresses due to the chamber forward joint load was calculated to be 18 ksi in the rhenium material, and lower stresses were calculated for the stainless steel. However, this joint is of a complex design, and precise resolution of its load carrying capability was beyond the scope of this effort.

Due to its complexity and critical nature, a more detailed analysis of the forward joint should be performed.

Redesign of the throat area is necessary, and it is recommended that additional support be provided through the throat to not only provide better load carrying capability, but to also raise the fundamental mode natural frequency of 75 Hz out of the critical excitation range. The specified base input drops to 5 G's in the 100-200 Hz frequency range, and to zero above that.

It is estimated that by adding a ring having an outside diameter of 1.8 in., spanning the length of the throat, with a thickness of 0.1 in., the resultant increased stiffness may raise the fundamental mode above 200 Hz. This estimation is supported by preliminary hand calculations (Appendix D), but in order to confirm the overall improvement in stresses, this analysis should be repeated.

Another possible design improvement may be to provide ribs across the throat area. As mentioned above, any design change should be verified through analysis.

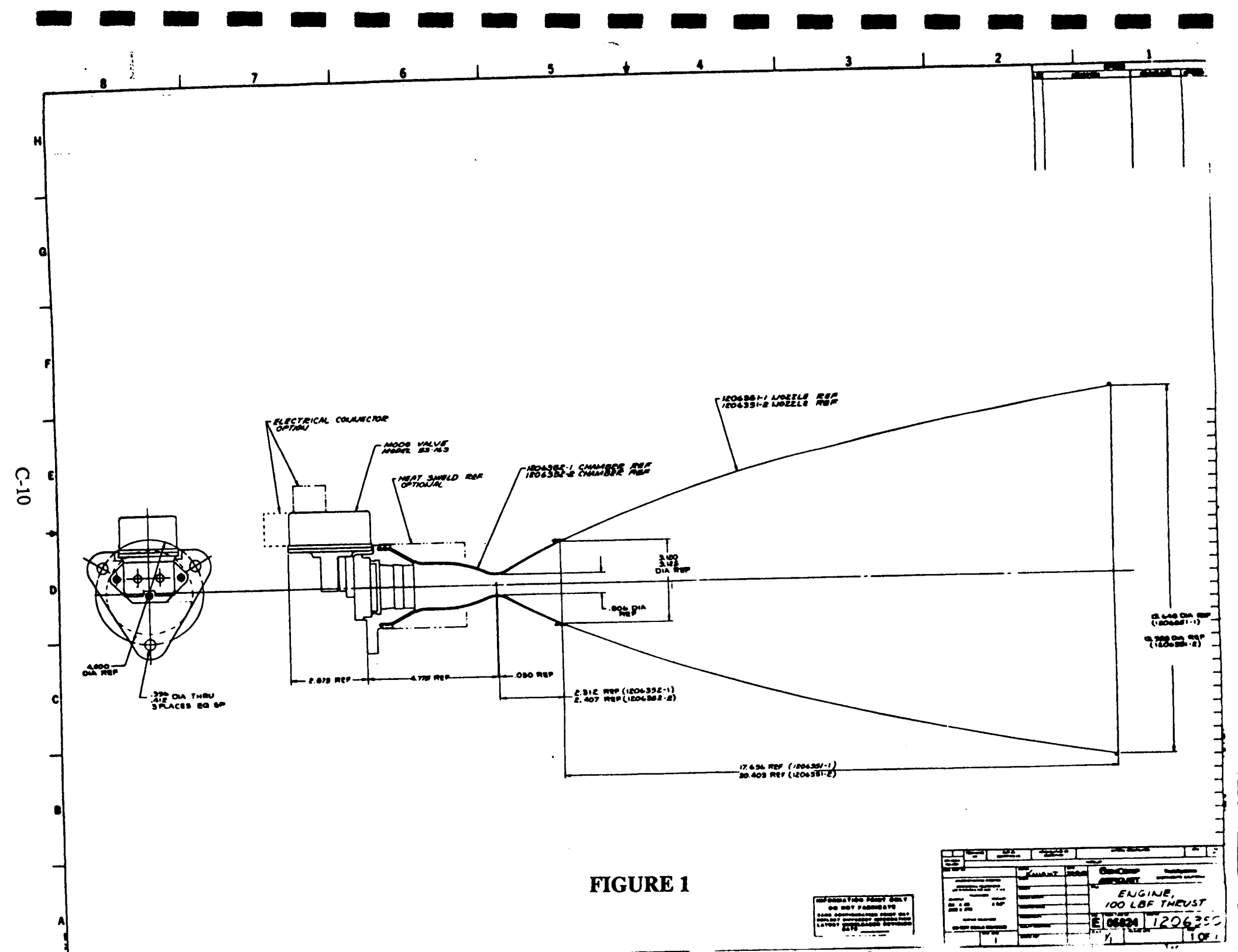
ELECTRICAL CONNECTOR OPTIONAL
MOOG VALVE MODEL 53-163
HEAT SHIELD REF OPTIONAL
1204361-1 CHAMBER REF
1204362-2 CHAMBER REF
1204361-1 NOZZLE REF
1204362-2 NOZZLE REF
3.120
3.118
DIA REF
.906 DIA REF
4.000 DIA REF
.396 DIA THRU
.312
3 PLACES EQ SP
2.878 REF
4.778 REF
.050 REF
2.512 REF (1204362-1)
2.407 REF (1204362-2)
17.656 REF (1204361-1)
20.409 REF (1204361-2)
ENGINE,
100 LBF THRUST
E
06624
1206250

FIGURE 1

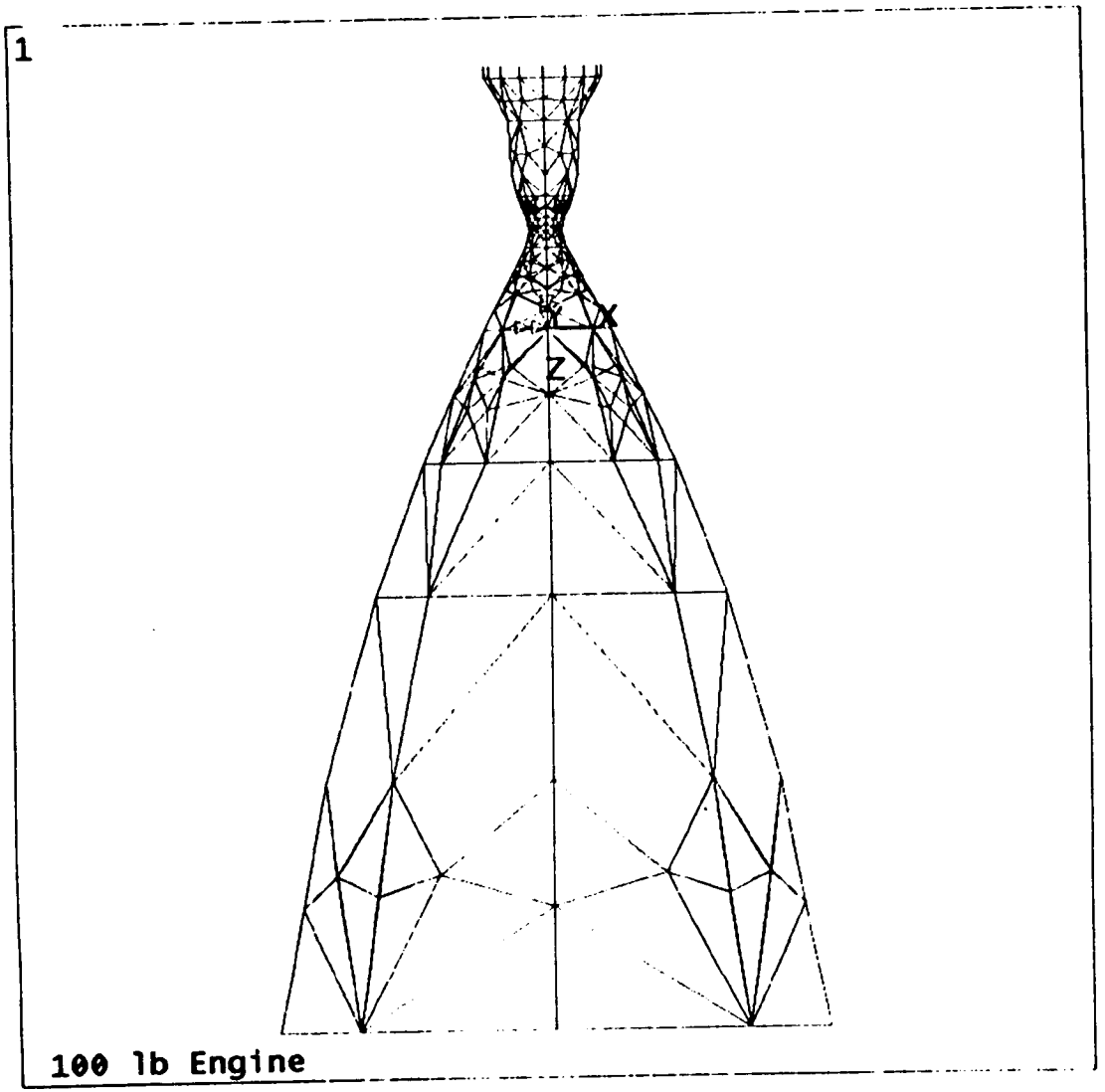

ANSYS 4.4
NOV 14 1990
18:15:10
PREP7 ELEMENTS
TYPE NUM
BC SYMBOLS

YV =1
DIST=13.288
ZF =5.48

FIGURE 2

ANALYSIS TYPE= 6
NUMBER OF ELEMENT TYPES= 3
545 ELEMENTS CURRENTLY SELECTED. MAX ELEMENT NUMBER = 545
293 NODES CURRENTLY SELECTED. MAX NODE NUMBER = 396

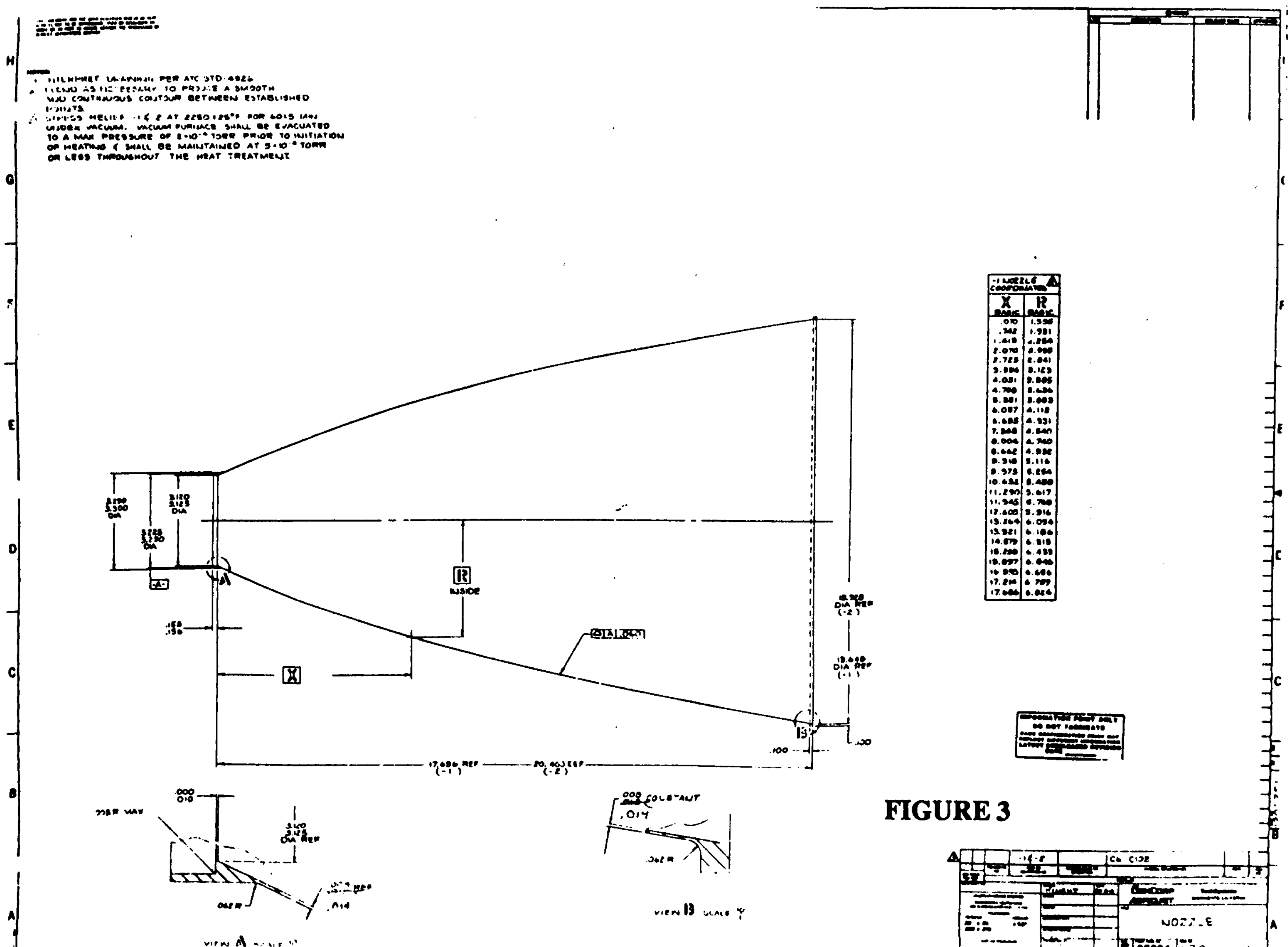

-1 NOZZLE COORDINATES

X BASIC	R BASIC
.010	1.536
.342	1.931
1.418	2.254
2.070	2.598
2.723	2.841
3.386	3.123
4.051	3.365
4.708	3.636
5.381	3.883
6.057	4.112
6.695	4.331
7.368	4.540
8.006	4.740
8.642	4.932
9.318	5.116
9.975	5.294
10.632	5.460
11.290	5.617
11.945	5.768
12.605	5.916
13.264	6.054
13.921	6.186
14.579	6.315
15.236	6.433
15.897	6.546
16.550	6.656
17.214	6.757
17.686	6.824

FIGURE 3

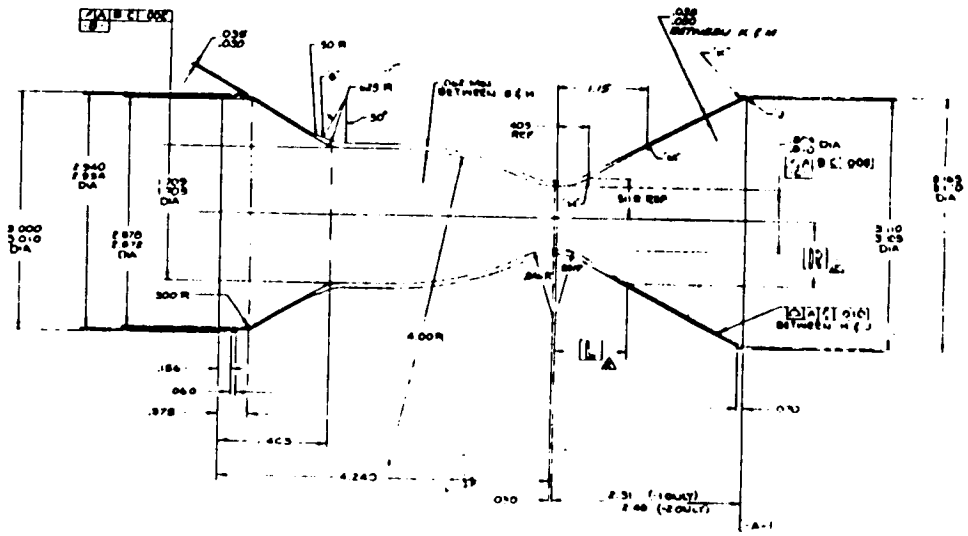

FIGURE 4

100 LB ENGINE
RANDOM VIBRATION ENVIRONMENT

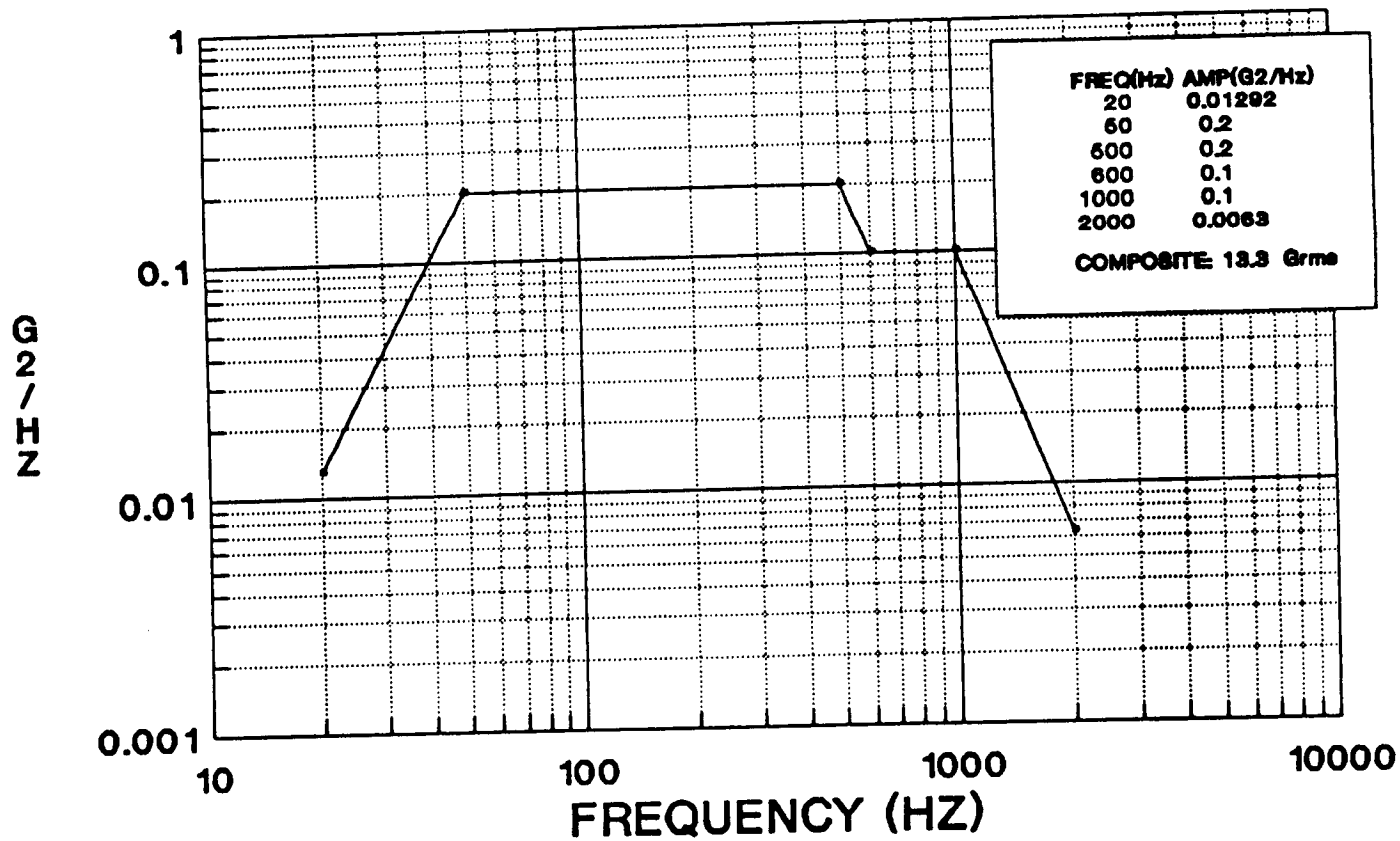

FIGURE 5

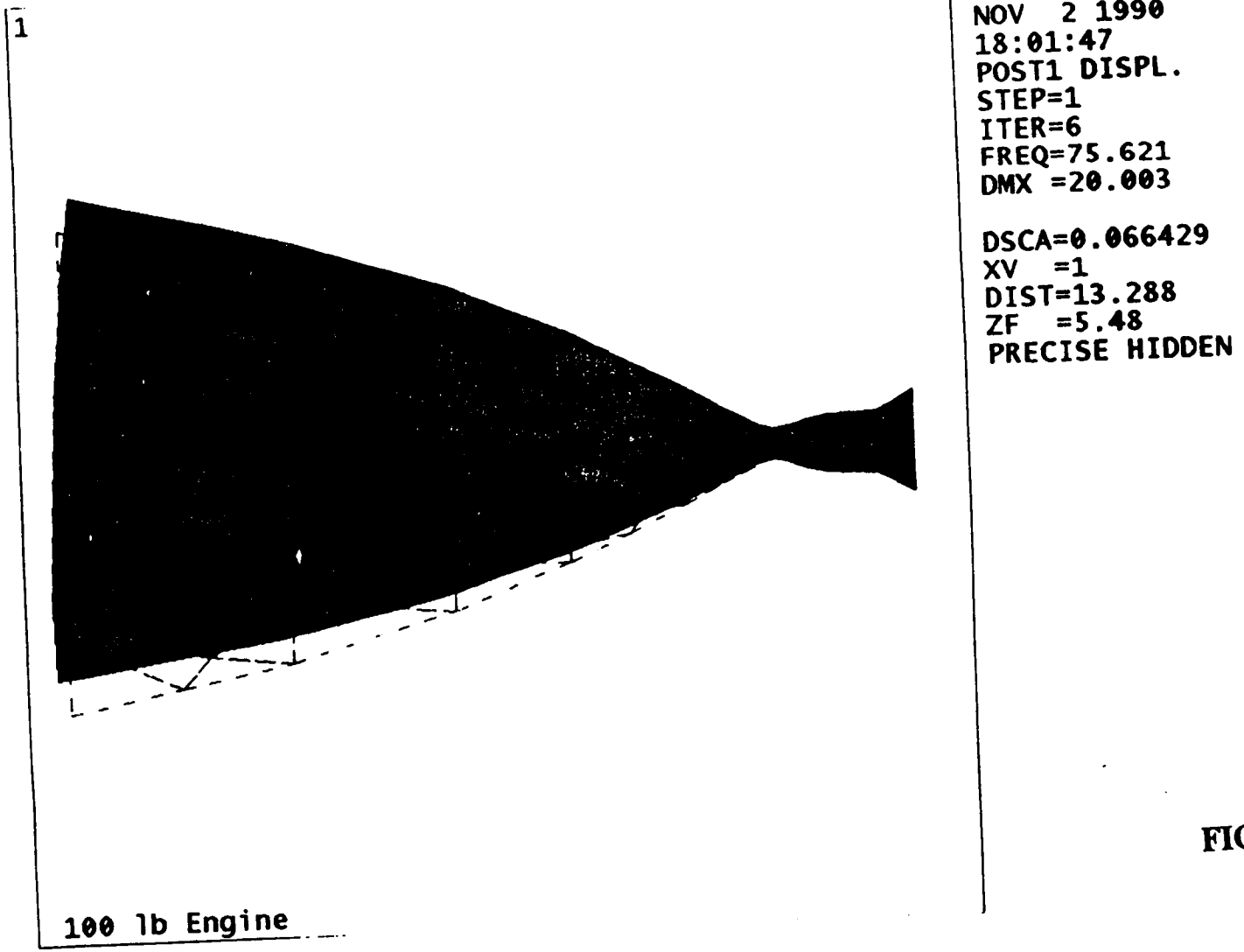
1
ANSYS 4.4
NOV 2 1990
18:01:47
POST1 DISPL.
STEP=1
ITER=6
FREQ=75.621
DMX =20.003
DSCA=0.066429
XV =1
DIST=13.288
ZF =5.48
PRECISE HIDDEN
100 lb Engine

FIGURE 6


1
ANSYS 4.4
NOV 6 1990
16:13:46
POST1 DISPL.
STEP=1
ITER=16
FREQ=908.482
DMX =23.251
DSCA=0.05715
YV =1
DIST=13.288
ZF =5.48
100 lb Engine

FIGURE 7

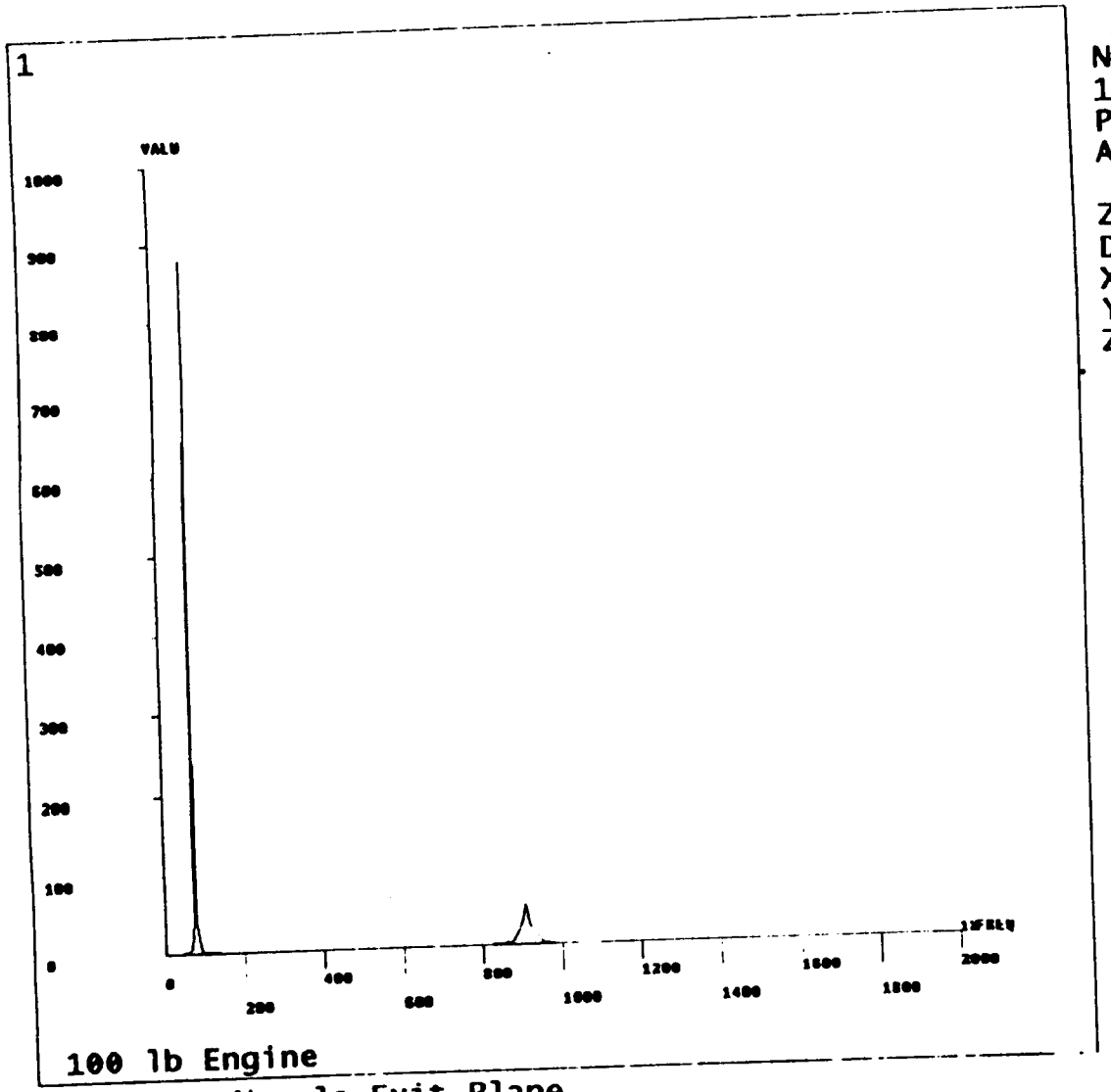

68 GRMS

FIGURE 8

***** PARTICIPATION FACTOR CALCULATION ***** X DIRECTION

MODE	FREQUENCY	PERIOD	PARTIC.FACTOR	RATIO	EFFECTIVE MASS	CUMULATIVE MASS FRACTION
1	21.5319	0.46443E-01	-0.94839E-08	0.000017	0.899449E-12	0.121697E-09
2	22.3726	0.44698E-01	0.69221E-05	0.000121	0.479169E-10	0.660481E-08
3	24.9149	0.40137E-01	-0.10063E-02	0.017662	0.101668E-05	0.137563E-03
4	24.9150	0.40136E-01	0.12523E-03	0.002194	0.156831E-07	0.139665E-03
5	33.1647	0.30162E-01	0.23801E-05	0.000042	0.566499E-11	0.139666E-03
6	75.6207	0.13224E-01	-0.43301E-01	0.756501	0.187499E-02	0.253830
7	75.6214	0.13224E-01	0.57088E-01	1.000000	0.325902E-02	0.694781
8	213.980	0.46733E-02	0.55858E-04	0.000976	0.312012E-08	0.694782
9	783.797	0.12892E-02	-0.20280E-02	0.035524	0.411270E-05	0.695338
10	789.832	0.13092E-02	0.20204E-02	0.045902	0.666681E-05	0.696267
11	770.082	0.12956E-02	-0.14727E-03	0.002580	0.216893E-07	0.696270
12	807.186	0.12390E-02	-0.80827E-04	0.000898	0.937998E-08	0.696270
13	897.241	0.11944E-02	0.93905E-04	0.001640	0.876196E-08	0.696271
14	910.170	0.10987E-02	-0.84491E-01	0.604186	0.110000E-02	0.857226
15	910.880	0.10977E-02	0.22172E-01	0.388383	0.491595E-03	0.923740
16	1039.19	0.96229E-03	0.16321E-03	0.002859	0.266388E-07	0.923744
17	1168.35	0.85591E-03	0.35847E-02	0.062498	0.127291E-04	0.925466
18	1182.88	0.84539E-03	-0.81421E-02	0.142625	0.662943E-04	0.934486
19	1208.91	0.82719E-03	0.77039E-02	0.134948	0.593498E-04	0.942466
20	1286.78	0.77713E-03	-0.16282E-02	0.028522	0.266117E-05	0.942824
21	1497.62	0.66769E-03	0.93617E-04	0.001640	0.870417E-08	0.942826
22	1483.47	0.67410E-03	-0.14701E-02	0.025761	0.216107E-05	0.943116
23	1484.34	0.67370E-03	0.21802E-02	0.037868	0.482348E-05	0.943744
24	1523.89	0.65621E-03	0.10182E-03	0.001783	0.103668E-07	0.943745
25	1640.99	0.60940E-03	-0.24109E-02	0.042231	0.581240E-05	0.944531
26	1644.83	0.60797E-03	0.31861E-02	0.055860	0.100243E-04	0.945888
27	1719.82	0.58149E-03	0.38093E-03	0.006676	0.152626E-06	0.945906
28	1760.64	0.56803E-03	0.10666E-03	0.002902	0.274612E-07	0.945912
29	1770.16	0.56492E-03	-0.14716E-03	0.002578	0.210641E-07	0.945915
30	1887.72	0.52974E-03	-0.88522E-04	0.001551	0.801424E-08	0.945916

TABLE I

APPENDIX A

```
/title, 100 lb Engine
et,1,63
mp,ex,1,13.1e6
mp,nuxy,1,0.3
mp,dens,1,8.259e-4
mp,ex,2,65.5e6
 p,nuxy,2,0.3
mp,dens,2,2.0e-3
mp,ex,3,27.6e6
mp,nuxy,3,0.3
mp,dens,3,7.25e-4
r,1,0.014
r,2,0.035
r,3,0.062
r,4,0.035
r,5,0.0375
CSYS,1
/com,                          ***/SHOW,4125,,1
K,1,6.824,,17.56
K,2,5.617,,11.29
K,3,4.331,,6.695
K,4,3.123,,3.396
K,5,1.595,,0.07
k,6,.511,,-2.012
k,7,.436,,-2.415
k,8,.5,,-2.765
k,9,.7,,-3.325
k,10,.82,,-3.885
k,11,.886,,-5.267
k,12,1.455,,-6.295
kgen,2,1,12,1,,90
A,1,2,14,13
 ,2,3,15,14
A,3,4,16,15
A,4,5,17,16
A,5,6,18,17
A,6,7,19,18
A,7,8,20,19
A,8,9,21,20
A,9,10,22,21
A,10,11,23,22
A,11,12,24,23
agen,4,1,11,1,,90
/com,                          ***/view,,1,1,1
/com,                          ***/pnum,area,1
/com,                          ***/pnum,line,1
/com,                          ***/pnum,kpoi,1
MAT,1   $REAL,1
ELSIZE,2,,1
AMESH,4,37,11
ELSIZE,4,,1
AMESH,3,36,11
ELSIZE,5,,1
AMESH,2,35,11
ELSIZE,6,,1
AMESH,1,34,11
MAT,2   $REAL,2
ELSIZE,.7,,1
AMESH,5,38,11
MAT,2   $REAL,3
ELSIZE,.3,,1
AMESH,6,39,11
AMESH,7,40,11
```

```
AMESH,8,41,11
ELSIZE,.7,,1
AMESH,9,42,11
ELSIZE,1,,1
AMESH,10,43,11
MAT,2     $REAL,4
 LSIZE,.6,,1
AMESH,11,44,11
nummrg,node
/com,                *** Dummy beams at injector forward joint
ET,2,4
MP,EX,4,30E6
MP,NUXY,4,.3
R,6,0.01,0.00032,0.00032,.25,.25
KNODE,,325
KNODE,,328
KNODE,,329
KNODE,,330
KGEN,2,97,100,1,0,0,--.305
L,97,101
L,98,102
L,99,103
L,100,104
LGEN,4,137,140,1,,90
TYPE,2   $MAT,2   $REAL,6
LMESH,137,152
NUMMRG,NODE
et,3,21
r,7,1e6
type,3
real,7
n,13
  ,13
d,13,uy,,,,,uz,rotx,roty,rotz
m,13,ux
cpsize,17
cp,1,ux,13,366,368,370,372,374,376,378,380
cp,1,ux,382,384,386,388,390,392,394,396
cp,2,uy,13,366,368,370,372,374,376,378,380
cp,2,uy,382,384,386,388,390,392,394,396
cp,3,uz,13,366,368,370,372,374,376,378,380
cp,3,uz,382,384,386,388,390,392,394,396
cp,4,rotx,13,366,368,370,372,374,376,378,380
cp,4,rotx,382,384,386,388,390,392,394,396
cp,5,roty,13,366,368,370,372,374,376,378,380
cp,5,roty,382,384,386,388,390,392,394,396
cp,6,rotz,13,366,368,370,372,374,376,378,380
cp,6,rotz,382,384,386,388,390,392,394,396
```

APPENDIX B

100# Environment per JPL
Fax sent 30 Aug 90

7. Engine Thermal Environment: Instrumentation shall be incorporated and termperatures monitored to allow determination of heat conduction and radiation from the engine to the critical spacecraft gimbal and mounting surfaces.

C. Environmental Testing

1. Propellant and Engine temperature: The REA shall demonstrate satisfactory and non-detrimental operation with a temperature range of 0°C to 55°C, and a difference in oxidizer and fuel temperature of ±15°C.

2. Sinusoidal Vibration: The following levels and frequencies shall be used to perform sine vibration on each REA:

Preliminary Requirements

Frequency, Hz	Amplitude
5-25	1.27 cm D.A. displacement
25-100	15.0g peak
100-200	5.0g peak

sweep rate = 2 octaves/minute up and down each of 3 axes.

D.A. = Double Amplitude

D. Random Vibration: Each REA shall be subjected to the following acceleration power spectral densities and overall RMS levels applied separately to each of the three axes of the REA for a duration of 3 minutes per axis:

Frequency, Hz	Accel Spectral Level
20	0.01292 g^2/Hz.
20-50	+9 dB/octave +9 dB/oct
50-500	0.2 g^2/Hz
	0.2 g^2/Hz

500-600	-9 dB/octave
600-1000	0.1 g^2/Hz
1000-2000	-12 dB/octave
2000	0.0063
overall	13.4 g(rms)

1. Acoustic Test:

The overall level is 149 dB reverberant random-incidence acoustic field specified in 1/3 octave bands. The design acoustic noise exposure time is 3 minutes. See Table 1.

APPENDIX C

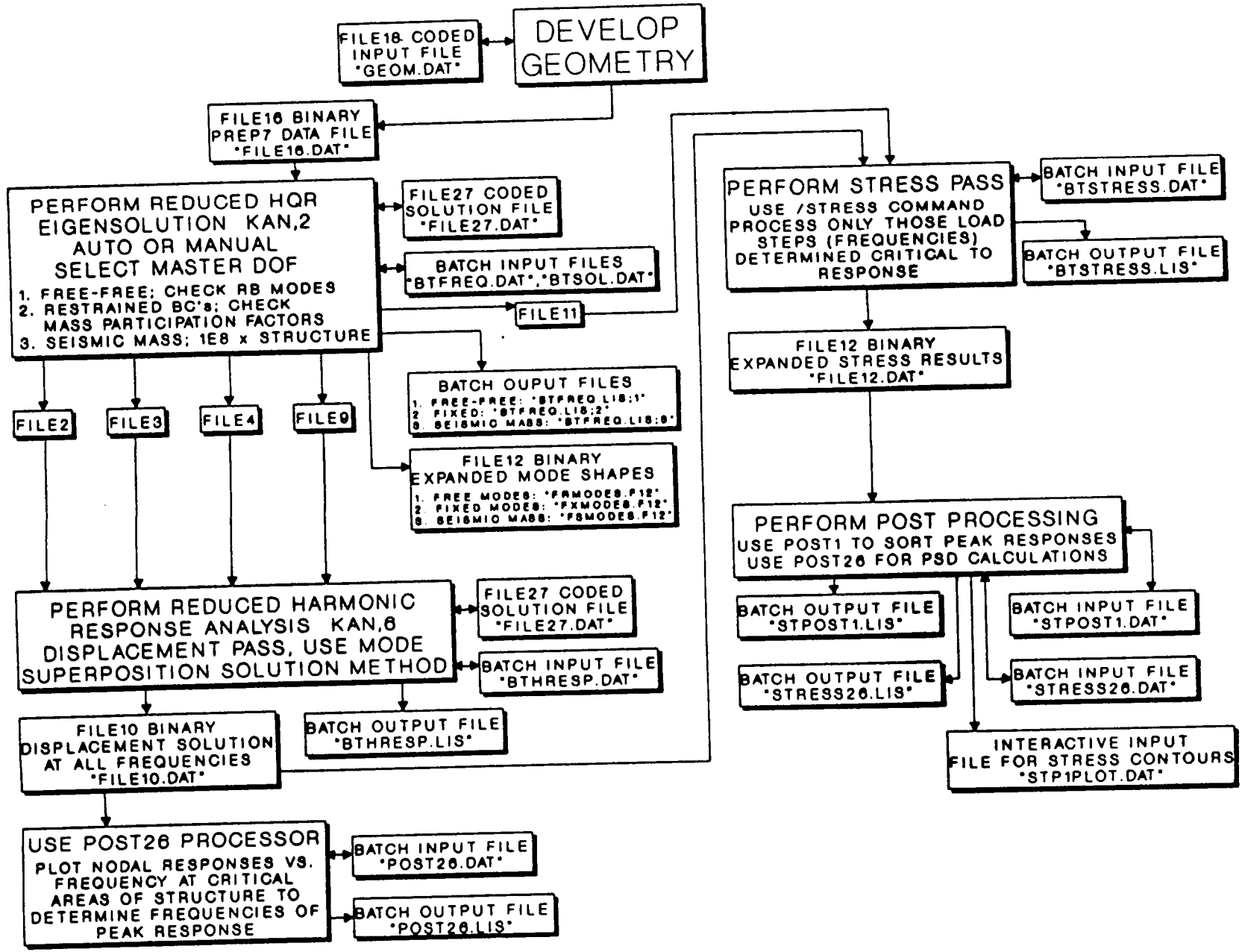
DEVELOP GEOMETRY
FILE18 CODED INPUT FILE "GEOM.DAT"
FILE16 BINARY PREP7 DATA FILE "FILE16.DAT"
PERFORM REDUCED HQR EIGENSOLUTION KAN,2 AUTO OR MANUAL SELECT MASTER DOF
1. FREE-FREE; CHECK RB MODES
2. RESTRAINED BC'S; CHECK MASS PARTICIPATION FACTORS
3. SEISMIC MASS; 1E8 x STRUCTURE
FILE27 CODED SOLUTION FILE "FILE27.DAT"
BATCH INPUT FILES "BTFREQ.DAT","BTSOL.DAT"
FILE11
BATCH OUPUT FILES
1. FREE-FREE: "BTFREQ.LIS;1"
2. FIXED: "BTFREQ.LIS;2"
3. SEISMIC MASS: "BTFREQ.LIS;3"
FILE12 BINARY EXPANDED MODE SHAPES
1. FREE MODES: "FRMODES.F12"
2. FIXED MODES: "FXMODES.F12"
3. SEISMIC MASS: "FSMODES.F12"
FILE2
FILE3
FILE4
FILE9
PERFORM REDUCED HARMONIC RESPONSE ANALYSIS KAN,6 DISPLACEMENT PASS, USE MODE SUPERPOSITION SOLUTION METHOD
FILE27 CODED SOLUTION FILE "FILE27.DAT"
BATCH INPUT FILE "BTHRESP.DAT"
FILE10 BINARY DISPLACEMENT SOLUTION AT ALL FREQUENCIES "FILE10.DAT"
BATCH OUTPUT FILE "BTHRESP.LIS"
USE POST26 PROCESSOR
PLOT NODAL RESPONSES VS. FREQUENCY AT CRITICAL AREAS OF STRUCTURE TO DETERMINE FREQUENCIES OF PEAK RESPONSE
BATCH INPUT FILE "POST26.DAT"
BATCH OUTPUT FILE "POST26.LIS"
PERFORM STRESS PASS
USE /STRESS COMMAND PROCESS ONLY THOSE LOAD STEPS (FREQUENCIES) DETERMINED CRITICAL TO RESPONSE
BATCH INPUT FILE "BTSTRESS.DAT"
BATCH OUTPUT FILE "BTSTRESS.LIS"
FILE12 BINARY EXPANDED STRESS RESULTS "FILE12.DAT"
PERFORM POST PROCESSING
USE POST1 TO SORT PEAK RESPONSES
USE POST26 FOR PSD CALCULATIONS
BATCH OUTPUT FILE "STPOST1.LIS"
BATCH INPUT FILE "STPOST1.DAT"
BATCH OUTPUT FILE "STRESS26.LIS"
BATCH INPUT FILE "STRESS26.DAT"
INTERACTIVE INPUT FILE FOR STRESS CONTOURS "STP1PLOT.DAT"

```
Directory DISK$1:[E24595.REA100.TESTE]

1102.F18;1                62    BTFREQ.DAT;1               2
BTFREQ.LIS;3             543    BTFREQ.LIS;2            1297
BTFREQ.LIS;1            1294    BTHRESP.DAT;1              4
BTHRESP.LIS;1           4494    BTSOL.DAT;1                1
BTSTRESS.DAT;1             1    BTSTRESS.LIS;2            42
FILE02.DAT;1            8097    FILE03.DAT;1            8097
FILE04.DAT;1            1278    FILE09.DAT;1             959
FILE10.DAT;1            3562    FILE11.DAT;1            6551
FILE12.DAT;1          179154    FILE16.DAT;1             511
FILE16.OLD;1             496    FILE18.DAT;2              19
FILE18.DAT;1              17    FILE19.DAT;2              48
FILE19.DAT;1              65    FILE23.DAT;1              10
FILE27.DAT;1              19    FILESTAT.DAT;1             1
FREIGEN.LIS;1              9    FRMODES.F12;1            863
FSMODES.F12;1           1773    FXEIGEN.LIS;1            114
FXMODES.F12;1            863    GEOM
GEOMSM.DAT;2               3    POST26.DAT;1               1
POST26.LIS;1             123    PSDX.DAT;7                 1
STP1PLOT.DAT;1             2    STPOST1.DAT;7              2
STPOST1.LIS;4            515    STPOST1.LIS;3           1792
STPOST1.LIS;1           1339    STRESS26.DAT;2             2
STRESS26.LIS;1           102

Total of 43 files, 224136 blocks.
```

APPENDIX D

GENCORP
AEROJET
TechSystems

REPORT NO

PAGE OF

SUBJECT

DATE

WORK ORDER

BY | CHK BY | DATE

INCREASED THROAT STIFFNESS CALCULATIONS

$$K = \frac{8EI}{l^3}$$

$$f_n = \frac{1}{2\pi}\sqrt{\frac{K}{m}}$$

$f_n^2 \approx K$, increase f_n by 3 (75 Hz to 225 Hz)

K must increase by 9, ∴ increase I by 9

$$I = \frac{\pi}{64}(D_o^4 - D_i^4)$$

Assume, $D_o = 1.8$

$D_i = 1.6$

$I = 0.1936\ in^4$

CHECK

$$K = \frac{8EI}{l^3}$$

$E = 65.5 \cdot 10^6$

$l = 17.656 + 2.31 = 19.966$ ins

$K = 12.745\ \frac{lb}{in}$

$$f_n = \frac{1}{2\pi}\sqrt{\frac{K}{m}}$$

$m = \frac{2.71\ lbs}{386\ \frac{in}{sec^2}}$

$= 215$ Hz ✓

GENCORP
AEROJET

Propulsion Division

Memo

2 April 1992
WAH:gg:5242:4831

TO: L. Schoenman/S.D. Rosenberg

FROM: W. A. Holzmann

SUBJECT: Structural Dynamics Design Study of 100 lbF Reaction Engine

COPIES TO: J.H. Beuttler, D.M. Jassowski, G.E. Nelson, N.R. Shimp, 5242 File

REFERENCE: (a) IOM 5242:4560, "100 lbF Thrust Engine Structural Dynamics Analysis", by J.H. Beuttler, dtd 21 November 1990

ENCLOSURE: (1) Structural Dynamics Design study of 100 lbF Reaction Engine

The results presented in this memo correspond to the design study recommendations made in Reference (a) for the 100 lbF Reaction Engine. Four alternate design configurations were investigated. Parameter iterations were made for each design concept until adequate stress margins were achieved.

W. A. Holzmann
Metallic Structures Section
Engineering Analysis Department

APPROVED BY:

E. Lueders, Manager
Metallic Structures Section
Engineering Analysis Department

ENCLOSURE (1)

STRUCTURAL DYNAMICS DESIGN STUDY OF 100 lbF REACTION ENGINE

PREPARED BY:
W.A. Holzmann
Structural Dynamics
Metallic Structures Department

APPROVED BY:
E. Lueders, Manager
Metallic Structures Department
Engineering Analysis

REVIEWED BY:
J.H. Beuttler
Structural Dynamics
Metallic Structures Department
Engineering Analysis

INTRODUCTION

The maximum predicted stresses in the throat region due to sinusoidal and random base excitations exceeded allowables for the baseline design, area ratio 286:1, refer to Reference (a). Consequently, the Research & Technology group requested that further studies be made to determine viable design alternatives. Prior to any analysis, it was agreed upon to investigate the following four cases:

(1) Increase throat wall thickness until the maximum principle equivalent stress in the throat region is less than the yield stress of annealed rhenium (F_{ty} = 135 ksi).

(2) Decrease the density of the nozzle material until the maximum equivalent stress in the throat region is less than the yield stress of annealed rhenium. Maintain nominal wall thickness of .062" at the throat.

(3) Increase the nominal nozzle wall thickness from 10 to 16 mils, and determine the required throat wall thickness so that the maximum equivalent stress is less than the yield stress of rhenium in the work hardened condition (F_{ty} = 310 ksi).

(4) Use the existing baseline design with the modified nozzle configuration and reduce the levels of the input PSD until the maximum equivalent stress is less than the yield stress of annealed rhenium.

ANALYSIS

The ANSYS finite element model described in Reference (a) was used for this analysis. Modifications were made to the nozzle geometry as per specifications provided by the Thermodynamic Analysis Section. Changes made included decreasing the wall thickness from 14 to 10 mils and reducing the overall length from the throat to the aft end from 19.98 to 15.40", i.e., reduce the area ratio from 286:1 to 170:1.

For the baseline design (area ratio 286:1), the first mode exhibiting a large system response occurred at 75 Hz and was described as a cantilever motion of the nozzle about the throat. This mode fell within the 50-100 Hz frequency range specified for the 15 G sinusoidal base input. The motivation for making the nozzle design changes described above was to lower its mass, thereby increasing this fundamental frequency. Naturally, for this application, this is an improvement only if the frequency is raised above 100 Hz.

The current design of the 100 lbF REA includes a columbium nozzle and a rhenium chamber. The allowable stresses used for these two materials are summarized below:

		Allowable Yield Stress	Allowable Ultimate Stress
rhenium			
	annealed	F_{ty} = 135 ksi	F_{tu} = 168 ksi
	reduced 30.7%	F_{ty} = 310 ksi	F_{tu} = 322 ksi
columbium		F_{ty} = 34 ksi	F_{tu} = 50 ksi

The finite element model of the engine was composed primarily of elastic quadrilateral shell elements. An area plot illustrating the discrete regions used to represent the varying wall thicknesses is shown in Figure 1. The following list is a breakdown of the thicknesses used in the baseline design:

Chamber, Conical Section	.035"
Chamber	.062"
Throat Region	.062"
Nozzle Top	.035"
Nozzle	.014"

The analytical procedure used to determine the maximum equivalent stresses due to the random vibration environment included running a normal modes analysis and then attaching a seismic mass to the system in order to generate transfer functions. Once the transfer functions were available, these were post processed with the input PSD to obtain displacement PSDs at selected locations of the engine. Referring to Figures 2 and 3, the modes exhibiting the largest response occur at 121 Hz, 807 Hz and 1195 Hz. A stress pass was then made with the solution expanded about these frequencies. Lastly, equivalent stress PSDs for selected elements were determined. Figure 4 shows an equivalent stress PSD for an element located at the throat. The square root of the area under this curve corresponds to the rms equivalent stress. The breakpoints and a plot of the random vibration environment as specified by the customer, NASA/Lewis are shown in Figure 5.

The random analysis was limited to a single coordinate direction in the lateral plane of the engine. This decision was made since the finite element model is axisymmetric and it was judged that the most critical load direction was in the lateral plane perpendicular to the axial axis of the engine.

RESULTS

Case I:

The initial iteration for this case involved updating the nozzle design while keeping the throat thickness at the nominal .062". This change increased the first high response frequency from 75 to 121 Hz, refer to Figure 6. The maximum equivalent stresses predicted in the throat and nozzle regions were 245 and 46 kpsi, respectively. Comparing these stresses with the allowables listed previously indicates negative margins in both areas. Three additional iterations were made on the throat and nozzle top wall thickness. A plot showing the maximum equivalent stress versus throat thickness is shown in Figure 7. Based on these results, the throat wall thickness is required to be approximately .13", which is twice the nominal value.

A summary of the stress margins and the corresponding wall thickness are listed in Tables I and II, respectively. Note that the nozzle top wall thickness was increased from .035 to .073". This was necessary because the load path shifted to this region after the throat thickness was increased.

Case II

In order to obtain a stress margin while holding the throat thickness at the baseline value, .062 in., the density of the nozzle material had to be reduced from 0.339 to 0.20 lb/in^3 .

Case III

For this case, it was assumed the rhenium in the throat could be work hardened and the nozzle wall thickness was increased from 10 to 16 mils. Without modifications to the throat or nozzle top thickness, the predicted maximum equivalent stress in the throat was 329 kpsi. This value exceeds both the yield and ultimate stress of rhenium in the work hardened condition and is unacceptable. In addition, the added mass of the nozzle reduced the first high response frequency to approximately 102 Hz. To compensate for this, the throat wall thickness must be increased to .08". Realizing that the load path would again transfer to the nozzle top, its thickness was scaled by a proportional amount.

Case IV

The requirement for this option was to retain the baseline thickness and lower the input PSD levels enough to meet stress allowables. Reducing the random input PSD shown in Figure 5 by 6 dB produced acceptable stress levels.

CONCLUSIONS

The analyses showed that the baseline 100 lbf thrust liquid apogee engine with the modified nozzle,area ratio 170:1, did not meet design allowables. As a result, four different options were proposed for further investigation. The subsequent parametric studies completed indicate that each of these four options is viable from a structural dynamics standpoint.

Option 1. Increase the throat thickness from .062 to 0.13 in.

Option 2. In order to implement the second option, a lower density nozzle material, such as titanium, would have to be used in place of the columbium.

Option 3. If the CVD rhenium could be work hardened in-place, a throat thickness of .080" would be adequate.

Option 4. The fourth option can be applied if a practical form of vibration isolation is utilized to reduce the propulsion system induced random vibration environment by 6 dB.

The first fundamental frequency was shifted out of the bandwidth corresponding to the specified sinusoidal vibration levels when the modified nozzle concept was modelled. This is a result of the reduced mass of the nozzle in comparison to the original design.

RECOMMENDATIONS

Obtain experimental data on strength/fatigue properties of annealed and work hardened rhenium.

Negative stress margins in the nozzle, area ratio 170:1, were predicted for the first and third cases. The maximum equivalent stresses for the nozzle occur at the rhenium/columbium interface for both of these cases. If either of these options is considered, it is recommended that the nozzle wall thickness be increased at the joint and the analysis repeated.

Maximum Equivalent 3-Sigma Stresses (kpsi)						
	Throat	Stress Margin* yield	ult.	Nozzle	Stress Margin yield	ult.
Case I	125.	.08	.34	49.0	-.31	.02
Case II	120.	.13	.40	22.4	.52	1.23
Case III	245.	.27	.31	37.0	-.08	.35
Case IV	123.	.10	.37	23.0	.48	1.17

TABLE I

Throat and Nozzle Wall Thickness			
	Throat (in.)	Nozzle Top (in.)	Nozzle (in.)
Case I	.129	.073	.010
Case II	.062	.035	.010
Case III	.08	.045	.016
Case IV	.062	.035	.010

TABLE II

* Yield Stress Margin = (Yield Stress/Actual Stress) - 1.0
Ultimate Stress Margin = (Ultimate Stress/Actual Stress) - 1.0

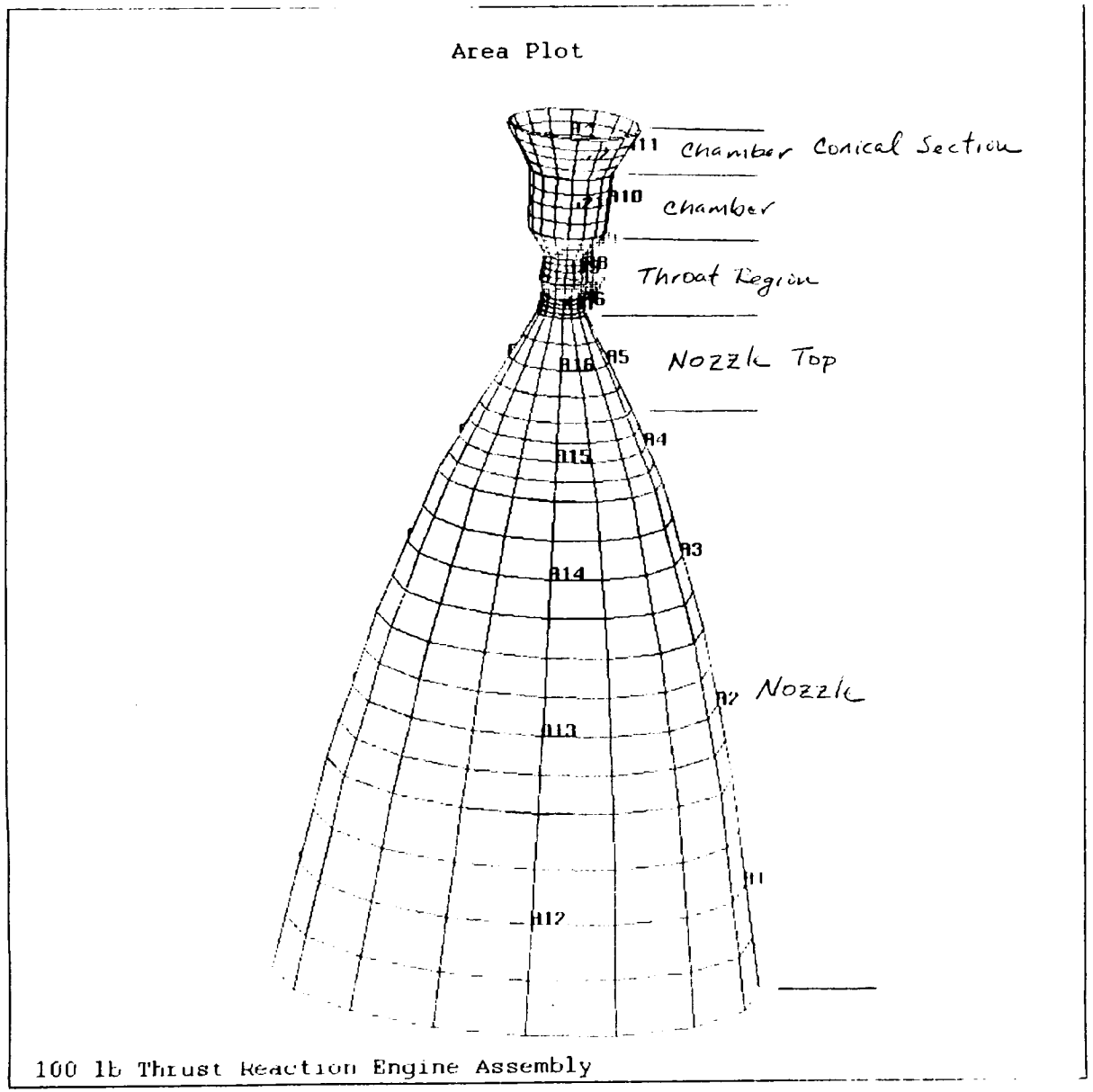
Area Plot
A11
Chamber Conical Section
A10
Chamber
Throat Region
A16
A5
Nozzle Top
A4
A15
A3
A14
A2
Nozzle
A13
A1
A12
100 lb Thrust Reaction Engine Assembly
ANSYS 4.4A1
MAR 12 1992
7:47:22
PREP7 AREAS
AREA NUM
XV =-0.725226
YV =0.64945
ZV =-0.228611
DIST=11.757
ZF =3.193
ANGZ=-105.66
SECTION

Figure 1

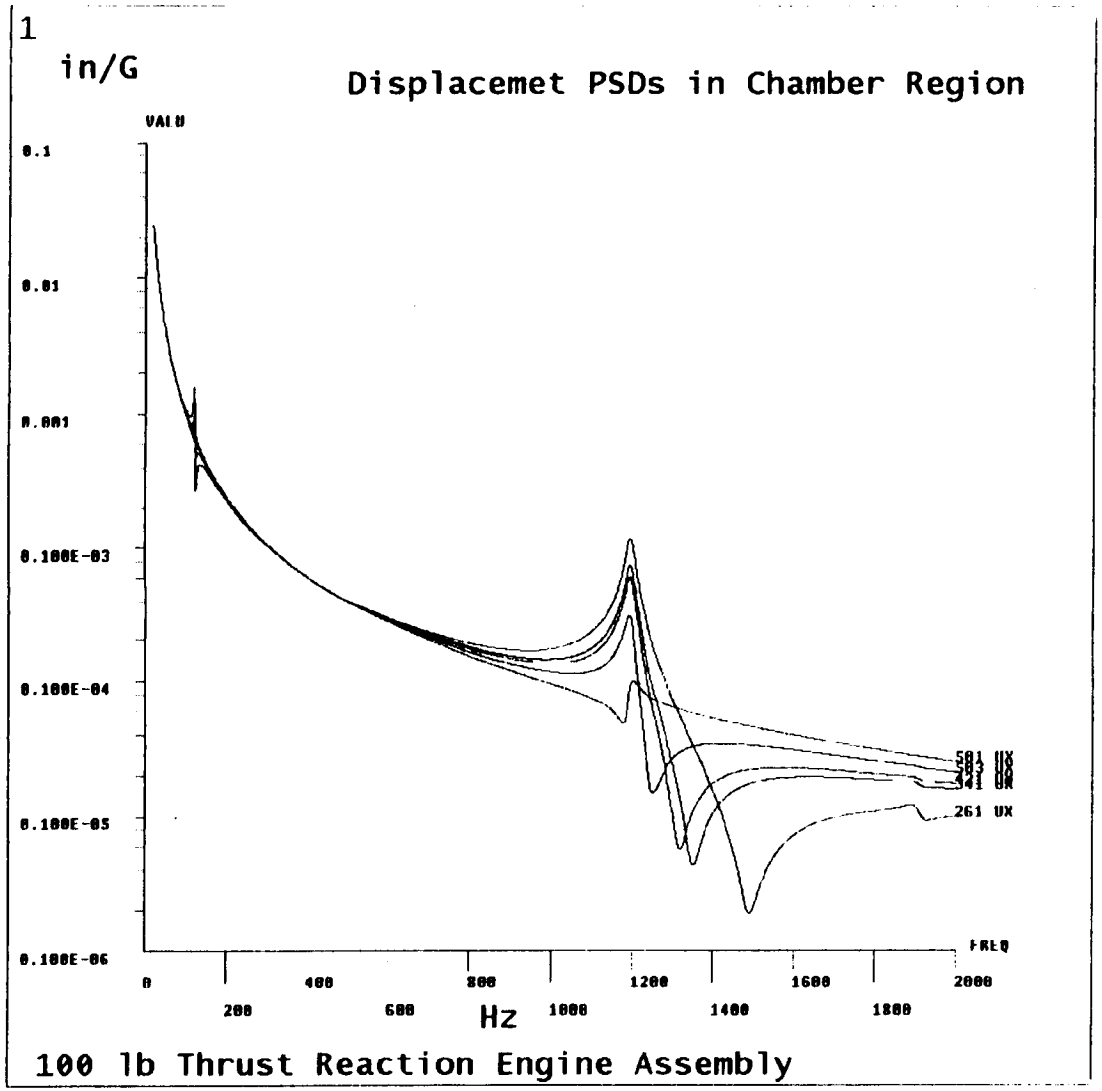
1
in/G
Displacemet PSDs in Chamber Region
VALU
0.1
0.01
0.001
0.100E-03
0.100E-04
0.100E-05
0.100E-06
501 UX
261 UX
FREQ
0
200
400
600
800
1000
1200
1400
1600
1800
2000
Hz
100 lb Thrust Reaction Engine Assembly
ANSYS 4.4A1
MAR 18 1992
10:24:46
POST26
AMPLITUDE
ZV =1
DIST=0.6666
XF =0.5
YF =0.5
ZF =0.5

Figure 2

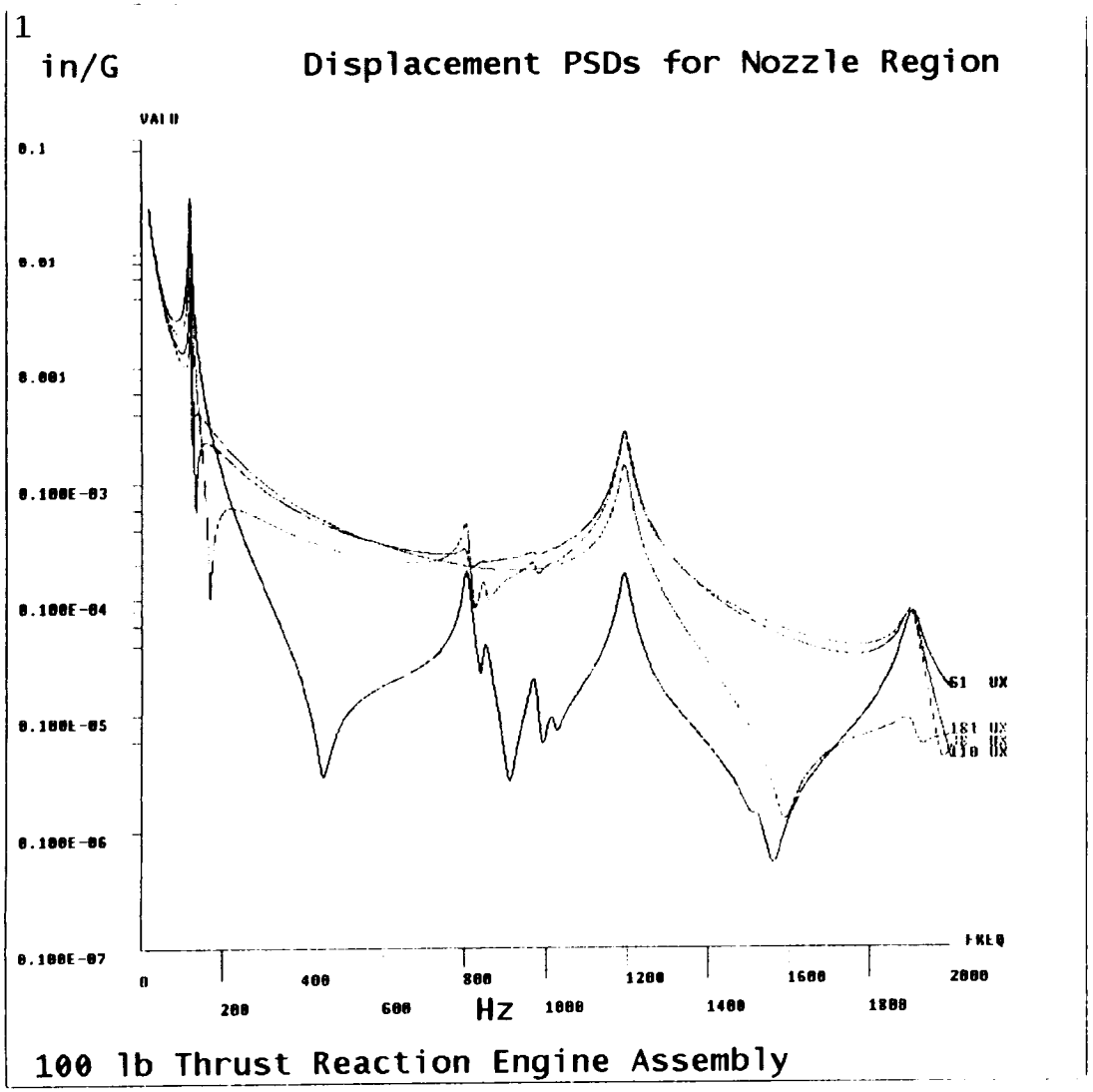
1
in/G
Displacement PSDs for Nozzle Region
VALUE
0.1
0.01
0.001
0.100E-03
0.100E-04
0.100E-05
0.100E-06
0.100E-07
0
200
400
600
800
1000
1200
1400
1600
1800
2000
Hz
FREQ
1 UX
181 UX
100 lb Thrust Reaction Engine Assembly
ANSYS 4.4A1
MAR 18 1992
10:58:35
POST26
AMPLITUDE
ZV =1
DIST=0.6666
XF =0.5
YF =0.5
ZF =0.5

Figure 3

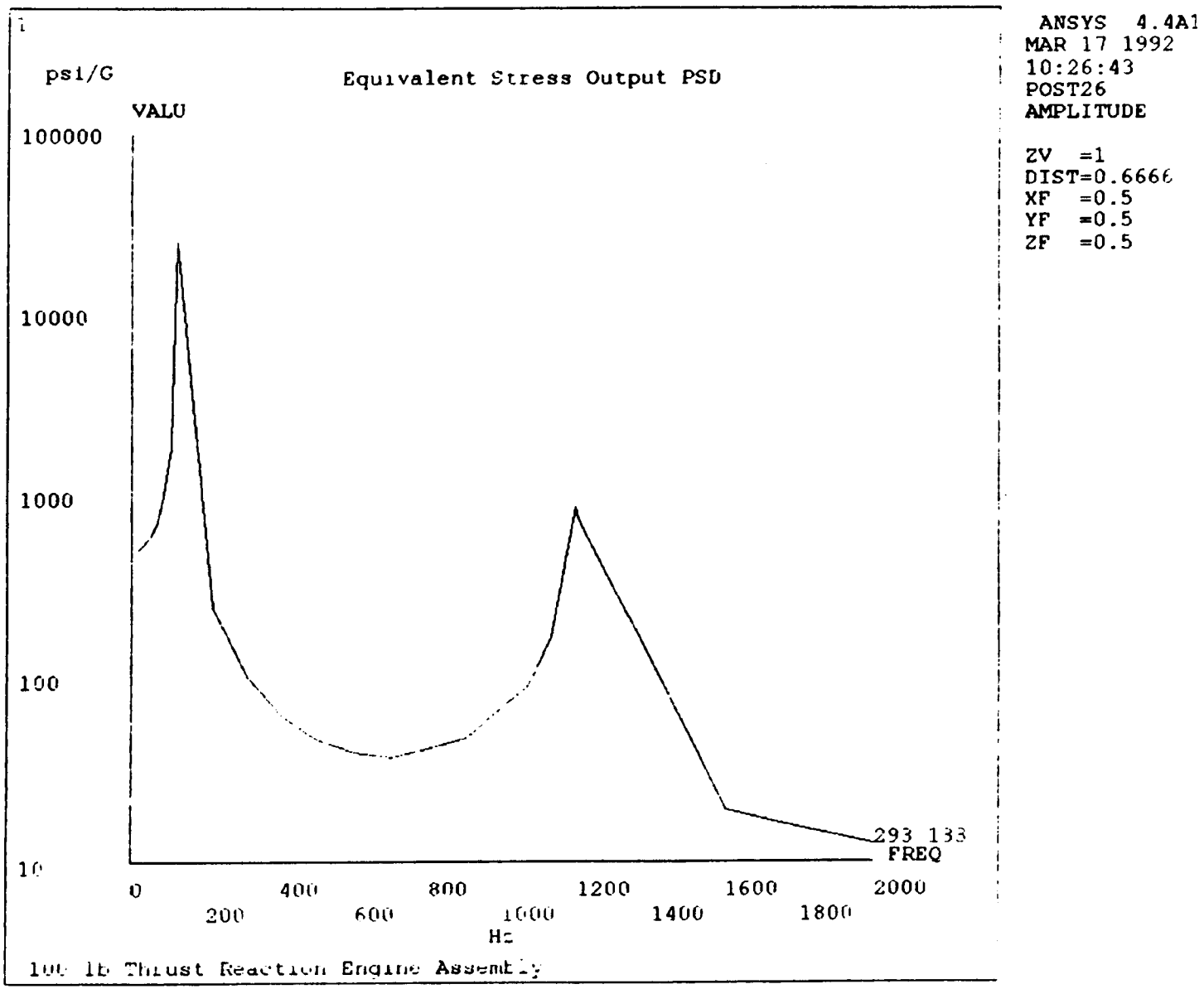
psi/G
Equivalent Stress Output PSD
VALU
100000
10000
1000
100
10
0
200
400
600
800
1000
1200
1400
1600
1800
2000
Hz
293.133
FREQ
ANSYS 4.4A1
MAR 17 1992
10:26:43
POST26
AMPLITUDE
ZV =1
DIST=0.6666
XF =0.5
YF =0.5
ZF =0.5

Figure 4

100 LB ENGINE
RANDOM VIBRATION ENVIRONMENT

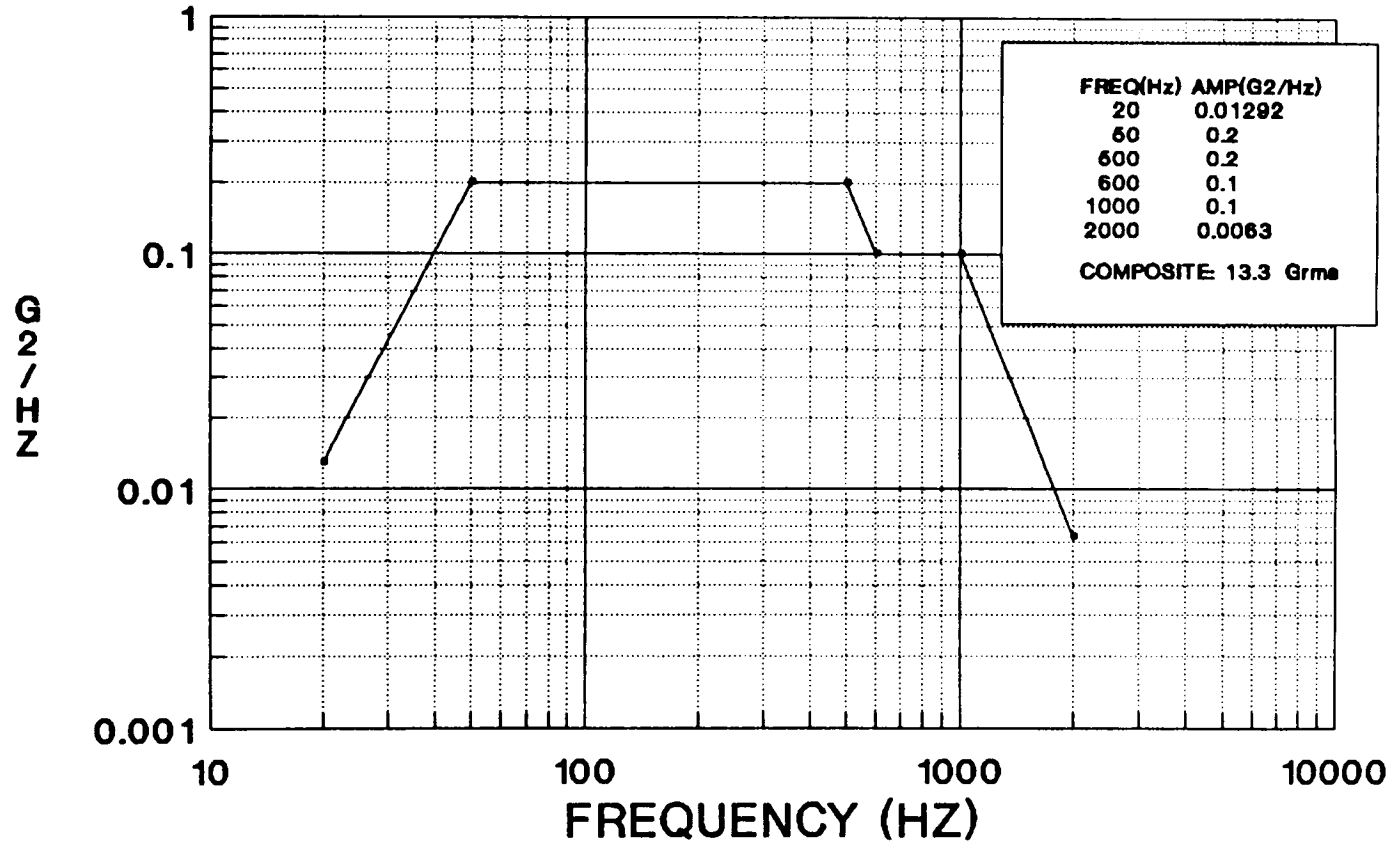

Figure 5

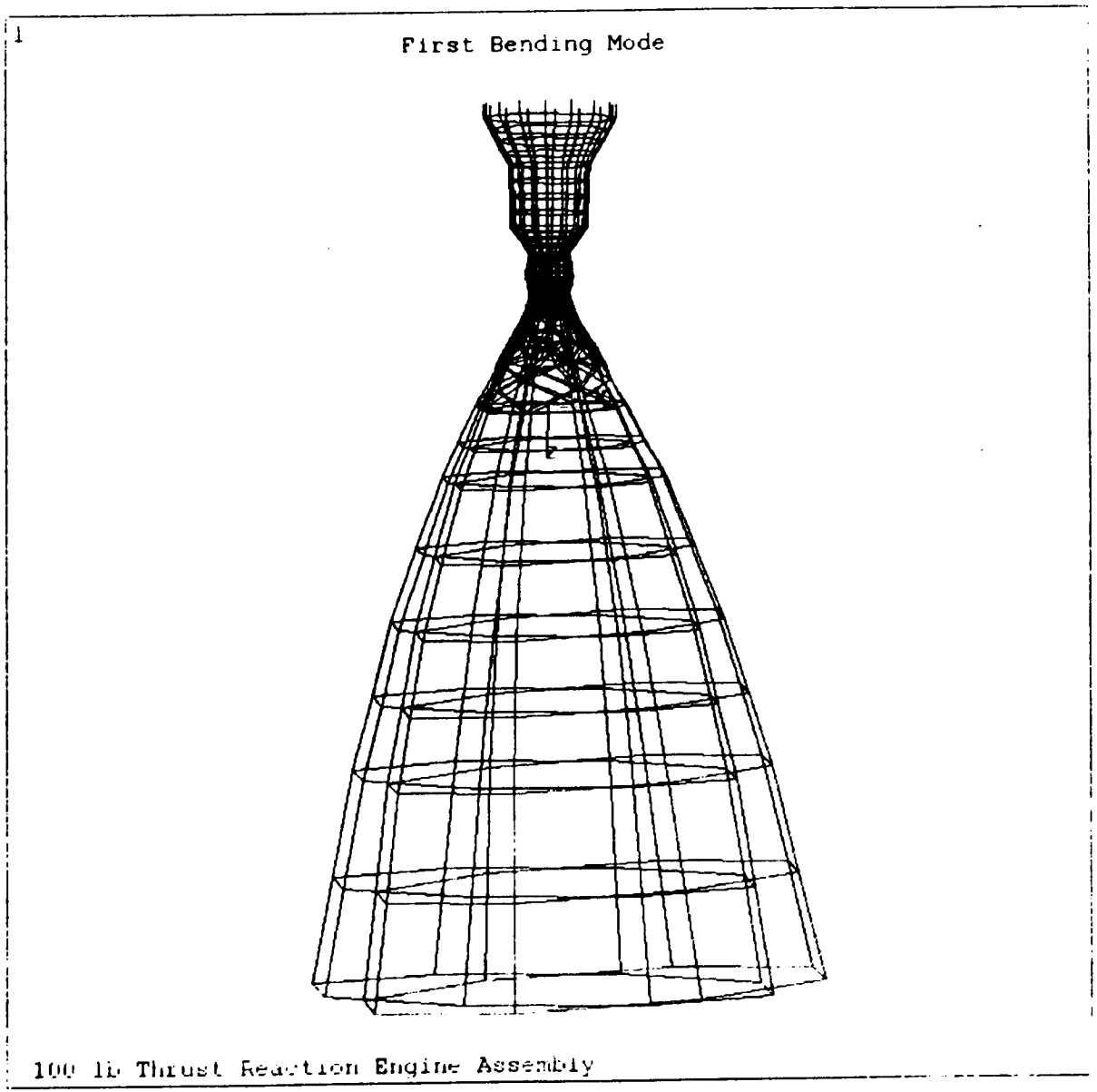
1
First Bending Mode
ANSYS 4.4A1
MAR 18 1992
9:22:11
POST1 DISPL.
STEP=1
ITER=6
FREQ=121.24
DMX =28.485
DSCA=0.041274
XV =-0.441963
YV =0.894184
ZV =-0.071436
*DIST=11.757
*ZF =3.192
ANGZ=-98.927
100 lb Thrust Reaction Engine Assembly

Figure 6

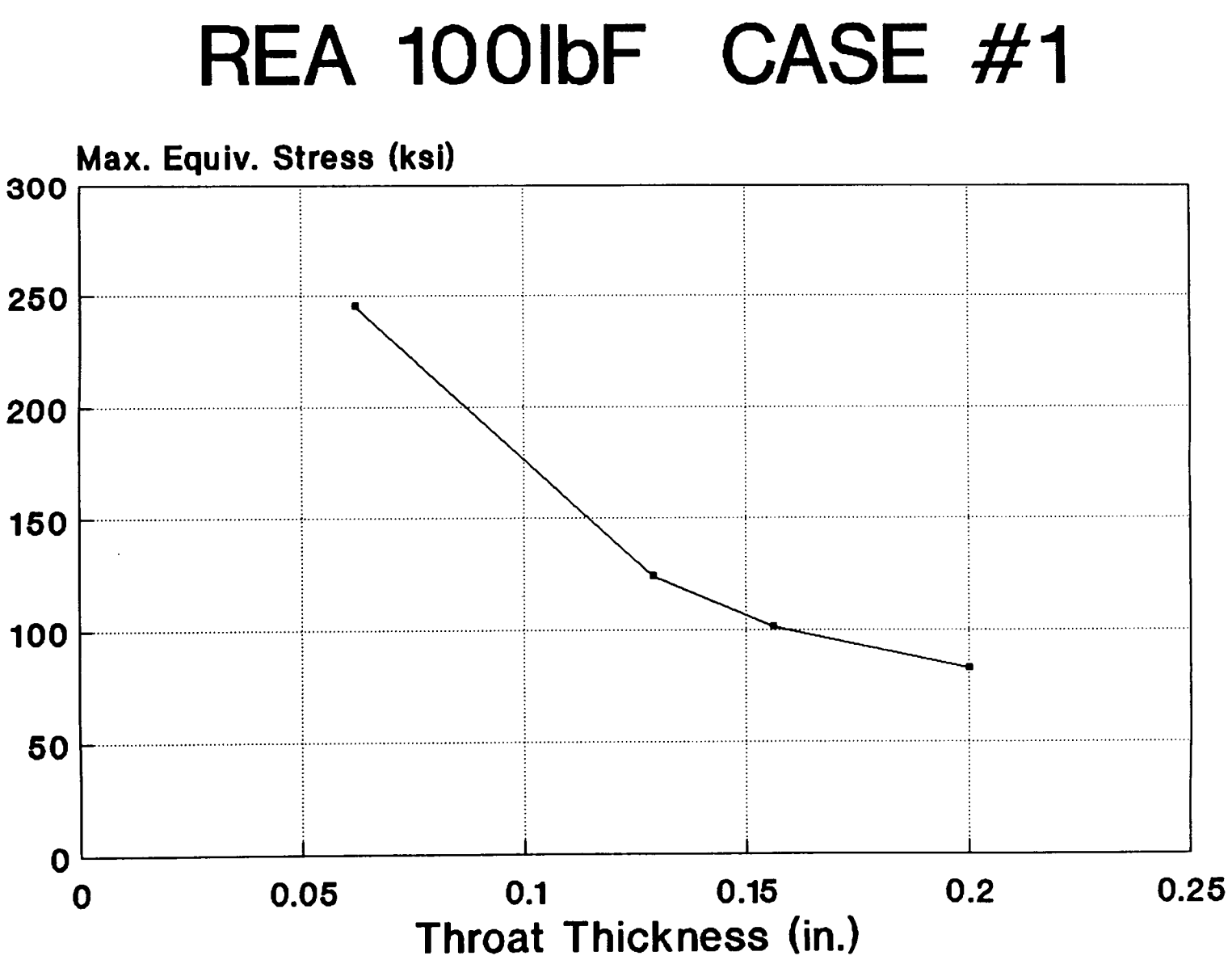
REA 100lbF CASE #1
Max. Equiv. Stress (ksi)
300
250
200
150
100
50
0
0
0.05
0.1
0.15
0.2
0.25
Throat Thickness (in.)

Figure 7

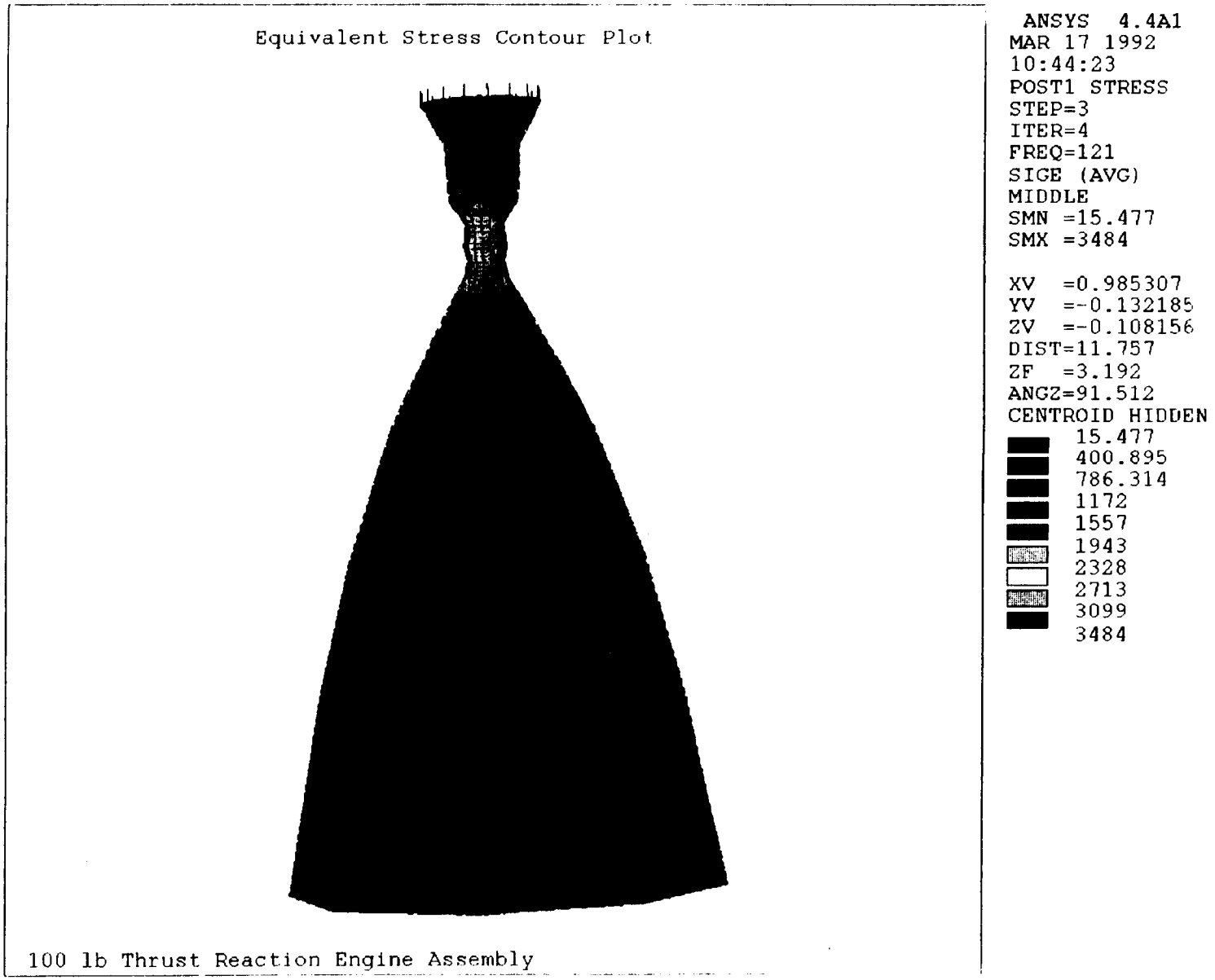
Equivalent Stress Contour Plot
ANSYS 4.4A1
MAR 17 1992
10:44:23
POST1 STRESS
STEP=3
ITER=4
FREQ=121
SIGE (AVG)
MIDDLE
SMN =15.477
SMX =3484
XV =0.985307
YV =-0.132185
ZV =-0.108156
DIST=11.757
ZF =3.192
ANGZ=91.512
CENTROID HIDDEN
15.477
400.895
786.314
1172
1557
1943
2328
2713
3099
3484
100 lb Thrust Reaction Engine Assembly

Figure 8

APPENDIX D

VALVE ACCEPTANCE DATA FROM MOOG

OMV valve
modified for vibration

INTERDEPARTMENTAL

memorandum

MOOG
MOOG INC EAST AURORA NEW YORK 14052

SPEM #66-91

S/N 001
RCD 7-8-91

DATE: June 28, 1991

FROM: D. Suarez

TO: B. Morrish

SUBJECT: **MOOG MODEL 53X179 (PART NUMBER B66637) PERFORMANCE DATA**

- Coil Resistance at at 70°F:

  Primary Coils: 31.7 Ω
  Secondary Coils: 29.8 Ω

$70°$ S.G. $_{OX} \cong 1.437$
$70°$ S.G. $_{FU} \cong 0.854$

- Insulation Resistance

  2.5 x 10^6 megohms

$$K_W = \frac{\dot{W}}{(S.G. * \Delta P)^{1/2}}$$

- Pressure Drop

  Oxidizer at .163 lb/sec H_2O: 11.0 psid
  Fuel at .127 lb/sec H_2O: 8.8 psid

$$K_{WO} = \frac{.163}{(11.0 * 11.0)^{1/2}} = 0.04915$$

$$K_{WF} = \frac{.127}{(1.0 * 8.6)^{1/2}} = 0.04281$$

- Pull-In Voltage at 260°F, 350 psig

  Primary: 18.0 vdc
  Secondary: 17.5 vdc

ΔP at 100 lbf
$\left(\frac{\dot{W}}{K_W}\right)^2 S_J$

.12 lb/sec fuel
.19 lb/sec ox

ox = 12.3 psi
fuel 8.3 psi

- Drop-Out Voltage at 20°F, 350 psig

  Primary: 2.6 vdc
  Secondary: 2.6 vdc

- Response, Pressurized at 350 psig
  41.7 V suppression diode

  Primary Coils
  Open, 22 vdc - 19.0 msec
  Close, 17.5 vdc - 4.2 msec

  Secondary Coils
  Open, 22 vdc - 19.5 msec
  Close, 17.5 vdc - 4.2 msec

- Response, Unpressurized
  41.7 V suppression diode

  Primary Coil
  Close, 17.5 vdc - 3.1 msec

  Secondary Coil
  Close, 17.5 vdc - 3.1 msec

- Valve Cleanliness

Micron Size	Fuel	Oxidizer
6 - 10	3	1
11 - 25	4	1
26 - 50	0	0
51- 100	0	0
> 100	0	0

- Internal Leakage

  50 psig Ox - 0.0 scc/hr
  Fuel - 0.0 scc/hr

  250 psig Ox - 0.0 scc/hr
  Fuel - 0.0 scc/hr

  450 psig Ox - 0.0 scc/hr
  Fuel - 0.0 scc/hr

- Valve subjected to random vibration of 24 grms.

- Internal Leakage

  50 psig Ox - 0.0 scc/hr
  Fuel - 0.0 scc/hr

  250 psig Ox - 0.0 scc/hr
  Fuel - 0.0 scc/hr

  450 psig Ox - 0.0 scc/hr
  Fuel - 0.0 scc/hr

cc: D. Ferguson

APPENDIX E

Ir-Re CHAMBER INSPECTION DATA

ULTRAMET
12173 Montague Street
Pacoima, Ca 91331
(818) 899-0236

INVOICE NO.: 016718

INVOICE DATE: 03/18/91

PAGE: 1

SOLD TO: AEROJET TECHSYSTEMS ACCOUNTS PAYABLE P.O. BOX 640 ORANGEVALE, CA 95662	SHIP TO: AEROJET TECHSYSTEMS BUILDING 2022 HWY 50 AND HAZEL AVENUE NIMBUS, CA 95670

SHIP VIA..: FED EXPRESS
SHIP DATE.: 03/18/91
DUE DATE..: 04/17/91
TERMS.....: 0-30-30

CUST. ID.....: AERO
P.O. NUMBER...: L823585H
P.O. DATE.....: 03/18/91
OUR ORDER NO..: 7574
SALESMAN.....: 0

PRODUCT I.D.	DESCRIPTION	ORDERED	SHIPPED	U/M	UNIT PRICE	AMOUNT	TX
	THRUST CHAMBER IRIDIUM LINED RHENIUM PER DWG #1206352-REV N/C **	1.00	1.00	EA	49000.00	49000.00	
	DELIVERY PERFORMANCE INCENTIVE	1.00	1.00	EA	15000.00	15000.00	

NET AMOUNT: 64,000.00
TAX: 0.00 *
TOTAL DUE: 64,000.00

** Fabricated per Patent # 4,917,968 and 3,982,148

Hardness Testing of Iridium Coating
Ref: Aerojet Tech. Systems, P.O. No. L823585

End Rings per Dwg. No. 1206352-2 & -3

Vickers Microhardness, with 300 gram load for 5 seconds.

End Ring/Sect.	Measured Hardness	Mean Hardness	S/N
* -2, sect. 1	553.6, 557.1, 560.7	557.1	T1-1
* -2, sect. 3	478.4, 484.1, 489.9	484.1	T1-3
** -3, sect. 1	590.3, 602.0, 614.0	602.1	B1-1
** -3, sect. 2	594.1, 590.3, 575.2	586.5	B1-2

* Lightly ground with 1 μ diamond disc.
** Ground with 70μ, 30μ, 9μ, 6μ, 1μ diamond disc

ULT: 7574

ULTRAMET 12173 MONTAGUE STREET · PACOIMA, CALIFORNIA 91331
TELEPHONE (818) 899-0236
TELEX (910) 496-3490
FAX (818) 890-1946

LEAK TEST CERTIFICATION

Company Aerojet Tech Systems Invoice 16718

P.O. # L823585 Date 3/18/91

This is to certify that the component shipped on the above mentioned invoice was tested for leaks by pressurizing internally to 100± 10 PSIG with Helium while immersed in water, in accordance with Drawing No. 1206352, Note 4. No bubbles passing through wall(s) permitted.

Pass PASS Date Tested 3-5-91

No Pass

Ultramet

Walter M. Abrams

Walter Abrams
Production Manager

L1:Leak

ULTRAMET
DISCREPANT MATERIAL REPORT

DATE 5 MAR 91 NO. 00041A

REJECTION NOTICE: IN-PROCESS MATERIAL... ☐
REJECTION NOTICE: PURCHASED MATERIAL.... ☐
MATERIAL DEVIATION REQUEST..... ■

AFFECTED ITEM		DESCRIBE: LIST SERIAL NUMBERS, DIMENSIONS, ETC.
PART NO. DWG # 1206352-1	REV. NO.	① .030/.035 RE/IR WALL IS .0254-.0348
PART NAME CHAMBER, RE ON IR		② .05 R ± .03 IS OMITTED - NOT A TRUE RADIUS
CUSTOMER AEROJET TECH SYSTEMS		③ HIGH EMISS. RE AT "K" (1.15 ± .03) IS 1.265 - 1.414
SHOP ORDER NO. 7574	PURCHASE ORDER NO. L823585	
RESPONSIBILITY		④ .025/.040 RE/IR WALL IS .0269-.0590, DISCREPANCY NOTED AT POINT "M"
DEPT. ■	VENDOR ☐	⑤ (2) SMOOTH AND CONTINUOUS CONTOUR HAS MACHINED 3.1188 DIA. X .049 STEP
P	NAME ULTRAMET	⑥ .156 ± .010 DIM. IS .1435
	CITY PACOIMA	⑦ NOTE 5, 600 VICKERS HARDNESS MAX. IS 602.1 AVERAGE, SAMPLE B1-1
	SOURCE INSPECTED YES ☐ NO ■	

DISPOSITION

RETURN TO VENDOR		REWORK		LOT QTY. 1	AQL	SAMPLE	QTY. DEF. 1	QTY. REJ.	DATE COMPLETED
USE AS IS		SCRAP		SUBMITTED BY Joseph Thorp DEPT. Q.A.					INSP. SIGNATURE Joseph Thorp
CORRECTIVE ACTION REQ.		REPLY REQUIRED		PURCHASING MGR.					DATE

DISPOSITION OR REWORK INSTRUCTIONS (DESCRIBE IN FULL)

DISPOSITION OF REWORK	ACCEPT	REJECT	INSPECTOR	Q.A. MGR.
VENDOR ACKNOWLEDGMENT		TITLE		DATE

VENDOR COMMENTS

DISPOSITION ACCEPTED
QUALITY ASSURANCE
Herbert R. Young 3-5-91
SIGNATURE DATE

QUALITY ASSURANCE
VERIFICATION OF COMPLETION

MATERIAL REVIEW BOARD	DATE	SIGNATURE
DEPT. MGR.		
ENG. MGR.		
Q.A. MGR.		
GEN. MGR.	3/18/91	

DMRF0310/90

ULTRAMET 12173 MONTAGUE STREET · PACOIMA, CALIFORNIA 91331
TELEPHONE (818) 899-0236
TELEX (910) 496-3490
FAX (818) 890-1946

INSPECTION REPORT

S.O.# 7574	DATE	☒ CUSTOMER AEROJET TECH SYSTEMS
P.O.# L823585	28 Feb 91	☐ SUPPLIER
PART NO. Dwg# 1206352-1		PART NAME CHAMBER, RE ON IR
QTY. OF LOT 1	QTY. INSP. 1	SERIAL NO. 7574-1-1
		PAGE 1 OF 2

NO.	PRINT DIM.	ACTUAL DIM.	ACC.	REJT	REWK	REMARKS
	⌖ A B-C .002	.0002	✓			
	.030/.035	.0254-.0348		✓		
	.50R ± .03	omitted		✓		Not a true Radius
△	HIGH EMISS. RE AT "G"	acceptable	✓			
	.625R ± .010	.625	✓			
	30 ± .5°	30°	✓			
"G"	.045 MIN.	.0610	✓			
"H"	.062 MIN	.0684	✓			
"J"	.062 MIN	.1091	✓			
"K"	.040 MAX	.0292	✓			
△	HIGH EMISS. RE @"K" (1.15 ± .03)	1.265 - 1.414		✓		
M	.025/.040	.0269-.0590		✓		Discrepancy noted at point "M"
Ø	.804/.810	.8085	✓			
	⌖ A B-C .005	.0010	✓			
Ø	3.105/3.110	3.1054	✓			
Ø	3.165/3.170	3.1672	✓			

INSP. BY Joseph Thorp

Q.A. MANAGER Herbert R George 3/5/91

WPF:INSP1

S.O. # 7574	PART NO. 1206352-1	PART NAME CHAMBER	QTY 1	DATE	PAGE 2 OF 2

NO.	PRINT DIM.	ACTUAL DIM.	ACC.	REJT	REWK	REMARKS
	32 ✓	< 32 ✓	✓			
	⌭ A C .010	.0014	✓			
	.070 ± .010	.0652 - .0660	✓			
	2.31 ± .03	2.2893	✓			
2	SMOOTH AND CONTINUOUS CONTOUR	3.1188 DIA X .049 step at point "M"		✓		
	.807 ± .00 R	.807	✓			
	.846 ± .010 R	.846	✓			
	.030 ± .010	.030	✓			
	4.240 ± .010	4.235	✓			
	4.00 ± .03 R	4.00	✓			
	1.403 ± .010	1.3975	✓			
	.375 ± .010	.3690	✓			
	.060 ± .010	.0639 - .0651	✓			
	.156 ± .010	.1435		✓		
	.300 ± .010 R	.300	✓			
Ø	3.000/3.010	3.0076	✓			
Ø	2.934/2.940	2.9378 - 2.9395	✓			
Ø	2.872/2878	2.8756	✓			
Ø	1.703/1.709	1.7072	✓			
NOTE 3	DYE PENETR.	No visible fractures	✓			
NOTE 4	LEAK TEST	acceptable	✓			
NOTE 5	600 VICKERS HARDNESS MAX.	T1-1 557.1, T1-3 484.1 B1-1 602.1, B1-2 586.5		✓		
NOTE 6	VISUAL INSP. AT 20X	No visible defects	✓			

ULTRAMET 12173 MONTAGUE STREET · PACOIMA, CALIFORNIA 91331
TELEPHONE (818) 899-0236
TELEX (910) 496-3490
FAX (818) 890-1946

#2

COVER SHEET

TO: Leo Schoeman
Aerojet

FROM: R. Tuffias

DATE: 4/24/91

FAX NUMBER: (916) 355-2589

This transmittal consists of this cover sheet plus 1 pages.

If this transmittal is unclear or incomplete, please call (818) 899-0236 and ask for the fax operator.

SPECIAL INSTRUCTIONS/NOTES:

ULTRAMET #2

DISCREPANT MATERIAL REPORT

DATE 4/19/91 NO. 00043A

REJECTION NOTICE: IN-PROCESS MATERIAL... ☐
REJECTION NOTICE: PURCHASED MATERIAL.... ☐
MATERIAL DEVIATION REQUEST..... ■

AFFECTED ITEM		DESCRIBE: LIST SERIAL NUMBERS, DIMENSIONS, ETC.
PART NO. 1206352-1	REV. NO. N/C	S/N 7574-1-11
PART NAME CHAMBER, RE ON IR		1. B/P DIM. 0.50R ± .03 IS NOT A TRUE RAD. (~.490 R.)
CUSTOMER AEROJET TECHSYSTEMS		2. B/P DIM. 30 ± .5° IS: 31° (LOCATION OF PT. "G")
SHOP ORDER NO. 7574	PURCHASE ORDER NO. 182358SH	3. B/P DIM. 1.15 ± .03 IS: 1.194/1.252 (Δ "HIGH EMISSIVITY RHENIUM" TO PT "K")
RESPONSIBILITY		4. B/P DIM. .025/.040 COATING "BEWEEN K & M" IS: .0536 AT PT. "M"
DEPT. ■	VENDOR ☐	5. B/P DIM. 3.105/3.110 DIA. IS: 3.118
PRODUCTION	NAME	6. Ⓐ "SMOOTH & CONTINUOUS" IS: .312 DIA. X .04 STEP AT PT. "M"
	CITY	
	SOURCE INSPECTED YES ☐ NO ☐	

DISPOSITION

				LOT QTY.	AQL	SAMPLE	QTY. DEF.	QTY. REJ.	DATE COMPLETED
RETURN TO VENDOR		REWORK							
USE AS IS		SCRAP		SUBMITTED BY		DEPT.			INSP. SIGNATURE
CORRECTIVE ACTION REQ.		REPLY REQUIRED		PURCHASING MGR.					DATE

DISPOSITION OR REWORK INSTRUCTIONS (DESCRIBE IN FULL)

DISPOSITION OF REWORK	ACCEPT	REJECT	INSPECTOR	Q.A. MGR.
VENDOR ACKNOWLEDGMENT			TITLE	DATE

VENDOR COMMENTS

DISPOSITION ACCEPTED
QUALITY ASSURANCE
Robert R. Gonzo 4/19/91
SIGNATURE DATE

QUALITY ASSURANCE
VERIFICATION OF COMPLETION

MATERIAL REVIEW BOARD	DATE	SIGNATURE
DEPT. MGR.		
ENG. MGR.		
Q.A. MGR.		
GEN. MGR. R.H. TUFFIAE	4-19-91	

DMRF0310/90

#2

ULTRAMET 12173 MONTAGUE STREET · PACOIMA, CALIFORNIA 91331
TELEPHONE (818) 899-0236
TELEX (910) 496-3490
FAX (818) 890-1946

INSPECTION REPORT

S.O.# 7574	DATE 20 Mar 91	☒ CUSTOMER AEROJET TECH SYSTEMS ☐ SUPPLIER	
P.O.#			
PART NO. Dwg# 1206352-1		PART NAME CHAMBER, RE ON IR	
QTY. OF LOT 1	QTY. INSP. 1	SERIAL NO. 7574-1-11	PAGE 1 OF 2

NO.	PRINT DIM.	ACTUAL DIM.	ACC.	REJT	REWK	REMARKS
	⌖ A B-C .002	.0007	✓			
	.030/.035	.0312-.0348	✓			
	.50R ± .03	~.490		✓		Not a true Radius
7	HIGH EMISS. RE AT "G"	acceptable	✓			
	.625R ± .010	.6300	✓			
	30 ± .5°	31°		✓		
"G"	.045 MIN.	.0673-.1065	✓			
"H"	.062 MIN	.0640	✓			
"J"	.062 MIN	.0888	✓			
"K"	.040 MAX	.0352-.0368	✓			
7	HIGH EMISS. RE @ "K" (1.15 ± .03)	1.194-1.252		✓		
M	.025/.040	.0312-.0536		✓		Discrepancy noted at point "M"
Ø	.804/.810	.8090	✓			
	⌖ A B-C .005	.0006	✓			
Ø	3.105/3.110	3.1180		✓		
Ø	3.165/3.170	3.1674-3.1696	✓			

INSP. BY Joseph Thorpe

Q.A. MANAGER [signature]

WPF:INSP1

#2

S.O. #	PART NO.	PART NAME	QTY	DATE	PAGE
7574	1206352-1	CHAMBER	1	20 Mar 91	2 OF 2

NO.	PRINT DIM.	ACTUAL DIM.	ACC.	REJT	REWK	REMARKS
	32 ✓	< 32 ✓	✓			
	⌭ | A | C | .010	.0008	✓			
	.070 ± .010	.0751	✓			
	2.31 ± .03	2.2984	✓			
2	SMOOTH AND CONTINUOUS CONTOUR	3.1195 Ø X .040 step at point M		✓		
	.807 ± .00R	.8100	✓			
	.846 ± .010 R	.8500	✓			
	.030 ± .010	.033	✓			
	4.240 ± .010	4.247	✓			
	4.00 ± .03R	4.0125	✓			
	1.403 ± .010	1.412	✓			
	.375 ± .010	.384	✓			
	.060 ± .010	.0647	✓			
	.156 ± .010	.154	✓			
	.300 ± .010R	.300	✓			
Ø	3.000/3.010	3.0092	✓			
Ø	2.934/2.940	2.9383 - 2.9396	✓			
Ø	2.872/2878	2.8757	✓			
Ø	1.703/1.709	1.7075	✓			
NOTE 3	DYE PENETR.	No visible fractures	✓			
NOTE 4	LEAK TEST		✓			
NOTE 5	600 VICKERS HARDNESS MAX					
NOTE 6	VISUAL INSP. AT 20X	No visible defects	✓			

#2

Hardness Testing of Iridium Coating
Ref: Aerojet Tech. Systems, P.O. No. L823585

End Rings Per Dwg. No. 1206352-2 & -3

Vickers Microhardness, with 300 gram load for 5 seconds.

End Ring/Sect.	Measured Hardness	Mean Hardness	S/N
-2, Sect. 1	412.6, 390.2, 441.3	414.7	2-T1-1
-2, Sect. 2	432.8, 441.3, 513.7	462.6	2-T1-2
-3, Sect. 1	397.5, 363.1, 383.1	381.2	2-B1-1
-3, Sect. 2	379.7, 393.8, 408.7	394.1	2-B1-2

7574-2

36:7574-2
04.10.91

#2

ULTRAMET 12173 MONTAGUE STREET · PACOIMA, CALIFORNIA 91331
TELEPHONE (818) 899-0236
TELEX (910) 496-3490
FAX (818) 890-1946

LEAK TEST CERTIFICATION

Company AEROJET TECHSYSTEMS Invoice # _____

P.O. # L823585 Date _____

This is to certify that the component shipped on the above mentioned invoice was tested for leaks by pressurizing internally to 100± 10 PSIG with Helium while immersed in water, in accordance with Drawing No. 1206352, Note 4. No bubbles passing through wall(s) permitted.

Pass PASS Date Tested 4-1-91

No Pass _____

Ultramet

Walter Abrams
Production Manager

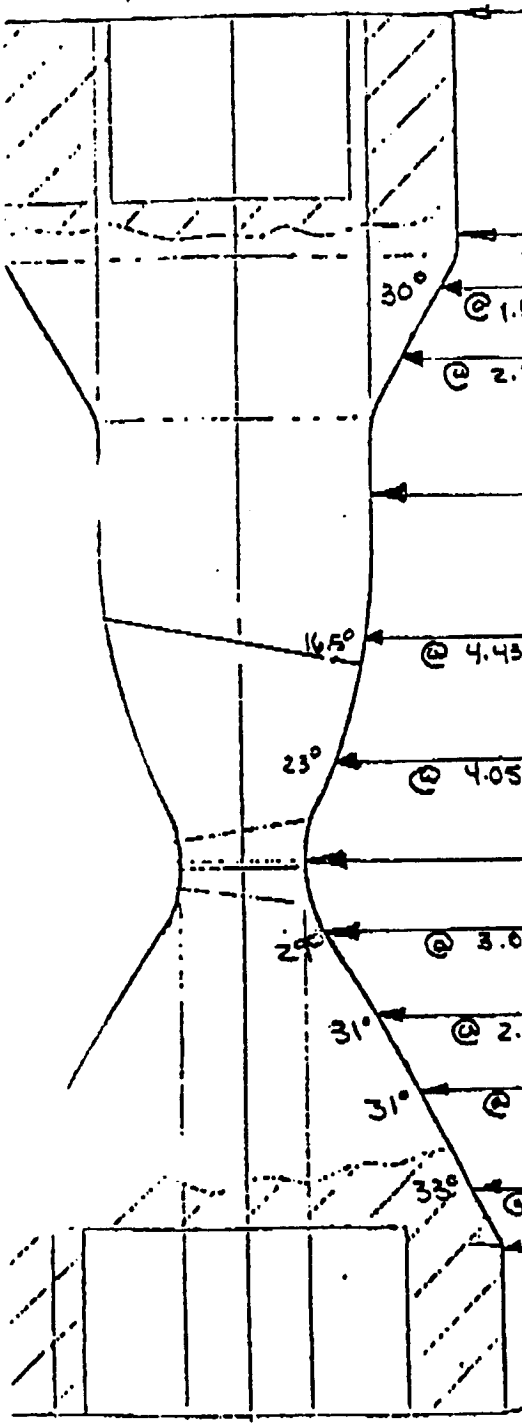

7574 Aerojet
S/N 1-11 Run# Ir 1

	original	Ir ctd	measured Ir wall		calculat Ir wal
	2.8741	2.8800	.0029		
	2.8757	2.8808	.0025		
30° @ 1.866	2.5218	2.5278	.0030		.0025
@ 2.207	2.1347	2.1404	.0028		.0026
	1.7075	1.7121	.0023		
165° @ 4.430	1.3665	1.3711	.0023		.0027
23° @ 4.050	1.0950	1.1006	.0024		.0022
	.8090	.8127	.0014		
@ 3.017	1.1418	1.1467	.0024		.0020
31° @ 2.367	1.8752	1.8793	.0020		.0017
31° @ 1.794	2.5019	2.5059	.0020		.0017
33° @ 1.207	3.1232	3.1269	.0018		.0015
	3.2550	3.2588	.0019		
	3.2555	3.2592	.0018		
INSP.					
DATE	11 Jan 91	24 Jan 91			
	Joseph Thorp	Joseph Thorp			

Ir dye pen
No visible fractures

TJ574 Aerojet #2 NASA Chamber

S/N 1-11 Run# Ir 1

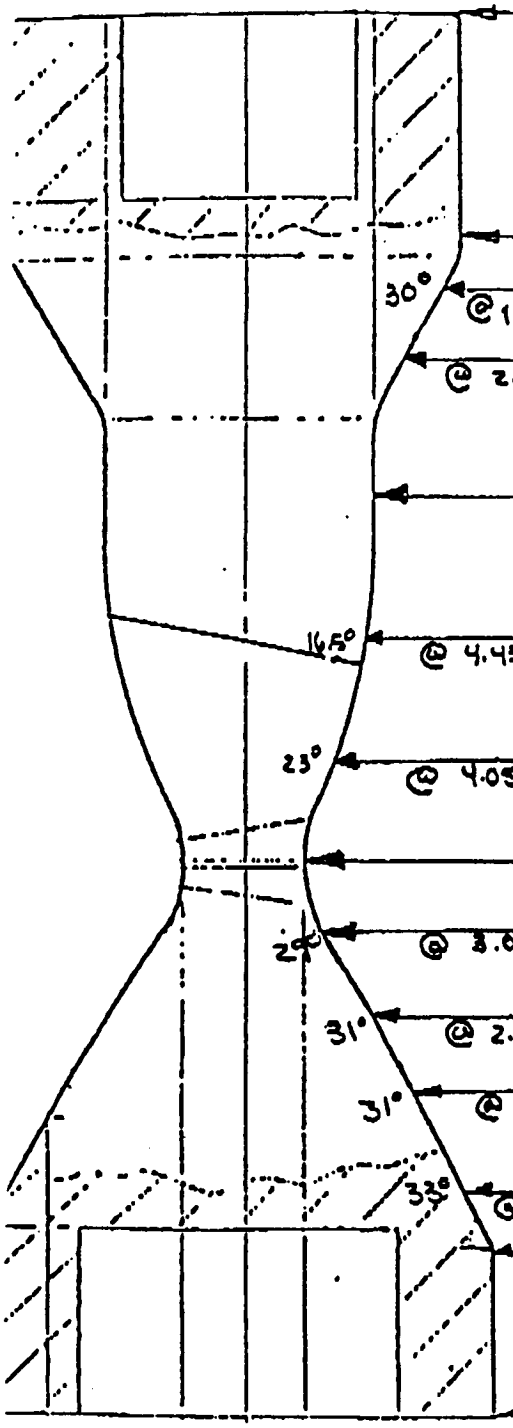

	original	Ir ctd	measured Ir wall		calc Ir
	2.8741	2.8800	.0029		
	2.8757	2.8808	.0025		
30° @ 1.866	2.8218	1.5278	.0030		.002
@ 2.207	2.1347	2.1404	.0028		.00
	1.7075	1.7121	.0023		
16.5° @ 4.430	1.3665	1.3711	.0023		.002
23° @ 4.050	1.0950	1.1006	.0024		.002
	.8090	.8127	(.0019)		
29° @ 3.017	1.1418	1.1467	.0024		.00
31° @ 2.867	1.8752	1.8793	.0020		(00
31° @ 1.744	2.8019	2.5059	.0020		(00
33° @ 1.207	3.1232	3.1269	.0018		(0015
	3.2580	3.2588	(0019)		
	3.2555	3.2592	(.0018)		
INSP. DATE	11 Jan 91 Joseph Thorp	24 Jan 91 Joseph Thorp			

Ir dye pen
No visible fractures

ULTRAMET 12173 MONTAGUE STREET · PACOIMA, CALIFORNIA 91331
TELEPHONE (818) 899-0236
TELEX (910) 496-3490
FAX (818) 890-1946

COVER SHEET

TO: Len Schuerman
Aerojet
x 2964

FROM: R. H. Tuffias

DATE: 4/8/91

FAX NUMBER: (916) 355-2589

This transmittal consists of this cover sheet plus __1__ pages.

If this transmittal is unclear or incomplete, please call (818) 899-0236 and ask for the fax operator.

SPECIAL INSTRUCTIONS/NOTES: _____

100 lb 91-1 Iridium

7574 Aerojet
S/N 1-1 Run # Ir 1

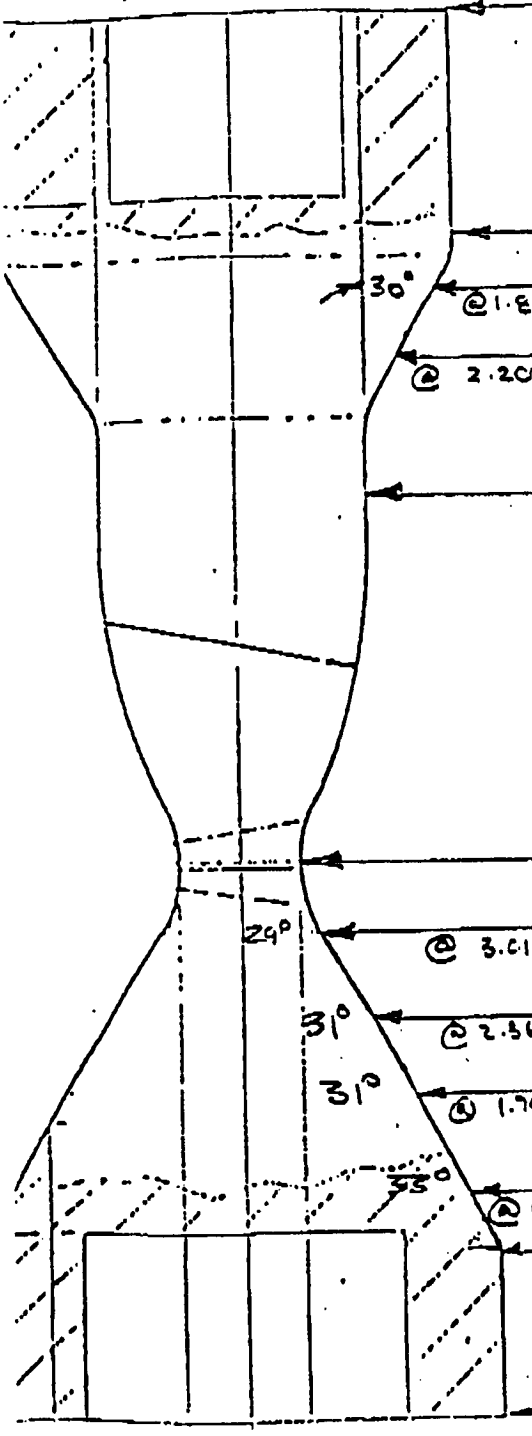

	original	Ir ctd	measured Ir wall		calculated Ir wall
	2.8745	2.8810	.0032		
	2.6756	2.6813	.0028		
@ 1.866	2.5224	2.5276	.0027		.0023
@ 2.207	2.1352	2.1410	.0029		.0025
	1.7072	1.7114	.0021		
	.8085	.8123	.0019		
@ 3.017	1.1404	1.1460	.0028		.002
@ 2.367	1.8737	1.8792	.0027		.002
@ 1.794	2.4998	2.5054	.0028		.002
@ 1.207	3.1220	3.1279	.0027		.002
	3.2535	3.2617	.0021		
	3.2543	3.2675	.0016		
INSP.	Joseph Thorp				
DATE	4 Jan 91	11 Jan 91			

Ir dye pen

20 X visual

GENCORP
AEROJET
Propulsion Division

10016 #1 Chamber

03/19/1991 08:48AM

RECEIVING ACTIVITY RECORD

INSP AREA N

AEROJET PROPULSION

O. NO  823585 LINE 001 DOCK DATE 03/19/91 BY

IST. NO  R2537

DELIVER TO:
L. SCHOENMAN 2964
2004/K

ENDOR UL104 ULTRAMET
UYER 2393 STAN RUSHTON
ARRIER FDEX
REIGHT BILL

TYPE

FOB SELLER'S PLANT

PART REV —
PART NUMBER 1206352-1
CHAMBER THRUST RHENIUM

APR 2 1991

DOCK QTY	= UM	ACCEPT QTY	+ SCRAP QTY	+ DIT QTY	+ REWORK QTY	+ RTV QTY
1.000	EA	1				

COST PER UNIT 73,500.0000
REQUISITION 106028
OWNERSHIP

DEBIT QTY

NR NO.
NR QTY

823585

INSPECTION SPECs:

CP	SP	INSP BY	DATE

MFG LOT # LOT/SER NO EXP. DATE

RECEIVED DEV STORES
823585
CONT PO# ON FILE DIST # R2537
SHOP WORKORDER KGH3239-1 OPER
PN 1206352-1 C/D
QTY 1 REV
INSP BY DATE STAMP
REC'D BY
DATE 4-1-91 SN
LOC 13-H-4R
NEW LOC

JOB KGH PROGRAM
GL NO KGH3239100

RTV SHIP REWORK

NOTES

D-00002 (REV. 6/90)

ULTRAMET
DISCREPANT MATERIAL REPORT

#1

DATE 5 MAR 91 NO. 00041A

REJECTION NOTICE: IN-PROCESS MATERIAL... ☐
REJECTION NOTICE: PURCHASED MATERIAL.... ☐
MATERIAL DEVIATION REQUEST..... ☐

AFFECTED ITEM		DESCRIBE: LIST SERIAL NUMBERS, DIMENSIONS, ETC.
PART NO. DWG # 1206352-1	REV. NO.	① .030/.035 RE/IR WALL IS .0254-.0348
PART NAME CHAMBER, RE ON IR		② .05 R ± .03 IS OMITTED - NOT A TRUE RAD
CUSTOMER AEROJET TECH SYSTEMS		③ HIGH EMISS. RE AT "K" (1.15 ± .03) IS 1.265 - 1.414
SHOP ORDER NO. 7574	PURCHASE ORDER NO. L823585	④ .025/.040 RE/IR WALL IS .0269-.0590, DISCREPANCY NOTED AT POINT "M"
RESPONSIBILITY		⑤ (2) SMOOTH AND CONTINUOUS CONTOUR HAS MACHINED 3.1188 DIA. X .049 STEP
DEPT. ■	VENDOR ☐	⑥ .156 ± .010 DIM. IS .1435
P	NAME ULTRAMET	⑦ NOTE 5, 600 VICKERS HARDNESS MAX. IS 602.1 AVERAGE, SAMPLE B1-1
	CITY PACOIMA	
	SOURCE INSPECTED YES ☐ NO ■	

DISPOSITION			
RETURN TO VENDOR		REWORK	
USE AS IS		SCRAP	
CORRECTIVE ACTION REQ.		REPLY REQUIRED	

LOT QTY.	AQL	SAMPLE	QTY. DEF.	QTY. REJ.	DATE COMPLETED
1			1		

SUBMITTED BY Joseph Thorp DEPT. Q.A. — INSP. SIGNATURE Joseph Thorp
PURCHASING MGR. — DATE

DISPOSITION OR REWORK INSTRUCTIONS (DESCRIBE IN FULL)

DISPOSITION OF REWORK	ACCEPT	REJECT	INSPECTOR	Q.A. MGR.
VENDOR ACKNOWLEDGMENT			TITLE	DATE

VENDOR COMMENTS

DISPOSITION ACCEPTED
QUALITY ASSURANCE
Kenneth R. Upson 3-5-91
SIGNATURE DATE

QUALITY ASSURANCE
VERIFICATION OF COMPLETION

MATERIAL REVIEW BOARD	DATE	SIGNATURE
DEPT. MGR.		
ENG. MGR.		
Q.A. MGR.		
GEN. MGR.	3/18/91	

DMRF03

#1

ULTRAMET 12173 MONTAGUE STREET · PACOIMA, CALIFORNIA 91331
TELEPHONE (818) 899-0236
TELEX (910) 496-3490
FAX (818) 890-1946

INSPECTION REPORT

impact

S.O.# 7574	DATE	☒ CUSTOMER AEROJET TECH SYSTEMS
P.O.# L823585	28 Feb 91	☐ SUPPLIER
PART NO. Dwg# 1206352-1		PART NAME CHAMBER, RE ON IR
QTY. OF LOT 1	QTY. INSP. 1	SERIAL NO. 7574-1-1
		PAGE 1 OF 2

NO.	PRINT DIM.	ACTUAL DIM.	ACC.	REJT	REWK	REMARKS
	↗ A B-C .002	.0002	✓			
①	.030/.035	.0254-.0348		✓		Less heat soak Reduced V.G. design margin
	.50R ± .03	omitted		✓		Not a true Radius
△7	HIGH EMISS. RE AT "G"	acceptable	✓			
	.625R ± .010	.625	✓			
	30 ± .5°	30°	✓			
"G"	.045 MIN.	.0610	✓			
"H"	.062 MIN	.0684	✓			
"J"	.062 MIN	.1091	✓			
"K"	.040 MAX	.0292	✓			
△7	HIGH EMISS. RE @"K" (1.15 ± .03)	1.265 - 1.414		✓		
M	.025/.040	.0269- .0590		✓		Discrepancy noted at point "M"
Ø	.804/.810	.8085	✓			
	↗ A B-C .005	.0010	✓			
Ø	3.105/3.110	3.1054	✓			
Ø	3.165/3.170	3.1672	✓			

OK to Order Too Thick at ext will skirt F.I.T?

INSP. BY Joseph Thorp

Q.A. MANAGER Herbert R. Gregor 3/5/91

WPF:INSP1

#1

S.O. # 7574	PART NO. 1206352-1	PART NAME CHAMBER	QTY 1	DATE	PAGE 2 OF 2

NO.	PRINT DIM.	ACTUAL DIM.	ACC.	REJT	REWK	REMARKS
	32 ✓	< 32 ✓	✓			
	⌓ | A | C | .010	.0014	✓			
	.070 ± .010	.0652 - .0660	✓			
	2.31 ± .03	2.2893	✓			
△2	SMOOTH AND CONTINUOUS CONTOUR	3.1188 Dia. X .049 step at point "M"		✓		
	.807 ± .010 R	.807	✓			
	.846 ± .010 R	.846	✓			
	.030 ± .010	.030	✓			
	4.240 ± .010	4.235	✓			
	4.00 ± .03 R	4.00	✓			
	1.403 ± .010	1.3975	✓			
	.375 ± .010	.3690	✓			
	.060 ± .010	.0639 - .0651	✓			
	.156 ± .010	.1435		✓		
	.300 ± .010 R	.300	✓			
Ø	3.000/3.010	3.0076	✓			
Ø	2.934/2.940	2.9378 - 2.9395	✓			
Ø	2.872/2878	2.8756	✓			
Ø	1.703/1.709	1.7072	✓			
NOTE 3	DYE PENETR.	No visible fractures	✓			
NOTE 4	LEAK TEST	acceptable	✓			
NOTE 5	600 VICKERS HARDNESS MAX	T1-1 557.1, T1-3 484.1, B1-1 602.1, B1-2 586.5		✓		
NOTE 6	VISUAL INSP. AT 20X	No visible defects	✓			

(?)

Custo[illegible] cut ss[illegible] ring mat[illegible]

.614 [illegible]

#1

Hardness Testing of Iridium Coating
Ref: Aerojet Tech. Systems, P.O. No. L823585

End Rings per Dwg. No. 1206352-2 & -3

Vickers Microhardness, with 300 gram load for 5 seconds.

End Ring/Sect.	Measured Hardness	Mean Hardness	S/N
* -2, sect. 1	553.6, 557.1, 560.7	557.1	T1-1
* -2, sect. 3	478.4, 484.1, 489.9	484.1	T1-3
** -3, sect. 1	590.3, 602.0, 614.0	602.1	B1-1
** -3, sect. 2	594.1, 590.3, 575.2	586.5	B1-2

* Lightly ground with 1 μ diamond disc.
** Ground with 70μ, 30μ, 9μ, 6μ, 1μ diamond disc

ULT: 7574

ULTRAMET 12173 MONTAGUE STREET · PACOIMA, CALIFORNIA 91331
TELEPHONE (818) 899-0236
TELEX (910) 496-3490
FAX (818) 890-1946

LEAK TEST CERTIFICATION

Company Aerojet Tech Systems Invoice 16718

P.O. # L823585 Date 3/18/91

This is to certify that the component shipped on the above mentioned invoice was tested for leaks by pressurizing internally to 100± 10 PSIG with Helium while immersed in water, in accordance with Drawing No. 1206352, Note 4. No bubbles passing through wall(s) permitted.

Pass PASS Date Tested 3-5-91

No Pass

Ultramet

Walter M. Abrams

Walter Abrams
Production Manager

L1:Leak

APPENDIX F

NOZZLE SKIRT FABRICATION AND INSPECTION

Thermo Electron
Tecomet

115 Eames Street
Wilmington, MA 01887

TEL (508) 658-9977
FAX (508) 658-4334

June 7, 1991

Dr. S. D. Rosenberg
Aerojet Propulsion
P.O. Box 13222
Sacramento, CA 95813
Dept. 5153
Bldg. 2019A

Re: Proposed manufacture process of 250:1 nozzle
Ref. Dwg. 1206351, P.O. L823586 (Revision A)

Dear Dr. Rosenberg:

Here is an alternate method of manufacture, 250:1 nozzle P/N 1206351:

1. C-103 material, .035 thick sheet will be rolled to a predetermined size to form nozzle.

2. Cleaned per ATC-10195 and eb welded per ATC-STD-4897-1 (weld # 1).

3. This nozzle will be spun to final shape per dimensions of Dwg. 1206351.

3A. Anneal per ATC-47044.

4. In process inspection.

5. Finish machine flange large end and small end of nozzle to final dimensions.

6. Chemical etch per ATC-10195 to achieve final thickness of .016.
Note: Flange and small end of nozzle will be masked during etching process.

7. Rough flange for small end of nozzle.

8. Clean nozzle and flange per ATC-10195.

9. Fixture and eb weld per ATC-STD-4897-1 per marked up Aerojet Dwg. 1206351. (weld # 2)

10. Radiographic inspect eb welds per ATC-STD-4818, quality level 2. Acceptance criteria per ATC-STD-4897-1.

11. In process inspection.

12. Clean per ATC-10195.

13. Anneal per ATC-47044 prior to coating.

14. Coat per Dwg. 1206351. Silicide coating R size (Hitemco).

15. Finish machine surfaces, view A, of Dwg. 1206351 to remove coating.

16. Final inspection. Estimated ship date 11/15/91.

If you have any questions regarding this process please contact Bill Baker, (508) 658-9977 Ext. 324.

Sincerely,

William Baker
Engineering Manager

cc: S. Rushton

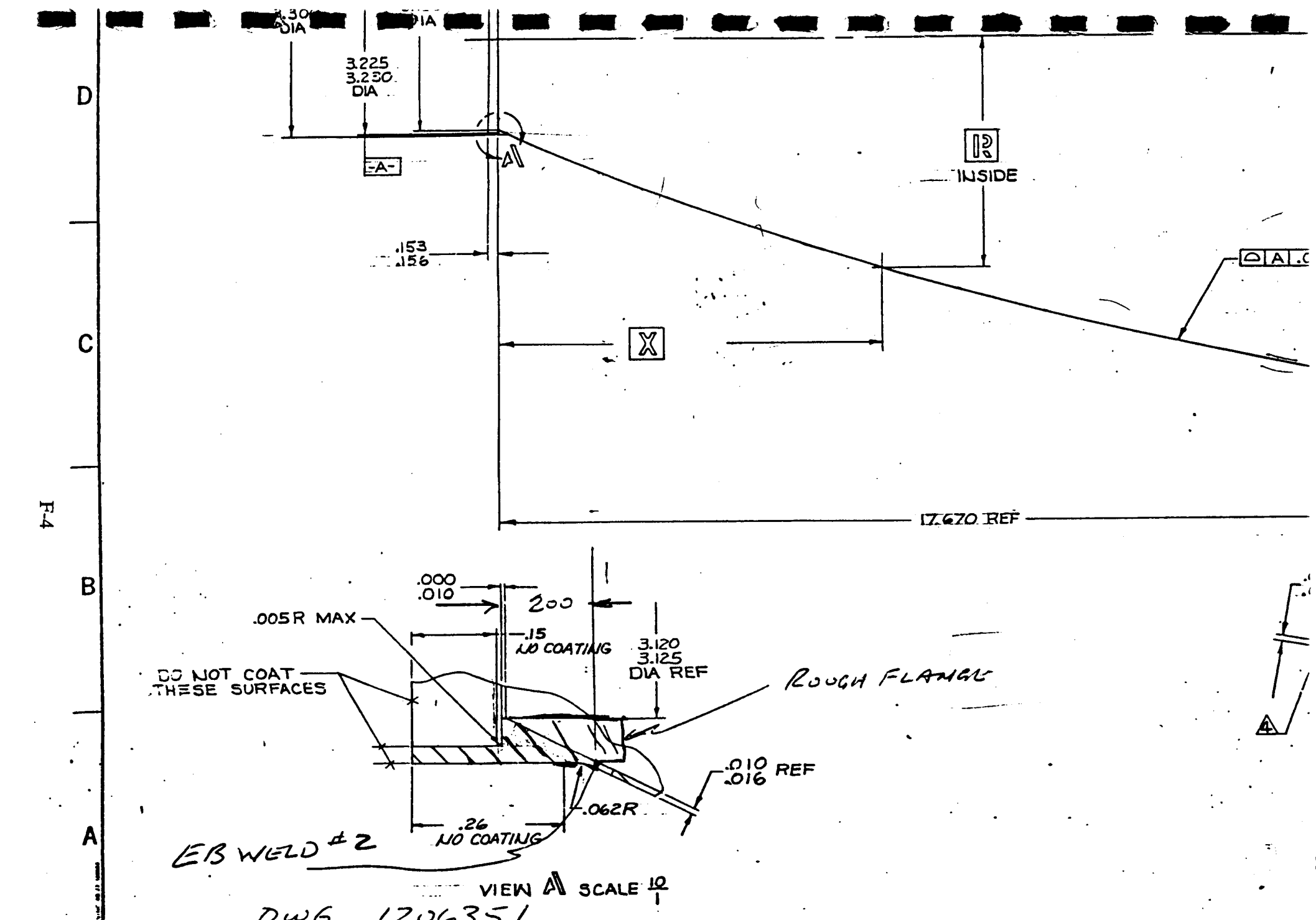
3.225
3.230
DIA
-A-
A1
INSIDE
.153
.156
X
17.670 REF
.000
.010
.200
.005R MAX
.15
NO COATING
3.120
3.125
DIA REF
DO NOT COAT
THESE SURFACES
ROUGH FLANGE
.010
.016 REF
.062R
.26
NO COATING
EB WELD #2
VIEW A1 SCALE 10/1
DWG 1206351
D
C
B
A
8
7
6
5
F-4

APPENDIX O

NONCONFORMANCE REPORT

GENCORP
AEROJET

Propulsion Division
P O Box 13222
Sacramento CA 95813-6000

Tel: 916-355-1000

S/N 02

15 January 1992

THERMO ELECTRON
115 Eames Street
Wilmington, MASS 01887

Attention: Donna Baker

Subject: **Part Number 1206351, C103 Nozzle Non Conformances**
Purchase Order L-823586

Enclosure: Non Conformance Report

Dear Ms. Baker:

Based upon the 1/13/92 data provided by Tecomet's Bill Baker, the reported Non Conformance items (01-04), as dispositioned by Engineering, are accepted as is.

Tecomet is authorized to proceed with nozzle processing as required. Please advise your estimated delivery schedule as soon as possible.

If you have any questions, please contact the undersigned.

Stan E. Rushton
Subcontract Manager

Orig. to Quality
Copy to: L. Schulman

AEROJET TechSystems COMPANY — PRINT OR TYPE IN BLACK INK

NONCONFORMANCE REPORT

G.F.M. ☐ NO. V-21534

PAGE 1 OF

AREA:

1. PART NUMBER	DASH	REV.	2. NOMENCLATURE	3. SERIAL NO.	4. PROGRAM	5. LOT SIZE	6. AOC.	7. DISC.
1206351-2						1		

8. WORK ORDER	9. SHOP ORDER	10. OPER. NO.	11. SUPPLIER NAME	NUMBER	12. P.O. NUMBER	13. DISTRIBUTION NO.	PREVIOUS NR NUMBER
L823585	9001-1157-01		THERMO ELECTRON		L823586		

ITEM	14. NONCONFORMANCE (A) DWG. ZONE, SPEC., PARA., SHOP ORDER OPER., ETC AS APPLICABLE (B) STATE REQUIREMENT (C) INSPECTION RESULTS	(A) CAUSE C/C	(B) FREQ. CODE	☐ MRB ITEMS	16. DISPOSITION/COMMENTS	☐ EPB ITEMS
1	.010 / .016 CONSTANT CHECKS .025 TO				Accept .008 is local Thin Spot .125 long by .030 wide per Fax 1-13-92 Bill Baker	
	(.008 ONE SPOT VIEW A)					
2	.062" MAX CHECKS .092				Accept - radius on end of nozzle is not critical use 0.092 Future parts.	
3	PROFILE A .060 IS OVER SIZE SEE ATTACHED HIGHLIGHTED INSPECTION SHEETS. DUE TO OUT OF ROUND CONDITION				Accept as is. Consider increase in Tollerance for future parts	
4	DEPRESSIONS IN WELD AT TOP OF CONE SEE VIEW A OF PRINT				Accept weld depression is .005 in in .025 Thick material. Per Fax 1-13-92 Baker.	

17. INITIATOR/IDENTITY — DATE — 18. REVIEWED BY — DATE — 19. PROG. REPR. — DATE — 20. INSPECT QTY — ACC. — DISC. — NEW WA NO. — INSPECTOR — DATE

21. MRB/ERB APPROVALS

ENG. REPR. — DATE — QA REPR. — DATE — CUST. REPR. — DATE

22. MRB/ERB RESUBMIT DECISIONS

ENG. REPR. — DATE — QA REPR. — DATE — CUST. REPR. — DATE — RESUBMIT FOR

23. CAUSE

24. CORRECTIVE ACTION

None / Continue by applying coating

C.I.A. SIGNATURE — DATE — 25. EFFECTIVITY: (DATE/SERIAL NUMBER/ETC.)

DISCREPANT MATERIAL DISPOSITION — RESPONSIBILITY: ☐ GFM ☐ SUPPLIER ☐ ATC — QTY — RTS — SHIPPER NO. — SALVAGE — PROC/MFG'G'S REPR. — DATE — QA REPR. — DATE — NO.

F-7

JAN 15 '92 13:43 P.2

CUSTOMER: AEROJET GENCORP CORP. | PART NAME: NOZZLE

DRAWING # 1206351 REV:

1/14/92 INSPECTION METHODS SHEET sheet 1 of 4

ITEM	CHARACTERISTIC	ZONE	INSPECTION METHOD 0°	90°	180°	270°
1	X.073/R 1.596		1.5833	1.5821	1.5839	1.5805
2	X .410/R 1.771		1.7962	1.7958	1.7904	1.7948
3	X .744/ R 1.931		1.9805	1.9755	1.9758	1.9693
4	X 1.090/R 2.098		2.101	2.0907	2.0988	2.0905
5	X 1.418/R 2.254		2.2626	2.2528	2.2497	2.2451
6	x 1.730/ R2.399		2.4179	2.4069	2.4078	2.3975
7	x 2.076/ R 2.555		2.587	2.580	2.571	2.553
8	X 2.410/ R 2.685		2716	2.711	2.727	2.689
9	X 2.729/ R 2.841		2.8592	2.8528	2.864	2.829
10	X 3.110/ R 3.003		3.0168	3.0261	3.0348	2.9975
11	X 3.402/R 3.126		3.1405	3.1403	3.1437	3.1199
12	X 3.770/R 3.277		2.2899	3.2918	3.2621	3.2832
13	X 4.058/ R 3.385		3.3996	3.4006	3.4013	3.3649
14	X 4.410/ R 3.516		3.536	3.546	3.536	3.5118
15	X 4.715/R3.636		3.641	3.672	3.6478	3.6156
16	X 5.090/ R 3.769		3.7783	3.8045	3.7801	3.7444
17	X 5.389/ R 3.882		3.8925	3.9124	3.8693	3.8683
18	X 5.730/ R 4.003		4.015	4.0259	4.0003	3.985
19	X 6.045/ R 4.111		4.1384	4.1674	4.1175	4.0833
20	X 6.410/ R 4.237		4.260	4.2985	4.2293	4.2146

CUSTOMER: AEROJET GENCORP CORP.	PART NAME: NOZZLE

DRAWING # 1206351 REV:

INSPECTION METHODS SHEET sheet 1 of 4

ITEM	CHARACTERISTIC	ZONE	INSPECTION METHOD 0°	90°	180°	270°
1	X.6.704/R 4.331		4.3325	4.3431	4.3218	4.306
2	X 7.110/R 4.461		4.4513	4.5231	4.4503	4.437
3	X 7.357/ R 4.539		4.544	4.5783	4.5251	4.5117
4	X 7.670/R 4.635		4.6575	4.654	4.616	4.6013
5	X 8.013/R 4.739		4.7431	4.7516	4.6998	4.7024
6	x 8.310/ R4.820		4.826	4.8762	4.7859	4.789
7	x 8.672/ R 4.931		4.939	4.961	4.8757	4.8907
8	X 9.090/ R 5.044		5.0519	5.064	4.988	5.006
9	X 9.324/ R 5.113		5.115	5.1196	5.0644	5.0686
10	X 9.730/ R 5.218		5.2092	5.2213	5.1765	5.179
11	X 9.984/R 5.287		5.279	5.296	5.2429	5.246
12	X 10.310/R 5.370		5.3683	5.4055	5.3287	5.340
13	X 10.644/R 5.455		5.4519	5.484	5.4098	5.4204
14	X 10.990/R5.538		5.5341	5.5483	5.496	5.4958
15	X 11.302/R5.614		5.5916	5.627	5.5778	5.583
16	X 11.610/ R 5.684		5.6541	5.6883	5.6394	5.6587
17	X 11.957/R5.766		5.826	5.7167	5.781	5.7298
18	X 12.290/R5.838		5.901	5.7905	5.8414	5.8748
19	X 12.618/R5.912		5.9573	5.888	5.9387	5.9303
20	X 12.970/R 5.988		6.0337	5.9633	6.0612	6.0193

CUSTOMER: AEROJET GENCORP CORP. | PART NAME: NOZZLE

DRAWING # 1206351 REV:

INSPECTION METHODS SHEET sheet 3 of 4

ITEM	CHARACTERISTIC	ZONE	INSPECTION METHOD 0°	90°	180°	270°
1	X.13.277/R 6.050		6.0576	5.9996	6.1254	6.1147
2	X 13.610/R 6.117		6.162	6.0695	6.134	6.116
3	X 13.934/R 6.183		6.201	6.1425	6.2184	6.2272
4	X 14.270/R 6.249		6.301	6.231	6.317	6.2745
5	X 14.593/R 6.309		6.3936	6.2771	6.3592	6.3693
6	x 14.910/R 6.371		6.4105	6.363	6.4196	6.4085
7	x 15.253/R 6.429		6.515	6.4083	6.4897	6.524
8	X 15.590/R 6.492		6.5692	6.475	6.5216	6.5708
9	X 15.911/R 6.543		6.575	6.5335	6.582	6.581
10	X 16.230/R 6.595		6.6175	6.565	6.614	6.643
11	X 16.570/R 6.651		6.6575	6.6325	6.654	6.682
12	X 16.910/R 6.705		6.750	6.6795	6.6831	6.7478
13	X 17.230/R 6.754		6.784	6.7214	6.752	6.811
14	X 17.450/R 6.788		6.7655	6.7496	6.7726	6.8216
15	X 17.670/R6.819		6.7965	6.780	6.813	6.857
16	3.290/3.300 DIA		3.2976			
17	3.225/3.230 DIA		3.2272			
18	3.120/3.125 DIA		3.1227			
19	.153/.156		.153/.155			
20	.000/.010		W/I			

CUSTOMER:AEROJET GENCORP CORP.	PART NAME:NOZZLE

DRAWING # 1206351 REV:

INSPECTION METHODS SHEET Sheet 4 of 4

ITEM	CHARACTERISTIC	ZONE	INSPECTION METHOD
1	.062 R		.062
2	.010/.016 CONSTANT		.024/.008
3	.062 R MAX		.070
4	PRO A .060		
5	.020/.100		.024/.025
6	.100		.096/.105
7	NOTE 1		✓
8	NOTE 2		✓
9	NOTE 3		✓
10	NOTE4		✓
11	NOTE 5		✓

WINCHESTER
TESTING
LABORATORY

NON-DESTRUCTIVE TEST/ANALYSIS REPORT JOB NO. F1-78

CUSTOMER	P.O. NO	DATE
Thermo Electron	61351	6/17/91

ADDRESS: 813 Woburn, Street, Wilmington, Mass. 01887

PART NAME	PART NO	SPEC NO
Nozzle	1206351-2	See Instructions

LOT SIZE	TEST QTY.	ACCEPT	REJECT	PART S/N	MATERIAL	STANDARD
1	1	1	0	N/A		MIL-STD-453

O RADIOGRAPHY	O MAGNETIC PARTICLE	O LEAK TESTING	O TEST PROCEDURES
XO FILM INTERPRETATION	O ULTRASONIC	O THICKNESS MEASUREMENT	O CONSULTATION
O PENETRANT	O EDDY CURRENT	O WELDER QUALIFICATION	O OTHER

SPECIAL INSTRUCTIONS

Radiographic inspect weld per MIL-STD-453, specifications ATC-STD-4897H and ATC-STD-4818 detailing the accept/reject criteria. Views A,B,C,D & E.

RESULTS

After radiographic inspection nozzle was found to be acceptable per above specification.

David Lavole 6-17-91
APPROVED BY DATE

P.O. Box 2151
13 Henshaw Street
Woburn, Massachusetts 01888
(617) 935-7674

Thermo Electron
Tecomet

115 Eames Street
Wilmington, MA 01887

TEL (508) 658-9977
FAX (508) 658-4334

CERTIFICATE OF CONFORMANCE

Purchase Order No.

1-823586

Teco Job No.

9001-1175-01

I certify that the shipment of

C103 NOZZLE

Shipped to:

AEROJET PROPULSION
HIGHWAY 50 & HAZEL AVE.
NIMBUS, CA 95670

were inspected and found to comply with all requirements of the contract.

12063551-2 Part Number

Rev No.

2 Qty Shipped

JULY 25, 1991 Date Shipped

Lloyd Peacock

Lloyd Peacock
Quality Assurance Manager

PACKING SLIP

HITEMCO

A Barson Company

No. 15189

160 SWEET HOLLOW ROAD
OLD BETHPAGE, N.Y. 11804
TEL. (516) 752-7882 • FAX (516) 752-7951

SOLD TO THERMO ELECTRON

ADDRESS 115 EAMES STREET

CITY WILMINGTON STATE MA. 01887

SHIP TO 813 WOBURN STREET

SAME AS SOLD TO UNLESS OTHERWISE INDICATED HERE

DATE	YOUR ORDER NO.	OUR ORDER NO.	SHIPPED VIA	CARTONS - PKGS.	TOTAL WEIGHT
7/18/91	61525	33710	FED.EX.#0045382875		

QUANTITY	DESCRIPTION
1	P/N 1206551 NOZZLE EXTENSION
	CERTIFICATIONS
	PROCESSED PER INSTRUCTIONS
	9001-1175-02
	COMPLETE

PLEASE NOTIFY US IMMEDIATELY IF ERROR IS FOUND IN SHIPMENT.

☐ ORDER COMPLETE

☐ BALANCE TO FOLLOW

PACKED BY _____ CHECKED BY _____

<<CERTS1>>

CERTIFICATE OF COMPLIANCE

TO: THERMO ELECTRON

ADDRESS: 813 WOBURN STREET

WILMINGTON, MA. 01887

REF. P.O. 61525 DATE REC'D 7/2/91 DATE SHIPPED 7/18/91

SHIPPER NO. 15189 INV. NO. 15189 JOB NO. 33710

REF P/N 1206551 DESCRIPTION NOZZLE EXTENSION QTY. 1

REF P/N _____ DESCRIPTION _____ QTY. _____

REF P/N _____ DESCRIPTION _____ QTY. _____

APPLICABLE SPEC. R512E

PROCESS FUSED SILICIDE

REMARKS COATING THICKNESS .002"/.004"

BASE ALLOY IS C-103

SMALL AREA ON I.D. NEAR NOZZLE

EXIT WAS SPOT REPAIRED IN

SECOND SHORT FUSION CYCLE.

We hereby certify that the above parts have been processed in compliance with the Instructions as outlined on your Purchase Order.

Authorized Signature Dennis Pepeio

Title Q.C. LAB MGR.

Hitemco, A Barson Company
160 Sweet Hollow Road
Old Bethpage, New York 11804

FORM 003

P.O.# 61525

PROJECT # 33710

DATE: 7-8-91

CUSTOMER: Thermo Electron

PARTS 1206351

SUBSTRATE C-103

COATING RS12E VIS. _____ AT _____ F _____ DIP TIME

BATCH # 371

Coupon Area = 20.6

S/N					
REC'D WT.	1856.4				
COATED WT. DIP-SPRAY	2034.8		9.52	9.01	
BLASTED WT.	1856.4		8.98	8.50	
△ WT. - 1	178.4		.54	.51	
Mg/cm^2 APPLIED	30.0		26.2	24.8	
DIFF. WT. -1	2015.9		9.15	8.98	
BLASTED WT.	1856.4		8.98	8.50	
△	159.5		.147	.48	
Mg/cm^2 -1	26.8		22.8	23.3	
Mg/cm^2 as dip only					
Mg/cm^2 as pre bead					
FINAL THICKNESS					
REC'D THICKNESS					
△ THICKNESS					

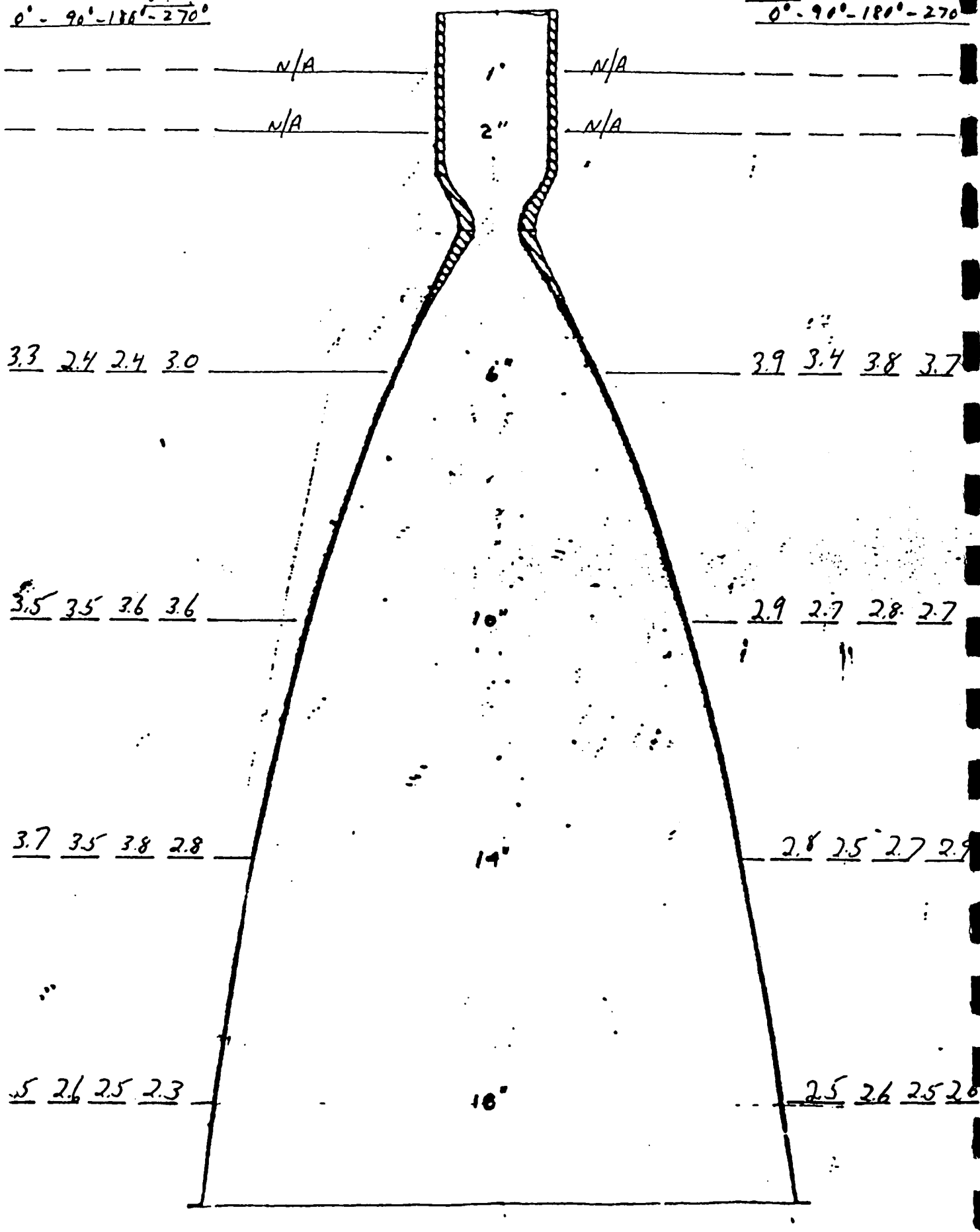
O.D.
0° - 90° - 180° - 270°
I.D.
0° - 90° - 180° - 270°
N/A
N/A
N/A
N/A
1"
2"
6"
10"
14"
18"
3.3 2.4 2.4 3.0
3.9 3.4 3.8 3.7
3.5 3.5 3.6 3.6
2.9 2.7 2.8 2.7
3.7 3.5 3.8 2.8
2.8 2.5 2.7 2.9
2.5 2.6 2.5 2.3
2.5 2.6 2.5 2.6

Customer Thermo Electron Proj # 33110 P/N 1206351 Coating RS12E Dermidron

O.D.
0° - 90° - 180° - 270°

I.D
0° - 90° - 180° - 270°

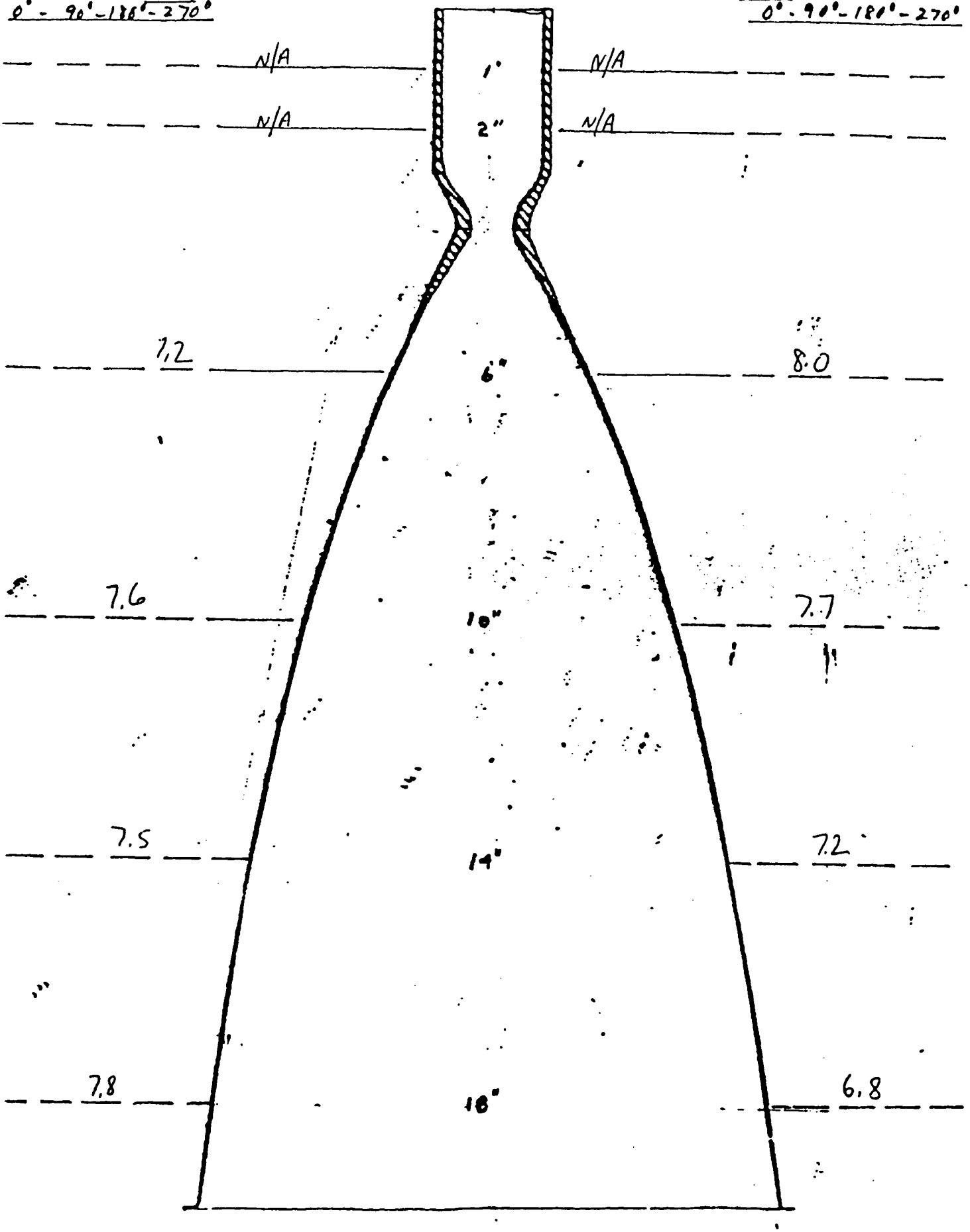

Thermo Electron CORPORATION

Tecomet
115 Eames Street
Wilmington, Massachusetts 01887
(508) 658-9977 TELEX 94-9337
FAX # (508) 658-4334

PURCHASE ORDER

THIS NUMBER MUST APPEAR ON ALL PAPERS AND PACKAGES
ORDER NUMBER 59136

DATE 11/29/90

VENDOR NO. 2313

BILL TO: 115 EAMES STREET, WILMINGTON, MA. 01887

TO TELEDYNE WAH CHANG, ALBANY
P.O. BOX 460-T
ALBANY, OR 97321

SHIP TO THERMO ELECTRON CORP.
813 WOBURN STREET
WILMINGTON, MA 01887

ACCOUNT NO.	DEPARTMENT	☐ CONFIRMING (DO NOT DUPLICATE)	☐ NOT CONFIRMED
09-9001175	GENERAL MACHINING		

BUYER NAME	CERTIFICATE OF ANALYSIS REQUIRED ☐ YES ☐ NO	GOVT RATING	CONFIRM TO	TAXABLE CODE TAX EXEMPT NO 042-208-186 IN
JOE HOSFER		DO6C	GRANT	

FOB POINT	SHIP VIA	P.R. CODE	PAYMENT TERMS	REQUESTED BY
SHIPPING POINT	UPS	NO	NET 15	R PAIGE

ITEM	QUANTITY	U/M	ACKNOWLEDGED DELIVERY DATE	PLEASE ENTER OUR ORDER FOR THE FOLLOWING (SUBJECT TO TERMS AND CONDITIONS ON FACE AND BACK HEREOF)
1	5.00	EA	3/05/91	9001117501 REQ. # 25653 C-103 SHEET, .125 THK X 15"X15"

P.O. #: 59136
JOB #: 9001-1175-61
CUST: Aerojet
DWG #: 1206351-2
HT #: 576560
Q.C. [illegible] 2-7-91
DATE: 2-7-91

ITEM	QUANTITY RECEIVED	DATE RECEIVED	BALANCE DUE	ITEM	QUANTITY RECEIVED	DATE RECEIVED	BALANCE DUE	ITEM	QUANTITY RECEIVED	DATE RECEIVED	BALANCE DUE
1	5	2/91	0								

RECEIVING COPY

PACKING LIST

TELEDYNE
WAH CHANG ALBANY

P.O. BOX 460
ALBANY, OR 97321
(503)926-4211
TWX (510)595-0973

REV. NO.: | REVISION DESC.: | REV. DATE:

CUSTOMER PURCHASE ORDER NO.	CUST NO.	PRO FORMA NEED	SLMN	OLD CD	ORDER DATE	TYPE	S/O NO.
59136	6242	NO	GFR	1M5	11/29/90		5169

PRODUCTION DEPT.	FORECAST NO.	INQUIRY NO.	EXPORT LIC NEED	INSPECTION	CAS COVERED	GOVT CONTRACT NO.	GOVT PRIORITY	CERT. REQUIRED
FAB			NONE	TWCA	NO			

Sold To:
THERMO ELECTRON
115 EAMES STREET
WILMINGTON, MA
01887

Ship To:
THERMO ELECTRON
813 WOBURN STREET
WILMINGTON, MA 01887

CUSTOMER SPECIFICATION: ASTM B654

MDS1 NO.:

SHIP VIA	F.O.B.	P/L NO.
UPS B/L	SOURCE	1
$	FREIGHT: PREPAY & ADD	DATE SHIPPED: 01/31/91

ORDERING DATA | SHIPPING DATA

TWCA ITEM	CUST ITEM	QUANTITY	UNIT MEAS	TOTAL POUNDS	MATERIAL DESCRIPTION	HEAT NUMBER	PACS NUMBER	QUANTITY SHIPPED	UNIT MEAS	WEIGHT SHIPPED	BALANCE
1	1	5.0	PC	47.0	C-103 PLATE, ANNEALED .125" X 16" X 16" PACS 88505 5.0 PC	576560	88505	5.0	PC	45.7	0.0

"KNOWINGLY OR WILLFULLY RECORDING OF FALSE, FICTITIOUS OR FRAUDULENT STATEMENTS OR ENTRIES ON THIS DOCUMENT MAY BE PUNISHABLE AS A FELONY UNDER FEDERAL STATUTES."

These products may be subject to U.S. Export Regulations for ECCN's 3604A, 3608A, 1649A, 1674A, 1675A or 6899G.

TELEDYNE
WAH CHANG ALBANY
P.O. BOX 460
ALBANY, OREGON 97321-0130
(503) 926-4211 TWX (510) 596-0973

TO ADDRESS: Thermo Electron
115 Eames Street
Wilmington, MA 01887

ATTENTION OF: Purchasing Agent

IN REGARD TO YOUR

Purchase Order No.:	59136
Item No.:	1
Description:	C-103 Sheet - Annealed
Dimensions:	0.125" X 15.000" X 15.000"
Specifications:	ASTM B654-79 and Purchase Order
Date:	January 31, 1991
Date Shipped:	Ref. P.L.#
Quantity Shipped:	5 pcs.
Weight Shipped:	45.7 lbs.
Sales Order No.:	5169
Heat No.:	576560 C103
PACS No.:	88505
Anneal Run No.:	9711

INGOT CHEMISTRY COMPOSITION: IN PERCENT

Element:	Spec.	Top	Bottom
Hf:	9-11	10	10
Ti:	.7-1.3	0.9	0.8
Nb:		B A L A N C E	

MAXIMUM IMPURITIES: IN PERCENT

Element:	Spec. Max.:	Top	Bottom
Zr:	0.700	0.500	0.440
Ta:	0.500	0.230	0.250
W:	0.500	0.082	0.100
O:	0.025	0.007	0.010
N:	0.010	0.003	0.003
H:	0.0015	<0.0005	<0.0005
C:	0.015	0.011	0.008

METALLOGRAPHY TEST: RESULTS
Micro No.: BR-770

Percent: Recrystallization

Sample:	Spec. Min.:	Results
Results:	90 %	100

Grain Size Test: Results
Method: ASTM E112

Sample:	Spec.	Results
1:	For Info Only:	8.5

CERTIFIED BY: L. R. Jackson, Manager Quality Assurance Dept.: L R Jackson 11/31/91
mw

A1.06.22.14.P1-2
C1.01.28.27

Sales Order No.: 5169
Purchase Order No.: 59136
Item No.: 1
Heat No.: 576560 C103
PACS No.: 88505

TELEDYNE
WAH CHANG ALBANY
P.O. BOX 460
ALBANY, OREGON 97321-0130
(503) 926-4211 TWX (510) 696-0973

ROOM TEMPERATURE TENSILE TEST: RESULTS
Method: ASTM E8

Test:	Spec. Min.:	Results
Tensile STR (Psi) Long. #1:	54000	59200
Yield Strength (Psi) (0.2% Offset) Long.. #1:	38000	43100
Elongation in 1" (%) Long. #1:	20	41
Tensile STR (Psi) Trans.#1:	54000	62000
Yield Strength (0.2% Offset) (Psi) Trans.#1:	38000	45000
Elongation in 1" (%) Trans.#1:	20	41

BEND TEST: RESULTS
Method: ASTM E290
Procedure: LP-BT-1 Rev. 1

Attribute:	Spec.	Results
Degree of bend:	90-120	105
Radius of bend:	2.5T	2.5t
Temperature:	RT	75°

Results: One transverse specimen was bent without showing signs of cracking.

APPENDIX G

I_S ERROR ANALYSIS

Date: 01-30-92

To: D.M. Jassowski

From: H.C. Howard

Subject: Estimate of measurement uncertainty for reported ISP for the 100 Lb-F Advanced Small Rocket Chamber Program.

Distribution: W.G. Hooper, A.R. Keller, S.D. Rosenberg, R.K. Schaplowsky, L. Schoenman, T.C. Smith, W.A. Thompson, E.M. Vanderwall, R.E. Werling, J.D. Wilkins

Enclosures: (1) Evaluation of measurement uncertainty for Isp-vacuum 44:1 nozzle for 100 Lb-F Advanced Small Rocket Program.

An estimate of measurement uncertainty in reported Isp-vacuum for the 100 Lb-F Advanced Small Rocket Chamber Program has been requested by Reaserch and Technology Engineering Department for assurance of minimum performance quotations for prospective customers.

Attached is Enclosure (1) that details the evaluation of this uncertainty estimate and is developed for a 1 sigma confidence interval at 0.706 Lb-F-secs/Lb-m. Wherever possible and reasonable this evaluation uses the actual test instruments calibration and hot-fire test data.

I would advise the reader that this uncertainty is an estimate and is applicable to test Bay A2 100 Lb-F thrust fixture and propellant feed systems using the current procedures for propellant pressurization, in-place propellant flowmeter calibrations and thrust calibration.

H C Howard

H. C. Howard
Engineering Data Analyst
Test Operations

Enclosure: (1) Evaluation of measurement uncertainty for Isp-vacuum 44:1 nozzle for 100 Lb-F Advanced Small Rocket Program.

Definitions: a. (L) designates limit of error, assumed to be 3 sigma, used when tolerances are stated with calibration procedures and where lack of data is available.
b. The uncertainty for NIST weight calibrations here is estimated to be 25% of the Balances tolerance per paragraph 5.2 of MIL-SRD-45662A.
c. (A) stands for assumed value.
d. ~ signifies the partial derivative function, and is applied to estimate uncertainties in computed parameters. Reference CPIA 180 section 1.5 and Appendix II, Propagation of errors by Taylor's series.

A. Standard dual bridge Load Cell S/N 5881 Lebow 200 Lb. Range

Metrology Laboratory evaluation at 100 lb level:	Mg (L)	1 sigma Lbs
1. NIST calibration of "S" class transfer weights. (4:1)	0.28	2.058e-7
2. Balances for periodic "S" class cal. use weights.	1.10	8.084e-7
3. "S" class weight transfer standard for "C" weights.	3.45	2.535e-6
4. "C" class weight transfer standard for "ASA" weights.	49.71	3.653e-5
5. "ASA" weight transfer standard for Lebow load cell. stack of 16 6.25# weights 1 sigma = 739.52 Mg		.0016305
6. Fluke DVM readout. +/-.003% +2counts or +/-.0032% (L) reading		.0010667
7. Lebow load cell cal. shunt to force repeatability	.06%FS(L)	.0400000
8. Lebow load cell cal. dead weight repeatability.	.07%FS(L)	.0466700
Total 1 sigma RSS =		.061497 lbs
% of nominal =		.064%

B. Field use A zone thrust calibrations and hot test precision evaluated at 100 Lb-F.

1. NEFF recording system resolution, linearity & repeatability. (10 cnts zero, + 5 cnts lin) +/-15cnts(L) based on sensitivity of .032 Lbs/cnt.@ 1 sigma 5 cnts.	.1600
2. Thrust calibrations standard load cell average of A&B bridge output, precision. +/-.175%(L) at 100 Lb load. Determined from deviations from average of stds "A"&"B"	.0582
3. Thrust calibrations average bias precision. +/-.032%@100lb-F	.0320
4. Firing test average of A&B bridge thrust measurement precision.	.0219
Total field use thrust calibration uncertainty RSS	.1746 lbs
% of nominal =	.182%

C. Total combined 1 sigma thrust measurement uncertainty RSS .1851 lbs
% of nominal = .193%

D. Volume Transfer standards PDFM S/N 89-03-01(N2O4) were used for in-place in-propellant flowmeter calibrations. Oxidizer flowmeters FMO-1 S/N .25-331 FMO-2 S/N .25-8407882

	1 sigma Lb/sec
1. PDFM volume, dia used laser measurement, length used vernier model T320312 S/N 001, resolution .001"	
Volume = .25*3.1415927*Dia*Dia*Length. = 120.122215 cu-in	
1 sigma Diameter = .0001882645 in. N=32	
1 sigma Length = .002461 in. N=10	
1 sigma Volume = .02599012 cu-in = .00093893 lbs H2O@4 Deg C.	
This uncertainty is +/-.021636% of FS, evaluated at .139 Lb/sec	.000030075
2. a. Rectilinear Potentiometer electrical end-end voltage DVM = .0032%(L) of reading taken twice per displacement, evaluated at .139 Lb/sec.	.000002965
b. Linearity and repeatability based on 10" displacement. N=18 1 sigma = .0049032V = .068824% by volume df=16	.000095667
t test applied	.000101407
3. A zone electrical ratio conformance to metrology lab data. (Deviation from 10 volt recorder calibration range) .033%(A)	.000045870
4. NEFF recorder frequency calibration & signal conditioning. linearity & repeatability. (10 cnts zero, + 5 cnts lin) = +/-15cnts(L) based on sensitivity of .107 Hz/cnt. @ 1 sigma 5 cnts. = .535 Hz (used avg K of both flowmeters)	.000098527
5. Calibration data precision based on residuals from 2nd order equation used to compute hot test flowrate. N=17 df=15	
S/N .25-331	.000038307
S/N .25-8407882	.000053298
Average of both	.000046412
t test applied	.000049452

Total calibration uncertainty, oxidizer volumetric flowrate Lb/sec H2O @ 4 Deg C, avg of 2 flowmeters	.000159542
% of nominal =	.115

E. Volume Transfer standards PDFM S/N 89-03-02(MMH) were used for in-place in-propellant flowmeter calibrations. Fuel flowmeters FMf-1 S/N .25-8407881 FMf-2 S/N .25-326

	1 sigma Lb/sec
1. PDFM volume, dia used laser measurement, length used vernier model T320312 S/N 001, resolution .001"	
Volume = .25*3.1415927*Dia*Dia*Length. = 123.670562 cu-in	
1 sigma Diameter = .000179156 in. N=32	
1 sigma Length = .002974 in. N=10 df=9	
1 sigma Volume = .03009925 cu-in = .001087374 lbs H2O@4 Deg C.	
This uncertainty is +/-.02435% of FS, evaluated at .140 Lb/sec	.000034095
2. a. Rectilinear Potentiometer electrical end-end voltage DVM = .0032%(L) of reading taken twice per displacement, evaluated at .140 Lb/sec.	.000002987
b. Linearity and repeatability based on 10" displacement. N=18 1 sigma = .0049032V = .068824% by volume df=16	.000096354
t test applied	.000102135
3. A zone electrical ratio conformance to metrology lab data. (Deviation from 10 volt recorder calibration range) .033%(A)	.000046200
4. NEFF recorder frequency calibration & signal conditioning. linearity & repeatability. (10 cnts zero, + 5 cnts lin) = +/-15cnts(L) based on sensitivity of .112 Hz/cnt. @ 1 sigma 5 cnts. = .560 Hz (used avg K of both flowmeters)	.000102208

5. Calibration data precision based on residuals from 2nd order equation used to compute hot test flowrate. N=17 df=15	1 sigma EU
S/N .25-8407882	.000100510
S/N .25-326	.000037733
Average of both t test applied	.000075914
	.000080887

Total calibration uncertainty, fuel volumetric flowrate Lb/sec H2O @ 4 Deg C, avg of 2 flowmeters .000175290

% of nominal = .125%

Nominal operating condition data used to evaluate 100Lb-F thruster performance uncertainties.

F meas = 95.8	Lbs	SGo = 1.46390	Wt = .327289	Lb/sec	
F-vac = 101.5	Lbs	Wo = .203483	Pexit = .235	psia	
FMO = 0.139	Lb/sec H2O	SGf = .884332	Ae = 24.279	Sq-in.	
FMF = 0.140	Lb/sec H2O	Wf = .123806	Ispvac= 310.1	secs.	

Evaluation of partial derivatives.

~FMo/Wo = SGo = 1.46390, ~SGo/Wo = FMo = .139
~FMf/Wf = SGf = .884332, ~SGf/Wf = FMf = .140
~Wo/Wt = 1., ~Wf/Wt = 1.
~Pexit/Fvac = Ae = 24.279, ~Ae/Fvac = Pexit = .235, ~Fmeas/Fvac = 1.
~Fvac/Ispvac = 1./Wt = 3.055403, ~Wt/Ispvac = -Fvac/(Wt*Wt) = -947.5523

F. Hot test redundant flowmeter average flowrate precision evaluated from test data deviation between flowmeters.	1 sigma EU	1 sigma %
Oxidizer N=18 df=16	.000023847	.017
Fuel n=15 df=13	.000071735	.051
Since the current test series is a limited sample and the data is significantly lower than the historical precision for flowmeters I am electing to use TM125's quote for the average of 2 flowmeters for both the oxidizer and fuel flowrate precision.	.000080596	.058

G. Total combined uncertainty RSS 1 sigma for 2 redundant flowmeter average volumetric flowrate Lb/sec H2O @ 4 Deg C.		
Oxidizer	.00017874	.129
Fuel	.00019293	.138

H. Uncertainty evaluation for propellant specific gravities combines propellant report Reference quotes and temperature and pressure uncertainties applied to the equations.

N2O4-NO report AFRPL-TR-73-105 quote of .0010(L) Gram/CC combined with 1.32 Deg F and 1.35 psi 1 sigma uncertainty entering specific gravity curve.	.00015694	.113
MMH report AFRPL-TR-69-149 quote of .0026(L) Gram/CC combined with 1.32 Deg F and 1.35 psi 1 sigma uncertainty entering specific gravity curve.	.00017528	.125

I. Uncertainty of mass propellant flowrate, Lb/sec.	1 sigma EU	1 sigma %
Oxidizer, Wo	.00026257	.129
Fuel, Wf	.00017237	.139
Total, Wt	.00031409	.096

J. Uncertainty in calculated vacuum thrust, lbs.

Where: Fvac + Fmeas + Pcell*Ae
Uncertainty 1 sigma in Pcell = .27% FS = .00405 psi
Uncertainty Ae is .001"(A) resolution in throat diameter
Uncertainty in Fmeas is C. above = .1851 Lbs

1 sigma combined uncertainty RSS in Fvac, lbs	.209597	.206

K. Uncertainty 1 sigma in computed Isp-vacuum, Lbf-sec/Lb-m.

Where: Isp-vac = Fvac/Wt, Lbf-sec/Lb-m	.706181	.228

APPENDIX A

UPDATE UNCERTAINTY IN VACUUM SPECIFIC IMPULSE MEASUREMENT FOR 286:1 NOZZLE PERFORMANCE TESTS

PERFORMANCE ANALYSIS UNCERTAINTY

The uncertainty estimate of Monthly Technical Report #32, Appendix B, has been updated to include a revised measure of cell pressure uncertainty. The effected sections are presented here.

J. UNCERTAINTY IN CALCULATED VACUUM THRUST, LBS

Nominal operating condition data used to evaluate 110 lbf 286:1 thruster performance uncertainties:

F meas	= 108.60 lbs	Wt	= .3451 lb/sec	Ae	= 145.374 sq-in.
F-vac	= 111.05 lbs	PVAC	= .0169 psia	Ispvac	= 321.8 sec

Evaluation of partial derivatives, which are designated as ~( )

~Fvac/Pexit = Ae = 145.374, ~Fvac/Ae = PVAC = .0169, ~Fv ac/Fmeas = 1

~Ispvac/Fvac = 1./Wt = 2.897711, ~Ispvac/Wt = -Fvac/(Wt*Wt) = -932.4566

where:

Fvac = Fmeas + PVAC*Ae

Met Lab. std. Uncertainty (L) 5 micron	1 sigma	=	.00003223 psi
Post test "AS IS" cal deviation at 1000 Microns		=	.00035005 psi
Digital recording system (L) + / -10 cnts.	1 sigma	=	.00004082 psi
Precision (L) assumed 0.25% of 10000 microns from Met Lab calibration data sheet 1 sigma		=	00016117 psi
Zero reference, estimate (L) .0030 psi	1 sigma	=	00100000 psi
Uncertainty 1 sigma in PVAC RSS		=	.00107295 psi
Uncertainty Ae is .001" resolution of meas.	1 sigma	=	.00712387 sq-in.
Uncertainty in Fmeas is		=	.1851 lb

	Eng. Unit	%
1 sigma combined uncertainty RSS in Fvac, lbs	.242057	.218

K. UNCERTAINTY 1 SIGMA IN COMPUTED ISP-VACUUM, LBF-SEC/LBM

			Eng. Unit	%
where:	Isp-vac = Fvac/Wt, lbf-sec/lbm		.760101	.236
	Uncertainty of total mass propellant flowrate, lb/sec Wt	1 sigma =	.0031409	.096

APPENDIX H

PERFORMANCE DATA

APPENDIX H

IR-RE Welded 286:1 Thruster Performance Test Data

Test data from the performance test series for the Ir-Re welded 286:1 thruster are presented in this Appendix. Test conditions are summarized in Table 2 of the main body of this report. The planning, instrumentation, and the purpose of each test were presented in the previous monthly report.

The control on thruster operating conditions is shown in Figures H-1 and H-2 where total propellant flow and mixture ratio are plotted versus time for the long duration tests. The resulting thruster operation is plotted in Figures H-3 and H-4 which show Pc and Fvac versus time.

Specific Impulse Results

Vacuum specific impulse for all tests (runs -259 through -278) is plotted as a function of mixture ratio in Figure H-5 and chamber pressure in Figure H-6.

This family of data includes tests with durations between 1 and 120 sec (Table 2). The specific impulse measurements are for a data sample period near the end of the firing which is indicated in the data summary table. The vacuum specific impulse is calculated from:

$$I_{s\,vac} = \left[(F_{bias} - F_{zro}) F_{bias} + P_a A_e \right] / (W_o + W_f)$$

where

F_{meas} is the measured thrust at 286:1

F_{zro} is the stand off set at the end of the test

F_{BIAS} is the bias measured during the post test stand calibration

P_a is the corrected cell pressure

A_e is the nozzle exit area (145.37 $in.^2$)

W_o is the oxidizer mass flow rate, and

W_f is the fuel flow rate

In this series, the tests of less than 10 sec duration (-259, -260 and -270) are far from reaching steady state conditions; their effect on trends in the data should be considered with this in mind.

Mixture ratio is seen to have a moderate effect on I_S, with a relatively flat maximum probably occurring between 1.6 and 1.8. The effect of chamber pressure on I_S is very nearly flat over the range of 104 to 128 psia.

To permit comparison of tests run at different mixture ratios, the set of data was used to determine the effect of mixture ratio on I_S. The best fit of the data is shown in Figure H-7, with data points from the long duration tests shown as well. Using these data, the performance measurements for all tests 10 sec or longer in duration have been analyzed to the standard MR of 1.650 in Figure H-8. It should be noted that this is a greatly expanded scale: the full range of the ordinate is less than 1%. The same data, for just the long duration tests, are shown in Figure H-9 with an expanded ordinate of 0.5% full range. At the nominal operating pressure of 115 psia, all of the normalized performance data are within a range of ± 0.25%. Any variations of I_S with P_C over the range of 104 to 128 psia is within less than 0.06%.

Specific impulse throughout each long duration test has been determined and is plotted in Figure H-10. The values are time averages for the interval between successive data points. Note that the I_S is nearly steady at the 120 sec duration. Note also that test -276 shows a 0.2% drop during the last averaging period which corresponds to the time at which the H_2 shroud flow was stopped. This time period is expanded in Figure H-11 to show thrust at cell pressure, cell pressure, and thrust corrected to vacuum. Hydrogen flow is terminated at 110 sec and falls to zero before 111 sec; cell pressure comes to a new steady value at about 118 sec. Although thrust at cell pressure rises, as expected, the corrected vacuum thrust falls very slightly, instead of remaining constant (Note that all data points are not shown in the plot, especially prior to 110 sec).

In previous tests at 44:1, the hydrogen flow was terminated to determine the effect on thrust; none was observed. In the present series of tests, hydrogen flow was terminated during post test coast, after the stand reached zero; no evidence of an effect on thrust was noted at the 0.01 lbf (0.01%) level. The apparent change in thrust corrected to vacuum could be explained by an error of 35 micron on cell pressure; it could also represent a transient effect on force or pressure which is important at the 0.2% level.

Normalized I_s versus time for the long duration test is plotted in Figure H-12. As expected, the data points fall on top of each other with the exception of test -273 which is about 0.4% higher than expected.

Characteristic Exhaust Velocity

Characteristic exhaust velocity has been calculated for the thruster as defined by:

$$C^{*} = \frac{P_c A_t g}{W_p}$$

where

P_c = chamber total pressure

A_t = throat area

$g = 32.174$

W_p = Total propellant and flow

Chamber pressure for this thruster is measured at a static port upstream of the trip and is not corrected for chamber gas velocity, Rayleigh line losses, or losses at the trip. The throat area is corrected for thermal expansion, using the optically measured chamber wall temperature and

$$A_t = (1 + k_t \Delta T)^2 A_{t_o}$$

where

K_t is the coefficient of thermal expansion of rhenium, 4.17×10^{-6} in/in.-°F

ΔT is the temperature rise of the chamber

and $A_o = 0.5077$ in.^{2}

The calculated throat diameter versus time is shown in Figure H-13 for the 120 sec tests.

Characteristic exhaust velocity for all tests is plotted in Figure H-14 versus mixture ratio and in Figure H-15 as a function chamber pressure. No trend with MR is evident, but a 1% drop is noted, as P_c increases from 104 to 128 psia. These trends are clearer where only the long duration tests are plotted, Figures H-16 and H-17.

Thrust Coefficient

Nozzle thrust coefficient is a measure of nozzle performance but also includes the effects of mixing and reaction downstream of the throat. Thrust coefficient defined as

$$C_F = \frac{I_{sva}g}{C^*}$$

is plotted in Figure H-18 as a function of mixture ratio for the long duration tests. A definite trend is seen, about 1% increase in C_f for an 18% increase in MR. A similar trend is evident for P_c in Figure H-19 with about a 1% increase in C_f for a 23% change in P_c.

Temperature

Chamber wall temperature, measured with a two-color optical pyrometer, is plotted in Figures H-20 and H-21 for all 286:1 tests as a function of mixture ratio and P_c, respectively. The data for the long duration tests are shown in the body of this report, Figures H-17 and H-18. The lower temperature limit for this pyrometer is about 2550°F.

Thermal data were monitored for a long coast period after the test to determine maximum soak back temperature. Generally, maximum values were reached in 600 sec or less.

The six locations plotted are #1, outside of the regeneratively cooled adapter, between the welds, #2, the thruster mounting point, #3, regen fuel inlet, #4, regen fuel out, #5, valve body, and #6, injector body. Where multiple thermocouples were used, the highest reading is shown.

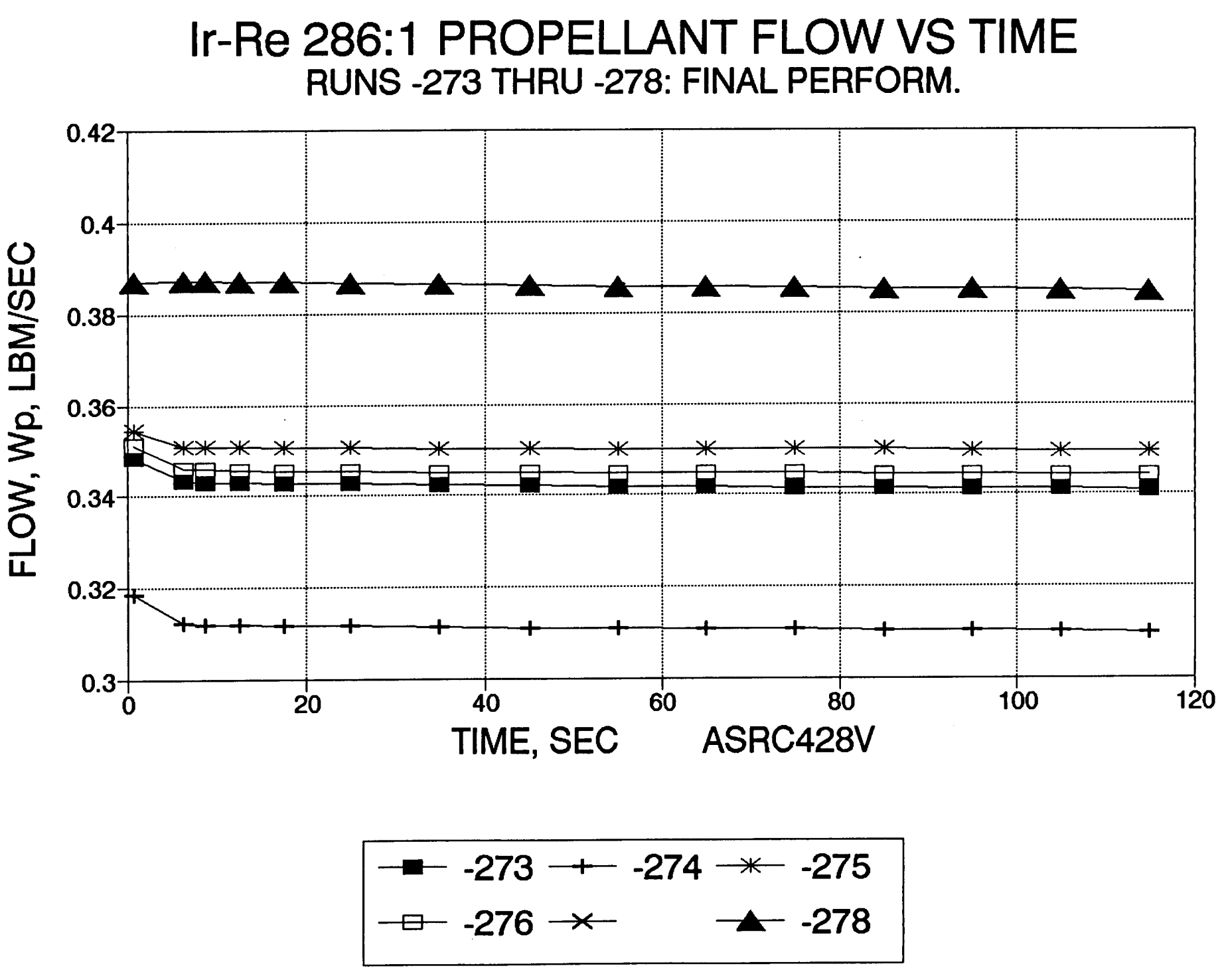
Ir-Re 286:1 PROPELLANT FLOW VS TIME
RUNS -273 THRU -278: FINAL PERFORM.
FLOW, Wp, LBM/SEC
0.42
0.4
0.38
0.36
0.34
0.32
0.3
0
20
40
60
80
100
120
TIME, SEC
ASRC428V
-273
-274
-275
-276
-278

Figure H-1

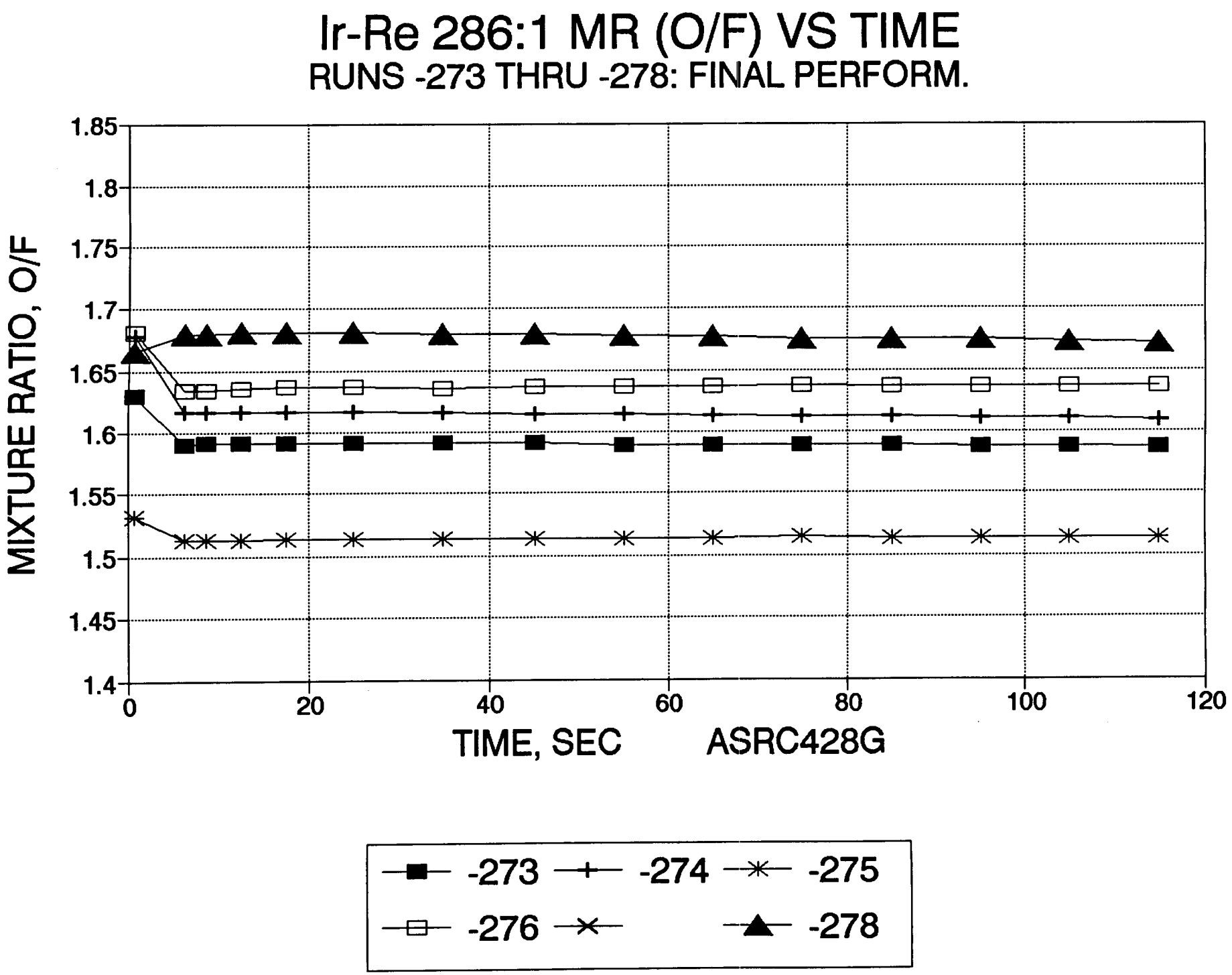
Ir-Re 286:1 MR (O/F) VS TIME
RUNS -273 THRU -278: FINAL PERFORM.
MIXTURE RATIO, O/F
1.85
1.8
1.75
1.7
1.65
1.6
1.55
1.5
1.45
1.4
0
20
40
60
80
100
120
TIME, SEC
ASRC428G
-273
-274
-275
-276
-278

Figure H-2

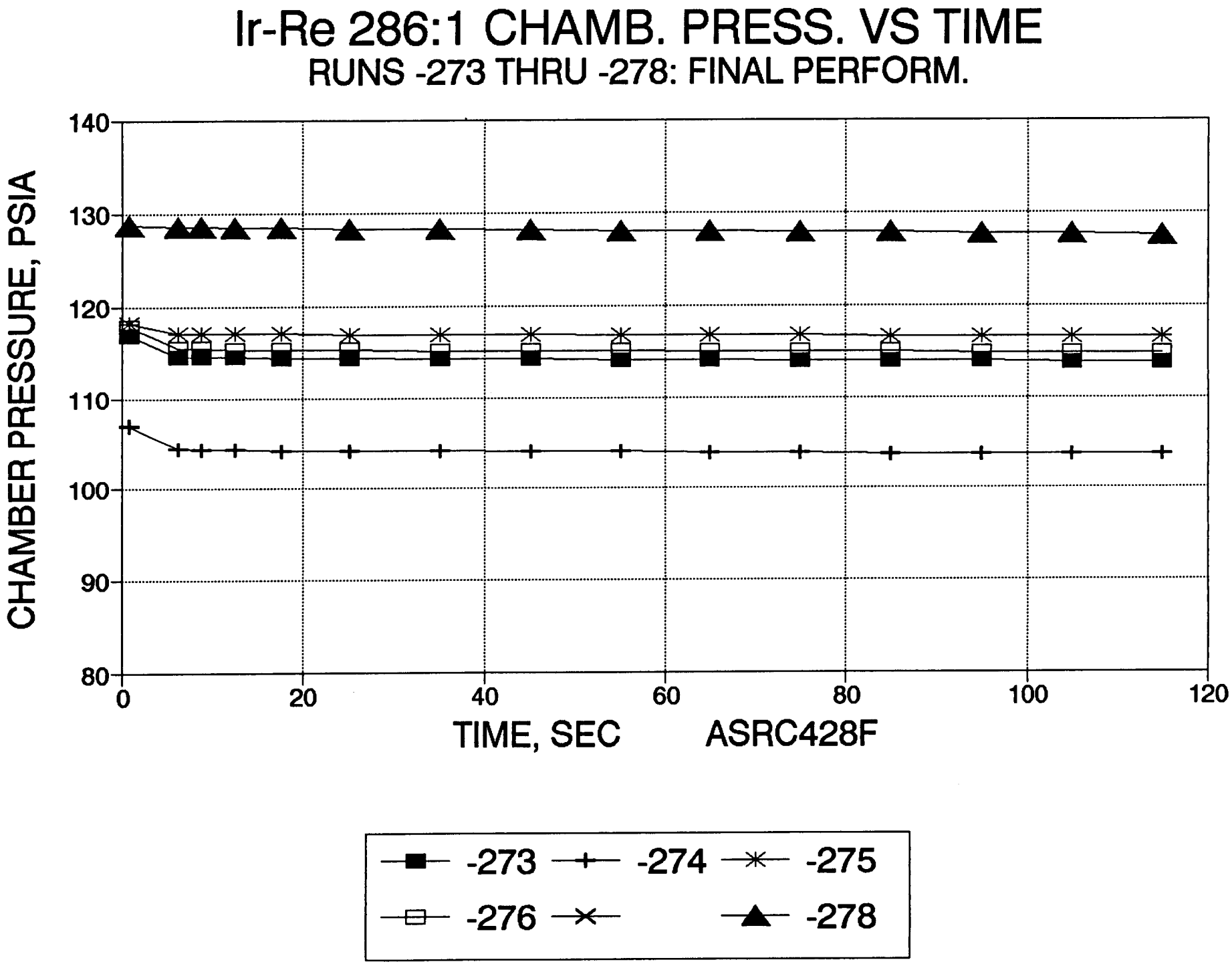
Ir-Re 286:1 CHAMB. PRESS. VS TIME
RUNS -273 THRU -278: FINAL PERFORM.
CHAMBER PRESSURE, PSIA
140
130
120
110
100
90
80
0
20
40
60
80
100
120
TIME, SEC
ASRC428F
-273
-274
-275
-276
-278

Figure H-3

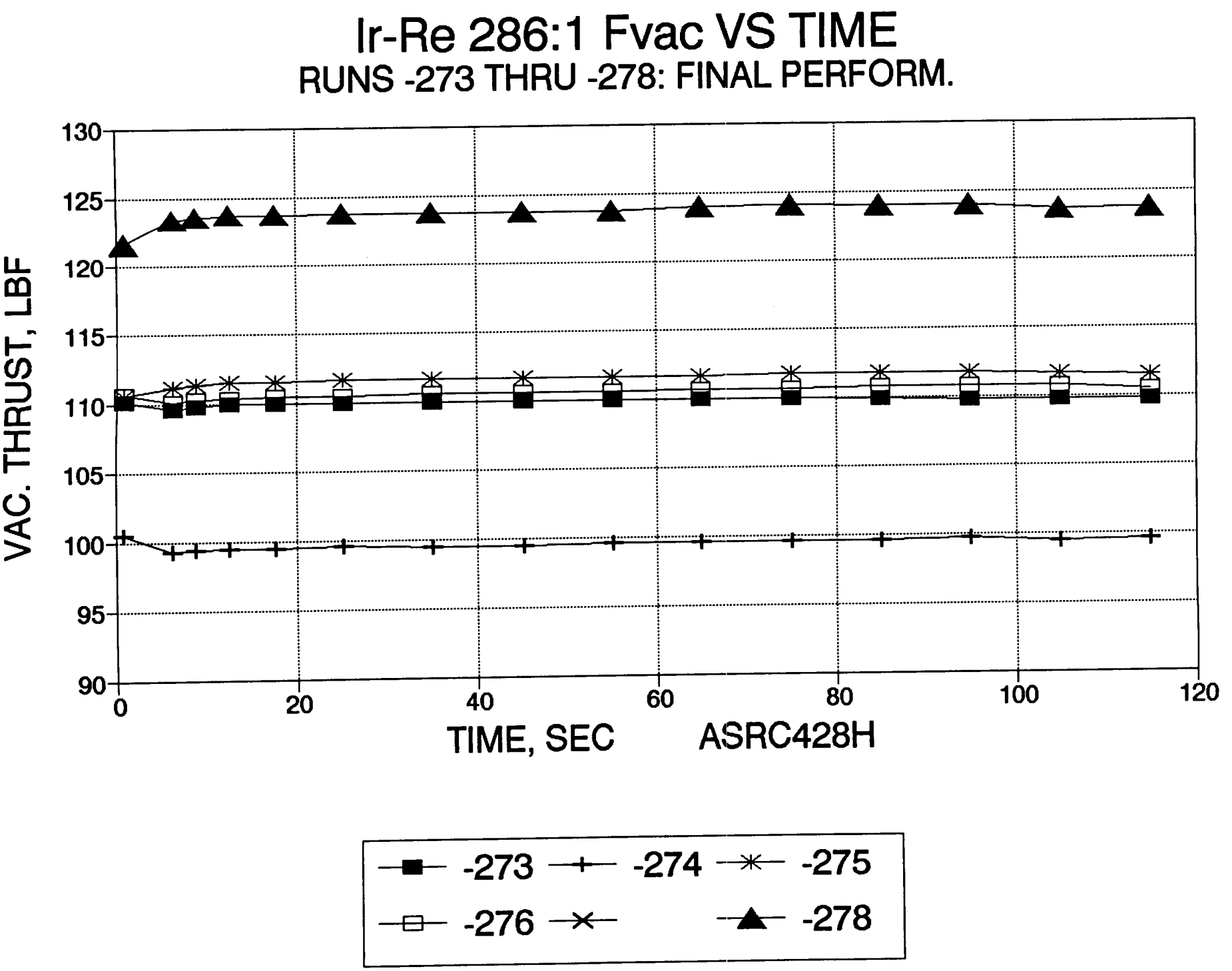
Ir-Re 286:1 Fvac VS TIME
RUNS -273 THRU -278: FINAL PERFORM.
VAC. THRUST, LBF
130
125
120
115
110
105
100
95
90
0
20
40
60
80
100
120
TIME, SEC
ASRC428H
-273
-274
-275
-276
-278

Figure H-4

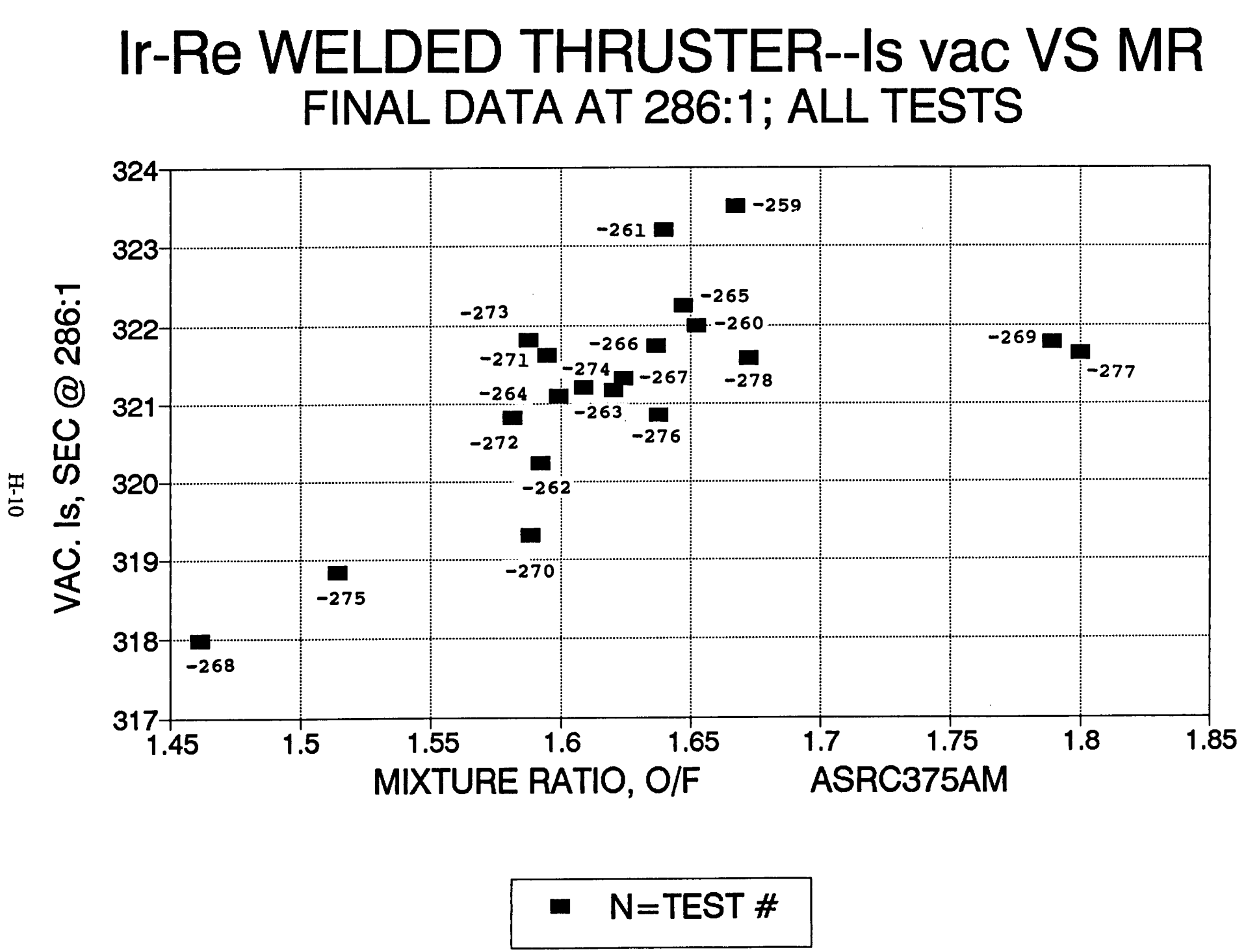
Ir-Re WELDED THRUSTER--Is vac VS MR
FINAL DATA AT 286:1; ALL TESTS
VAC. Is, SEC @ 286:1
MIXTURE RATIO, O/F
ASRC375AM
324
323
322
321
320
319
318
317
1.45
1.5
1.55
1.6
1.65
1.7
1.75
1.8
1.85
-259
-261
-265
-273
-260
-269
-266
-271
-274
-267
-278
-277
-264
-263
-272
-276
-262
-270
-275
-268
N=TEST #

Figure H-5

Ir-Re WELDED THRUSTER-- Is vac VS PC-1

FINAL DATA AT 286:1; ALL TESTS

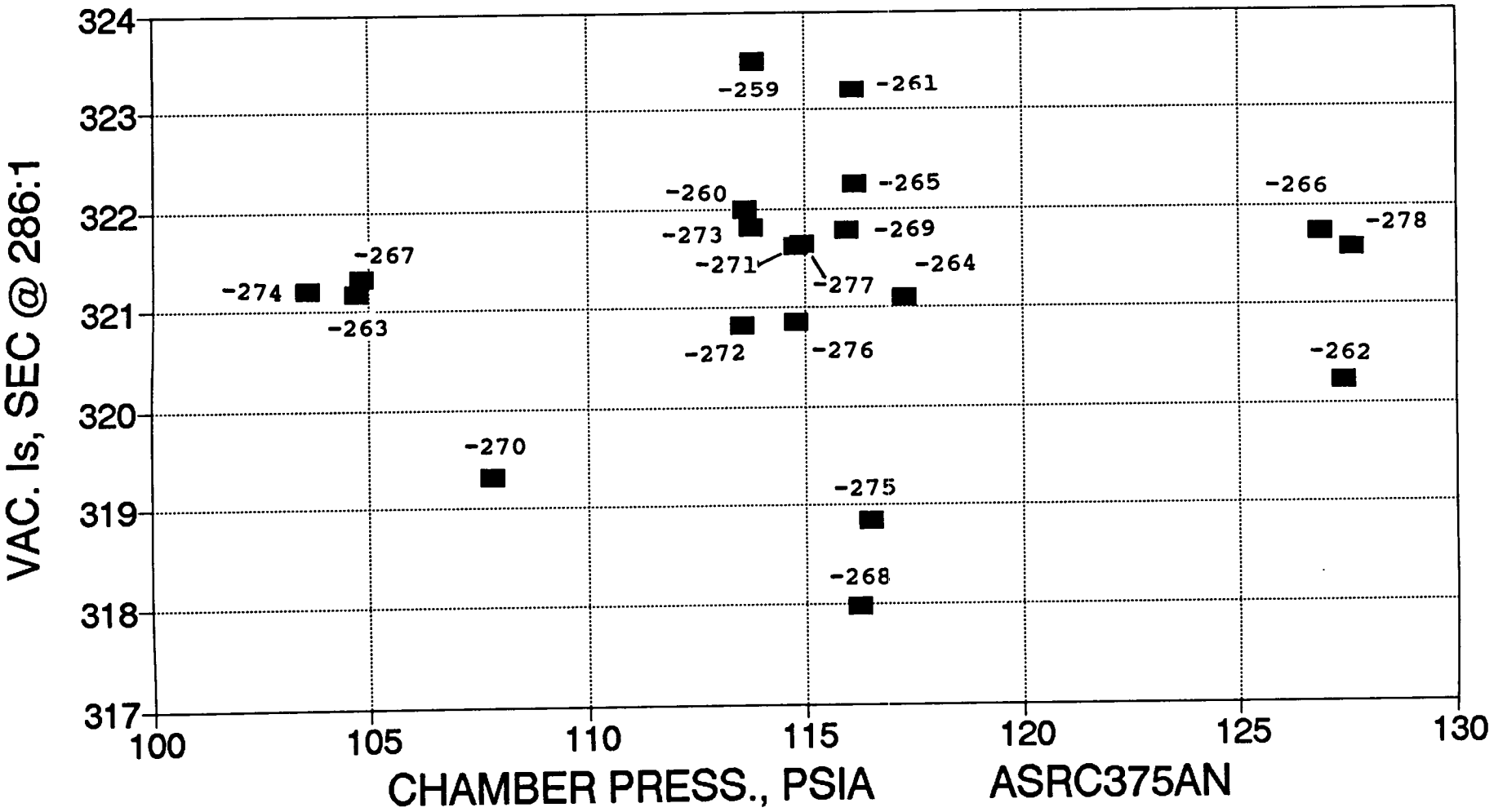

Figure H-6

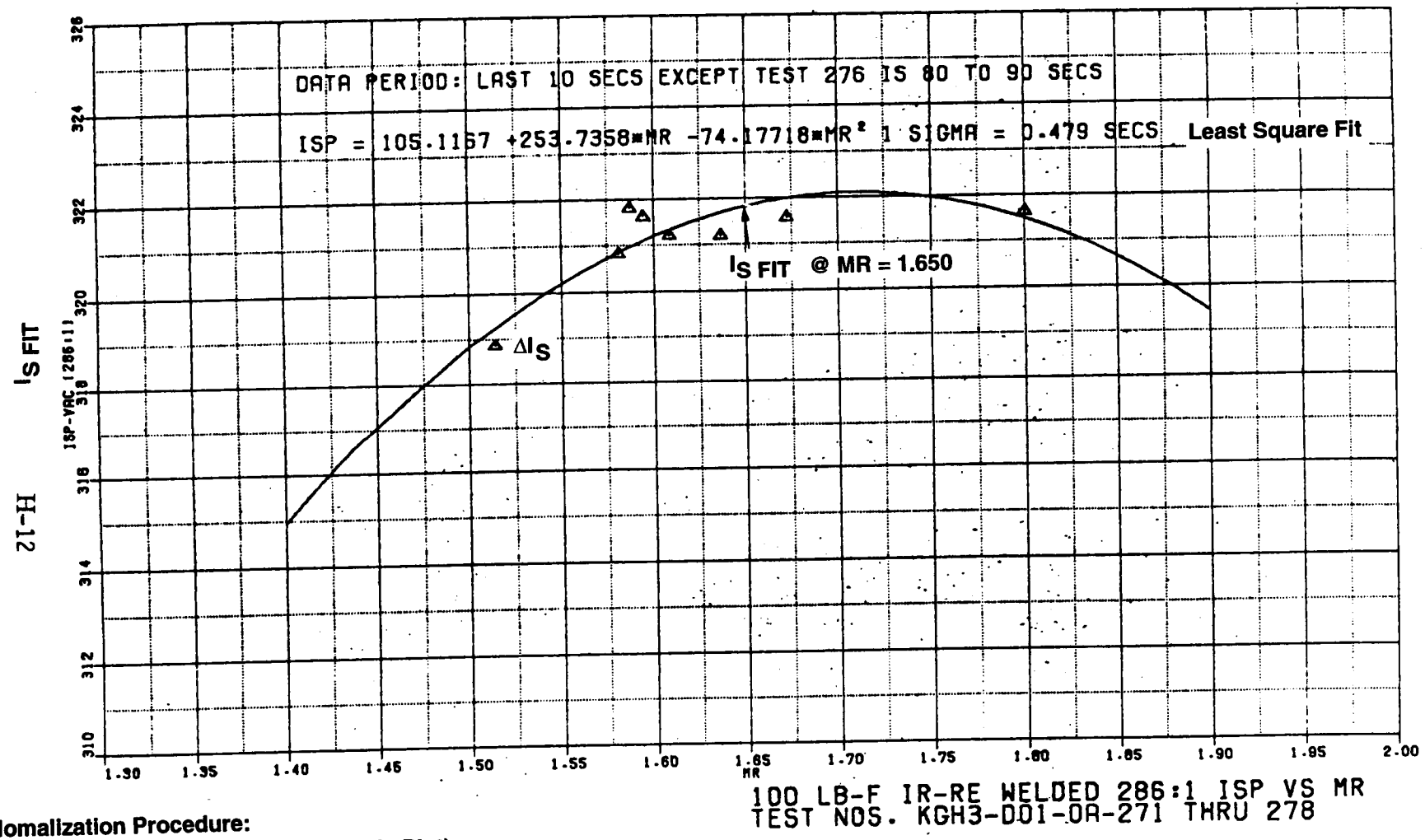

Nomalization Procedure:

1. **Make Least Square Fit to Data (This Plot)**
2. **Take Difference Between Measured $I_{S\ VAC}$ and $I_{S\ FIT}$ = ΔI_S**
3. **Add ΔI_S to Value of $I_{S\ FIT}$ @ MR = 1.650. This Is Normalized I_S @ 1.650 for the Test**

[To Do: ASRC 428K.]

Figure H-7. Curve Fit of $J_{s_{vac}}$ vs MR

Replotted $I_{S\ NORM}$ Curves Are Identified by (.) Post Script , e.g., ASRC 375BC, ASRC 375 CT.

Ir-Re WELDED ENGINE-- Is NORM. VS PC-1

FINAL DATA AT 286:1; ALL TESTS

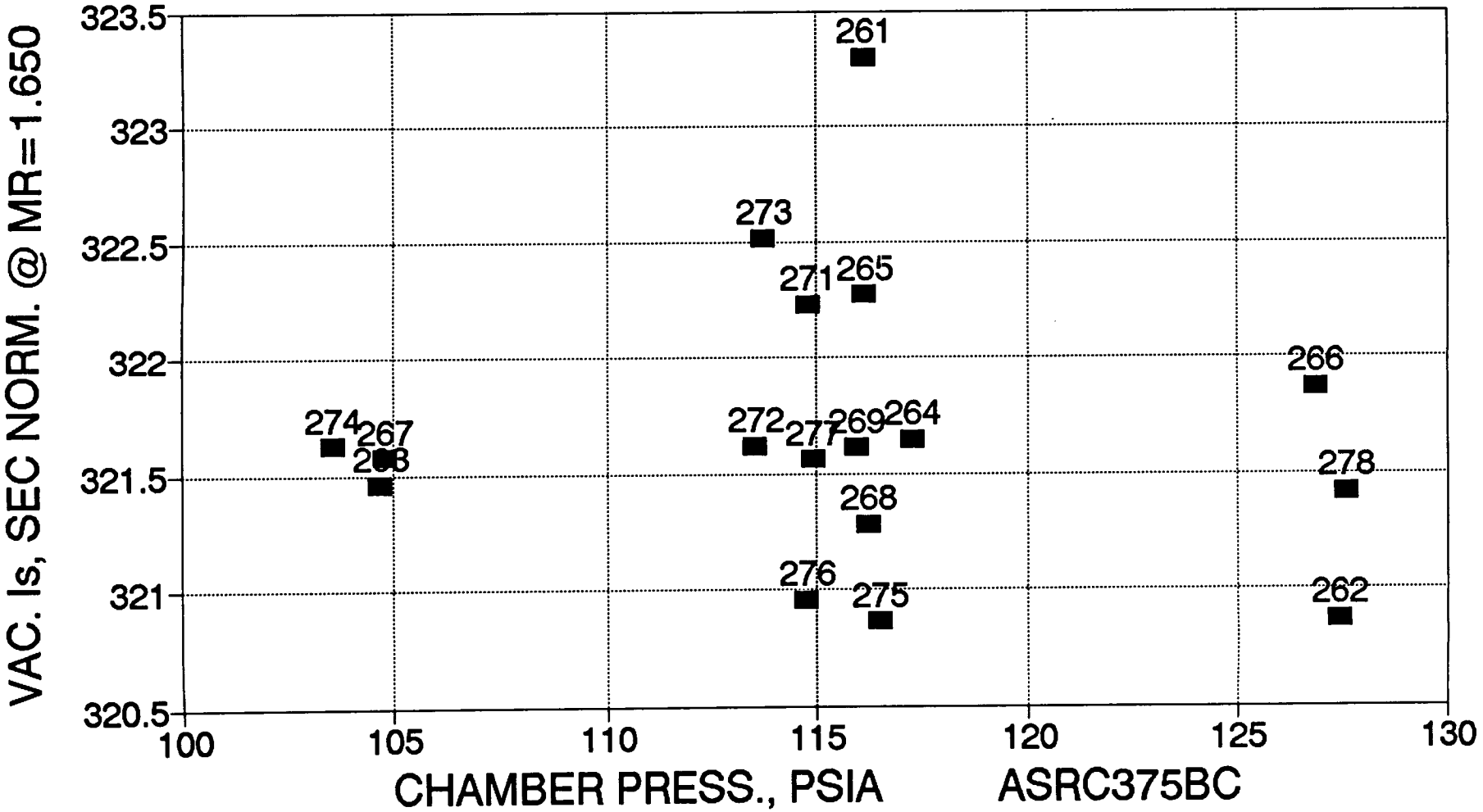

Figure H-8

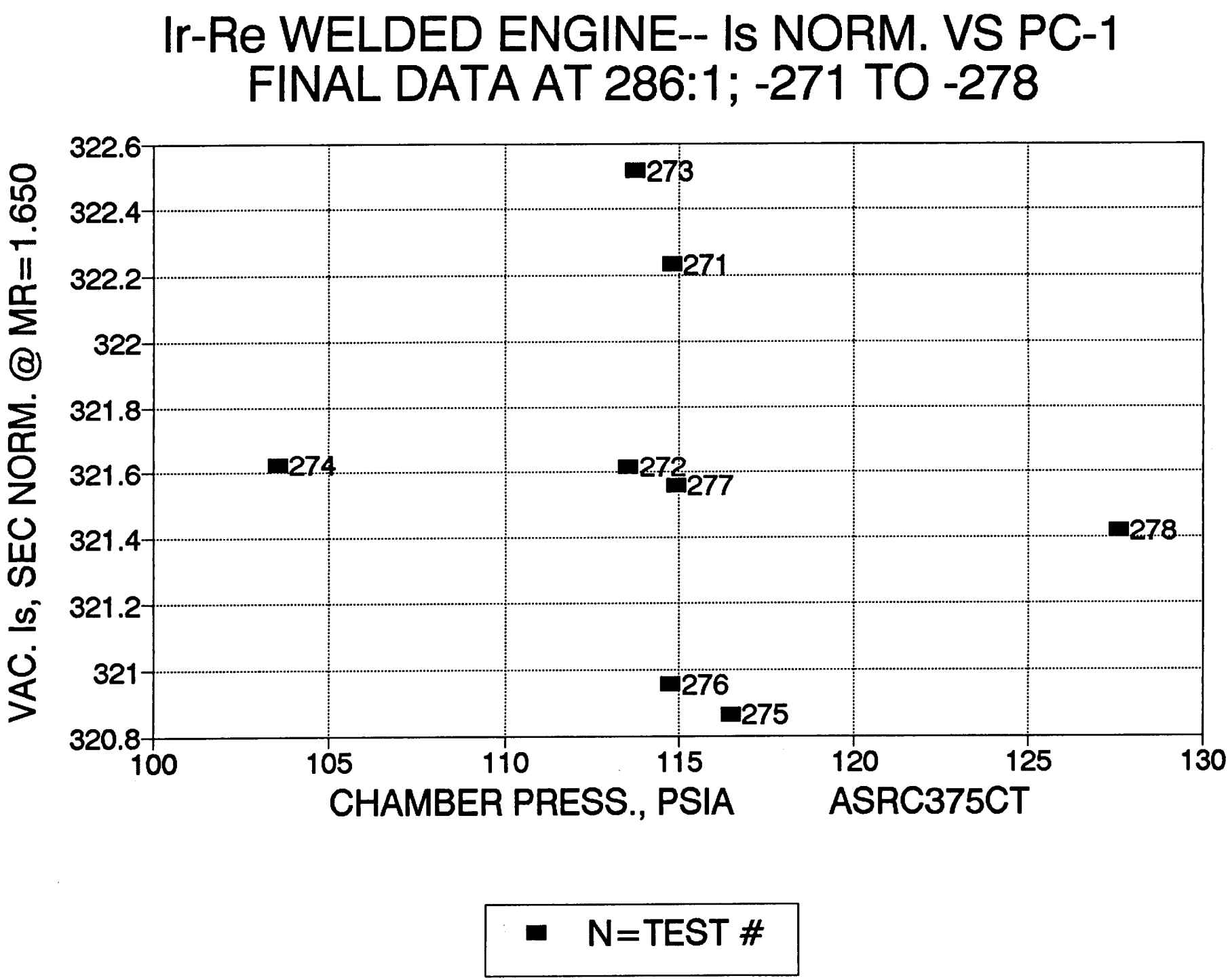
Ir-Re WELDED ENGINE-- Is NORM. VS PC-1
FINAL DATA AT 286:1; -271 TO -278
VAC. Is, SEC NORM. @ MR=1.650
322.6
322.4
322.2
322
321.8
321.6
321.4
321.2
321
320.8
273
271
274
272
277
278
276
275
100
105
110
115
120
125
130
CHAMBER PRESS., PSIA
ASRC375CT
N=TEST #

Figure H-9

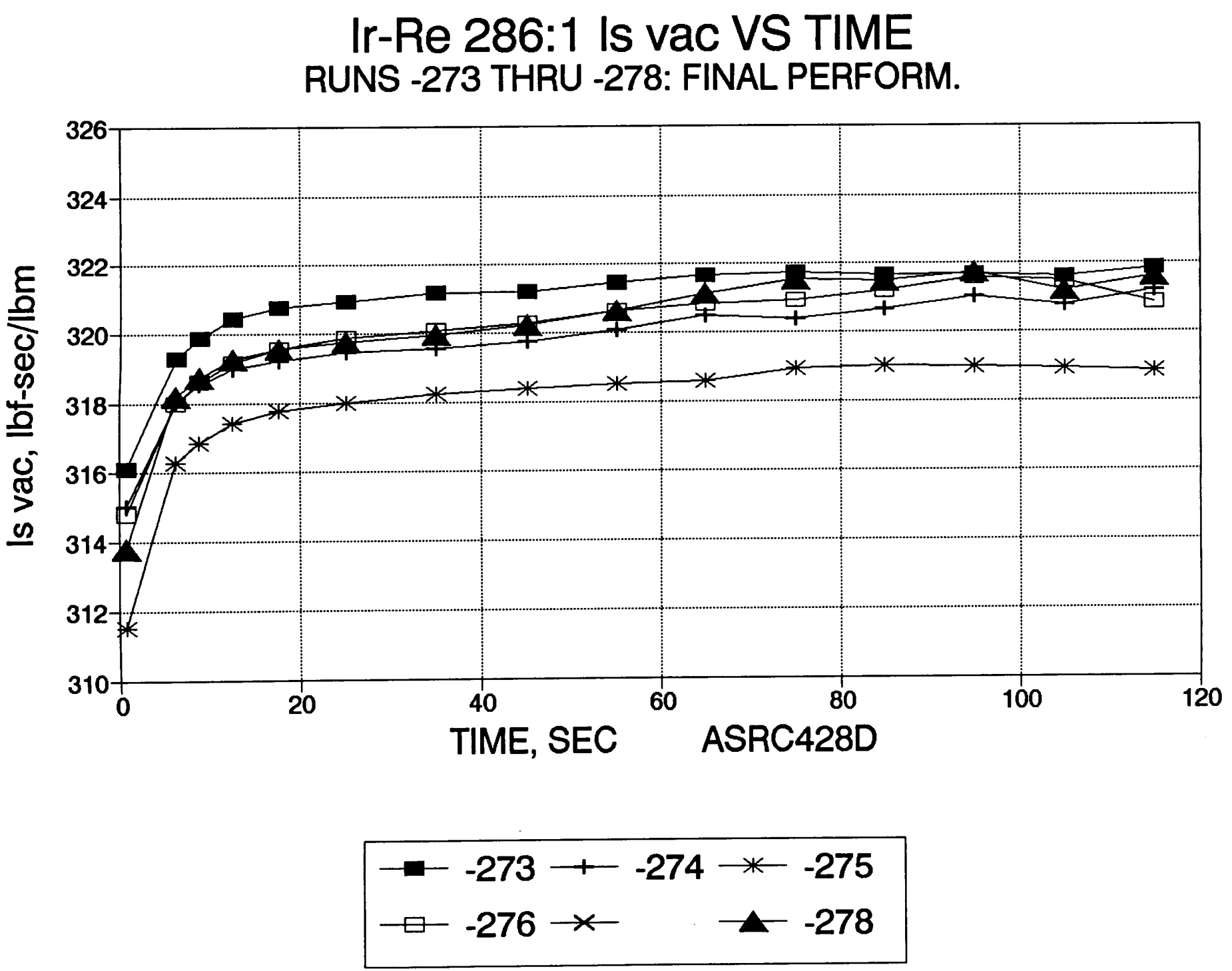
Ir-Re 286:1 Is vac VS TIME
RUNS -273 THRU -278: FINAL PERFORM.
Is vac, lbf-sec/lbm
326
324
322
320
318
316
314
312
310
0
20
40
60
80
100
120
TIME, SEC
ASRC428D
-273
-274
-275
-276
-278

Figure H-10

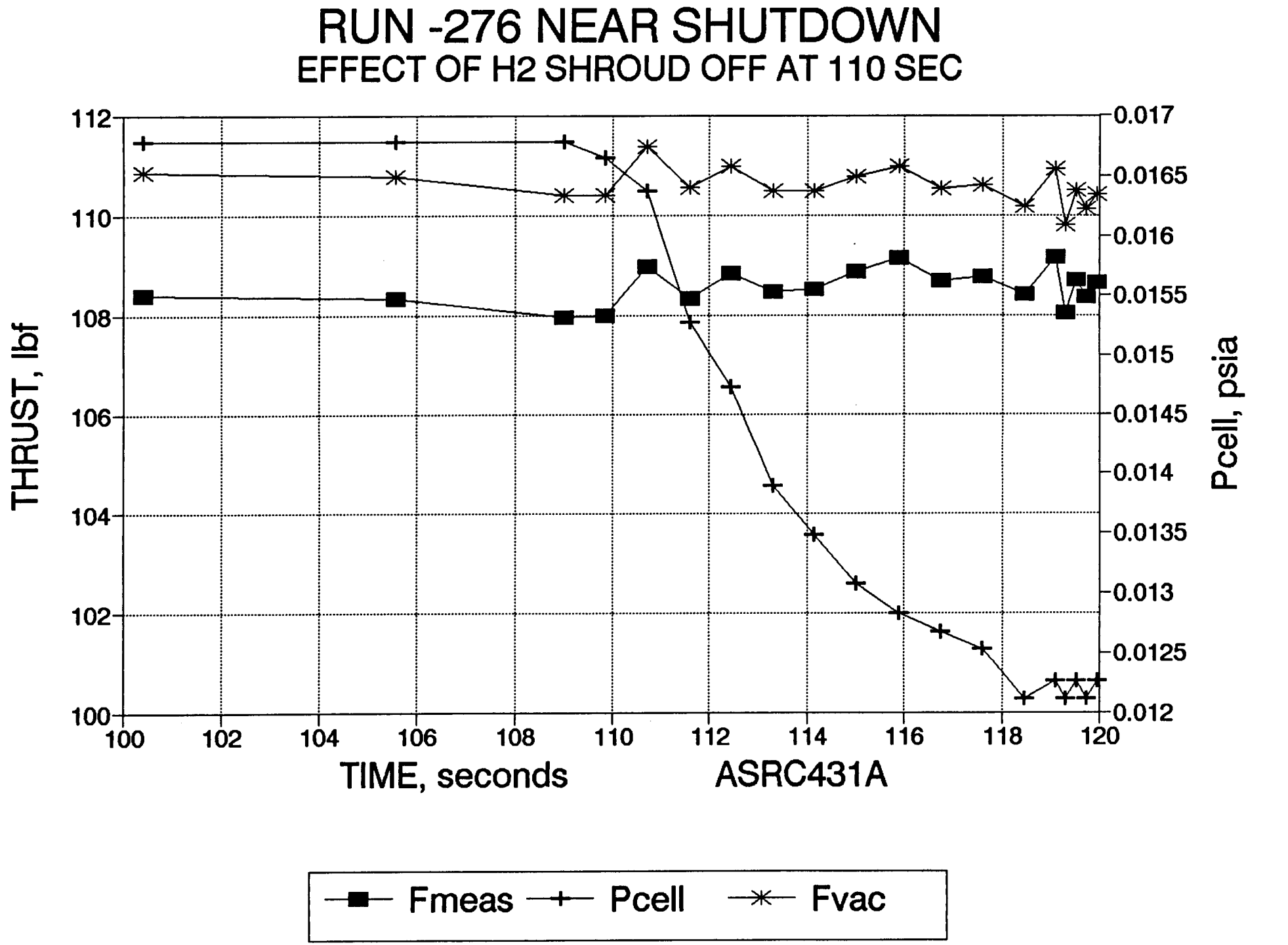
RUN -276 NEAR SHUTDOWN
EFFECT OF H2 SHROUD OFF AT 110 SEC
THRUST, lbf
Pcell, psia
TIME, seconds
ASRC431A
112
110
108
106
104
102
100
0.017
0.0165
0.016
0.0155
0.015
0.0145
0.014
0.0135
0.013
0.0125
0.012
100
102
104
106
108
110
112
114
116
118
120
Fmeas
Pcell
Fvac

Figure H-11

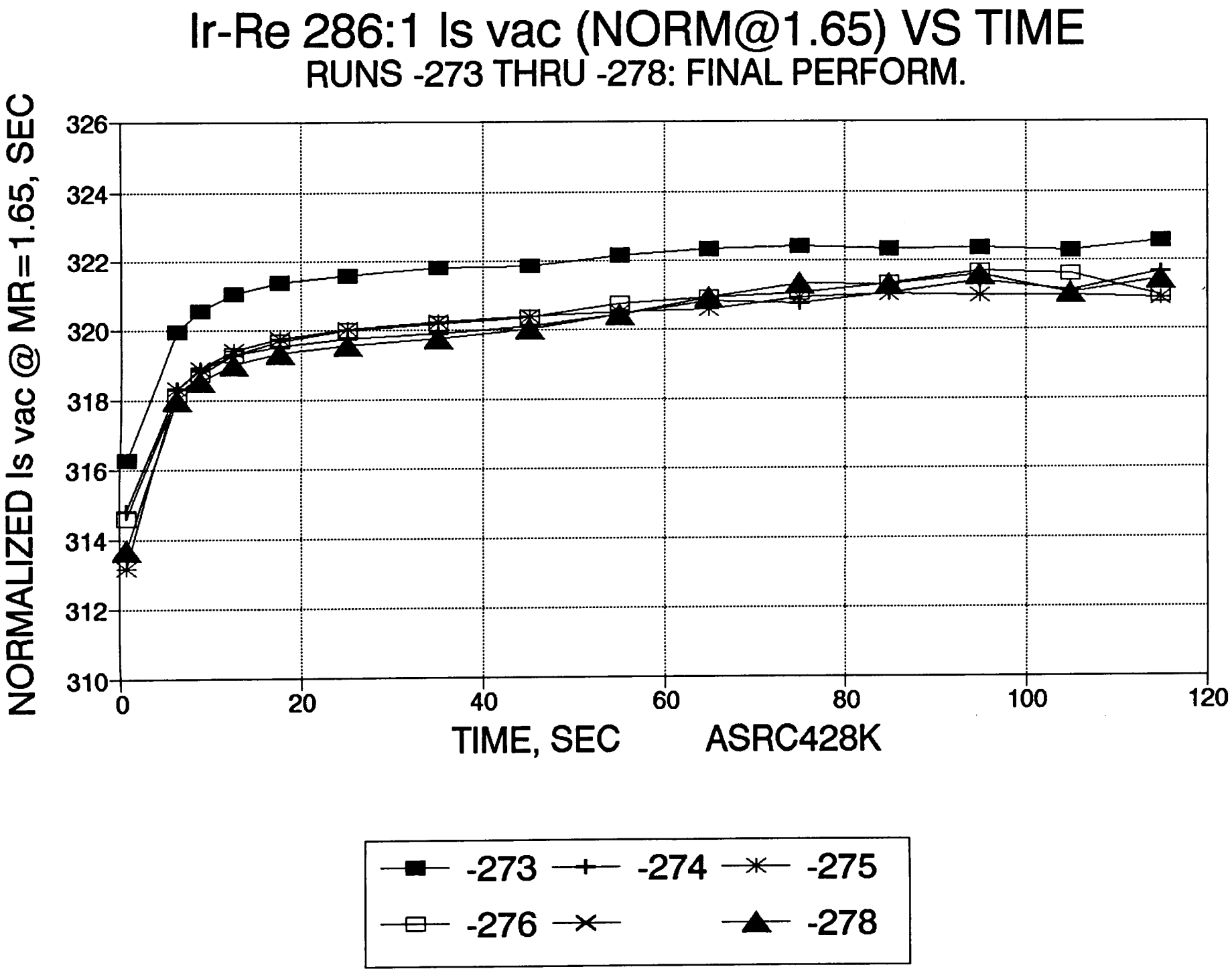
Ir-Re 286:1 Is vac (NORM@1.65) VS TIME
RUNS -273 THRU -278: FINAL PERFORM.
NORMALIZED Is vac @ MR=1.65, SEC
326
324
322
320
318
316
314
312
310
0
20
40
60
80
100
120
TIME, SEC
ASRC428K
-273
-274
-275
-276
-278

Figure H-12

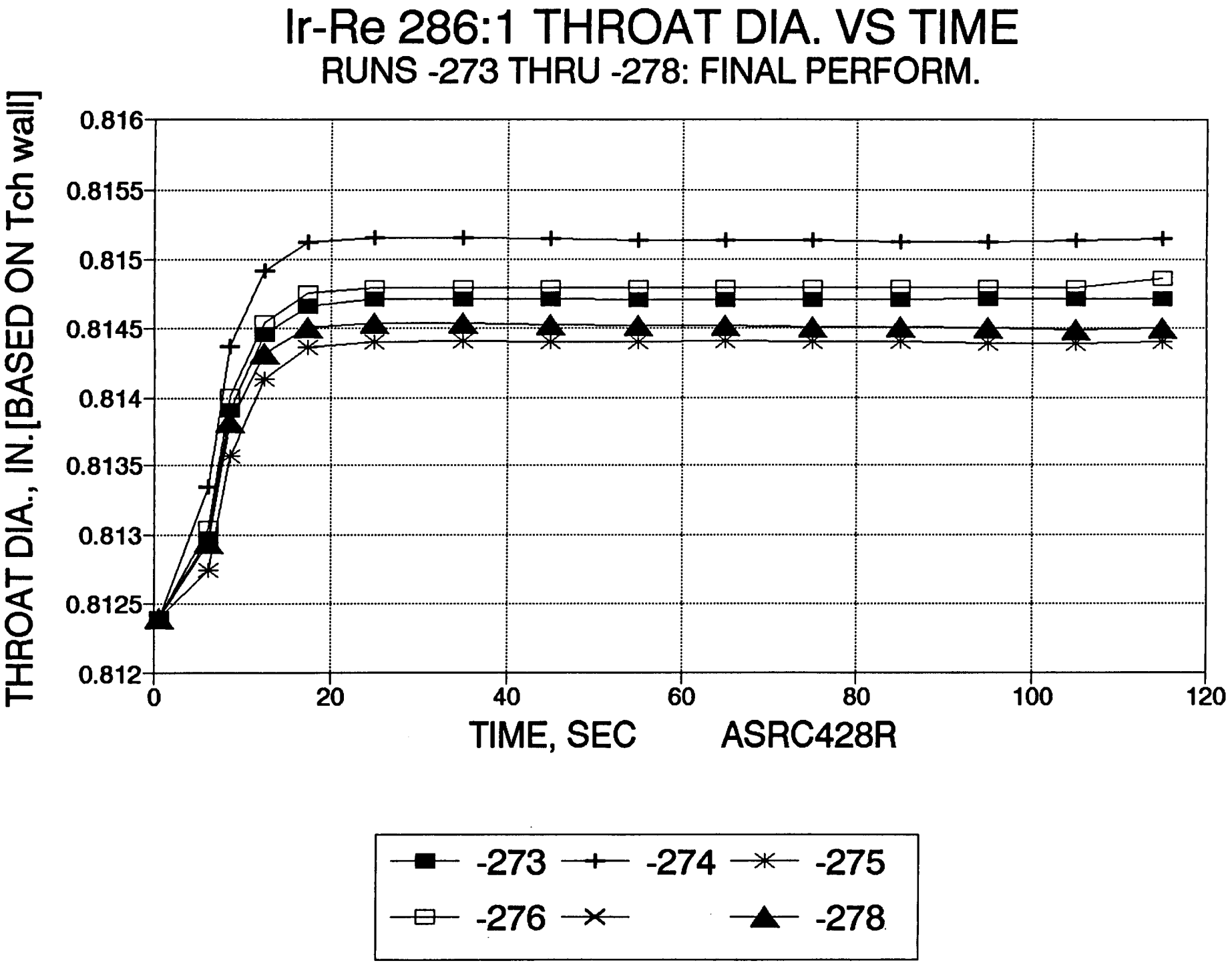
Ir-Re 286:1 THROAT DIA. VS TIME
RUNS -273 THRU -278: FINAL PERFORM.
THROAT DIA., IN.[BASED ON Tch wall]
0.816
0.8155
0.815
0.8145
0.814
0.8135
0.813
0.8125
0.812
0
20
40
60
80
100
120
TIME, SEC
ASRC428R
-273
-274
-275
-276
-278

Figure H-13

Ir-Re WELDED THRUSTER-- C* VS MR
FINAL DATA AT 286:1; ALL TESTS

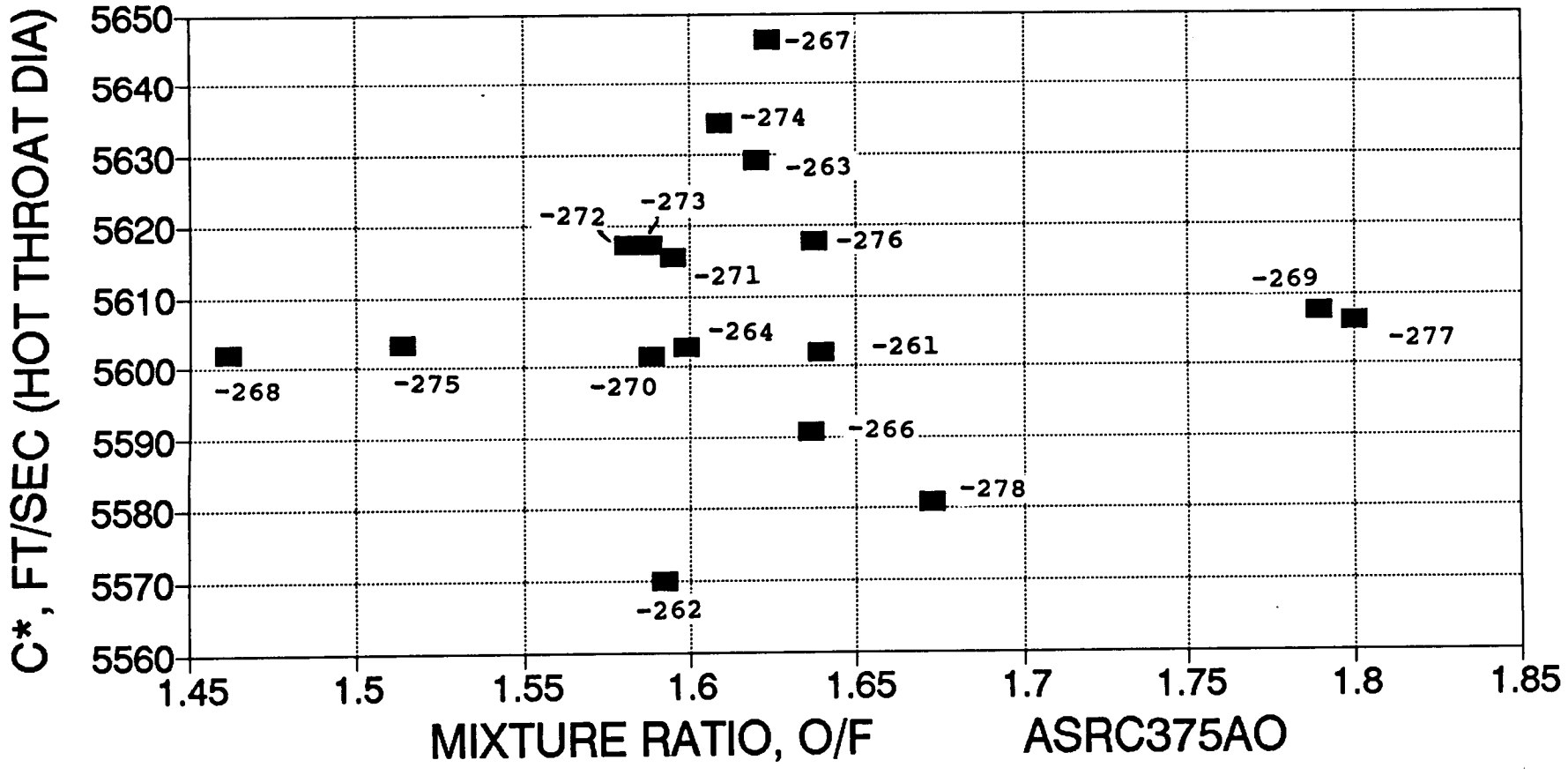

Figure H-14

Ir-Re WELDED THRUSTER--C* VS PC
FINAL DATA AT 286:1; ALL TESTS

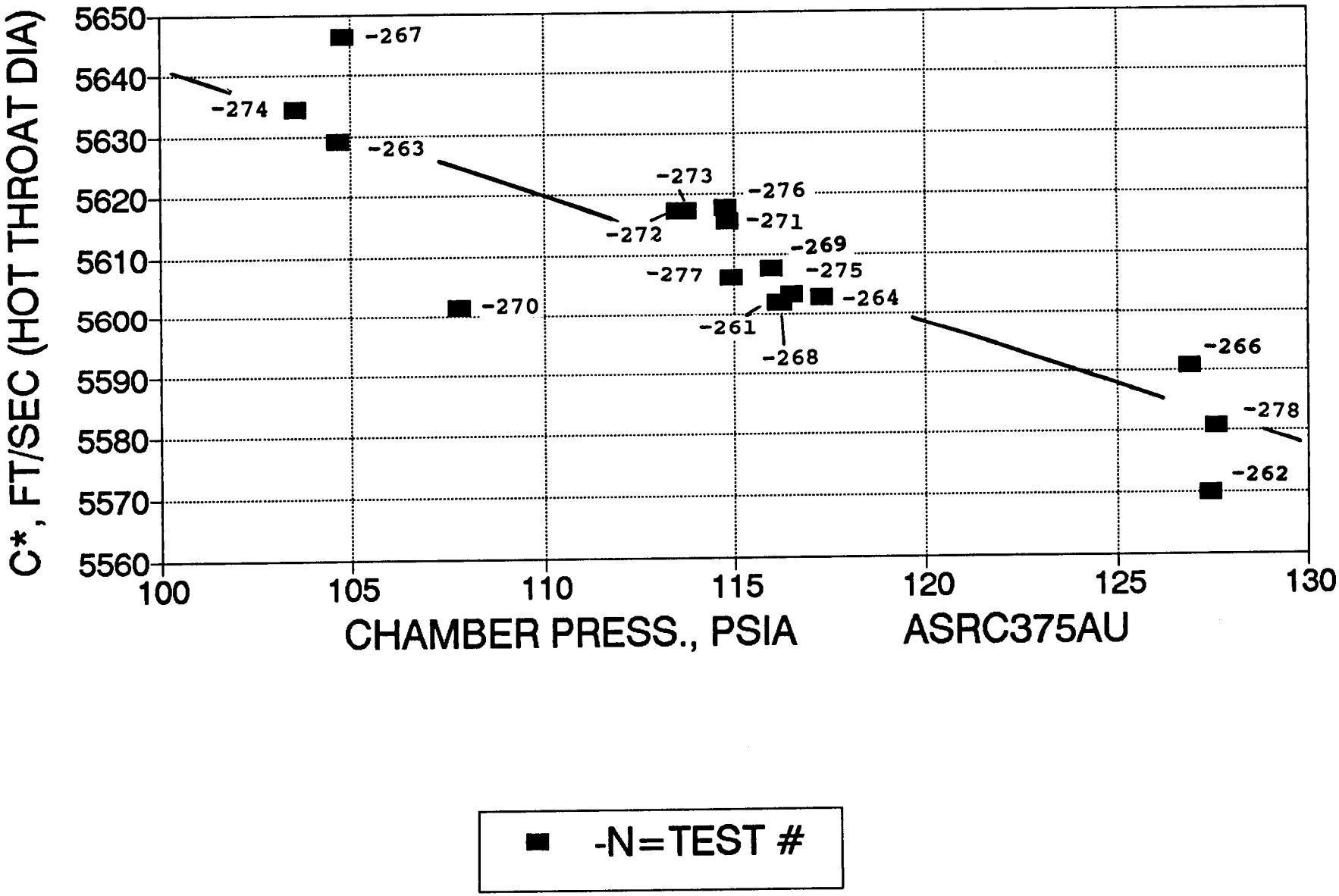

Figure H-15

Ir-Re WELDED THRUSTER-- C* VS MR

FINAL DATA AT 286:1; -271 TO -278

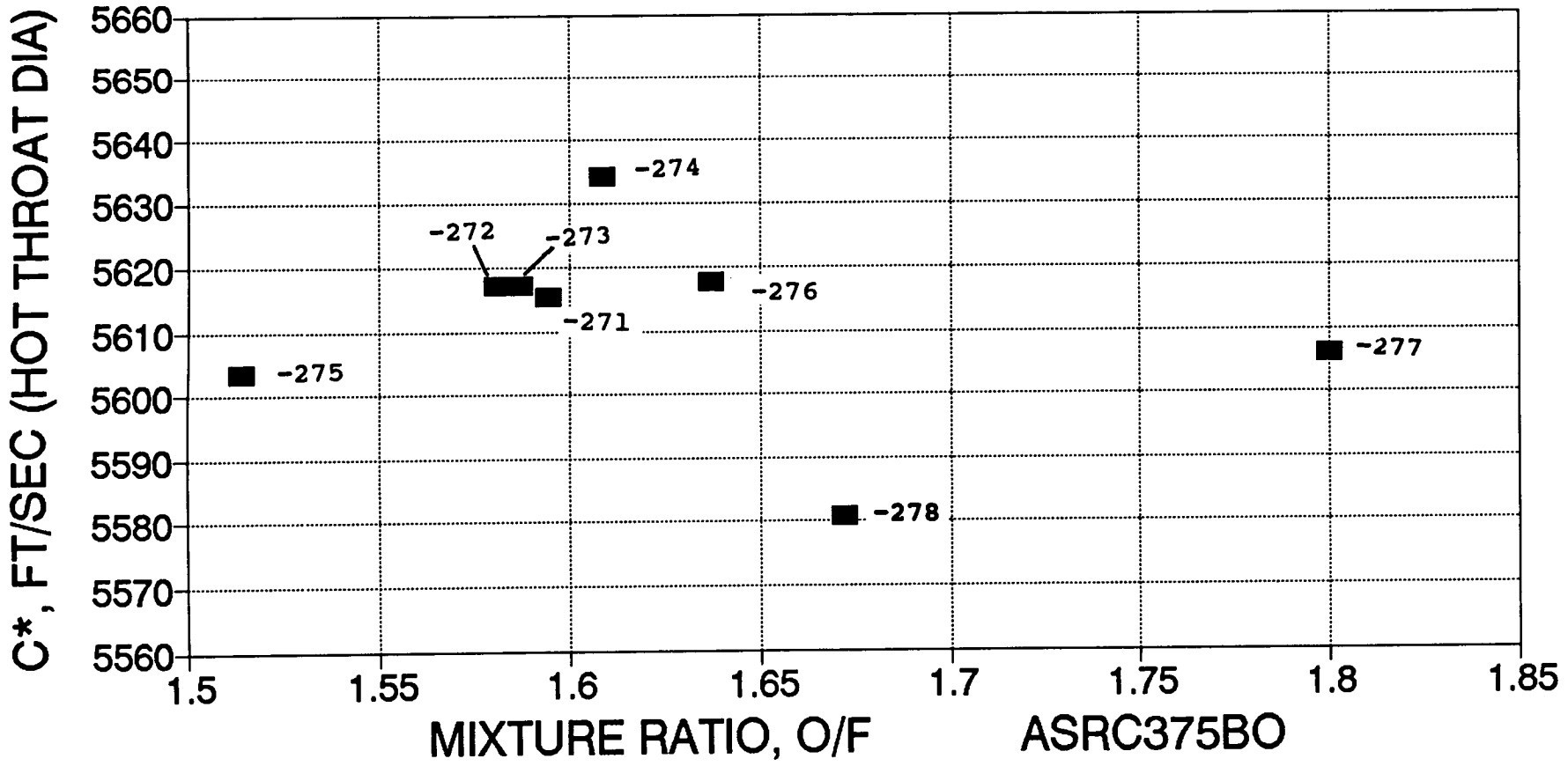

Figure H-16

Ir-Re WELDED THRUSTER--C* VS PC
FINAL DATA AT 286:1; -271 TO -278

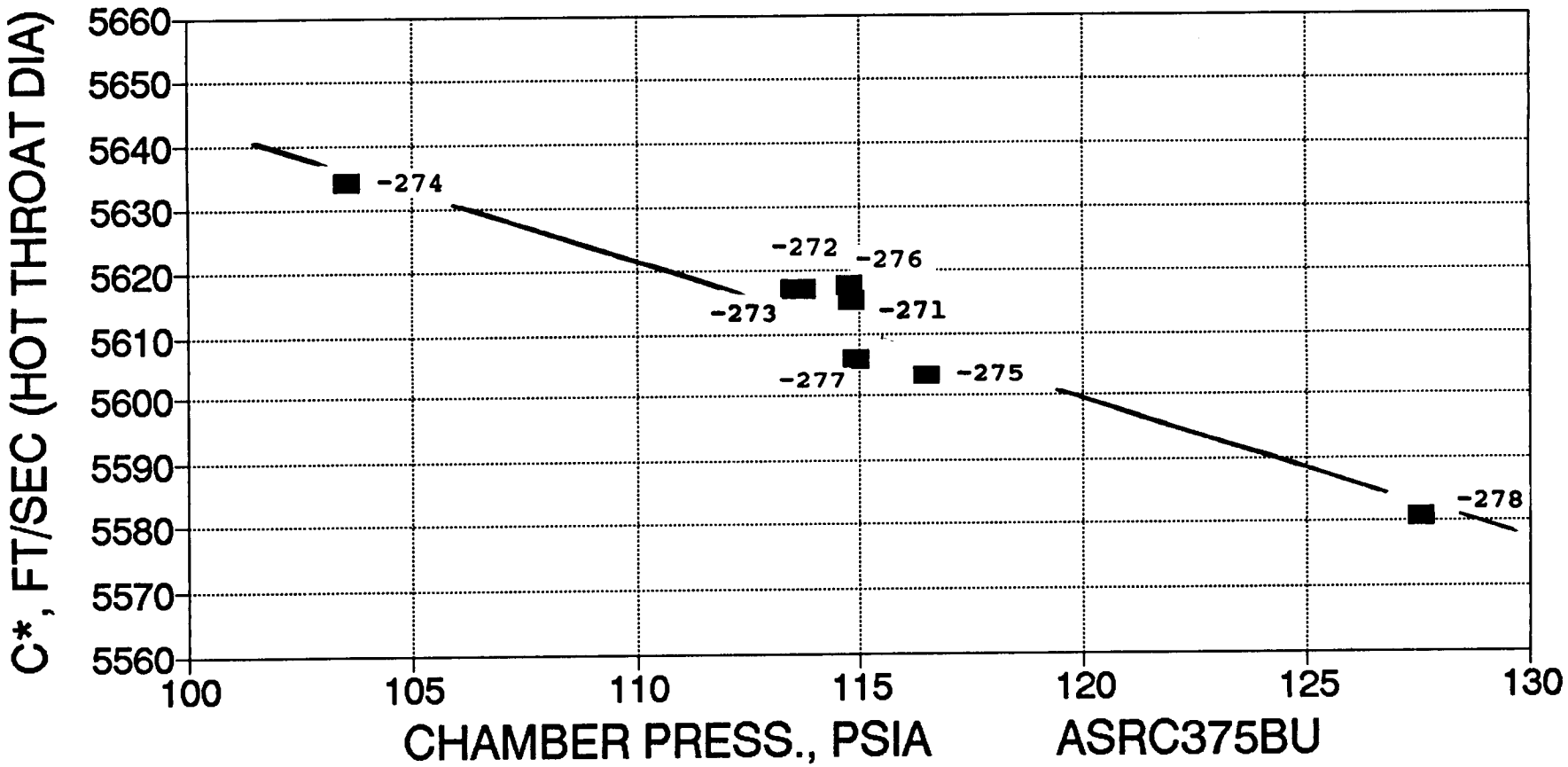

Figure H-17

Ir-Re WELDED THRUSTER--Cf VS MR

FINAL DATA AT 286:1; -271 TO -278

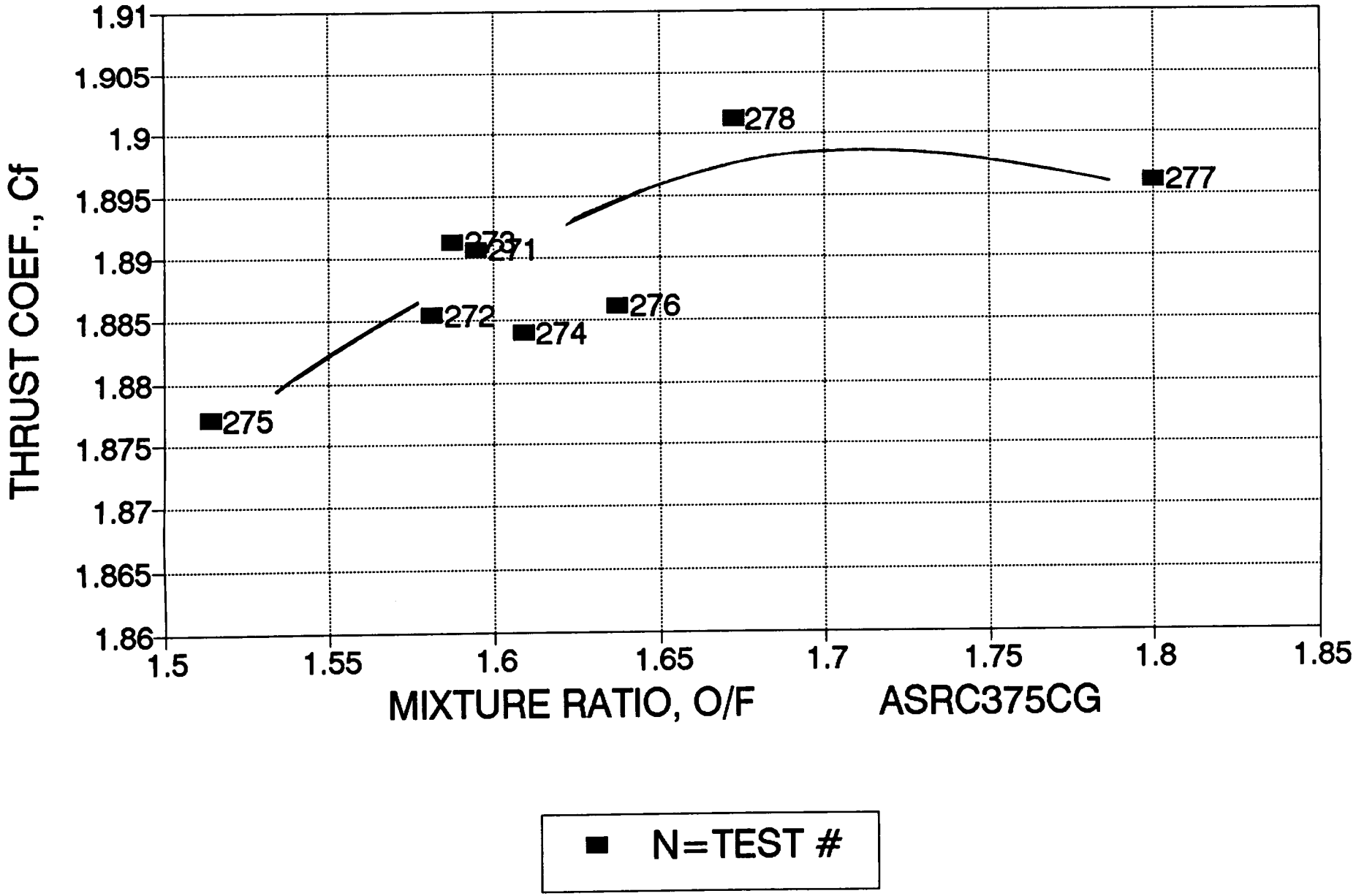

Figure H-18

Ir-Re WELDED THRUSTER--Cf VS Pc

FINAL DATA AT 286:1; -271 TO -278

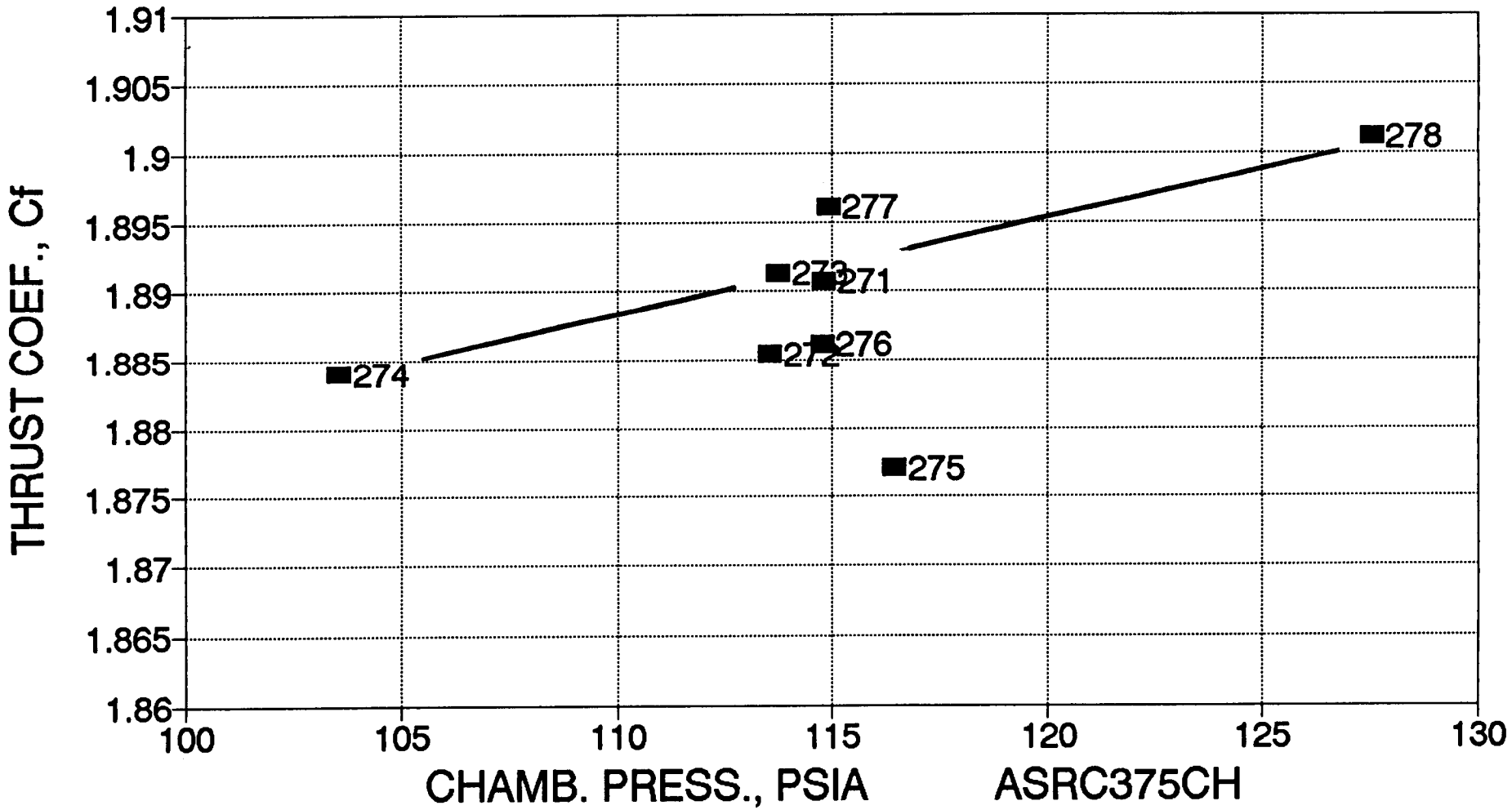

Figure H-19

Ir-Re WELDED ENGINE--Tchamb wall VS MR

FINAL DATA AT 286:1; ALL TESTS

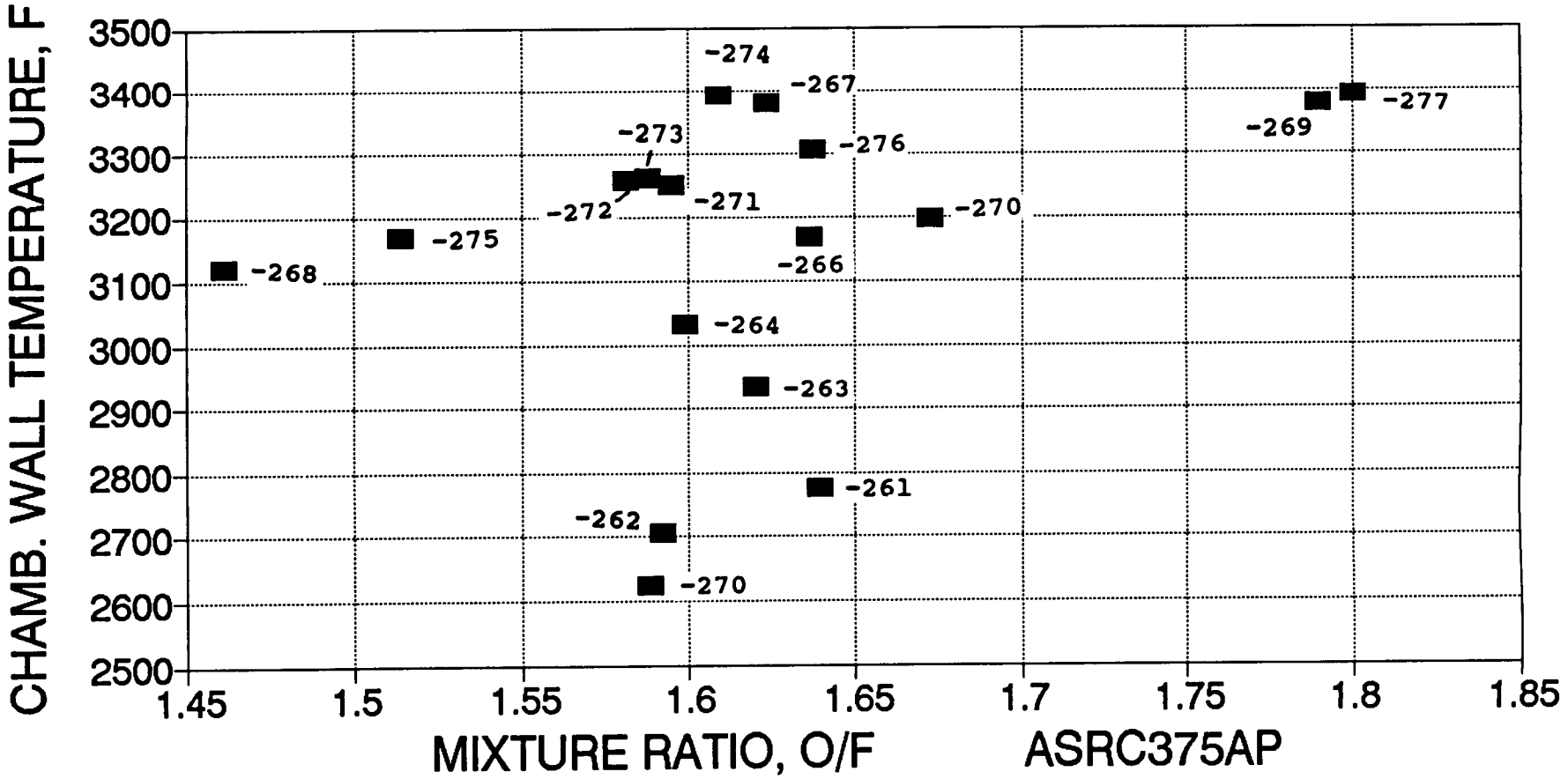

Figure H-20

Ir-Re WELDED ENGINE-Tchamb wall VS PC

FINAL DATA AT 286:1; ALL TESTS

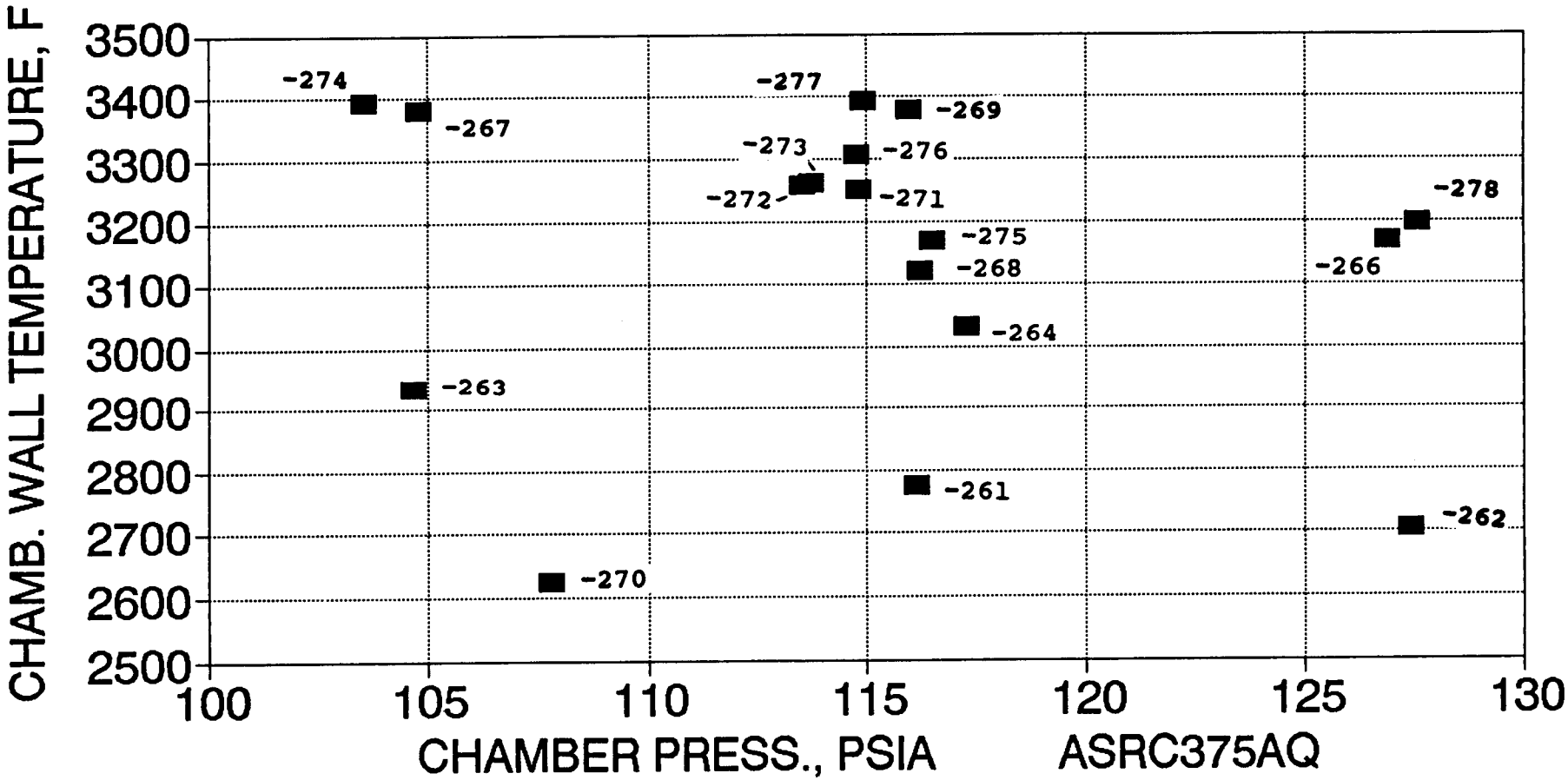

Figure H-21

APPENDIX I

THERMAL DATA

APPENDIX I

THERMAL DATA FOR 286:1 THRUSTER

Temperature measurements for Test -276 are presented here. This test was run for 120 sec at nominal conditions. It differs from other tests in the 286:1 test series in that the hydrogen shroud flow, which is used to protect the exterior of the chamber from oxidation by the recirculating test cell gases, was terminated at 100 sec. This was done to determine the effect the hydrogen flow might have on engine operation. Temperature measurement locations are defined in Figure I-1.

Temperature in and out of the fuel cooled adapter and the fuel temperature rise are plotted in Figure I-2. A log time scale is used to show detail of the temperatures over the 120 sec firing time and 516 sec post fire coast. It should be noted that post test temperatures are measured in the fuel lines and show thermal soak back through the (static) fuel and lines. Fuel delta T is close to a steady value of 140°F but has not quite reached equilibrium at 120 sec. Soak back temperature on the fuel inlet rises after the test; it has not reached a steady value at the end of the 516 sec coast.

Ambient cell temperature and Moog bipropellant valve body temperature are shown in Figure I-3. The valve body temperature is rising throughout the test. Part of this is a delayed response to heating of the valve mass by the heated fuel passing through it. Some of the temperature rise is due to the electrical heating of the valve (approximately 30W) from the energized coil. In these short duration tests, the valve was operated at a constant 28 VDC. In long duration tests, the valve will be opened at 28 VDC and then held at reduced voltage (10 VDC); this reduces the electrical input to about 4W. Valve body temperature peaks at 180°F during the firing, falls off to 153°F because the direct heat input from the fuel and coil have been removed. It then starts to rise again at about 130 sec into the coast, rising to 169°F at the end of the coast.

Test cell temperature, measured on a 0.032 dia thermocouple in free air behind the engine valve rose to about 184°F at 100 sec when the H_2 shroud flow was stopped. It then rose to 193 by 120 sec (FS-2). It then rose rapidly when the diffuser unloaded after shutdown, reaching a peak of 222°F at 124 sec.

Temperature of the injector body (TJB) and valve-to-injector adapter plate are shown in Figure I-4. The injector body temperatures reach a steady value in the 230°F range at shutdown, dip and then rise to a maximum of about 260°F before the end of

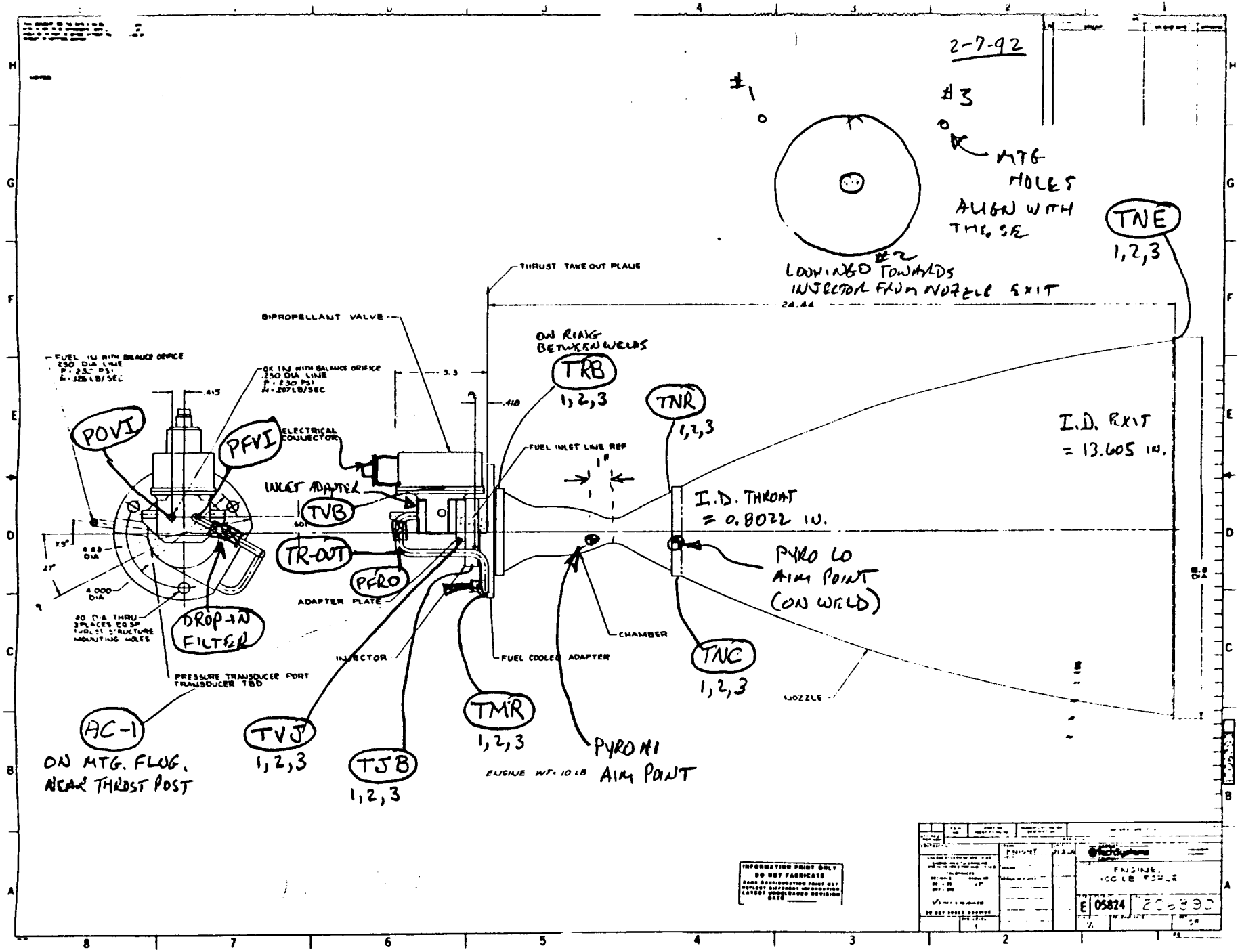

Figure I-1. Instrumentation Locations For 286:1 490N Welded Thruster

THRUSTER TEMPERATURE VS TIME

TEST -276

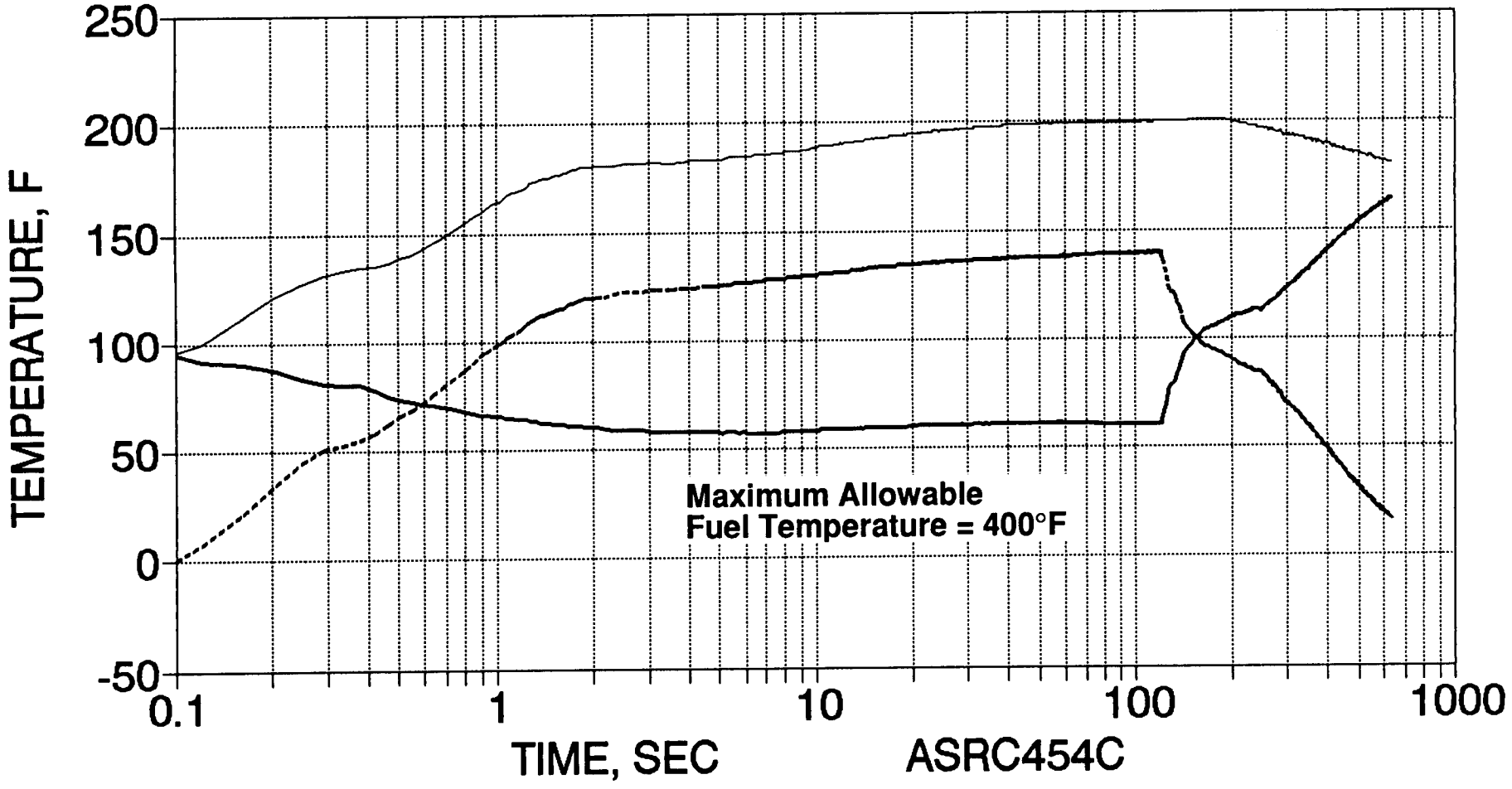

Figure I-2. Thruster Temperature vs Time - Test -276

VALVE AND FACILITY TEMPS. VS TIME

TEST -276

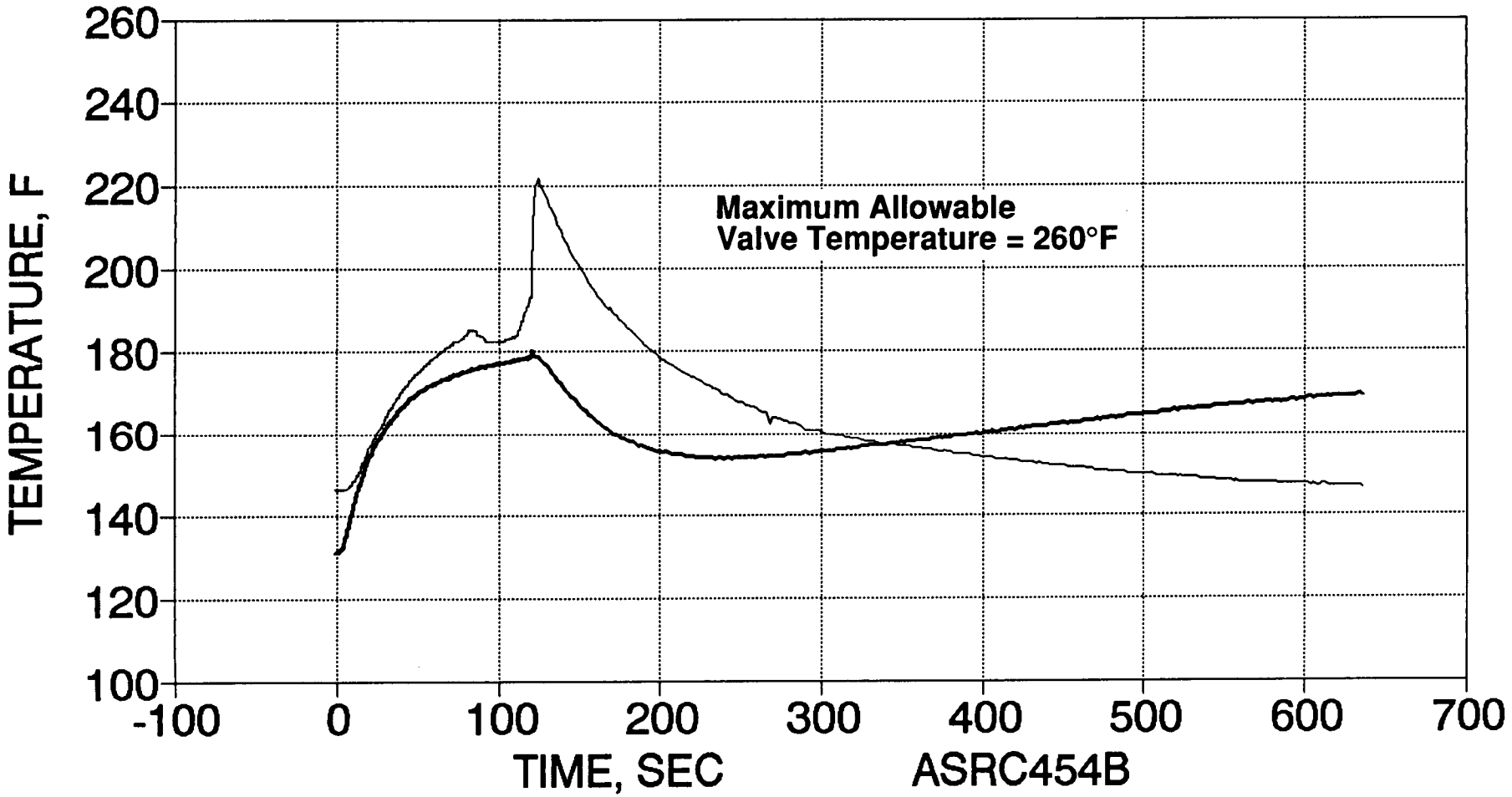

Figure I-3. Valve and Facility Temperature vs Time - Test -276

THRUSTER TEMPERATURE VS TIME

TEST -276

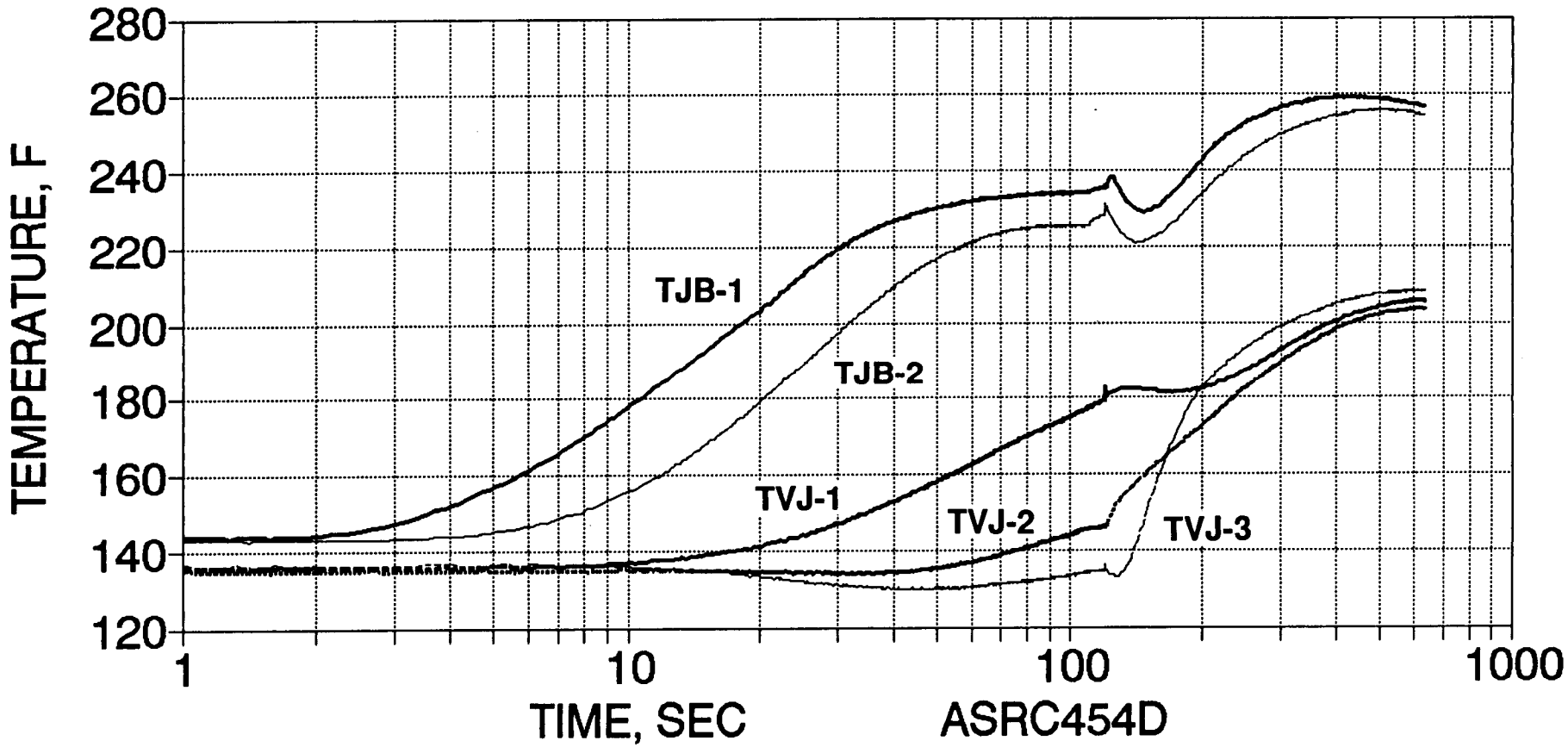

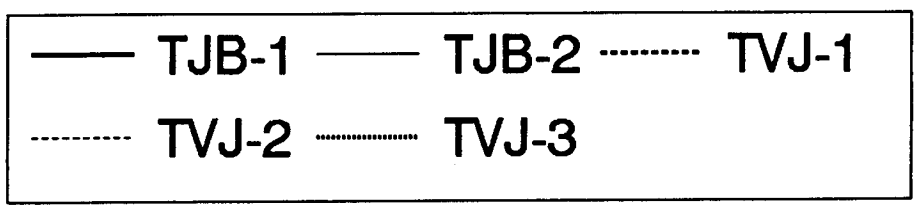

Figure I-4. Thruster Temperature vs Time - Test -276

THRUSTER TEMPERATURE VS TIME

TEST -276

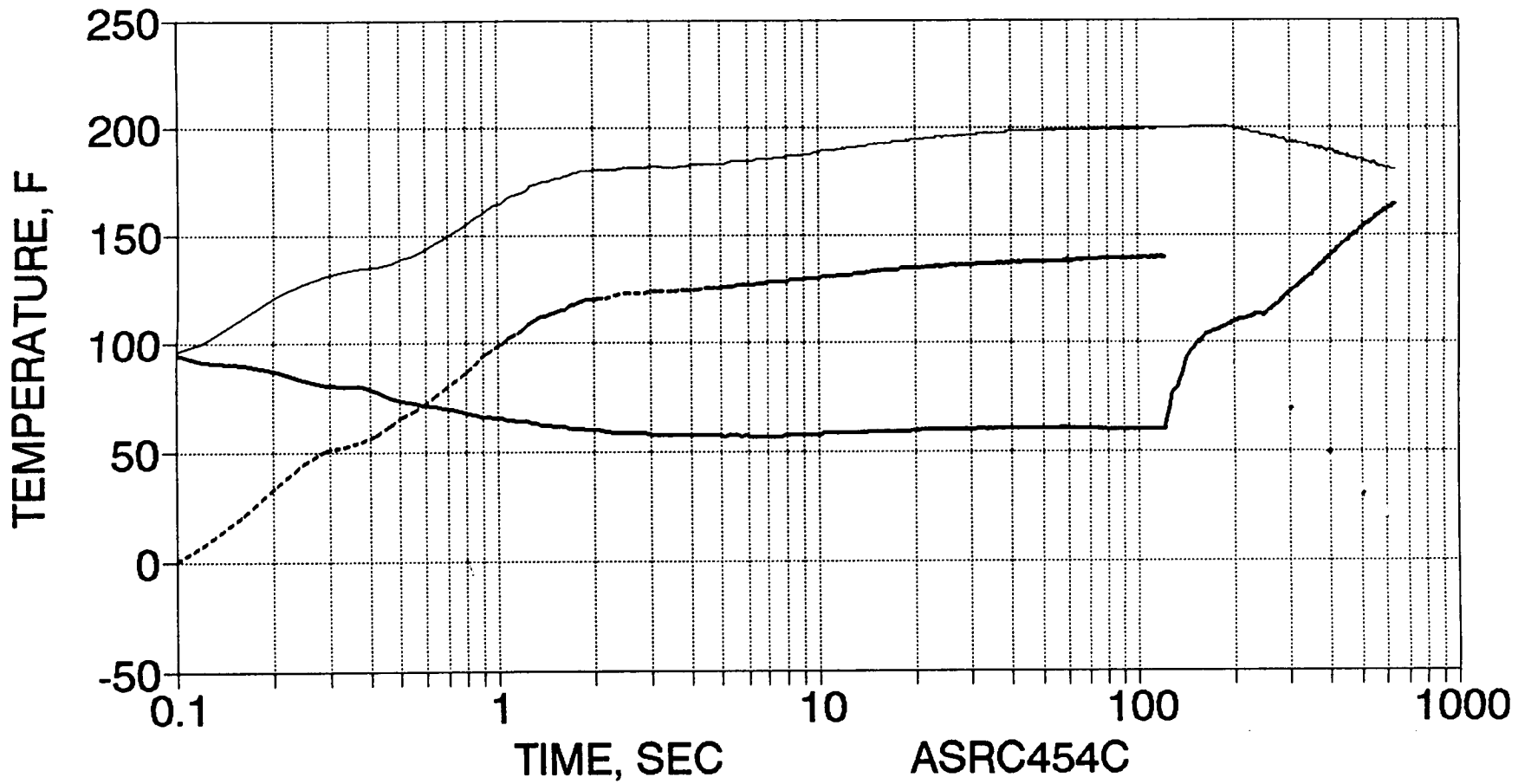

coast. The three adapter plate temperatures show a wider spread during the firing, which depends on the proximity to the fuel circuit. The maximum value reached during the firing was about 180°F and rising (maximum fuel temperature was 200°F). The temperatures reached a maximum of about 210°F at the end of coast.

Temperatures of the exterior of the cooled adapter between the stainless-to-stainless welds (TRB) and temperatures at the mounting flange holes (TRM) are shown in Figure I-5. Again, these temperatures are biased depending on their location relative to fuel inlet (cooler) or outlet (hotter). The mounting point temperatures start at the hot restart temperature of about 150°F and generally fall during the test to between 85 and 125°F. Post test they reach a maximum near the end of coast of about 260°F. The cooled adapter body cools initially from the hot restart temperature of 150°F and then rises to a maximum of about 290°F at FS-2. It then rises to a maximum of 336°F at 40 sec into the coast and then steadily falls.

Temperatures on the chamber outer wall and on the nozzle are shown in Figure I-6. Chamber wall temperature measured with a two-color optical pyrometer (gray body scale) rises to a steady value of 3288°F in about 24 sec. Chamber temperature rises an additional 28°F to 3316°F when the shroud hydrogen flow is terminated at 110 sec. The nozzle temperatures are measured near the Re-to-C-103 transition joint with type K thermocouples. TNR-1 and -3 are on the Re; they reach a maximum value of about 2130°F at 33 sec. The C-103 skirt temperature at the weld adaption is monitored with TNC-2 and -3. They reach steady values of 1855°F for TNC-2 and 1630°F for TNC-3 at 41 sec. TNC-2 shows a 25°F drop in temperature when the H_2 shroud flow is stopped.

These thermal data obtained for the 286:1 thruster at design conditions show that it has satisfactory thermal margins for all components. The margin on valve temperature is 90°F; the maximum fuel temperature is about 200°F below the design allowable of 400°F. Rhenium chamber temperature is running 700°F below the previously demonstrated long term operating temperature of 4000°F. The C-103 nozzle maximum temperature is about 800°F below the maximum allowable temperature of 2500°F. The overall demonstrated thermal margin for the 286:1 engine is excellent.

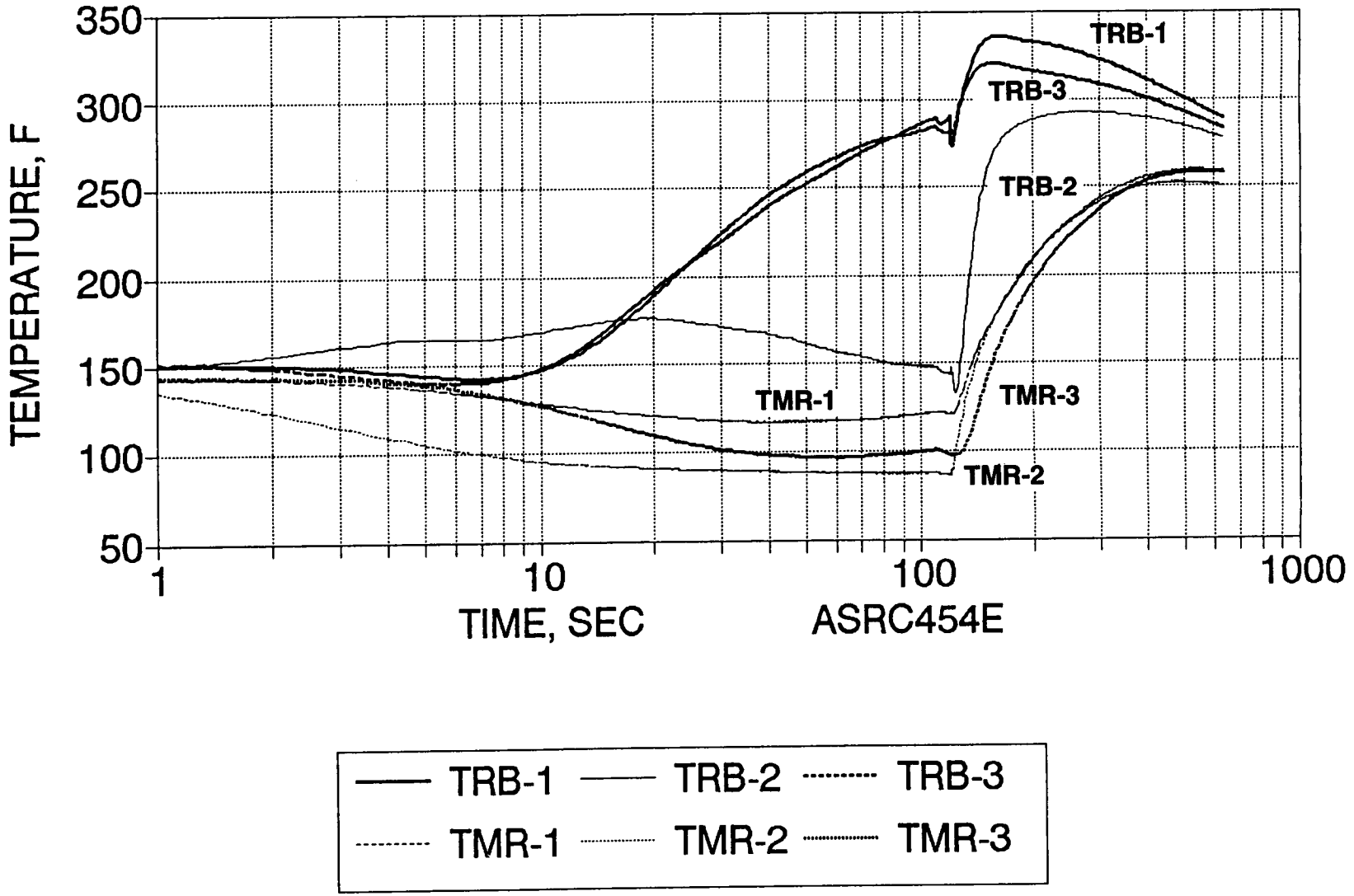

Figure I-5. Thruster Temperature vs Time – Test-246

THRUSTER TEMPERATURE VS TIME

TEST -276

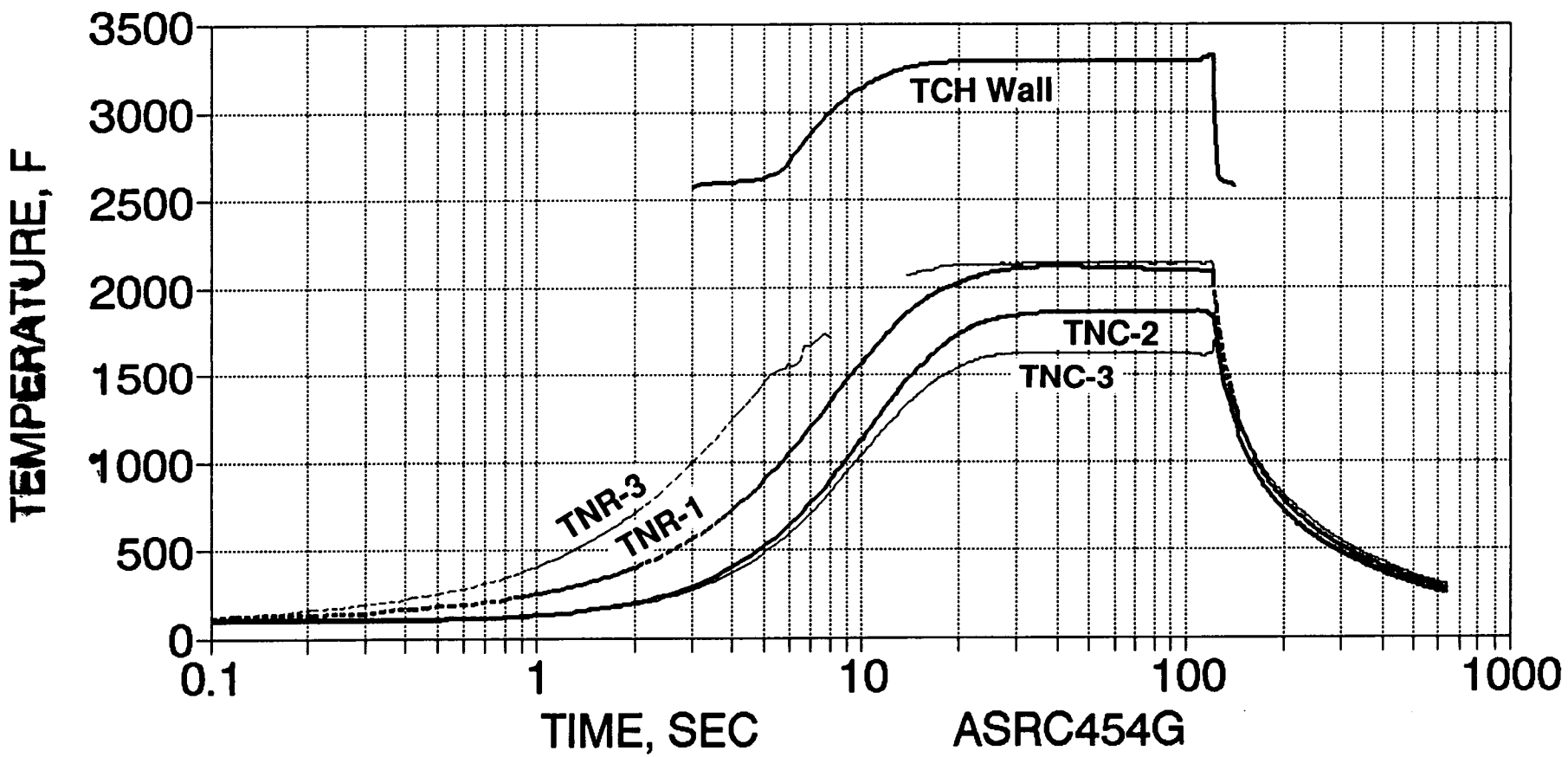

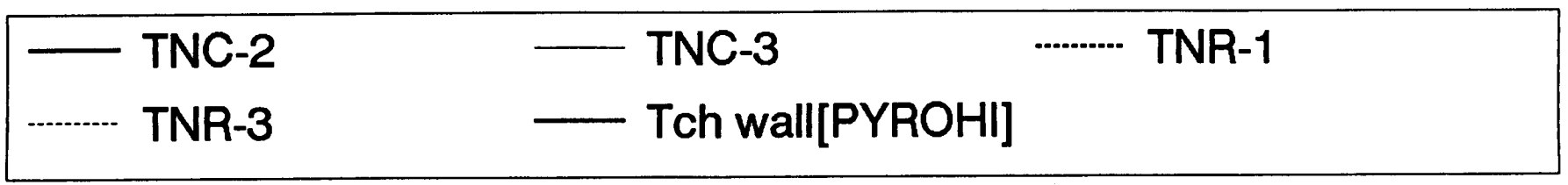

Figure I-6. Thruster Temperature vs Time - Test -276

APPENDIX J

TEST FACILITY AND INSTRUMENTATION

Some characteristics of the Bay A-2 altitude test facility are shown in this appendix, for the system as set up for testing of the 286:1 welded Ir-Re chamber, in tests KGH3-D01-0A-259 through KGH3-D01-OA-278. In these tests the cell was equipped with the 16 in. second throat water cooled diffuser (1203664).

A detailed instrumentation list was presented in Table 6.3-6.

Thrust was measured with the 100 lbf steady state stand using a dual output calibration cell and a single output measuring cell.

Thrust bias for the test stand, defined as (actual thrust)/(indicate thrust), is measured immediately before and after each test. The test stand is loaded directly through the calibration cell by a pneumatic actuator, in a series of force steps which bracket the planned thrust level. It is necessary that the force ratio, the bias, be precisely repeatable; by design, the value is very close to 1.000. The value must not shift with time, either over the minutes of a firing or the days of a test campaign. The pre and post test thrust bias for the performance test series is shown in Figure J-1 with the calculated 3 sigma range of the measurements, which is ± 0.1%.

Propellant flow was measured with three types of flow meters, positive displacement flow meters, (PDFM's), turbine and Micromotion vibrating tube meters. The PDFM's were used for test durations of up to 25 sec. The other meters were used for all test durations. Redundant turbine meters were used. These were calibrated with propellant using the PDFM's as standards in tests - 261 through -269. The standardized turbine flow meter data were then used for propellant flow measurement in all tests.

The Micromotion flow meters were run in series with the other meters as part of an evaluation of their operation, under test conditions. Although not used for data reduction, their output, which is direct mass flow, has been compared to the mass flow computed from the turbine meter volume flow measurements and propellant density measurements based on temperature and pressure corrections. The percent difference between the oxidizer Micromotion and turbine flow meters is very small throughout the tests, about ±.05%, as shown in shown Figure J-2. The fuel meters show the same order of agreement except for test -274 where the Micromotion is very consistently 0.96% lower than the turbine flow meters as shown in Figure J-3. This difference for this one test has not been explained. Both turbine and Micromotion flow meters have their own

idiosyncrasies, unique electronics and error/failure modes. However, the general agreement of the Micromotion meters with the turbine meters, plus their lack of bearings and wearing parts gives hope that they can replace the less reliable turbine meters.

Cell pressure (nozzle ambient pressure) was measured with two 0-1 psia straingage transducers and two 0-10,000 micron Baratron transducers.

During some test shutdowns, the thermal pulse as the cell repressurized was sufficient to cause a zero shift in the Baratron pressure sensors. The magnitude of these shifts was determined from pre and post test calibrations and the cell pressure data were corrected accordingly. As a check on the correction, the correlation between cell pressure and chamber pressure was made, as shown in Figure J-4. The deviation of the correlation corresponds to a 3σ error of calculated vacuum thrust of less than $\pm 0.1\%$.

A complete error analysis of the performance data is included in Appendix G.

The diffuser operated satisfactorily in all tests; its maximum capability is in excess of 120 sec operation at 100 lbf engine flows with the 286:1 nozzle. The cell pressure versus time for the long duration tests is shown in Figure J-5. The difference in operating pressures is related to the difference in thruster flow rates. The abrupt drop in cell pressure at the end of run-276 is the result of turning off the hydrogen shroud flow used to protect the thruster exterior from reaction with the residual gases in the cell.

The diffuser pressure recovery ratio, defined as the ratio of cell pressure to diffuser exit pressure, is shown in Figure J-6. The ratio increases as the exhaust flow must be pumped from the fixed, low cell pressure to the higher, and rising diffuser exit pressure. The effect of stopping the hydrogen shroud flow is evident in this plot. At some higher exit pressure, or more precisely, larger ratio of exit to cell pressure, the diffuser will breakdown and pumping will cease. The data from test -276 show that this will occur at pumping ratios of greater than 65:1.

One concern of long duration altitude testing is continual heating of the ambient cell environment, by recirculating hot gas and/or thruster thermal radiation. The cell ambient temperature versus time in the 120 sec tests is shown in Figure J-7. This temperature is measured with a .0625 dia sheathed thermocouple in the space behind

the engine thrust mount, shielded from direct radiation. As can be seen, the temperature was close to steady state, after relatively modest temperature rise of 30 to 50 F. Note that hot starts had approximately the same thermal rise as cold starts, indicating that for very long test times, the slow climb at 120 sec will reach at least the values seen in the hot start tests. No evidence of pre-and post test thermal effect on stand zero or bias was seen in the 120 sec tests. Data from tests up to 650 sec duration gave no evidence of thermal effects on the thrust measurements.

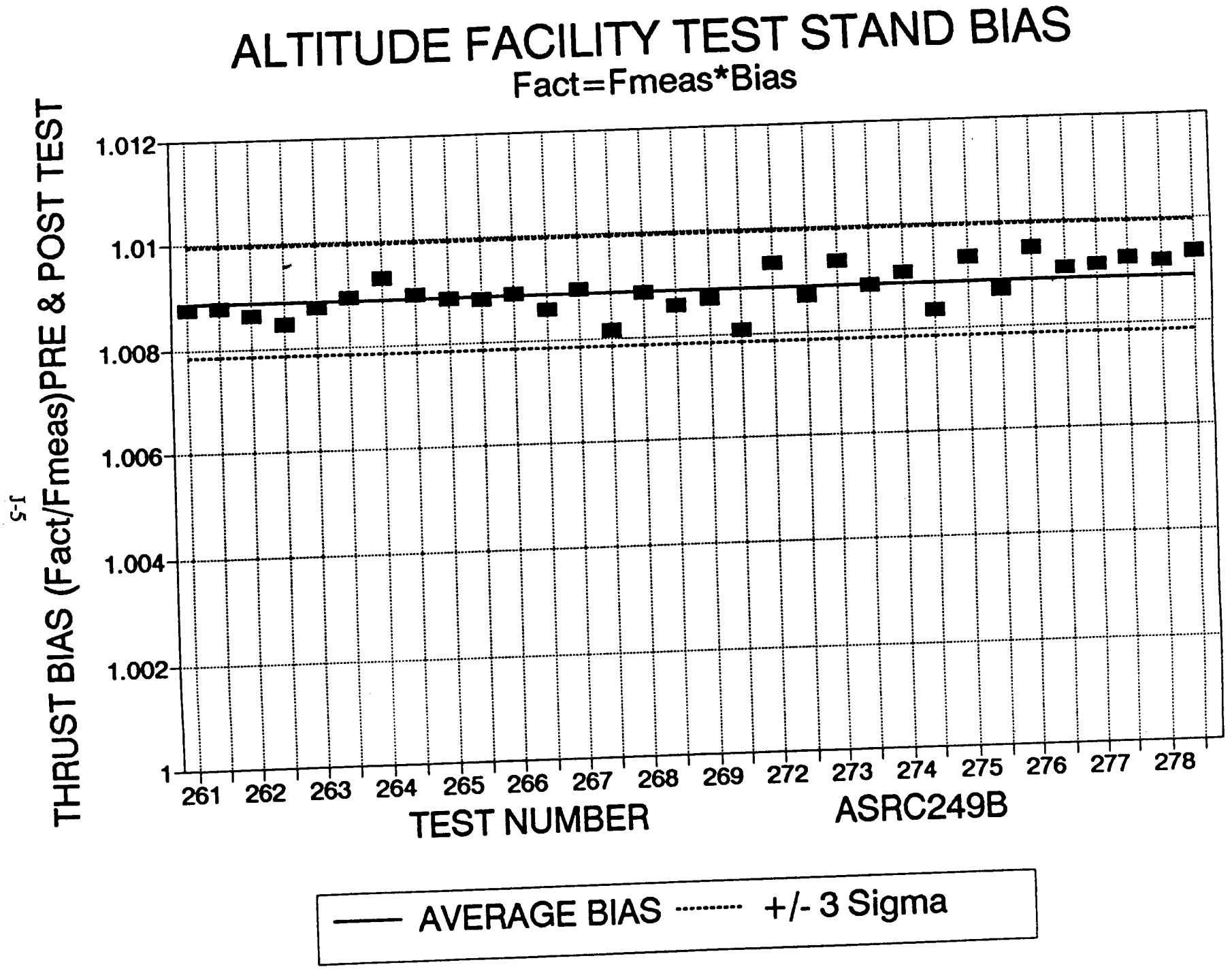
ALTITUDE FACILITY TEST STAND BIAS
Fact=Fmeas*Bias
THRUST BIAS (Fact/Fmeas)PRE & POST TEST
1.012
1.01
1.008
1.006
1.004
1.002
1
261 262 263 264 265 266 267 268 269 272 273 274 275 276 277 278
TEST NUMBER
ASRC249B
AVERAGE BIAS
+/- 3 Sigma

Figure J-1

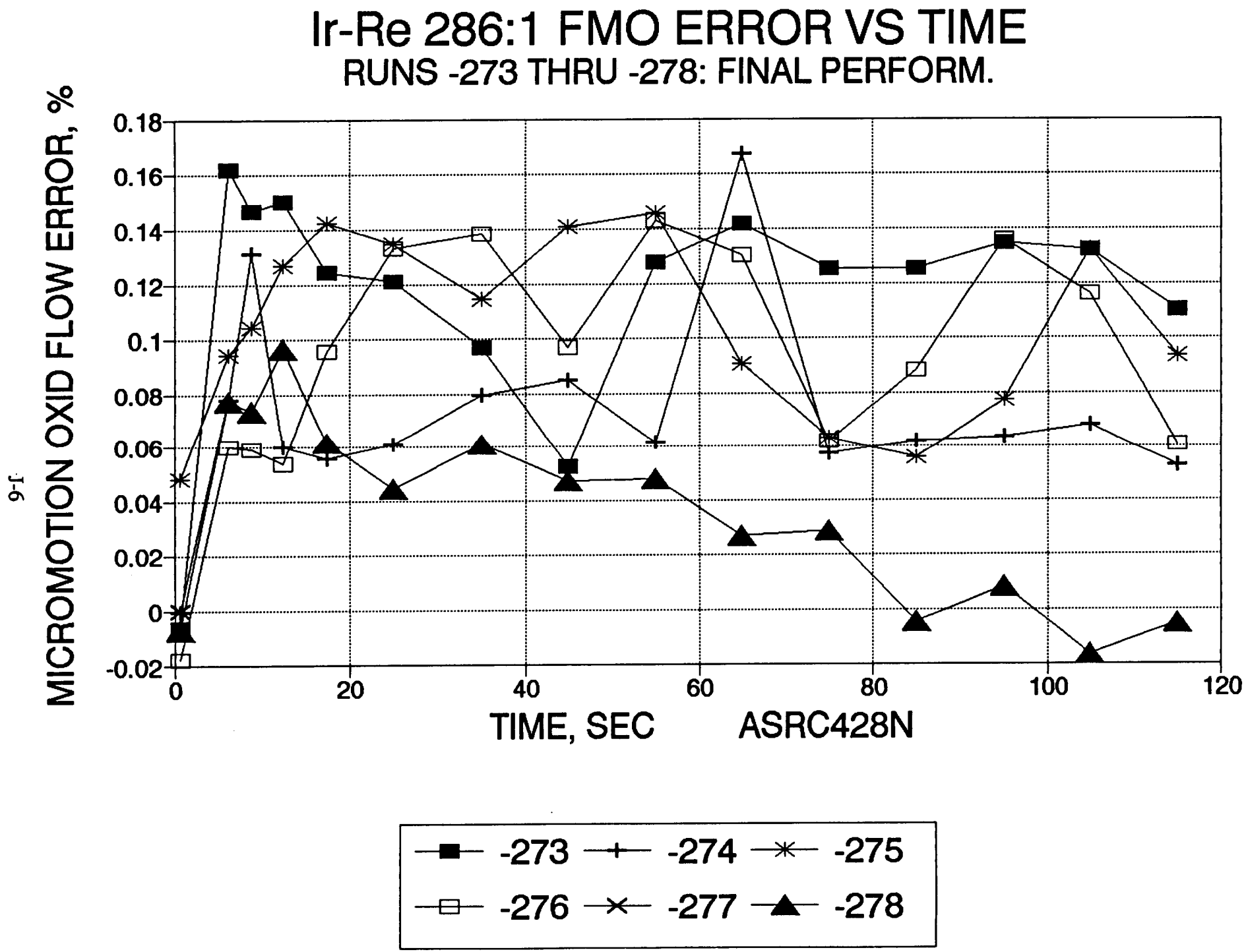
Ir-Re 286:1 FMO ERROR VS TIME
RUNS -273 THRU -278: FINAL PERFORM.
MICROMOTION OXID FLOW ERROR, %
0.18
0.16
0.14
0.12
0.1
0.08
0.06
0.04
0.02
0
-0.02
0
20
40
60
80
100
120
TIME, SEC
ASRC428N
-273
-274
-275
-276
-277
-278

Figure J-2

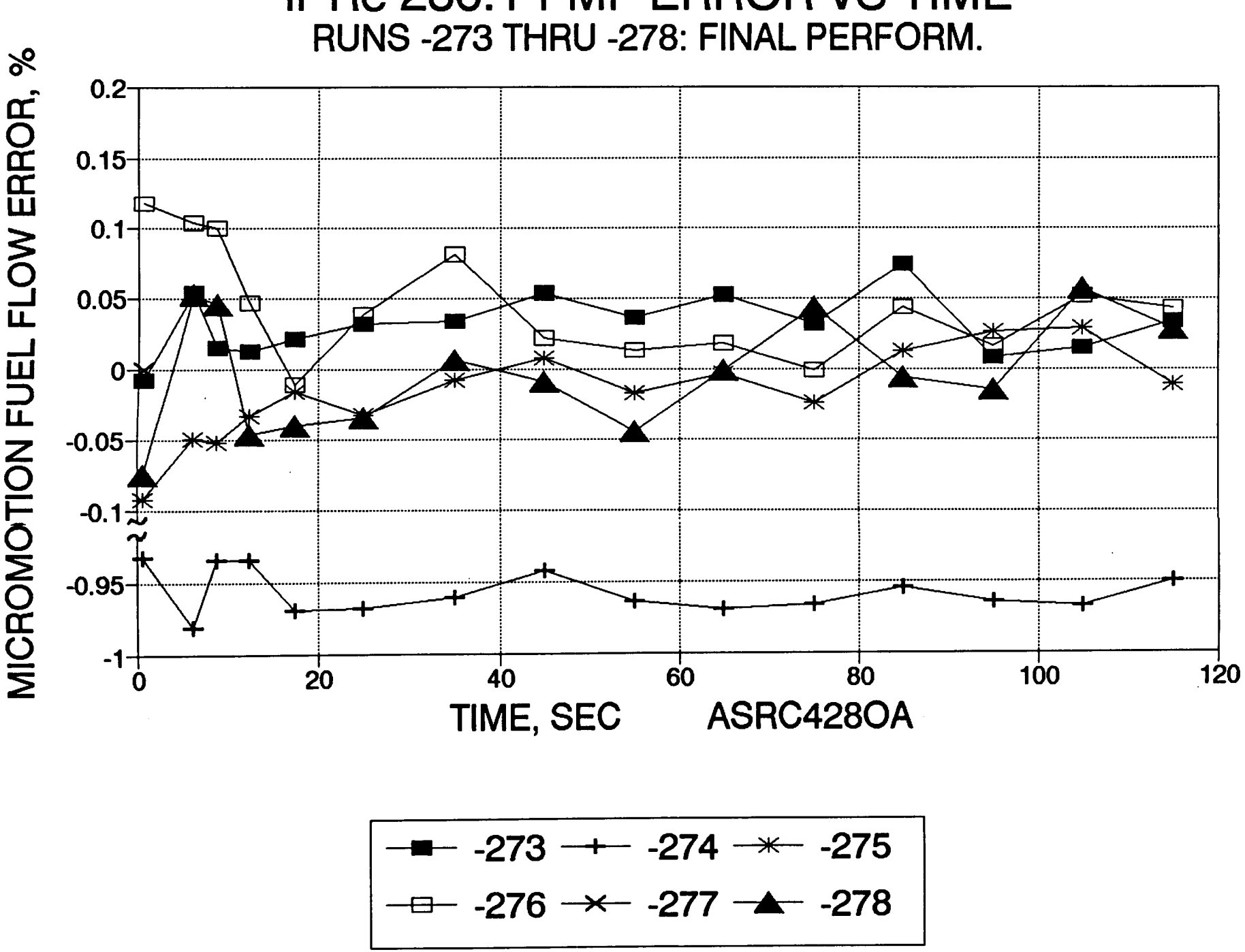
Ir-Re 286:1 FMF ERROR VS TIME
RUNS -273 THRU -278: FINAL PERFORM.
MICROMOTION FUEL FLOW ERROR, %
0.2
0.15
0.1
0.05
0
-0.05
-0.1
-0.95
-1
0
20
40
60
80
100
120
TIME, SEC
ASRC428OA
-273
-274
-275
-276
-277
-278

Figure J

FIG 2.

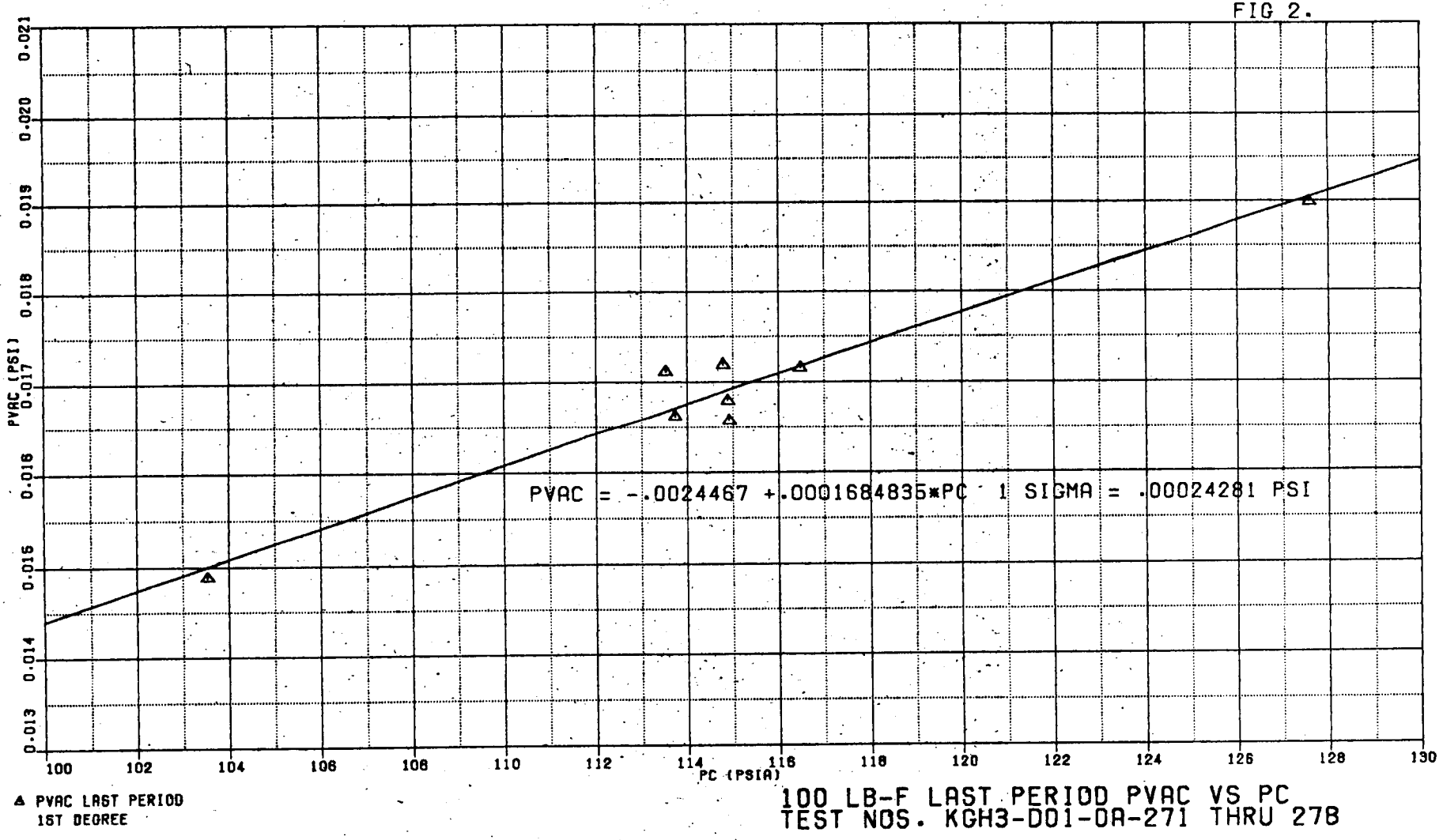

Figure J-4

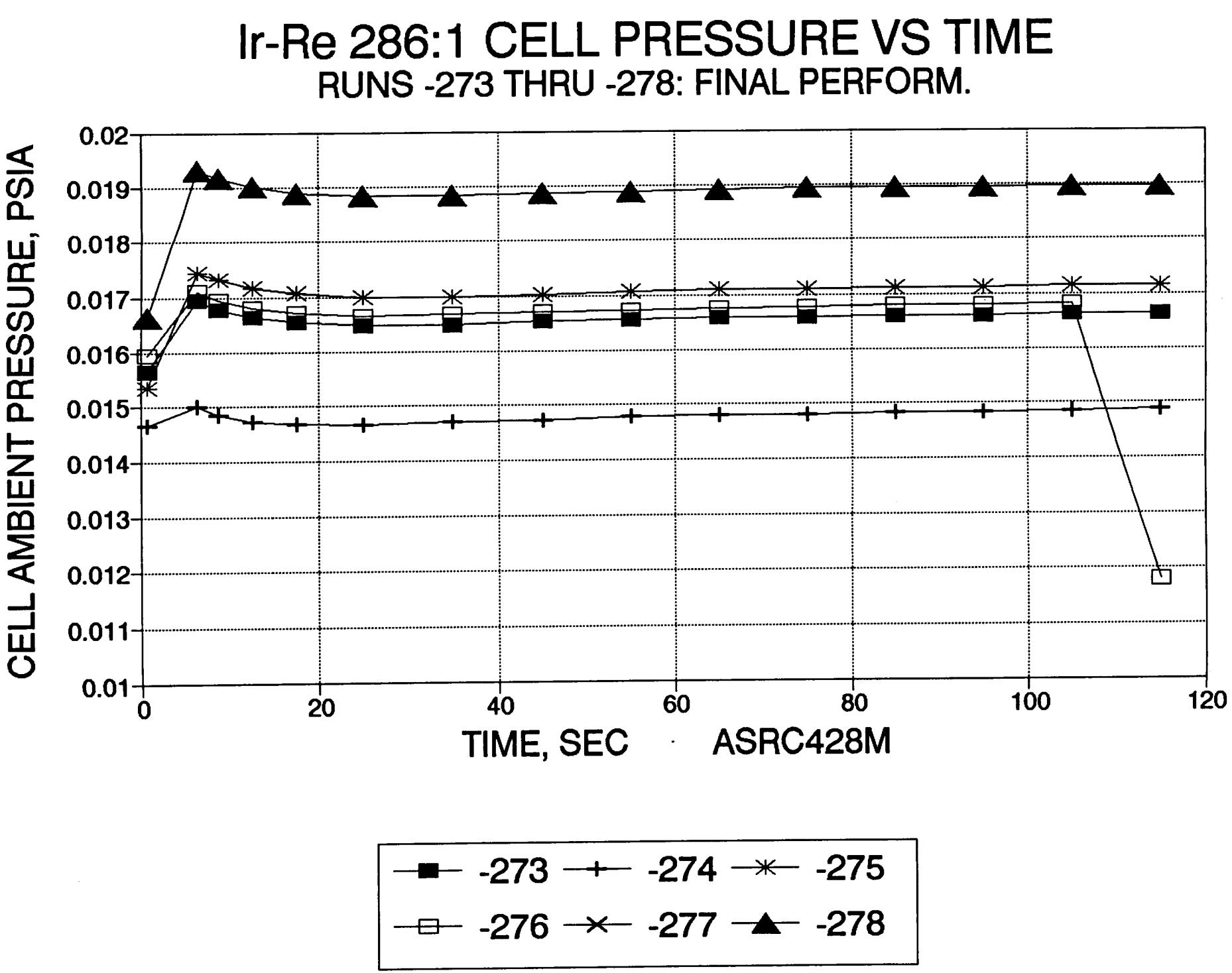
Ir-Re 286:1 CELL PRESSURE VS TIME
RUNS -273 THRU -278: FINAL PERFORM.
CELL AMBIENT PRESSURE, PSIA
0.02
0.019
0.018
0.017
0.016
0.015
0.014
0.013
0.012
0.011
0.01
0
20
40
60
80
100
120
TIME, SEC
ASRC428M
-273
-274
-275
-276
-277
-278

J-9

Figure J-5

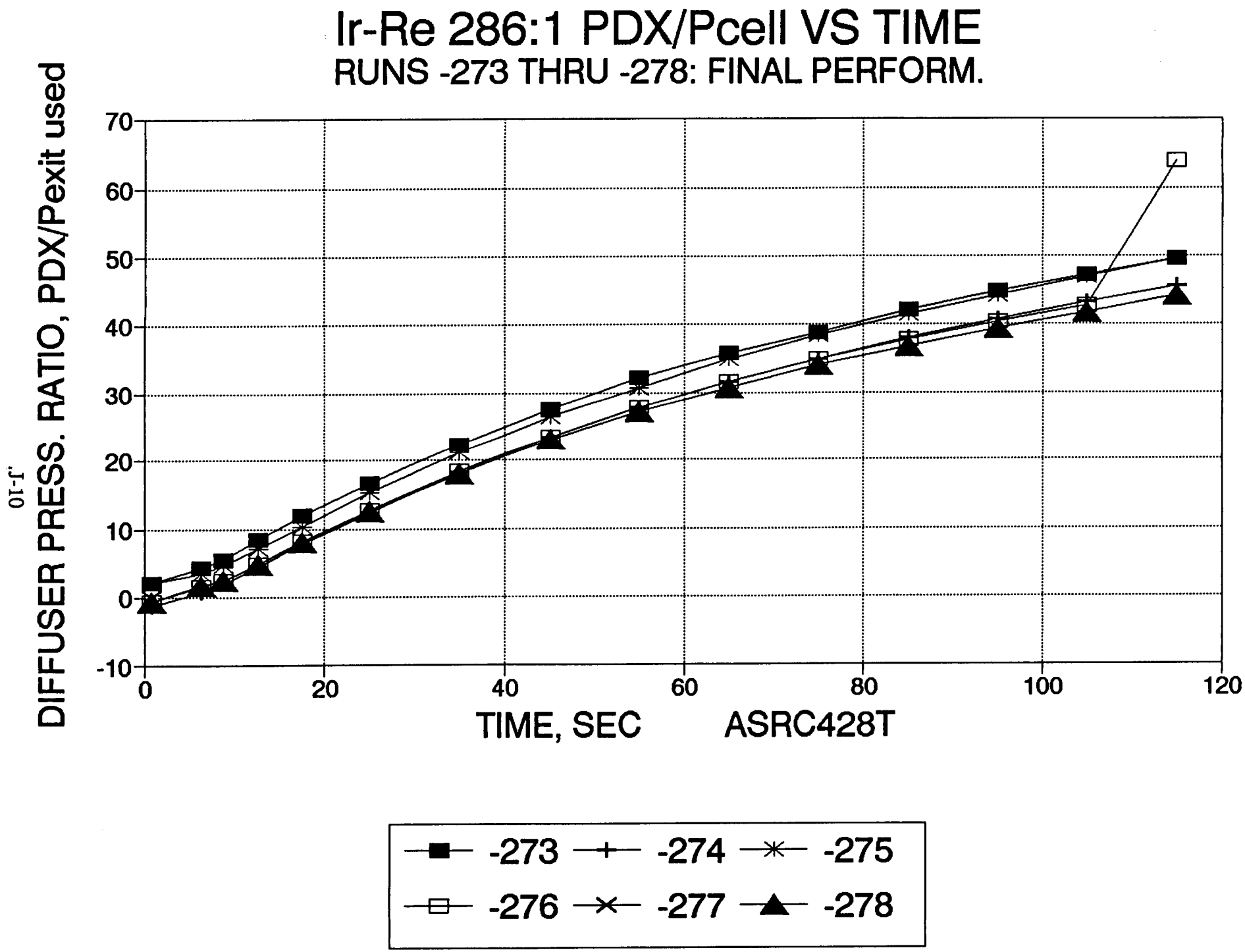
Ir-Re 286:1 PDX/Pcell VS TIME
RUNS -273 THRU -278: FINAL PERFORM.
DIFFUSER PRESS. RATIO, PDX/Pexit used
70
60
50
40
30
20
10
0
-10
0
20
40
60
80
100
120
TIME, SEC
ASRC428T
-273
-274
-275
-276
-277
-278

Figure J-6

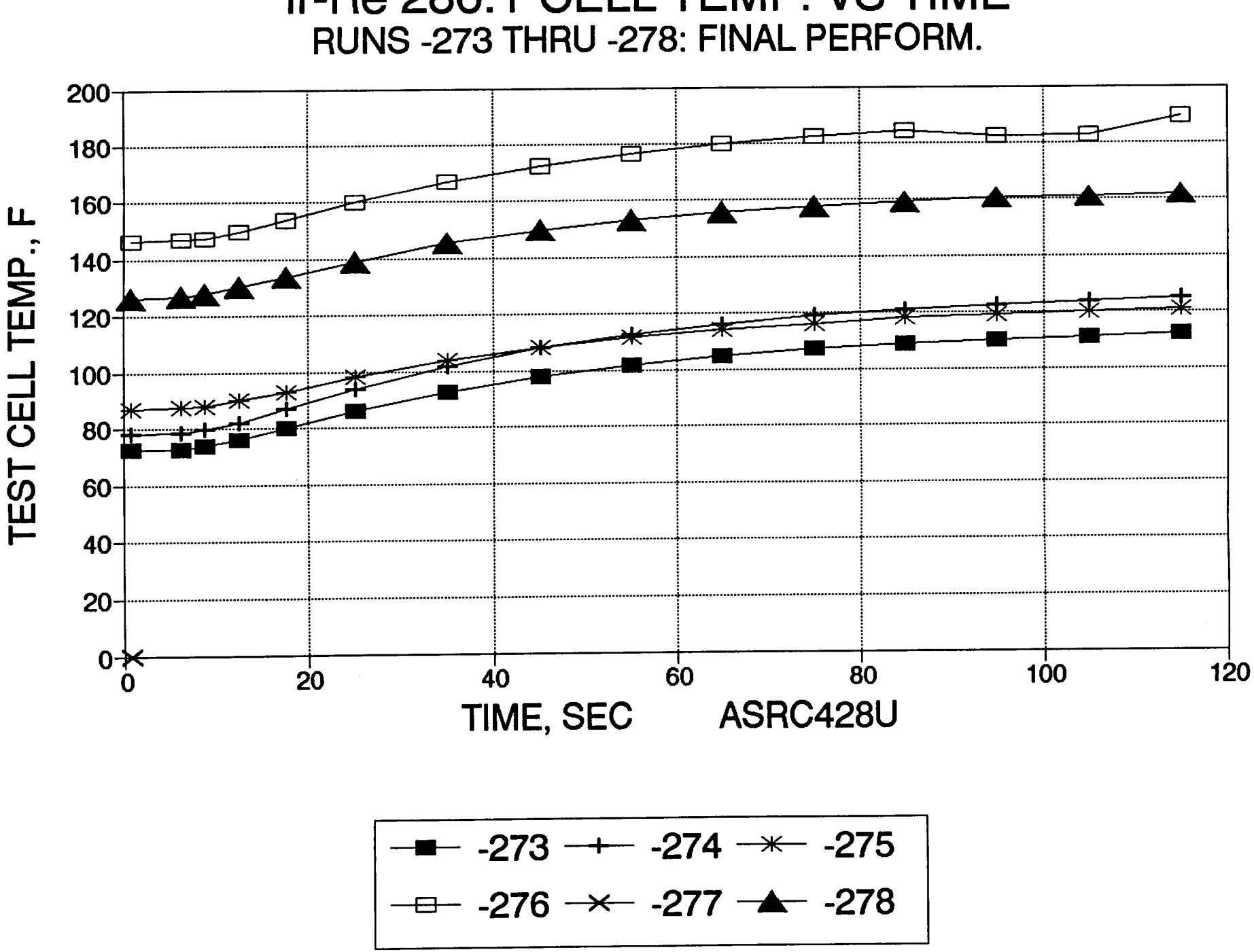
Ir-Re 286:1 CELL TEMP. VS TIME
RUNS -273 THRU -278: FINAL PERFORM.
TEST CELL TEMP., F
200
180
160
140
120
100
80
60
40
20
0
0
20
40
60
80
100
120
TIME, SEC
ASRC428U
-273
-274
-275
-276
-277
-278

Figure I-7

APPENDIX K

DURABILITY DATA LISTINGS

ASRC501 [FILE7] LAST TIME SLICES OF DURABILITY TEST PERFORMANCE DATA
7-27-92 [GRAPHS LISTED] FROM ASRC500
UPDATE 12-22-92

	TEST NUMBER	291	293	294	295	296	297	298	299	300	301	302
	TIME HR:MIN:SE	19	8	8	8	8	19	19	19	19	19	
	PROGRAM		100	100	100	100						
LINE No.	PARAMETER											
14	TIME-AVG	17.026	7.4898	7.4914	7.503	5.7527	17.0294	17.0296	17.0333	17.0215	17.0276	8.5083
15	T1	15.0691	5.0239	5.0255	5.0372	5.0359	15.0725	15.0728	15.0692	15.0646	15.0706	8.0209
16	T2	18.9829	9.9556	9.9573	9.9688	6.4695	18.9864	18.9865	18.9973	18.9785	18.9845	8.9958
17												
18												
19												
20	FMMO μM	0.21849	0.22977	0.18636	0.24655	0.20102	0.20973	0.22511	0.19342	0.23653	0.21691	0.20946
21	FMO-1	0.15136	0.15972	0.13017	0.17228	0.14074	0.14665	0.15728	0.13505	0.16509	0.15137	0.14605
22	FMO-2	0.15163	0.15976	0.13015	0.17219	0.14062	0.1466	0.15727	0.13509	0.16515	0.15134	0.14628
23	FMF-1	0.1461	0.17599	0.14528	0.15361	0.12364	0.15679	0.13865	0.13215	0.16328	0.15168	0.1508
24	FMF-2	0.14595	0.17586	0.14523	0.15355	0.12362	0.15675	0.13871	0.1322	0.16334	0.15179	0.15053
25	FMMF μM	0.12779	0.15408	0.12692	0.13412	0.108	0.13722	0.12143	0.11569	0.14294	0.13276	0.1307
26	POTR	22.5633	20.5465	23.6367	78.8703	23.1136	22.8812	24.3532	19.3953	27.6158	20.7859	33.1852
27	PFTR	14.4695	14.4752	14.4514	16.7311	14.4214	14.9248	17.1424	14.8046	18.295	14.7264	14.3114
28	PVT	0.90487	0.54789	0.38792	0.45315	0.28054	0.82295	0.76738	0.70351	0.87143	0.82248	0.13946
29	POVI	224.52	248.053	185.746	266.481	198.99	217.574	232.267	191.172	255.205	225.579	214.575
30	PFRI	234.336	295.139	221.108	256.462	189.96	250.367	222.886	201.869	271.944	243.656	237.329
31	PC-1	115.154	126.715	104.554	125.476	102.933	115.442	114.709	103.323	125.659	116.28	113.33
32	PFVI	207.118	256.506	194.253	226.632	169.692	220.127	198.443	179.488	239.425	215.432	209.479
33	PGODP	262.081	288.587	217.172	311.877	233.701	254.492	272.41	225.148	298.192	264.428	14.5387
34	PGFDP	255.245	322.882	241.53	278.956	206.172	273.62	242.112	219.594	296.522	265.353	26.7549
35	FCAL-A	-0.297	-0.307	-0.2852	-0.3081	-0.304	-0.3031	-0.3049	-0.3002	-0.3133	-0.3061	-0.359
36	FCAL-B	-0.6492	-0.5454	-0.4588	-0.4396	-0.4207	-0.3893	-0.373	-0.3654	-0.3663	-0.366	-0.4128
37	F	99.3896	108.58	89.195	108.915	89.2342	99.5598	99.9396	89.613	108.98	100.703	97.4312
38	PH2-UP	25.9378	27.995	27.5787	27.9499	31.272	26.4303	26.6799	26.8256	26.7008	26.9042	31.9464
39	PH2-DN	10.0538	10.6948	10.5345	10.7215	11.9241	10.229	10.416	10.479	10.3858	10.4903	12.1631
40	PDX	0.14315	0.04432	0.03302	0.03356	0.00816	0.14137	0.13582	0.11519	0.15319	0.13904	0.04195
41	PDW	69.0468	70.4046	70.4556	70.3832	70.6273	70.2742	70.2456	70.3042	70.3229	70.0738	70.3094
42	POL-1	235.355	262.384	193.967	286.435	210.102	230.79	248.616	201.632	274.153	240.504	211.38
43	PFL-1	248.848	315.369	235.384	272.137	200.531	266.591	236.012	213.869	289.498	258.933	252.104
44	PEXIT-1	0.14481	0.15515	0.12922	0.15974	0.11814	0.13986	0.14021	0.12321	0.15377	0.14172	0.13739
45	PEXIT-2	0.14785	0.16168	0.13103	0.16153	0.12569	0.14225	0.14243	0.12491	0.15607	0.14338	0.13984
46	TDUCT	90.9392	85.8254	85.8867	89.5458	89.9297	86.8233	94.6666	96.052	96.7709	99.7741	88.6043
47	TVP	89.3319	86.4154	90.0074	92.8456	91.691	103.147	105.292	105.33	108.49	108.525	89.0256
48	VTCV	28.2261	28.2699	28.2746	28.2996	28.3273	28.3173	28.3204	28.3346	28.3241	28.3357	28.2898
49	TOL	72.0571	74.8091	78.7274	80.5741	80.8664	78.7883	77.9686	77.4207	76.984	76.489	81.1287
50	TFL	68	67	70	70	70	66	65	66	66	66	75
51	TCELL	82.4367	97.0187	94.9262	96.4796	126.752	100.228	111.168	117.037	109.424	115.01	77.6467
52	TOJ[OX IN]	73.7099	77.5434	82.986	83.3537	85.1169	81.1465	79.774	78.9211	78.1987	78.0241	82.2843
53	TRIN	70.9281	68.67	72.5804	73.1357	71.9579	71.5889	72.1822	72.3957	71.7127	72.6188	79
54	TR-OUT	202.689	166.335	191.925	200.744	232.528	186.264	216.821	222.54	185.498	200.471	194.011
55	TRI	200.935	164.503	190.928	198.509	231.709	184.568	215.646	221.248	183.951	198.06	193.556
56	TVB	112.218	123.571	126.836	153.448	170.902	133.734	148.119	163.479	139.808	165.264	93.2828
57	TJB-1	188.315	143.082	156.552	195.567	210.043	182.144	205.824	218.353	188.821	223.615	139.599
58	TJB-3	218.599	165.207	165.565	215.305	215.406	239.919	239.306	260.312	247.585	291.348	143.845
59	TRB-1	147.43	119.329	118.145	176.936	187.455	154.291	181.923	212.896	178.887	222.252	94.5689
60	TRB-2	154.782	129.492	137.214	194.298	181.212	152.443	169.651	177.666	162.412	201.861	120.458
61	TVJ-1	76.4612	119.426	117.628	158.896	176.679	109.336	117.492	145.704	116.952	169.206	74.4853
62	TVJ-2	71.7535	116.089	116.064	158.338	177.69	101.991	108.378	136.469	109.396	162.383	73.9014
63	TVJ-3	66.4998	118.496	116.35	156.948	176.433	102.778	108.93	138.942	110.674	166.443	74.4569
64	TMR-1	72.3695	104.168	110.099	162.098	183.377	91.0634	100.025	128.515	105.657	162.481	77.2847
65	TMR-2	73.0139	83.3206	91.3541	118.297	134.382	79.836	84.1167	96.8834	85.7877	112.51	78.1072
66	TMR-3	69.7115	99.0721	107.033	157.897	179.413	86.7292	95.6429	119.654	101.21	147.692	76.0043
N.G. 67	TNR-1	1938.63	1134.33	1090.23	1301.14	1034.2	1804.94	1986.36	1922.3	1854.97	1862.06	1232.69
N.G. 68	TNR-2	1623.54	771.62	704.545	885.839	600.058	1523.06	1681.12	1630.01	1578.74	1594.4	896.913

	TEST NUMBER	291	293	294	295	296	297	298	299	300	301	302
69	TMR-3	292.377	127.067	130.41	157.343	132.414	249.97	366.764	406.888	283.973	302.839	137.338
70	TMC-1	1709.11	860.944	801.327	977.406	677.84	1563.7	1738.36	1682.59	1524.32	1574.81	887.825
71	TAC	397.402	318.604	293.494	343.592	307.344	435.582	404.913	423.213	441.299	474.11	289.301
72	TPC	138.032	132.754	122.501	175.273	171.101	168.005	203.368	237.365	203.778	248.147	116.753
73	THF-1	143.391	181.521	137.37	251.197	279.924	228.539	320.706	380.931	315.092	375.833	106.669
74	THF-2	169.197	195.742	145.636	266.637	293.663	259.275	364.773	447.695	355.911	435.055	115.368
75	THF-3	261.202	231.997	211.02	323.961	324.799	378.769	514.301	574.53	482.299	523.408	140.916
76	TMS-1	70.829	100.004	98.0807	114.546	126.498	100.052	101.895	107.968	103.423	112.415	73.6254
77	WOPDFM	2.79367	1.39816	1.16901	1.4946	1.02051	2.68033	2.86877	2.50454	2.97807	2.76339	0.16279
78	WFPDFM	2.6084	1.41844	1.18363	1.25132	0.80346	2.78878	2.46908	2.35413	2.89933	2.69483	0.0761
79	PVAC-1	7864.08	8569.99	6998.16	8565.84	6672.91	7611.78	7613.16	6701.17	8319.79	7656.38	7607.31
80	PVAC-2	7859.54	8591.07	7012.27	8587.99	6747.27	7600.29	7603.81	6694.14	8309.21	7645.08	7596.22
81	TMS-1	77.9793	100.267	97.1788	113.189	123.737	100.697	103.739	108.486	103.39	110.86	75.0483
82	TMS-3	999999	999999	999999	999999	999999	999999	999999	999999	999999	999999	999999
83	PYRO-LO	2152.64	1659.3	1626.31	1905.89		2039.37	2219.9	2199.36	2074.03	2088.68	
84	PYRO-HI	3256.99	2665.83	2757.14	2845.3	2739.5	3119.2	3352.69	3372.38	3139.08	3197.84	2845.49
85	POTS	13.8848	12.6228	12.8233	13.7764	13.0406	22.3433	23.8251	24.3671	25.2544	25.4758	238.759
86	PFTS	14.7621	14.7361	14.6125	14.5954	14.6367	29.7743	30.2595	30.3546	30.4649	30.49	254.795
87												
88												
89												
90												
91	TIME-AVG	17.026	7.4898	7.4914	7.503	5.7527	17.0294	17.0296	17.0333	17.0215	17.0276	8.5083
92	T1	15.0691	5.0239	5.0255	5.0372	5.0359	15.0725	15.0728	15.0692	15.0646	15.0706	8.0209
93	T2	18.9829	9.9556	9.9573	9.9688	6.4695	18.9864	18.9865	18.9973	18.9785	18.9845	8.9958
94												
95												
96												
97	FMO1	0.15141	0.15975	0.13007	0.17216	0.14076	0.1467	0.15732	0.13501	0.16506	0.15143	0.1461
98	FMO2	0.15166	0.15977	0.13009	0.17212	0.14063	0.14663	0.1573	0.13507	0.16514	0.15137	0.14608
99	PCT WO	-0.163	-0.0142	-0.0178	0.02591	0.09799	0.04525	0.01345	-0.0435	-0.0428	0.03714	0.01409
100	FMF1	0.14614	0.17587	0.14532	0.15364	0.12356	0.15682	0.13867	0.13214	0.16327	0.15172	0.15084
101	FMF2	0.14598	0.17578	0.14526	0.15358	0.12355	0.15677	0.13873	0.13219	0.16334	0.15183	0.15057
102	PCTWF	0.11108	0.05599	0.03906	0.03821	0.00615	0.02734	-0.0398	-0.0363	-0.0375	-0.0697	0.18384
103	SGO	1.43556	1.43212	1.4263	1.42461	1.42356	1.42652	1.42776	1.4281	1.42929	1.42967	1.42336
104	SGF	0.87502	0.87552	0.87384	0.8739	0.87385	0.87592	0.87625	0.8761	0.87599	0.87582	0.87122
105	WO	0.21754	0.2288	0.18553	0.24523	0.20029	0.20922	0.2246	0.19285	0.23598	0.21645	0.20794
106	WF	0.12781	0.15394	0.12696	0.13424	0.10797	0.13734	0.12154	0.11579	0.14305	0.13293	0.1313
107	WT	0.34535	0.38274	0.31249	0.37948	0.30826	0.34656	0.34613	0.30864	0.37903	0.34938	0.33924
108	MR	1.70207	1.4863	1.46135	1.82678	1.85507	1.5234	1.848	1.66557	1.64958	1.62836	1.58371
109	FSL	100.379	109.59	89.9792	109.813	89.7998	100.254	100.502	90.0952	109.601	101.263	98.1596
110	F-ALT	104.1	113.651	93.2951	113.873	92.9759	103.854	104.104	93.2654	113.537	104.884	101.758
111	ISP	301.437	296.944	298.552	300.078	301.619	299.668	300.761	302.181	299.546	300.203	299.962
112	CSTR[COLD TH	5418.48	5380.03	5436.98	5373.19	5426.26	5413	5385.29	5439.99	5387.36	5408.35	5428.82
113	CF	1.78863	1.77456	1.76548	1.79557	1.78715	1.77994	1.79562	1.78596	1.78767	1.78464	1.77648
114	SGOJ	1.43337	1.42848	1.42058	1.42088	1.41784	1.42336	1.42535	1.42609	1.42767	1.42762	1.42181
115	SGFJ	0.80463	0.82361	0.81025	0.80565	0.78906	0.81321	0.79726	0.79427	0.81361	0.80579	0.80916
116	BIAS-A	1.00529	1.00513	1.00478	1.00483	1.00441	1.00531	1.00495	1.00468	1.00484	1.00483	1.00454
117	BIAS-B	1.00529	1.00513	1.00478	1.00483	1.00441	1.00531	1.00495	1.00468	1.00484	1.00483	1.00454
118	FA-CORR	100.379	109.59	89.9792	109.813	89.7998	100.254	100.502	90.0952	109.601	101.263	98.1596
119	FB-CORR	100.379	109.59	89.9792	109.813	89.7998	100.254	100.502	90.0952	109.601	101.263	98.1596
120	AE	24.4808	24.4808	24.4808	24.4808	24.4808	24.4808	24.4808	24.4808	24.4808	24.4808	24.4808
121	AT	0.50542	0.50542	0.50542	0.50542	0.50542	0.50542	0.50542	0.50542	0.50542	0.50542	0.50542
122	AVG PEXIT	0	0	0	0	0	0	0	0	0	0	0
123	PRE FZERO	-0.4612	-0.4512	-0.3566	-0.37	-0.1714	-0.1641	-0.0677	-0.0628	-0.0935	-0.0726	-0.2847
124	HZO1	837.763	883.826	721.135	952.947	779.352	811.855	870.362	747.987	913.34	837.848	808.563
125	HZO2	864.427	909.999	744.054	979.66	802.712	836.277	896.078	771.746	940.212	862.813	833.177
126	HZF1	829.376	1001.11	824.639	872.492	700.335	890.772	786.553	749.218	928.065	861.428	856.384
127	HZF2	818.638	985.789	814.62	861.139	693.854	878.992	778.184	741.792	915.803	851.304	844.259
128	ROTV	-6138.6	-6236	-6730.1	-4455.9	-6253.9	-6357.1	-5896.8	-6608.7	-5853.5	-6261.5	-5983.6
129	RFTV	-10333	-8954.4	-9760.7	-10192	-11654	-9542	-10769	-10776	-9478.2	-9961.4	-9876.3
130	ROLJ	-136.31	-135.66	-138.97	-134.79	-137.58	-136.82	-135.81	-138.13	-135.17	-136.31	-136.82
131	RFLJ	-141.33	-137.94	-140.82	-140.6	-144.78	-139.91	-142.67	-143.54	-139.48	-140.87	-140.3
132	ROJT	3461	3458.52	3502.43	3477.75	3544.91	3469.96	3469.45	3519.33	3468.3	3478.9	3478.32
133	RFJT	4677.63	4656.21	4656.78	4669.04	4669.41	4659.9	4667.87	4661.53	4669.09	4668.69	4660.13
134	KOTV	0	0	0	0	0	0	0	0	0	0	0
135	KFTV	0	0	0	0	0	0	0	0	0	0	0
136	KOLJ	0	0	0	0	0	0	0	0	0	0	0

	TEST NUMBER	291	293	294	295	296	297	298	299	300	301	302
137	KFLJ	0	0	0	0	0	0	0	0	0	0	0
138	KOJT	0.017	0.017	0.0169	0.01696	0.0168	0.01698	0.01698	0.01686	0.01698	0.01695	0.01696
139	KFJT	0.01462	0.01465	0.01465	0.01463	0.01463	0.01465	0.01464	0.01465	0.01463	0.01464	0.01465
140	POVIT	224.923	248.492	186.061	266.975	199.345	217.955	232.693	191.506	255.668	225.98	214.952
141	PFVIT	207.366	256.837	194.498	226.899	169.886	220.402	198.673	179.702	239.719	215.695	209.737
142	POJT	229.42	253.457	189.422	272.673	203.23	222.158	237.496	195.106	260.937	230.45	219.11
143	PFJT	210.115	260.684	197.194	229.916	171.916	223.527	201.191	182.006	243.098	218.655	212.616
144	RFRC	1457.97	1427.34	1455.89	1446.52	1519.4	1404.3	1450.01	1462.54	1392.01	1398.96	1407.48
145	KFRC	0.02619	0.02647	0.02621	0.02629	0.02565	0.02669	0.02626	0.02615	0.0268	0.02674	0.02666
146												
147	[VALUES BELOW ARE CALCULATED OUTSIDE PERFORMANCE PROGRAM AND/OR USED FOR											
148	DATA PLOTTING]											
149	Cp	0.7132	0.70966	0.71239	0.71322	0.71625	0.71148	0.71432	0.71489	0.71139	0.71284	0.71307
150	FUEL DT BASED	134.858	99.4562	121.817	130.761	162.443	120.152	151.342	156.77	119.508	134.159	118.897
151	FUEL DT BASED	131.761	97.6647	119.345	127.608	160.57	114.675	144.639	150.144	113.785		
152	TEST DURATION	20	16.08									
153	PC-1[ROUNDED	115	127	105	125	103	115	115	103	126		113
154	MR{ROUNDED]											1.58
155	TIME-AVG[rnd]											9
156	MR[MICROM]	1.71	1.49	1.47	1.84	1.86	1.53	1.85	1.67	1.65	1.63	1.60
157	MRfm/MRmm	0.99551	0.99669	0.99526	0.99371	0.99661	0.99673	0.99688	0.99623	0.99685	0.99667	0.98822
158	KWOJT[MICRO]	0.01745	0.01745	0.01735	0.01742	0.01723	0.0174	0.01739	0.01728	0.01739	0.01736	0.01746
159	KWFJT[MICRO]	0.01486	0.0149	0.01489	0.01486	0.01488	0.01487	0.01486	0.01487	0.01486	0.01485	0.01482
160	Wt[MICROM.]	0.34628	0.38385	0.31328	0.38067	0.30902	0.34696	0.34654	0.30911	0.37947	0.34967	0.34017
161	C*[MICROM]	5403.84	5364.45	5423.26	5356.38	5412.85	5406.83	5378.95	5431.71	5381.18	5403.84	5413.96
162	PYRO-HI[120SEC.=]											
163	MR/Pc [MARKER	1.73/115	1.5/127	1.5/104	1.86/126	1.9/103	1.55/116	1.87/115	1.69/103	1.66/126	1.64/116	1.58/113
164	TR-OUT [Q>=120SEC]											
165	FUEL D T[Q>=120SEC]											
166	FUEL T IN [RNDED]											
167	PFVI[Q>=120SEC]											
168	MMH T~PFVI [V.P.]											
169	q, BTU/SEC	12.2911	10.8749	11.0145	12.5078	12.5654	11.7306	13.1276	12.9658	12.152	12.6966	11.0813
170	MARKER 1		1									
171	MARKER 2					2						
172	MARKER 3								3			
173	MARKER 4											4
174	MARKER 5											
175	MARKER 6											
176	MR ERROR, %; F	-0.4494	-0.3309	-0.4744	-0.6293	-0.339	-0.3273	-0.3122	-0.377	-0.3146	-0.3333	-1.1781
177	TOL/TFL/2 VS R	69.9441	70.8438	74.4178	75.2783	75.4756	72.4502	71.724	71.5953	71.4871	71.4005	78.121
178	Dt [HOT]	0.82833	0.82435	0.82497	0.82556	0.82485	0.8274	0.82898	0.82911	0.82754	0.82793	0.82556
179	C*[HOT] uM	5766	5669	5739	5677	5727	5756	5748	5806	5730	5760	5738
180												
181												
182												
183												
184												
185												
186												
187												
188												
189												
190												

graph id below

STOP	STOP	STOP	STOP	STOP	STOP	STOP	STOP	STOP	STOP	STOP	STOP	STOP

GRAPH
ASRC501 PLOT

A FUEL DT VS MR, Pc LABLES[FM]
B FUEL DT VS Pc, MR LABLES [FM]
C " " DATA TIME LABLES

D MRfm/MRuM VS RUN#, Pc LABLES
E FUEL DT VS MR, Pc LABLES [uM}
F FUEL DT VS Pc, MR LABLES [uM]
G Kwojt VS MR [uM]?
H Kwfjt VS MR [uM]?
I Kwojt & Kwfjt VS RUN # [uM]
J " " " [FM]
K Kwojt VS Wo [uM]
L Kwfjt VS Wf [uM]
M Kwojt VS Wo [FM]
N Kwfjt VS Wf [FM]
O C* VS Wt [uM]
P C* VS Wt [FM]
Q MICROMOTION OXID FLOW ERROR, % [NOT PLOTTED YET]
R MICROMOTION FUEL FLOW ERROR, % [NOT PLOTTED YET]
S FUEL DT VS MR @ HIGH INLET TEMP
T TR-OUT VS MR
U Tchamb VS Pc
V Tchamb VS RUN #
W Tchamb VS MR [FM]
X FUEL TR-OUT VS Pc [FM]
Y PFVI VS TR-OUT [MMH V.P. ADDED]
Z BIAS VS RUN NUMBER
AA POVI VS PFRI[PARAMETER=RUN#]
AA1 POVI VS PFRI[PARAMETER=MR]
AA2 POVI VS PFRI[PARAMETER=Pc]
AB POVI VS Wo uM
AC PFRI VS Wf uM
AD q VS RUN No.
AE DT, TFL, TOUT, Cp, Wf VS RUN No.
AF Tpyro_lo VS RUN #
AG Tpyro-hi
AH THRUST BIAS VS RUN #
AI q VS Pc
AJ q VS MR
AK MR VS Pc
AL MR ERROR VS RUN No.[FM REL TO uM]
AM Fvac VS Pc
AO AVG PROP LINE TEMP VS RUN #
AP HOT Dt VS RUN #
AQ HOT C* VS RUN#
AR C*HOT VS MR
AS C* HOT VS Pc

ASRC501 [FILE7]
7-27-92
UPDATE 12-22-92

	TEST NUMBER	303	304	305	306	307	308	309	310	311	312	313
	TIME HR:MIN:SEC						37					55
	PROGRAM											
LINE No.	PARAMETER											
14	TIME-AVG	41.0536	39.5293	112.052	440.119	493.045	642.031	352.021	223.005	454.514	444.528	405.478
15	T1	36.1219	35.085	105.106	405.253	455.14	635.092	305.113	205.114	405.139	405.132	369.006
16	T2	45.9852	43.9735	118.998	474.985	530.95	648.969	398.93	240.897	503.888	483.925	441.949
17												
18												
19												
20	FMMO	0.21455	0.21309	0.21588	0.2169	0.21648	0.2093	0.21439	0.21557	0.21443	0.19093	0.21394
21	FMO-1	0.15022	0.14895	0.15009	0.15051	0.14945	0.14449	0.14833	0.14912	0.14815	0.13202	0.14864
22	FMO-2	0.15034	0.14898	0.1502	0.15081	0.14965	0.14467	0.14812	0.14928	0.148	0.13213	0.14875
23	FMF-1	0.14847	0.15008	0.14761	0.14759	0.14992	0.14883	0.14781	0.14842	0.14827	0.15262	0.15083
24	FMF-2	0.14796	0.14982	0.14762	0.14753	0.14991	0.1487	0.14753	0.1484	0.14832	0.15272	0.15045
25	FMMF	0.1282	0.12982	0.12834	0.12821	0.1306	0.1305	0.12949	0.12972	0.12953	0.13371	0.13157
26	POTR	36.2798	32.2295	26.6371	23.9157	34.1135	26.8326	24.6354	24.3732	18.9104	23.2145	24.9349
27	PFTR	14.2767	14.2698	14.2822	14.2133	14.3795	17.9779	19.6342	19.3866	19.234	18.06	17.951
28	PVT	0.43187	0.45532	0.97756	999999	999999	3.08622	2.23636	1.748	2.96335	2.73626	3.01604
29	POVI	222.772	220.834	222.522	225.198	223.49	215.251	219.939	221.763	220.584	192.231	222.152
30	PFRI	235.676	238.47	236.37	218.085	241.477	236.655	236.578	237.528	237.424	236.558	241.224
31	PC-1	114.23	114.25	114.49	114.52	115.34	112.89	114.30	114.79	114.20	107.98	114.85
32	PFVI	208.819	210.914	209.335	211.487	216.045	212.821	211.075	211.53	211.839	209.847	214.542
33	PGODP	14.6134	14.6265	14.6748	14.7327	14.6182	14.5698	14.6629	14.7524	14.8051	14.801	14.9375
34	PGFDP	26.7352	26.7203	26.7116	26.7135	14.5897	14.5718	14.7045	14.7053	14.7294	14.4514	14.4984
35	FCAL-A	-0.3533	-0.3485	-0.333	-0.3012	-0.4359	-0.42	-0.3979	-0.529	-0.5159	-0.3948	-0.5194
36	FCAL-B	-0.1792	-0.1433	-0.088	-0.0227	-0.557	-0.6587	-0.6378	-0.3713	-0.2487	-0.7474	-0.4601
37	F	98.893	98.8649	99.3586	99.6402	99.9087	97.8378	99.0582	99.7216	99.3303	93.2258	100.017
38	PH2-UP	32.3808	32.5574	32.6992	32.8249	36.1669	17.7016	19.5591	32.3563	32.28	29.275	29.1851
39	PH2-DN	12.532	12.5953	12.7036	12.8781	14.0195	7.55347	8.67748	12.6006	12.6751	11.4145	11.4424
40	PDX	0.35455	0.37496	0.93207	2.87864	2.97181	3.13816	2.18014	1.66473	2.87085	2.67233	2.89163
41	PDW	70.3438	69.9542	69.5642	68.915	64.7224	75.0001	65.5489	65.7758	65.072	67.9643	68.8479
42	POL-1	220.849	219.065	221.932	224.165	248.013	238.612	245.44	247.364	245.265	212.82	246.069
43	PFL-1	249.828	252.756	250.697	252.477	258.239	254.245	252.806	253.694	253.672	254.402	258.273
44	PEXIT-1	0.13955	0.13902	0.13298	0.13324	0.1384	0.13462	0.1424	0.14082	0.14236	0.12696	0.13506
45	PEXIT-2	0.14046	0.13965	0.13884	0.13873	0.14521	0.13997	0.1422	0.14256	0.14205	0.1269	0.13612
46	TDUCT	109.395	103.908	122.041	141.703	137.937	139.614	132.483	133.588	135.236	135.423	133.637
47	TVP	106.375	93.5606	102.307	108.045	96.487	78.3076	84.4504	96.3031	98.9962	88.2894	100.185
48	VTCV	28.4132	28.4718	28.5498	28.6102	28.5623	28.6462	28.599	28.5836	28.6303	28.622	28.6284
49	TOL	81.3266	78.7054	73.0884	73.1551	68.3157	73.4223	66.7434	66.9256	64.627	68.8294	71.1071
50	TFL	77	74	69	70	65	70	64	68	68	69	67
51	TCELL	109.081	117.978	115.146	122.511	116.264	125.618	122.658	101.605	109.59	169.415	183.056
52	TOJ[OX IN]	85.7776	83.0657	76.5556	75.6147	71.869	67.9745	72.1131	73.337	70.3059	70.217	76.6964
53	TRIN	85	82	73	74	70	64	78	79	999999	79	81
54	TR-OUT	217.173	212.934	213.958	219.503	214.606	208.607	216.454	220.434	223.699	201.678	213.555
55	TRI	214.887	210.447	211.946	219.347	212.441	208.014	215.735	219.566	223.045	199.22	211.114
56	TVB	168.491	186.515	196.606	204.645	193.648	218.837	211.639	243.425	210.197	189.687	201.575
57	TJB-1	243.041	245.013	250.491	253.61	242.794	243.59	239.513	246.785	303.718	227.527	241.855
58	TJB-3	328.636	342.366	359.184	362.442	355.23	352.425	358.336	361.24	364.025	351.056	359.168
59	TRB-1	243.643	255.528	321.473	431.084	404.212	409.97	323.855	353.25	387.464	366.467	367.709
60	TRB-2	178.967	184.081	163.075	179.373	175.201	177.222	194.003	179.226	193.733	174.727	180.315
61	TVJ-1	143.538	182.298	201.844	210.645	201.837	201.524	201.367	202.752	210.785	189.893	200.982
62	TVJ-2	122.764	153.879	151.763	154.109	148.104	147.861	150.13	152.046	150.893	139.493	148.588
63	TVJ-3	78.7473	80.1886	81.7759	85.5513	72.5216	64.5654	154.603	76.0319	81.2871	65.3846	80.7849
64	TMR-1	112.562	144.793	153.34	211.721	213.78	213.324	153.751	184.747	229.729	208.667	201.648
65	TMR-2	98.222	109.578	102.654	113.038	107.333	109.019	101.79	106.905	115.142	103	107.99
66	TMR-3	104.01	126.724	134.431	180.159	167.445	193.491	129.383	145.65	171.905	150.648	169.602
N.G. 67	TMR-1	1984.52	1976.87	1878.43	2077.56	500.054	670.275	253.999	250.732	264.691	337.574	294.696
N.G. 68	TMR-2	1799.46	1790.39	927.014	602.145	197.664	387.703	71.8303	79.6501	83.0478	70.1156	82.557

		TEST NUMBER	303	304	305	306	307	308	309	310	311	312	313
N.G.	69	TNR-3	368.703	342.238	360.766	461.252	346.071	626.343	68.7573	76.6713	80.0891	67.8808	80.0245
N.G.	70	TAC-1	1561.45	1506.4	1340.16	899.511	3157.75	4032.88	3473.69	-15301	-14113	999999	999999
	71	TAC	526.208	536.005	549.427	552.782	547.484	543.979	550.338	554.444	558.005	549.463	552.432
	72	TPC	265.299	265.74	371.316	636.149	662.32	728.906	356.046	420.584	501.646	488.492	465.562
	73	THF-1	321.793	371.602	609.473	1019.87	947.751	1229.23	1127.37	765.872	977.967	947.691	1002.97
	74	THF-2	385.781	467.604	823.382	1297.45	1306.67	1391.61	1172.99	1096.24	1328.04	1280.14	1286.49
	75	THF-3	375.876	459.893	802.965	1371.99	1389.44	1432.71	1116.13	1185.09	1384.11	1336.34	1208.56
	76	TMS-1	93.6841	124.702	143.036	149.127	112.007	131.506	80.7932	97.3199	111.691	92.8081	103.846
	77	WOPDFM	0.16272	0.16271	0.16274	0.16271	0.16305	0.16281	0.16256	0.1627	0.16272	0.16316	0.16324
	78	WFPDFM	0.0761	0.07617	0.07611	0.07612	0.07626	0.07625	0.07602	0.07598	0.07601	0.07654	0.07643
	79	PVAC-1	7637.82	7603.88	7558.93	7541.08	7614.93	7322.88	7617.92	7546.4	7485.73	6833.18	7311.58
	80	PVAC-2	7628.09	7592.88	7550.86	7530.72	7604.78	7310.81	7597.54	7524.86	7464.82	6804.1	7280.75
	81	TMS-1	100.129	126.465	145.9	161.251	128.428	149.892	111.183	109.099	121.157	104.757	112.717
	82	TMS-3	999999	999999	999999	999999	999999	999999	999999	999999	1159.73	103.457	108.111
	83	PYRO-LO	2087.13	2064.02	2092.3	2105.53	2187.74	2100.14	2379.9	2175.83	2096.77	1923.93	1966.84
	84	PYRO-HI	3228.04	3206.63	3246.57	3254.8	3336.9	3334.03	2714.56	3504.64	3484.79	3296.27	3407.48
	85	POTS	247.969	245.67	248.102	249.828	249.665	240.35	246.303	248.211	245.722	214.127	247.523
	86	PFTS	252.217	255.219	252.924	254.755	257.428	253.825	253.847	254.224	253.988	255.585	258.622
	87												
	88												
	89												
	90												
	91	TIME-AVG	41.0536	39.5293	112.052	440.119	493.045	642.031	352.021	223.005	454.514	444.528	405.478
	92	T1	36.1219	35.085	105.106	405.253	455.14	635.092	305.113	205.114	405.139	405.132	369.006
	93	T2	45.9852	43.9735	118.998	474.985	530.95	648.969	398.93	240.897	503.888	483.925	441.949
	94												
	95												
	96												
	97	FMO1	0.15028	0.14901	0.15015	0.15057	0.14951	0.14453	0.14838	0.14918	0.14821	0.13194	0.14869
	98	FMO2	0.15025	0.14898	0.15012	0.15054	0.14968	0.14469	0.14815	0.14931	0.14803	0.13209	0.14879
	99	PCT WO	0.01596	0.01578	0.01595	0.01594	-0.1144	-0.1097	0.1577	-0.0885	0.12	-0.1077	-0.0637
	100	FMF1	0.14851	0.15013	0.14765	0.14764	0.14996	0.14887	0.14785	0.14847	0.14831	0.15266	0.15087
	101	FMF2	0.14799	0.14985	0.14765	0.14756	0.14994	0.14873	0.14757	0.14843	0.14836	0.15275	0.15049
	102	PCTWF	0.35065	0.1822	0.00018	0.0502	0.01427	0.09408	0.19264	0.02183	-0.0301	-0.0596	0.2534
	103	SGO	1.42317	1.42667	1.43417	1.43411	1.4405	1.43366	1.44253	1.44231	1.4453	1.43954	1.4368
	104	SGF	0.87001	0.87204	0.87457	0.87379	0.87643	0.8741	0.87688	0.87518	0.87487	0.8742	0.8756
	105	WO	0.21385	0.21256	0.21532	0.21591	0.21549	0.20733	0.21388	0.21525	0.21407	0.19004	0.21371
	106	WF	0.12898	0.1308	0.12913	0.12897	0.13142	0.13007	0.12952	0.12992	0.12977	0.13349	0.13193
	107	WT	0.34284	0.34336	0.34446	0.34488	0.34691	0.33739	0.3434	0.34517	0.34384	0.32353	0.34564
	108	MR	1.65804	1.62516	1.66742	1.67412	1.6397	1.594	1.65128	1.6568	1.6496	1.4236	1.61983
	109	FSL	99.4488	99.5164	99.9612	100.337	100.633	98.296	99.7913	100.412	99.9577	96.5374	104.138
	110	F-ALT	103.062	103.113	103.537	103.904	104.235	101.759	103.392	103.979	103.496	99.765	107.592
	111	ISP	300.616	300.306	300.583	301.275	300.465	301.605	301.083	301.235	300.997	308.362	311.285
	112	CSTR[COLD TH	5414.19	5406.99	5401.4	5395.94	5402.89	5436.99	5408.89	5404.19	5397.18	5423.61	5399.82
	113	CF	1.78517	1.7857	1.7892	1.79514	1.78801	1.78353	1.7897	1.79216	1.79306	1.82799	1.85345
	114	SGOJ	1.41719	1.42082	1.42956	1.43084	1.4358	1.44087	1.43545	1.43384	1.43784	1.43771	1.42936
	115	SGFJ	0.79707	0.79929	0.79875	0.79586	0.79841	0.80155	0.79745	0.79537	0.79367	0.80516	0.79896
	116	BIAS-A	1.00473	1.00469	1.00474	1.00476	1.00438	1.00468	1.00469	1.00476	1.0047	1.01023	1.01029
	117	BIAS-B	1.00473	1.00469	1.00474	1.00476	1.00438	1.00468	1.00469	1.00476	1.0047	1.01023	1.01029
	118	FA-CORR	99.4488	99.5164	99.9612	100.337	100.633	98.296	99.7913	100.412	99.9577	96.5374	104.138
	119	FB-CORR	99.4488	99.5164	99.9612	100.337	100.633	98.296	99.7913	100.412	99.9577	96.5374	104.138
	120	AE	24.4808	24.4808	24.4808	24.4808	24.4808	24.4808	24.4808	24.4808	24.4808	24.4808	24.4808
	121	AT	0.50542	0.50542	0.50542	0.50542	0.50542	0.50542	0.50542	0.50542	0.50542	0.50542	0.50542
	122	AVG PEXIT	0	0	0	0	0	0	0	0	0	0	0
	123	PRE FZERO	-0.0881	-0.1866	-0.131	-0.2222	-0.2853	0	-0.2678	-0.2141	-0.1596	-2.3345	-3.0609
	124	HZO1	831.52	824.52	830.802	833.105	827.293	799.976	821.1	825.46	820.12	731.308	822.791
	125	HZO2	856.551	849.424	855.82	858.165	853.339	825.42	844.762	851.253	844.078	755.137	848.324
	126	HZF1	842.979	852.251	838.046	837.942	851.304	845.036	839.18	842.715	841.826	866.813	856.518
	127	HZF2	829.87	840.262	827.975	827.462	840.75	833.992	827.49	832.336	831.903	856.457	843.804
	128	ROTV	-5815.6	-5967.5	-6071.7	-6204.3	-5886.9	-6296.9	-6171.2	-6156.7	-6372.8	-6750	-6216.8
	129	RFTV	-10187	-10037	-10243	-10376	-10247	-10081	-10020	-9975.6	-10019	-9421.4	-9902.4
	130	ROLJ	-136.59	-136.71	-136.54	-136.45	-136.6	-136.61	-136.83	-136.79	-136.86	-138.53	-136.8
	131	RFLJ	-141.41	-141.26	-141.67	-141.87	-141.68	-141.31	-141.97	-141.96	-142.09	-140.73	-141.52
	132	ROJT	3512.13	3500.33	3479.49	3545.54	3492.49	3580.88	3463.66	3458.9	3486.58	3505.32	3506.83
	133	RFJT	4679.51	4663.44	4690.13	4786.84	4802.22	4882.19	4747.3	4705.47	4748.51	4749.41	4722.82
	134	KOTV	0	0	0	0	0	0	0	0	0	0	0
	135	KFTV	0	0	0	0	0	0	0	0	0	0	0
	136	KOLJ	0	0	0	0	0	0	0	0	0	0	0

TEST STAND ERROR - THRUST REQUIRES CORRECTION

	TEST NUMBER	303	304	305	306	307	308	309	310	311	312	313
137	KFLJ	0	0	0	0	0	0	0	0	0	0	0
138	KOJT	0.01687	0.0169	0.01695	0.01679	0.01692	0.01671	0.01699	0.017	0.01694	0.01689	0.01689
139	KFJT	0.01462	0.01464	0.0146	0.01445	0.01443	0.01431	0.01451	0.01458	0.01451	0.01451	0.01455
140	POVIT	223.166	221.224	222.919	225.596	223.886	215.625	220.331	222.158	220.975	192.557	222.544
141	PFVIT	209.071	211.171	209.586	211.738	216.303	213.075	211.328	211.784	212.092	210.111	214.802
142	POJT	227.565	225.563	227.34	230.037	228.296	219.71	224.68	226.566	225.326	196.035	226.903
143	PFJT	211.893	214.062	212.41	214.564	219.225	215.929	214.173	214.652	214.961	213.098	217.744
144	RFRC	1404.51	1404.66	1417.9	346.646	1290.5	1231.49	1332.99	1348	1329.12	1310.35	1342.2
145	KFRC	0.02668	0.02668	0.02656	0.05371	0.02784	0.0285	0.02739	0.02724	0.02743	0.02763	0.0273
146												
147												
148												
149	Cp	0.71549	0.71472	0.71435	0.71502	0.71408	0.71393	0.71417	0.71486	0.71522	0.71325	0.71413
150	FUEL DT BASED	139.729	139.381	145.265	149.309	149.47	139.008	152.177	152.905	155.562	132.269	146.816
151	FUEL DT BASED ON TRIN			141.074	145.173	144.874	144.791	138.203	141.027	-999775	122.64	132.085
152	TEST DURATION											
153	PC-1[ROUNDED	114	114	114	115	115	113	114	115	114	108	115
154	MR{ROUNDED]	1.66	1.63	1.67	1.67	1.64	1.59	1.65	1.66	1.65	1.42	1.62
155	TIME-AVG[rnd]	41	40	112	440	493	642	352	223	455	445	405
156	MR[MICROM]	1.67	1.64	1.68	1.69	1.66	1.60	1.66	1.66	1.66	1.43	1.63
157	MRfm/MRmm	0.99072	0.9901	0.99129	0.98962	0.98922	0.99387	0.99739	0.99701	0.99647	0.99697	0.99617
158	KWOJT[MICRO]	0.0173	0.01732	0.01737	0.01724	0.01737	0.01723	0.01741	0.01741	0.01734	0.01735	0.01727
159	KWFJT[MICRO]	0.01476	0.01477	0.01475	0.0146	0.01456	0.01458	0.01474	0.01479	0.01471	0.01476	0.01474
160	Wt[MICROM.]	0.34275	0.34291	0.34423	0.34511	0.34708	0.3398	0.34388	0.34529	0.34396	0.32464	0.3455
161	C*[MICROM]	5415.54	5414.06	5404.99	5392.33	5400.29	5398.53	5401.38	5402.42	5395.34	5405.09	5401.92
162	PYRO-HI[120SE			3246.57	3254.8	3336.9	3334.03		3504.64	3484.79	3296.27	3407.48
163	MR/Pc [MARKER	1.66/114	1.63/114	1.67/115	1.67/115	1.64/115	1.59/113	1.65/114	1.66/115	1.65/114	1.43/108	1.62/115
164	TR-OUT [Q>=120SEC]			213.958	219.503	214.606	208.607	216.454	220.434	223.699	201.678	213.555
165	FUEL D T[Q>=120SEC]			141.074	145.173	144.874	144.791	138.203	141.027	-999775	122.64	132.085
166	FUEL T IN [RNDED]			73								81
167	PFVI[Q>=120SEC]			209.335	211.487	216.045	212.821	211.075	211.53	211.839	209.847	214.542
168	MMH T~PFVI [V.P.]			XXX	21.5	23.7	21.6	21.5	21	2	380	380
169	q, BTU/SEC	12.8167	12.9326	13.3182	13.6881	13.9393	12.9509	14.0732	14.1792	14.4119	12.6145	13.7943
170	MARKER 1									1		
171	MARKER 2											
172	MARKER 3											
173	MARKER 4											
174	MARKER 5			5								
175	MARKER 6						6					
176	MR ERROR, %; F	-0.928	-0.9896	-0.8709	-1.0381	-1.0777	-0.6133	-0.2613	-0.2985	-0.353	-0.3033	-0.3826
177	TOL/TFL/2 VS R	79.3854	76.1292	70.8911	71.6744	66.726	71.5105	65.5105	67.2277	66.3819	69.1192	68.9228
178	Dt [HOT]	0.82814	0.82799	0.82826	0.82832	0.82887	0.82885	0.82468	0.83	0.82987	0.8286	0.82935
179	C*[HOT] uM	5775	5772	5766	5753	5769	5767	5712	5787	5778	5771	5778
180												
181												
182												
183												
184												
185												
186												
187												
188												
189												
190												

ASRC501 [FILE7]
7-27-92
UPDATE 12-22-92

LINE No.	PARAMETER	TEST NUMBER 314	316	317	318	320	321	322	323	324	326	327
		TIME HR:MIN:SEC										
		PROGRAM										
14	TIME-AVG	432.55	455.083	435.016	437.54	455.998	453.016	535.541	547.065	547.523	471.717	387.648
15	T1	405.139	405.135	405.139	405.14	406.051	405.133	505.148	505.145	505.145	430.486	345.385
16	T2	459.961	505.031	464.893	469.94	505.946	500.9	565.934	588.984	589.901	512.949	429.912
17												
18												
19												
20	FMMO	0.215	0.20984	0.21165	0.21148	0.20881	0.20927	0.21133	0.21461	0.24102	0.23375	0.18513
21	FMO-1	0.14921	0.14785	0.14949	0.14932	0.14793	0.14822	0.14984	0.14897	0.16737	0.1621	0.12801
22	FMO-2	0.14932	0.14799	0.14928	0.14944	0.14804	0.14836	0.14998	0.14911	0.16757	0.16228	0.1283
23	FMF-1	0.1475	0.15035	0.14811	0.14749	0.15102	0.14942	0.14803	0.15224	0.16583	0.17703	0.14119
24	FMF-2	0.14796	0.15019	0.148	0.14738	0.15093	0.14932	0.1475	0.15218	0.16533	0.1769	0.14097
25	FMMF	0.12922	0.13147	0.12938	0.12882	0.13156	0.13019	0.12906	0.13376	0.14566	0.15545	0.12419
26	POTR	20.4701	22.4508	23.2085	21.1201	21.5822	20.0348	22.7565	13.062	12.9643	12.9039	203.131
27	PFTR	17.8547	14.9283	14.7681	14.7143	14.6228	14.4778	26.3101	15.327	15.1767	14.9662	229.025
28	PVT	3.02154	2.8144	3.05096	3.02085	2.96164	2.9518	3.04541	3.05025	3.37418	3.34551	2.35385
29	POVI	222.359	219.728	222.454	222.474	219.657	220.33	222.819	221.839	261.723	253.688	184.747
30	PFRI	236.8	239.966	237.223	236.057	240.551	237.904	236.252	245.301	280.516	301.4	215.863
31	PC-1	114.30	114.83	114.64	114.34	114.69	114.24	114.37	115.54	127.30	127.91	102.63
32	PFVI	210.544	213.898	211.353	210.112	214.059	211.626	210.041	218.192	247.881	263.999	190.841
33	PGODP	14.9868	14.7666	14.9091	14.9099	14.6714	14.632	14.5605	14.7602	14.7325	14.1572	14.0743
34	PGFDP	14.516	14.7548	14.7892	14.8043	14.681	14.6664	14.6313	14.7579	14.756	14.6429	14.5978
35	FCAL-A	0.03888	-0.2986	-0.8192	-1.1663	-0.0862	-0.2999	-0.37	0.18612	0.11783	-0.0168	-0.0474
36	FCAL-B	-0.091	-0.5537	-0.5031	-0.3425	-0.2851	-0.2375	-0.1269	0.18562	0.13189	0.21981	0.24515
37	F	99.0188	101.406	101.594	100.642	101.417	100.785	101.267	104.018	114.124	113.733	91.1819
38	PH2-UP	29.07	35.5031	35.5814	35.1671	31.8324	31.5778	31.1941	28.6259	52.117	51.4379	59.528
39	PH2-DN	11.3759	13.6935	13.8503	13.7154	12.4939	12.4251	12.3665	11.6291	19.7834	19.4771	22.537
40	PDX	2.90832	2.7784	2.95098	2.98199	2.96116	3.0169	2.9228	3.13706	3.43242	3.40192	2.56218
41	PDW	68.7949	69.1294	69.1753	69.1705	65.3426	65.593	65.437	64.7276	64.8508	64.9893	65.1699
42	POL-1	246.322	244.704	247.226	247.361	244.438	244.715	247.633	246.635	291.335	282.164	204.406
43	PFL-1	253.095	257.46	253.908	252.488	257.646	254.553	252.509	262.008	299.338	322.098	229.62
44	PEXIT-1	0.13392	0.1361	0.14123	0.14124	0.13533	0.13613	0.1332	0.1319	0.15782	0.15591	0.12365
45	PEXIT-2	0.13503	0.13543	0.1408	0.13946	0.13524	0.13506	0.13556	0.1346	0.15887	0.15699	0.12461
46	TDUCT	131.338	129.437	125.292	117.759	133.682	131.252	134.928	133.353	141.683	138.903	121.445
47	TVP	103.608	85.7459	98.3161	97.6787	85.9221	82.8613	87.0551	85.0508	83.698	84.9784	75.1003
48	VTCV	28.6602	28.6179	28.6219	28.6663	28.653	28.6866	28.6803	28.6539	28.6546	28.6674	28.6693
49	TOL	69.5253	66.6381	66.9512	64.5199	72.8469	71.6009	78.6487	76.1662	76.5938	73.5058	69.2838
50	TFL	68	65	64	63	74	72	76	70	71	71	66
51	TCELL	192.966	216.418	185.247	223.37	183.403	192.982	206.405	185.465	180.257	176.177	181.313
52	TOJ[OX IN]	74.6408	69.1197	72.5391	71.6494	74.8043	75.0652	78.8622	72.0663	72.931	71.4697	69.2541
53	TRIN	86	79	81	82	86	89	92	80	77	75	76
54	TR-OUT	219.637	211.107	216.028	217.556	214.686	218.015	223.121	205.667	194.011	181.029	213.157
55	TRI	217.191	209.776	214.147	216.541	212.402	215.505	221.597	202.93	192.216	179.407	211.258
56	TVB	207.829	197.663	203.255	205.758	201.255	205.645	210.516	193.234	184.472	172.165	200.682
57	TJB-1	251.128	240.514	245.297	219.083	238.901	243.954	253.288	238.8	227.724	216.5	246.34
58	TJB-3	364.252	356.456	357.663	357.539	360.005	361.303	364.161	352.117	352.74	353.138	349.611
59	TRB-1	375.335	372.015	375.244	376.612	375.026	381.09	392.579	385.443	365.533	330.735	363.976
60	TRB-2	183.747	178.569	183.199	184.008	182.618	185.853	191.797	179.841	177.338	167.409	175.213
61	TVJ-1	209.258	197.554	203.441	208.905	201.697	208.557	213.405	195.161	189.469	176.855	203.844
62	TVJ-2	150.825	142.916	147.627	148.418	146.827	149.49	155.713	141.494	137.714	131.607	145.793
63	TVJ-3	86.7049	67.772	79.1409	83.1975	83.1036	86.7162	88.6916	87.5007	90.5645	90.4278	89.9378
64	TMR-1	217.17	210.499	212.42	224.742	215.066	226.265	233.849	216.038	213.466	190.789	212.007
65	TMR-2	111.977	106.769	110.759	113.549	112.678	115.77	120.403	106.262	104.951	100.901	106.972
66	TMR-3	168.068	168.856	180.596	182.112	170.236	171.606	179.448	165.495	155.865	146.171	149.03
67	TNR-1	306.704	375.343	368.021	376.635	395.712	376.062	341.562	398.065	387.91	381.074	382.901
68	TNR-2	89.3554	71.7109	81.0138	88.6135	83.6558	92.61	94.5827	90.3186	98.2878	96.5568	96.3495

	TEST NUMBER	314	316	317	318	320	321	322	323	324	326	327
69	TNR-3	86.1884	68.5635	77.7322	84.4687	80.2421	88.5883	90.8051	86.8241	94.1793	93.2009	93.1602
70	TNC-1	999999	999999	999999	999999	999999	999999	999999	999999	999999	999999	999999
71	TAC	557.088	554.253	549.445	547.559	556.682	555.161	555.565	547.774	557.365	570.251	535.972
72	TPC	492.057	487.217	473.574	492.098	507.149	512.4	531.139	510.512	483.823	425.057	466.162
73	THF-1	988.356	962.298	1026.15	1009.32	991.739	1010.29	1056.46	1000.92	756.494	679.749	789.669
74	THF-2	1327.38	1322.1	1313.58	1337.66	1315.87	1329.41	1373.23	1327.36	1210.8	1117.56	1241.58
75	THF-3	1338.48	1302.9	1273.74	1286.1	1310.99	1375.39	1375.22	1371.09	1241.11	1130.13	1250.41
76	TMS-1	132.41	97.2549	107.573	150.185	117.673	149.518	146.923	116.851	151.348	138.584	147.966
77	WOPDFM	0.16318	0.16271	0.16282	0.16268	0.16292	0.16285	0.16289	0.16263	0.16266	0.16256	0.16249
78	WFPDFM	0.07662	0.07632	0.07642	0.07639	0.07637	0.07642	0.07626	0.07593	0.076	0.07592	0.07576
79	PVAC-1	7268.71	7452.53	7711.88	7650.42	7323.7	7299.98	7340.89	7384.96	8594.48	8507.32	6819.69
80	PVAC-2	7239.47	7424.01	7682.69	7620.8	7294	7270.33	7312.14	7354.24	8564.85	8477.51	6794.95
81	TMS-1	142.232	105.747	114.525	155.564	128.185	158.172	158.296	127.462	161.175	148.931	160.507
82	TMS-3	141.135	101.632	111.669	157.436	125.519	160.441	161.505	125.741	163.664	148.25	162.898
83	PYRO-LO	1993.39	2073.48	2083.77	2094.08	2133.85	2150.88	2167.74	2080.53	1931.56	1852.27	1943.37
84	PYRO-HI	3439.23	3432.19	3533.84	3540.87	3401.89	3415.34	3434.57	3390.41	3304.28	3161.87	3440.56
85	POTS	247.271	246.083	248.613	248.794	246.73	247.123	250.533	247.873	293.532	284.156	205.658
86	PFTS	253.731	255.209	255.774	254.332	259.403	256.324	256.735	264.098	298.862	324.777	231.806
87												
88												
89												
90												
91	TIME-AVG	432.55	455.083	435.016	437.54	455.998	453.016	535.541	547.065	547.523	471.717	387.648
92	T1	405.139	405.135	405.139	405.14	406.051	405.133	505.148	505.145	505.145	430.486	345.385
93	T2	459.961	505.031	464.893	469.94	505.946	500.9	565.934	588.984	589.901	512.949	429.912
94												
95												
96												
97	FMO1	0.14927	0.1479		0.14938	0.14798	0.14827	0.1499	0.14902	0.16732	0.16211	
98	FMO2	0.14935	0.14802		0.14948	0.14807	0.14839	0.15001	0.14914	0.16754	0.16228	
99	PCT WO	-0.0547	-0.0799	0.15237	-0.0669	-0.0615	-0.0798	-0.0749	-0.0775	-0.1272	-0.1077	-0.2691
100	FMF1	0.14754	0.15039		0.14753	0.15107	0.14946	0.14807	0.15228	0.16581	0.17691	0.14122
101	FMF2	0.14799	0.15022		0.14742	0.15107	0.1495	0.1473	0.15203	0.16536	0.17663	0.14086
102	PCTWF	-0.3025	0.11354	0.08131	0.0792	0.06943	0.07412	0.3621	0.04952	0.2957	0.05912	0.15489
103	SGO	1.43889	1.44266	1.44228	1.44545	1.43447	1.43613	1.42676	1.43007	1.42988	1.43391	1.43887
104	SGF	0.87483	0.87646	0.87696	0.8778	0.87198	0.87311	0.87052	0.8738	0.87359	0.87347	0.8759
105	WO	0.21484	0.21345	0.21552	0.21599	0.21234	0.21302	0.21395	0.2132	0.2394	0.23257	0.18425
106	WF	0.12927	0.13174	0.12987	0.12945	0.13168	0.13045	0.12867	0.13303	0.14463	0.15448	0.1236
107	WT	0.34411	0.34519	0.34539	0.34544	0.34402	0.34347	0.34261	0.34623	0.38404	0.38705	0.30784
108	MR	1.66192	1.62032	1.65944	1.66846	1.61252	1.63305	1.66276	1.60259	1.65524	1.50552	1.49071
109	FSL	102.863	103.328	104.164	102.586	103.187	102.476	103.144	105.048	114.438	114.257	91.4606
110	F-ALT	106.297	106.849	107.808	106.2	106.647	105.924	106.612	108.537	118.499	118.277	94.6828
111	ISP	308.903	309.537	312.131	307.431	310.006	308.394	311.172	313.484	308.561	305.588	307.567
112	CSTR[COLD TH	5397.68	5405.79	5393.63	5378.86	5417.5	5405.1	5424.66	5422.65	5386.56	5370.17	5415.81
113	CF	1.84	1.841	1.86061	1.83763	1.83981	1.83444	1.84429	1.85868	1.84175	1.82957	1.8259
114	SGOJ	1.43211	1.4394	1.4349	1.43608	1.43187	1.43152	1.42648	1.43553	1.43474	1.43661	1.43891
115	SGFJ	0.79579	0.80024	0.79767	0.79687	0.79837	0.79664	0.79397	0.80308	0.80916	0.81594	0.79917
116	BIAS-A	1.00736	1.01046	1.01009	1.00986	1.01014	1.00993	1.00975	1.00863	1.00931	1.00926	1.00942
117	BIAS-B	1.00736	1.01046	1.01009	1.00986	1.01014	1.00993	1.00975	1.00863	1.00931	1.00926	1.00942
118	FA-CORR	102.863	103.328	104.164	102.586	103.187	102.476	103.144	105.048	114.438	114.257	91.4606
119	FB-CORR	102.863	103.328	104.164	102.586	103.187	102.476	103.144	105.048	114.438	114.257	91.4606
120	AE	24.4808	24.4808	24.4808	24.4808	24.4808	24.4808	24.4808	24.4808	24.4808	24.4808	24.4808
121	AT	0.50542	0.50542	0.50542	0.50542	0.50542	0.50542	0.50542	0.50542	0.50542	0.50542	0.50542
122	AVG PEXIT	0	0	0	0	0	0	0	0	0	0	0
123	PRE FZERO	-3.093	-0.8524	-1.5304	-0.9421	-0.7345	-0.6836	-0.8812	-0.1316	0.74127	0.52446	0.57473
124	HZO1	825.962	818.437	827.475	826.559	818.877	820.496	829.415	824.615	925.921	896.889	709.267
125	HZO2	851.482	844.019	851.29	852.193	844.315	846.118	855.171	850.299	953.763	924.114	733.674
126	HZF1	837.415	853.77	840.929	837.357	857.655	848.423	840.457	864.658	942.713	1007.11	801.132
127	HZF2	829.86	842.313	830.108	826.654	846.458	837.449	827.331	853.431	926.931	991.579	790.847
128	ROTV	-6306.1	-6258.8	-6199.1	-6251.1	-6314.3	-6351.1	-6248.3	-6581.1	-6217.8	-6395.3	766.074
129	RFTV	-10101	-10062	-10234	-10248	-10042	-10129	-9674.1	-10029	-9730.4	-9127.6	2175.88
130	ROLJ	-136.71	-136.7	-136.73	-136.81	-136.66	-136.72	-136.38	-136.22	-134.72	-135.19	-139.05
131	RFLJ	-141.95	-141.5	-141.93	-142.11	-141.26	-141.61	-141.76	-140.91	-139.55	-138.38	-142.27
132	ROJT	3501.45	3462.76	3479.25	3477.21	3482.46	3495.3	3528.29	3506.2	3511.77	3488.08	3634.28
133	RFJT	4730.39	4715.19	4720.8	4701.08	4722.34	4706.1	4735.33	4805.27	4809.93	4798.34	4764.46
134	KOTV	0	0	0	0	0	0	0	0	0	0	0.03613
135	KFTV	0	0	0	0	0	0	0	0	0	0	0.02144
136	KOLJ	0	0	0	0	0	0	0	0	0	0	0

	TEST NUMBER	314	316	317	318	320	321	322	323	324	326	327
137	KFLJ	0	0	0	0	0	0	0	0	0	0	0
138	KOJT	0.0169	0.01699	0.01695	0.01696	0.01695	0.01691	0.01684	0.01689	0.01687	0.01693	0.01659
139	KFJT	0.01454	0.01456	0.01455	0.01458	0.01455	0.01458	0.01453	0.01443	0.01442	0.01444	0.01449
140	POVIT	222.754	220.118	222.85	222.871	220.045	220.719	223.213	222.23	262.196	254.138	185.058
141	PFVIT	210.796	214.156	211.606	210.364	214.319	211.881	210.292	218.455	248.18	264.331	191.076
142	POJT	227.15	224.44	227.265	227.301	224.345	225.046	227.588	226.551	267.587	259.233	188.338
143	PFJT	213.636	217.086	214.465	213.208	217.252	214.767	213.112	221.429	251.65	268.241	193.671
144	RFRC	1374.47	1316.54	1345.05	1359.03	1332.2	1348.36	1378.18	1338.47	1362.9	1369	1434.73
145	KFRC	0.02697	0.02756	0.02727	0.02713	0.0274	0.02723	0.02694	0.02733	0.02709	0.02703	0.0264
146												
147												
148												
149	Cp	0.71484	0.71374	0.71411	0.71411	0.71489	0.715	0.71596	0.7137	0.71264	0.71142	0.71404
150	FUEL DT BASED	151.433	146.019	151.91	155.046	141.016	146.51	146.668	135.494	123.439	110.222	146.998
151	FUEL DT BASED	134.01	132.595	135.437	135.534	129.144	128.896	131.346	125.655	116.841	105.92	137.092
152	TEST DURATION											
153	PC-1[ROUNDED	114	115	115	114	115	114	114	116	127	128	103
154	MR{ROUNDED]	1.66	1.62	1.66	1.67	1.61	1.63	1.66	1.60	1.66	1.51	1.49
155	TIME-AVG[rnd]	433	455	435	438	456	453	536	547	548	472	388
156	MR[MICROM]	1.66	1.60	1.64	1.64	1.59	1.61	1.64	1.60	1.65	1.50	1.49
157	MRfm/MRmm	0.99885	1.01519	1.01442	1.01629	1.01598	1.01596	1.01544	0.99881	1.00037	1.00122	1.00006
158	KWOJT[MICRO]	0.01728	0.01708	0.01702	0.01697	0.01703	0.01698	0.01699	0.01737	0.01736	0.01739	0.01703
159	KWFJT[MICRO]	0.01476	0.01477	0.01473	0.01475	0.01477	0.01478	0.01481	0.01473	0.01475	0.01475	0.01479
160	Wt[MICROM.]	0.34421	0.34131	0.34103	0.3403	0.34038	0.33946	0.34038	0.34837	0.38668	0.3892	0.30932
161	C*[MICROM]	5396.08	5467.3	5462.57	5460.2	5475.39	5469.03	5460.25	5389.32	5349.73	5340.48	5389.96
162	PYRO-HI[120SE	3439.23	3432.19	3533.84	3540.87	3401.89	3415.34	3434.57	3390.41	3304.28	3161.87	3440.56
163	MR/Pc [MARKER	1.66/114	1.62/115	1.66/115	1.67/114	1.61/115	1.63/114	1.66/114	1.6/116	1.66/127	1.51/128	1.49/103
164	TR-OUT [Q>=1	219.637	211.107	216.028	217.556	214.686	218.015	223.121	205.667	194.011	181.029	213.157
165	FUEL D T[Q>=1	134.01	132.595	135.437	135.534	129.144	128.896	131.346	125.655	116.841	105.92	137.092
166	FUEL T IN [RND	86		81	82	86	89	92	80			
167	PFVI[Q>=120SE	210.544	213.898	211.353	210.112	214.059	211.626	210.041	218.192	247.881	263.999	190.841
168	MMH T~PFVI [V.	380	380	380	380	380	380	380	386	395	403	370
169	q, BTU/SEC	13.9879	13.7018	14.0356	14.2625	13.2633	13.6381	13.5519	12.9346	12.8135	12.1895	13.0357
170	MARKER 1											
171	MARKER 2	2										
172	MARKER 3				3							
173	MARKER 4							4				
174	MARKER 5										5	
175	MARKER 6											
176	MR ERROR, %; F	-0.1151	1.51948	1.44225	1.62938	1.59798	1.59623	1.54427	-0.1192	0.03678	0.12175	0.00604
177	TOL/TFL/2 VS R	68.8644	65.863	65.5349	63.5148	73.2582	71.5527	77.5507	73.1694	73.583	72.1564	67.7213
178	Dt [HOT]	0.82956	0.82951	0.8302	0.83025	0.82931	0.8294	0.82953	0.82923	0.82865	0.82769	0.82957
179	C*[HOT] uM	5774	5850	5855	5853	5856	5850	5843	5763	5712	5689	5770
180												

ASRC501 [FILE7]
7-27-92
UPDATE 12-22-92

	TEST NUMBER	329	330	331	332	333	334	335	336	337	338	339
	TIME HR:MIN:SE	22					6	6	6	6	6	6
	PROGRAM											
LINE No.	PARAMETER											
14	TIME-AVG	113.541	539.537	552.055	535.544	552.056	17.0847	17.0873	17.0801	17.0851	17.0879	17.0904
15	T1	108.086	505.13	505.146	505.151	505.147	15.1851	15.1878	15.1805	15.1855	15.1884	15.1836
16	T2	118.996	573.944	598.964	565.937	598.965	18.9842	18.9869	18.9797	18.9846	18.9875	18.9972
17												
18												
19												
20	FMMO	0.20179	0.19015	0.22277	0.21276	0.21533	0.21677	0.23669	0.19068	0.24695	0.20202	0.21078
21	FMO-1	0.13738	0.13188	0.15494	0.14795	0.14822	0.15004	0.16408	0.13186	0.17043	0.13891	0.14483
22	FMO-2	0.13752	0.13194	0.15505	0.148	0.14837	0.15012	0.16434	0.13194	0.17066	0.13902	0.14498
23	FMF-1	0.14117	0.13196	0.14144	0.15211	0.14718	0.14839	0.17148	0.14023	0.15722	0.12057	0.15821
24	FMF-2	0.14084	0.13193	0.14101	0.15184	0.14697	0.14825	0.17156	0.14	0.15719	0.1203	0.15811
25	FMMF	0.12577	0.11611	0.12453	0.13317	0.12914	0.13029	0.15168	0.12381	0.13883	0.10653	0.13909
26	POTR	224.635	25.8705	26.9783	28.6008	22.1043	35.6525	27.3533	48.1335	44.8748	361.764	69.4646
27	PFTR	240.06	14.3186	14.2087	13.8923	13.725	14.4767	49.4669	47.2661	41.6395	55.845	82.2461
28	PVT	0.82805	2.4429	2.66857	2.79823	2.66553	0.22123	0.25558	0.21517	0.28059	0.20975	0.24991
29	POVI	200.612	187.018	230.308	222.521	220.238	221.981	256.326	187.861	266.371	194.917	216.664
30	PFRI	223.511	201.35	228.489	243.977	236.455	238.685	291.086	216.17	265.83	195.524	254.073
31	PC-1	109.31	102.17	114.87	114.93	114.29	115.239	128.185	104.822	127.109	102.257	116.045
32	PFVI	198.159	180.238	204.091	215.863	209.763	211.287	254.942	191.365	235.456	174.002	223.565
33	PGODP	14.4191	14.3997	14.3743	14.2551	14.2363	260.317	298.88	221.334	311.592	230.219	253.258
34	PGFDP	18.2279	18.1783	18.1518	18.087	18.0986	256.548	314.85	232.706	286.043	207.911	273.73
35	FCAL-A	-0.1552	-0.1287	-0.1313	-0.2562	-0.3533	0.12909	0.1528	0.12382	0.16422	0.12997	0.13963
36	FCAL-B	-0.2556	-0.1645	-0.1109	-0.0478	-0.0025	0.1345	0.1161	0.13275	0.1494	0.13713	0.15115
37	F	93.8712	89.4472	101.576	100.789	100.398	100.445	111.266	90.4565	110.596	88.9544	100.235
38	PH2-UP	69.1991	51.4757	51.3859	50.4268	49.5413	43.6212	43.5517	43.5823	43.6717	43.3931	43.0009
39	PH2-DN	25.5022	19.4404	19.416	19.0054	18.7601	16.493	16.4117	16.4415	16.5264	16.3855	16.2646
40	PDX	0.88734	2.43167	2.59879	2.69519	2.69179	0.21615	0.17758	0.14557	0.33129	0.19393	0.29921
41	PDW	85.2997	64.6119	64.9155	64.9043	65.0187	72.3875	72.3931	71.9363	71.6973	72.3904	71.4261
42	POL-1	223.141	207.526	256.283	246.708	245.526	247.677	285.895	208.876	297.909	218.162	241.347
43	PFL-1	238.22	214.482	242.96	259.947	251.532	253.703	311.167	230.007	282.916	205.89	270.791
44	PEXIT-1	0.14215	0.13103	0.14933	0.15044	0.15084	0.14035	0.15637	0.12603	0.15902	0.12493	0.14164
45	PEXIT-2	0.14896	0.13413	0.15278	0.15189	0.15204	0.14235	0.16099	0.12761	0.16122	0.12613	0.14308
46	TDUCT	106.497	119.551	126.608	126.845	124.219	101.154	81.8386	86.9678	92.6145	77.3799	75.7935
47	TVP	87.4433	81.7491	85.8956	79.6485	76.0427	85.3559	84.2081	88.9939	83.5733	67.7322	67.7938
48	VTCV	28.5265	28.6636	28.6796	28.6613	28.6697	28.3847	28.4439	28.4488	28.4661	28.4332	28.4168
49	TOL	46.8215	70.4179	72.2275	69.26	59.3498	67.4165	69.3768	66.2007	65.2567	59.3876	59.6282
50	TFL	39	62	62	61	58	61	51	53	53	58	60
51	TCELL	128.479	185.332	179.933	181.482	186.445	82.5145	89.5729	97.0055	106.485	86.8582	84.9895
52	TOJ[OX IN]	54.7118	75.9964	77.1075	73.7375	66.1806	70.1384	72.7364	69.0148	69.0977	63.8481	64.13
53	TRIN	57	80	79	77	77	60	59	-186	52	69	65
54	TR-OUT	198.82	238.302	227.011	203.736	212.191	195.548	164.417	203.028	193.698	236.327	185.164
55	TRI	195.075	236.182	224.838	201.922	210.691	192.763	161.196	199.4	189.345	234.563	182.2
56	TVB	180.419	223.489	214.419	192.963	199.627	115.093	117.554	160.079	173.046	146.907	126.313
57	TJB-1	219.67	262.794	256.949	235.404	243.509	174.061	162.302	213.033	219.644	209.243	179.834
58	TJB-3	324.022	362.865	358.005	345.463	351.038	212.357	224.611	272.781	293.351	236.532	235.279
59	TRB-1	275.983	406.24	388.274	358.274	359.108	140.517	139.789	199.807	230.441	193.098	150.808
60	TRB-2	146.051	190.499	185.199	168.816	177.2	151.788	143.703	189.873	214.392	143.302	159.106
61	TVJ-1	164.226	225.921	217.746	196.587	203.625	78.9907	93.0214	152.786	178.542	109.961	100.877
62	TVJ-2	121.293	160.131	154.929	142.928	142.813	73.3109	85.7512	146.27	169.144	99.6652	93.8108
63	TVJ-3	92.3028	92.5451	94.462	91.4177	90.1426	89.1533	89.7047	90.3851	90.4801	88.9403	87.9322
64	TMR-1	124.851	249.794	238.941	217.627	221.027	74.2377	76.2049	150.374	176.121	100.68	96.5409
65	TMR-2	76.6205	115.758	113.629	105.225	107.415	70.7103	65.9497	102.937	111.793	83.3209	81.8308
66	TMR-3	94.5392	169.204	177.455	169.918	177.101	74.2902	75.836	132.659	157.243	95.1934	93.7065
67	TNR-1	357.963	349.384	352.832	355.259	358.805	343.821	339.201	338.979	339.108	338.313	337.638
68	TNR-2	93.5341	96.9079	102.707	98.4025	97.6359	90.774	90.4818	90.4518	90.8189	90.7815	89.4622

	TEST NUMBER	329	330	331	332	333	334	335	336	337	338	339
69	TNR-3	91.3407	94.0136	99.2069	95.5437	94.7413	89.3256	89.2266	89.1237	89.1161	89.0666	88.2323
70	TNC-1	999999	999999	999999	999999	999999	999999	999999	999999	999999	999999	999999
71	TAC	508.392	543.134	540.241	533.827	542.499	390.18	428.542	444.863	469.401	399.951	430.27
72	TPC	266.218	534.242	515.557	479.975	468.403	92.5826	95.2279	167.832	206.218	116.454	112.153
73	THF-1	454.413	949.88	917.174	835.771	884.051	184.871	199.863	289.825	382.915	240.3	221.895
74	THF-2	700.1	1389.22	1329.36	1214.35	1256	171.64	199.417	373.421	483.977	265.829	240.732
75	THF-3	844.805	1409.95	1396.75	1295.34	1343.1	470.364	464.504	587.339	735.027	602.205	483.38
76	TMS-1	88.6339	141.719	157.105	143.03	153.924	77.4898	94.152	96.9832	104.282	97.5467	91.9598
77	WOPDFM	0.16279	0.16268	0.16265	0.16289	0.16256	2.76354	2.97283	2.46351	3.12745	2.54629	2.67155
78	WFPDFM	0.07601	0.07587	0.07581	0.07594	0.07577	2.65294	3.04544	2.50969	2.8823	2.24004	2.81144
79	PVAC-1	7933.66	7208.19	8164.35	8108.03	8108.71	8026.25	9027.48	7275.48	9008.25	7209.02	8102.62
80	PVAC-2	7900.85	7173.98	8130.09	8073.73	8076.52	7991.32	8991.36	7240.76	8982.9	7173.37	8067.96
81	TMS-1	95.4773	158.779	166.785	150.204	158.509	79.3669	93.7614	96.5947	104.825	98.1944	92.6079
82	TMS-3	91.5812	159.449	169.237	151.168	161.296	78.3994	94.301	100.118	111.005	103.098	95.7771
83	PYRO-LO	2011.11	2067.23	2076.21	1969.69	2024.98	1955.51	1875.19	1971.31	1990.44	2141.87	1906.92
84	PYRO-HI	3541.56	3598.04	3549.17	3414.97	3492.83	3467.41	3264.97	3496.06	3434.75	3792.26	3332.17
85	POTS	68.886	208.506	258.313	248.573	247.675	80.3479	81.2801	81.4817	81.6044	81.8002	15.2559
86	PFTS	61.3233	214.933	243.025	256.476	252.686	18.3364	18.0582	18.0257	17.86	17.4901	22.5143
87												
88												
89												
90												
91	TIME-AVG	97.993	455.067	455.027	455.031	455.028	17.0847	17.0873	17.0801	17.0851	17.0879	17.0904
92	T1	88.0149	405.119	405.136	405.14	405.137	15.1851	15.1878	15.1805	15.1855	15.1884	15.1836
93	T2	107.971	505.015	504.917	504.921	504.918	18.9842	18.9869	18.9797	18.9846	18.9875	18.9972
94												
95	← TEST STAND ERROR; THRUST REQUIRES CORRECTION →											
96												
97	FMO1	0.13737	0.13181	0.15499	0.148	0.14828	0.1501	0.16407	0.13178	0.17034	0.13892	0.14487
98	FMO2	0.13751	0.1319	0.15507	0.14803	0.1484	0.15015	0.16433	0.13189	0.17061	0.13902	0.145
99	PCT WO	-0.1042	-0.0725	-0.0534	-0.016	-0.0816	-0.0344	-0.1614	-0.0867	-0.1585	-0.0736	-0.0921
100	FMF1	0.1412	0.13194	0.14147	0.15215	0.14722	0.14843	0.17141	0.14026	0.15725	0.12045	0.15824
101	FMF2	0.14086	0.13192	0.14103	0.15187	0.14701	0.14829	0.17151	0.14002	0.15721	0.12021	0.15813
102	PCTWF	0.24383	0.01824	0.31067	0.18432	0.14873	0.09788	-0.0584	0.16501	0.02439	0.20423	0.06702
103	SGO	1.46742	1.43739	1.43539	1.43924	1.45211	1.44166	1.43939	1.44296	1.44487	1.45185	1.45172
104	SGF	0.89032	0.8782	0.87801	0.87841	0.88012	0.87856	0.88394	0.88276	0.8826	0.88032	0.87899
105	WO	0.20168	0.18952	0.22253	0.21303	0.2154	0.21643	0.23635	0.19023	0.24631	0.20176	0.21041
106	WF	0.12556	0.11586	0.12402	0.13353	0.12948	0.13034	0.15156	0.12371	0.13877	0.10593	0.13904
107	WT	0.32724	0.30539	0.34655	0.34656	0.34488	0.34677	0.38791	0.31395	0.38508	0.30769	0.34945
108	MR	1.60618	1.6358	1.79433	1.59541	1.66361	1.66049	1.55943	1.53774	1.77497	1.90469	1.51328
109	FSL	95.5634	91.0363	103.127	102.513	102.131	101.472	111.939	91.1168	111.415	90.1301	101.338
110	F-ALT	99.311	94.4401	106.983	106.342	105.961	105.263	116.204	94.5524	115.673	93.534	105.165
111	ISP	303.477	309.249	308.71	306.852	307.24	303.55	299.566	301.175	300.386	303.991	300.945
112	CSTR[COLD TH	5428.28	5436.56	5386.33	5388.84	5384.97	5400.23	5369.9	5425.7	5363.88	5400.57	5396.35
113	CF	1.79748	1.82888	1.84272	1.83077	1.83441	1.80726	1.79361	1.7847	1.80053	1.80977	1.79303
114	SGOJ	1.45781	1.42997	1.42889	1.43331	1.44327	1.43808	1.43495	1.43926	1.43985	1.44609	1.44591
115	SGFJ	0.80665	0.78605	0.79194	0.80409	0.79967	0.80836	0.82461	0.80446	0.80933	0.78708	0.81378
116	BIAS-A	1.00907	1.00971	1.00964	1.00929	1.00899	1.00944	1.00948	1.00978	1.00949	1.00887	1.00965
117	BIAS-B	1.00907	1.00971	1.00964	1.00929	1.00899	1.00944	1.00948	1.00978	1.00949	1.00887	1.00965
118	FA-CORR	95.5634	91.0363	103.127	102.513	102.131	101.472	111.939	91.1168	111.415	90.1301	101.338
119	FB-CORR	95.5634	91.0363	103.127	102.513	102.131	101.472	111.939	91.1168	111.415	90.1301	101.338
120	AE	24.4808	24.4808	24.4808	24.4808	24.4808	24.4808	24.4808	24.4808	24.4808	24.4808	24.4808
121	AT	0.50542	0.50542	0.50542	0.50542	0.50542	0.50542	0.50542	0.50542	0.50542	0.50542	0.50542
122	AVG PEXIT	0	0	0	0	0	0	0	0	0	0	0
123	PRE FZERO	-0.8337	-0.7136	-0.567	-0.7801	-0.8225	-0.0781	0.37823	0.22252	0.22811	-0.3832	-0.1343
124	HZO1	760.811	730.559	857.497	819.019	820.518	830.54	907.79	730.421	942.741	769.26	801.819
125	HZO2	785.333	754.112	883.585	844.083	846.156	855.977	935.68	754.073	971.115	793.742	827.161
126	HZF1	801.053	748.097	802.575	863.897	835.579	842.511	975.175	795.621	893.262	682.681	898.964
127	HZF2	790.072	740.299	791.023	851.545	824.356	831.508	961.753	785.413	881.437	675.325	886.598
128	ROTV	853.923	-6461.6	-5905.8	-6162.3	-6213.2	-5746.9	-5912	-5584.3	-5286.8	5938.1	-4839.3
129	RFTV	2352.58	-10869	-10853	-9963.5	-10305	-10191	-7919.4	-8325.3	-8895.9	-9284.9	-6438.1
130	ROLJ	-138.13	-138.78	-136.18	-136.8	-136.89	-136.5	-135.36	-138.63	-134.95	-137.79	-137.11
131	RFLJ	-142.75	-144.43	-143.05	-141.2	-142.07	-141.11	-138.74	-142.43	-140.74	-145.84	-140.01
132	ROJT	3422.49	3529.23	3478.89	3547.01	3444.46	3425.57	3438.72	3453.87	3451.48	3441.84	3435.47
133	RFJT	4693.49	4720.45	4741.78	4698.98	4701.44	4717.42	4695.82	4697.21	4699.94	5183.58	4672.38
134	KOTV	0.03422	0	0	0	0	0	0	0	0	0.01298	0
135	KFTV	0.02062	0	0	0	0	0	0	0	0	0	0
136	KOLJ	0	0	0	0	0	0	0	0	0	0	0

	TEST NUMBER	329	330	331	332	333	334	335	336	337	338	339
137	KFLJ	0	0	0	0	0	0	0	0	0	0	0
138	KOJT	0.01709	0.01683	0.01695	0.01679	0.01704	0.01709	0.01705	0.01702	0.01702	0.01705	0.01706
139	KFJT	0.0146	0.01455	0.01452	0.01459	0.01458	0.01456	0.01459	0.01459	0.01459	0.01389	0.01463
140	POVIT	200.965	187.342	230.726	222.911	220.632	222.38	256.787	188.187	266.864	195.272	217.044
141	PFVIT	198.398	180.452	204.327	216.127	210.015	211.541	255.262	191.6	235.735	174.192	223.846
142	POJT	204.806	190.819	235.435	227.233	225.02	226.82	262.048	191.668	272.541	199.143	221.234
143	PFJT	201.051	182.782	206.962	219.12	212.85	214.383	258.993	194.184	238.938	176.155	227.044
144	RFRC	1431.61	1381.18	1392.78	1385.06	1401.29	1416.88	1390.9	1430.75	1392.13	1688.47	1387.11
145	KFRC	0.02643	0.02691	0.0268	0.02687	0.02671	0.02657	0.02681	0.02644	0.0268	0.02434	0.02685
146												
147												
148												
149	Cp	0.71005	0.71601	0.71497	0.71268	0.71317	0.71188	0.70794	0.71182	0.71097	0.71543	0.71081
150	FUEL DT BASED	160.294	176.545	164.89	142.4	154.125	134.492	113.675	150.018	140.38	178.632	124.93
151	FUEL DT BASED	141.938	158.22	147.7	127.018	135.292	135.931	105.781	389.41	141.354	167.44	120.53
152	TEST DURATION											
153	PC-1[ROUNDED	109	102	115	115	114	115	128	105	127	102	116
154	MR{ROUNDED]	1.61	1.64	1.79	1.60	1.66	1.66	1.56	1.54	1.77	1.90	1.51
155	TIME-AVG[rnd]	114	540	552	536	552	17	17	17	17	17	17
156	MR[MICROM]	1.60	1.64	1.79	1.60	1.67	1.66	1.56	1.54	1.78	1.90	1.52
157	MRfm/MRmm	1.00111	0.99881	1.00304	0.99858	0.99771	0.99803	0.99937	0.99848	0.99782	1.00433	0.99858
158	KWOJT[MICRO]	0.01749	0.01726	0.01735	0.01713	0.01741	0.0175	0.01745	0.01744	0.01744	0.01745	0.01747
159	KWFJT[MICRO]	0.01486	0.01482	0.01481	0.01478	0.01478	0.01479	0.01484	0.01484	0.01483	0.01418	0.01487
160	Wt[MICROM.]	0.32756	0.30626	0.34731	0.34593	0.34447	0.34706	0.38837	0.31449	0.38578	0.30855	0.34986
161	C*[MICROM]	5423.03	5421.08	5374.6	5398.69	5391.33	5395.73	5363.5	5416.37	5354.15	5385.48	5389.98
162	PYRO-HI[120SE	3541.56	3598.04	3549.17	3414.97	3492.83						
163	MR/Pc [MARKER	1.61/109	1.64/102	1.79/115	1.6/115	1.66/114	1.66/115	1.56/128	1.54/105	1.77/127	1.9/102	1.51/116
164	TR-OUT [Q>=1	198.82	238.302	227.011	203.736	212.191						
165	FUEL D T[Q>=1	141.938	158.22	147.7	127.018	135.292						
166	FUEL T IN [RND	57	80					59	52	52		
167	PFVI[Q>=120SE	198.159	180.238	204.091	215.863	209.763						
168	MMH T~PFVI [V.	373	365	378	382	380						
169	q, BTU/SEC	14.3149	14.6766	14.6812	13.5147	14.1949	12.4742	12.2066	13.2211	13.8557	13.6139	12.3511
170	MARKER 1					1						
171	MARKER 2								2			
172	MARKER 3											3
173	MARKER 4											
174	MARKER 5											
175	MARKER 6		6									
176	MR ERROR, %; F	0.11094	-0.1189	0.3044	-0.142	-0.2288	-0.1968	-0.0631	-0.1524	-0.2184	0.43295	-0.1417
177	TOL/TFL/2 VS R	42.6734	66.0874	67.1743	65.2981	58.708	64.2364	60.0599	59.6056	59.2875	58.5412	59.9311
178	Dt [HOT]	0.83025	0.83063	0.8303	0.8294	0.82992	0.82975	0.82839	0.82994	0.82953	0.83194	0.82884
179	C*[HOT] uM	5813	5816	5762	5775	5774	5777	5723	5802	5729	5796	5758
180												

ASRC501 [FILE7]
7-27-92
UPDATE 12-22-92

	TEST NUMBER	340	341	342	343	344	345	346	347
	TIME HR:MIN:SE	6	6	6					
	PROGRAM								
LINE No.	PARAMETER								
14	TIME-AVG	17.0845	17.0852	17.0868	112.393	112.334	112.327	112.381	112.39
15	T1	15.1849	15.1857	15.174	105.791	105.797	105.79	105.779	105.788
16	T2	18.9841	18.9848	18.9995	118.995	118.872	118.865	118.983	118.992
17									
18									
19									
20	FMMO	0.22394	0.19666	0.23817	0.22109	0.22655	0.20391	0.21178	0.21572
21	FMO-1	0.15387	0.13513	0.16348	0.15585	0.16026	0.14585	0.15171	0.13826
22	FMO-2	0.15403	0.13523	0.16364	0.15592	0.16058	0.14346	0.15181	0.15282
23	FMF-1	0.14538	0.13385	0.16734	0.16755	0.16387	0.16537	0.15482	0.15374
24	FMF-2	0.14531	0.13363	0.16726	0.16694	0.1636	0.16478	0.15539	0.15349
25	FMMF	0.12788	0.11767	0.14711	0.14416	0.14102	0.14222	0.13337	0.13128
26	POTR	14.423	56.3725	57.768	265.665	275.33	247.631	257.432	273.83
27	PFTR	14.2232	65.9854	61.9783	293.203	286.923	281.679	263.018	260.892
28	PVT	0.28912	0.27674	0.33587	1.09133	1.06835	1.04037	0.9978	0.95547
29	POVI	230.189	192.83	256.132	238.49	247.122	224.112	232.443	247.675
30	PFRI	235.429	206.365	281.093	272.061	266.972	261.741	245.409	243.91
31	PC-1	116.414	104.618	127.125	121.272	122.018	115.055	114.893	115.314
32	PFVI	209.165	183.632	247.839	240.653	236.64	230.821	217.62	216.521
33	PGODP	269.106	226.315	297.954	14.4343	14.5049	14.4552	14.3414	14.3174
34	PGFDP	252.379	220.962	303.035	14.0829	13.9752	13.9144	13.9324	13.8899
35	FCAL-A	0.15895	0.14577	0.13644	-0.6054	-0.5607	-0.579	-0.5767	-0.5812
36	FCAL-B	0.15816	0.1529	0.14492	-0.7762	-0.6178	-0.5313	-0.4851	-0.4124
37	F	101.268	90.8004	110.082	104.532	105.47	98.7994	99.2482	99.8521
38	PH2-UP	43.0779	43.555	43.1008	64.447	64.19	63.9236	63.6769	63.2185
39	PH2-DN	16.3407	16.4662	16.2311	23.6676	23.6363	23.5224	23.4969	23.353
40	PDX	0.32336	0.23959	0.3876	1.16321	1.03663	0.99443	0.94644	0.90114
41	PDW	71.8492	71.981	72.0566	65.5773	65.5809	65.6073	65.3073	65.4389
42	POL-1	257.121	214.903	285.879	264.305	273.987	246.653	256.516	272.811
43	PFL-1	250.064	218.952	299.985	290.791	284.918	279.743	261.481	259.292
44	PEXIT-1	0.14432	0.12747	0.1577	0.1506	0.15131	0.14196	0.14144	0.14392
45	PEXIT-2	0.14567	0.12866	0.15911	0.15167	0.15253	0.14152	0.14204	0.14279
46	TDUCT	82.5485	82.4384	84.9992	125.503	123.105	117.752	119.856	115.308
47	TVP	67.7968	67.274	68.5978	100.045	95.6564	95.4608	95.4602	94.8797
48	VTCV	28.4133	28.4721	28.4868	28.5147	28.5793	28.5912	28.6005	28.5979
49	TOL	59.6519	59.5365	59.2346	92.3132	96.1094	106.62	107.647	117.771
50	TFL	60	60	60	103	102	102	102	114
51	TCELL	100.135	105.348	106.018	126.43	138.195	134.791	140.324	142.722
52	TOJ[OX IN]	64.5849	64.8636	64.5665	91.6064	95.3884	105.74	107.09	118.248
53	TRIN				106	107	106	108	119
54	TR-OUT	212.362	226.103	186.856	217.623	222.217	215.486	229.464	244.349
55	TRI	208.739	222.967	182.965	214.391	220.172	213.339	227.6	242.722
56	TVB	165.997	185.489	177.362	201.472	209.653	205.256	218.087	229.367
57	TJB-1	224.752	238.272	218.297	250.614	258.055	250.637	265.851	269.513
58	TJB-3	278.586	293.821	303.038	362.026	366.243	361.098	362.285	363.69
59	TRB-1	206.861	202.279	215.603	279.918	292.578	279.22	298.08	319.116
60	TRB-2	212.069	205.398	212.604	185.646	190.195	183.384	192.352	220.168
61	TVJ-1	158.265	182.843	191.789	184.435	205.382	204.652	215.838	219.551
62	TVJ-2	149.616	171.951	179.178	147.524	158.735	162.986	169.446	176.928
63	TVJ-3	88.1757	87.9969	88.1158	82.7825	84.8321	85.7484	86.4894	87.1619
64	TMR-1	154.941	167.21	179.518	151.062	174.096	169.786	179.579	181.118
65	TMR-2	108.219	115.739	115.534	118.036	125.115	124.323	127.61	137.16
66	TMR-3	140.341	145.245	160.446	125.935	142.246	142.765	147.171	150.59
67	TMR-1	336.691	336.437	336.277	226.501	241.634	250.655	260.149	270.344
68	TMR-2	89.8484	89.6872	89.7935	82.6931	85.6629	87.6813	89.4053	89.8926

D.G.
D.G.

	TEST NUMBER	340	341	342	343	344	345	346	347
O.G.	69 TNC-3	88.0494	88.0494	88.1804	80.9929	83.5403	85.3942	86.7565	87.3729
O.G.	70 TNC-1	999999	999999	999999	999999	999999	999999	999999	999999
	71 TAC	450.984	458.131	493.566	568.744	561.235	550.092	538.213	529.45
	72 TPC	171.681	180.691	195.893	299.414	338.773	313.151	345.131	343.511
	73 THF-1	324.484	250.103	348.8	400.029	462.05	452.762	500.378	479.441
	74 THF-2	397.318	347.581	432.506	651.773	757.16	706.656	771.677	742.428
	75 THF-3	649.41	616.162	653.554	627.563	730.332	747.077	830.905	759.684
	76 TMS-1	98.0588	112.479	120.656	89.019	135.098	147.765	153.622	142.301
	77 WOPDFM	2.83305	2.51805	3.01767	0.16485	0.16479	0.16496	0.165	0.16502
	78 WFPDFM	2.5991	2.3943	2.99407	0.07863	0.07866	0.07881	0.07881	0.07899
	79 PVAC-1	8224.51	7334.32	8916.5	8142.01	8200.44	7640.96	7667.39	7738.87
	80 PVAC-2	8190.5	7300.93	8883.54	8107.63	8166.51	7607.02	7633.57	7701.07
	81 TMS-1	99.5958	113.904	122.426	93.4629	136.044	145.688	151.275	140.878
	82 TMS-3	104.11	123.304	132.875	93.0908	140.521	153.694	159.699	148.163
	83 PYRO-LO	2019.64	2044.19	1919.48	1927.47	1961.06	1896.03	1973.09	1995.42
	84 PYRO-HI	3501.25	3578.5	3294.43	3210.27	3260.37	3174.29	3309.58	3344.13
	85 POTS	14.2478	13.5903	13.4019	69.0731	148.063	128.759	115.535	44.5348
	86 PFTS	22.4315	22.3723	22.1941	64.8106	126.352	84.121	62.6852	28.0757
	87								
	88								
	89								
	90								
	91 TIME-AVG	17.0845	17.0852	17.0868	112.393	112.334	112.327	112.381	112.39
	92 T1	15.1849	15.1857	15.174	105.791	105.797	105.79	105.779	105.788
	93 T2	18.9841	18.9848	18.9995	118.995	118.872	118.865	118.983	118.992
	94	TEST STAND ERROR							
	95	THRUST REQUIRES CORRECTION							
	96								
	97 FMO1	0.15392	0.1351	0.16347	0.15589	0.16028	0.14589	0.15177	0.15287
	98 FMO2	0.15406	0.13521	0.16363	0.15594	0.16059	0.14348	0.15185	0.15285
	99 PCT WO	-0.0939	-0.0829	-0.0976	-0.0329	-0.1909	1.66886	-0.0498	0.01529
	100 FMF1	0.14543	0.13385	0.16731	0.16752	0.16387	0.16535	0.15485	0.15378
	101 FMF2	0.14534	0.13363	0.16723	0.16691	0.16359	0.16477	0.15542	0.15352
	102 PCTWF	0.05828	0.16912	0.04409	0.36365	0.1663	0.34903	-0.3627	0.17181
	103 SGO	1.4518	1.45164	1.45255	1.40856	1.40354	1.38912	1.38783	1.37427
	104 SGF	0.87919	0.87931	0.87937	0.85685	0.85712	0.85718	0.8574	0.85115
	105 WO	0.22356	0.1962	0.23757	0.21962	0.22518	0.20099	0.21068	0.21007
	106 WF	0.12782	0.1176	0.14709	0.14328	0.14033	0.14149	0.13301	0.13078
	107 WT	0.35138	0.31379	0.38466	0.3629	0.36551	0.34248	0.3437	0.34085
	108 MR	1.74906	1.66838	1.6151	1.5328	1.60457	1.42053	1.58394	1.60634
	109 FSL	102.007	91.3854	110.89	105.586	106.452	99.7599	100.169	100.669
	110 F-ALT	105.892	94.8492	115.103	109.432	110.325	103.369	103.79	104.323
	111 ISP	301.358	302.265	299.233	301.548	301.838	301.828	301.983	306.064
	112 CSTR[COLD TH	5383.7	5417.71	5370.45	5430.37	5424.72	5459.24	5432.17	5497.56
	113 CF	1.79971	1.7938	1.79143	1.78537	1.78895	1.77758	1.78735	1.78996
	114 SGOJ	1.44544	1.44475	1.44568	1.40951	1.40451	1.39031	1.38858	1.37362
	115 SGFJ	0.79959	0.79241	0.8129	0.79684	0.79444	0.79795	0.79066	0.78289
	116 BIAS-A	1.00964	1.00974	1.00949	1.00464	1.00453	1.00469	1.00473	1.00406
	117 BIAS-B	1.00964	1.00974	1.00949	1.00464	1.00453	1.00469	1.00473	1.00406
	118 FA-CORR	102.007	91.3854	110.89	105.586	106.452	99.7599	100.169	100.669
	119 FB-CORR	102.007	91.3854	110.89	105.586	106.452	99.7599	100.169	100.669
	120 AE	24.4808	24.4808	24.4808	24.4808	24.4808	24.4808	24.4808	24.4808
	121 AT	0.50542	0.50542	0.50542	0.50542	0.50542	0.50542	0.50542	0.50542
	122 AVG PEXIT	0	0	0	0	0	0	0	0
	123 PRE FZERO	0.23474	0.29654	0.23404	-0.5662	-0.5013	-0.495	-0.4494	-0.4095
	124 HZO1	851.578	748.464	904.483	862.48	886.771	807.437	839.737	845.82
	125 HZO2	877.912	772.531	931.733	888.474	914.586	818.645	865.475	871.111
	126 HZF1	825.258	758.998	951.395	952.643	931.48	940.066	879.462	873.282
	127 HZF2	815.066	749.792	937.695	935.903	917.246	923.875	871.392	860.757
	128 ROTV	-6279.5	-5158.9	-5117.2	781.481	768.852	796.297	769.074	802.313
	129 RFTV	-10504	-7494.3	-7566.6	2180.86	2175.83	2165.16	2187.2	2195.23
	130 ROLJ	-136.26	-138.31	-135.51	-135.78	-135.41	-136.85	-136.15	-136.12
	131 RFLJ	-142.14	-143.78	-139.6	-139.18	-139.6	-139.22	-140.48	-140.76
	132 ROJT	3438.4	3461.59	3451.58	3573.37	3612.82	3902.8	3825.75	4268.08
	133 RFJT	4686.77	4676.38	4681.04	4779.45	4769.79	4760.4	4737.46	4779.53
	134 KOTV	0	0	0	0.03577	0.03606	0.03544	0.03606	0.0353
	135 KFTV	0	0	0	0.02141	0.02144	0.02149	0.02138	0.02134
	136 KOLJ	0	0	0	0	0	0	0	0

	TEST NUMBER	340	341	342	343	344	345	346	347
137	KFLJ	0	0	0	0	0	0	0	0
138	KOJT	0.01705	0.017	0.01702	0.01673	0.01664	0.01601	0.01617	0.01531
139	KFJT	0.01461	0.01462	0.01462	0.01446	0.01448	0.01449	0.01453	0.01446
140	POVIT	230.608	193.171	256.594	238.905	247.554	224.475	232.834	248.066
141	PFVIT	209.412	183.851	248.146	240.952	236.929	231.114	217.885	216.781
142	POJT	235.309	196.847	261.872	243.552	252.444	228.452	237.188	252.438
143	PFJT	212.178	186.23	251.715	244.407	240.258	234.481	220.901	219.727
144	RFRC	1413.35	1445.44	1351.56	1310.89	1320.09	1323.98	1346.72	1363.06
145	KFRC	0.0266	0.0263	0.0272	0.02762	0.02752	0.02748	0.02725	0.02709
146									
147									
148									
149	Cp	0.71336	0.71464	0.7109	0.71793	0.71831	0.71766	0.71895	0.7215
150	FUEL DT BASED	152.502	166.474	127.351	114.97	120.075	113.469	127.869	130.786
151	FUEL DT BASED	212.362	226.103	186.856	111.79	115.26	109.682	121.755	125.741
152	TEST DURATION								
153	PC-1[ROUNDED	116	105	127	121	122	115	115	115
154	MR{ROUNDED]	1.75	1.67	1.62	1.53	1.60	1.42	1.58	1.61
155	TIME-AVG[rnd]	17	17	17	112	112	112	112	112
156	MR[MICROM]	1.75	1.67	1.62	1.53	1.61	1.43	1.59	1.64
157	MRfm/MRmm	0.99877	0.99824	0.99758	0.99948	0.99879	0.99075	0.99754	0.97754
158	KWOJT[MICRO]	0.01746	0.01742	0.01744	0.0172	0.01709	0.01656	0.01658	0.016
159	KWFJT[MICRO]	0.01485	0.01487	0.01485	0.01478	0.01478	0.0148	0.0148	0.01475
160	Wt[MICROM.]	0.35182	0.31433	0.38527	0.36525	0.36757	0.34613	0.34515	0.347
161	C*[MICROM]	5377.07	5408.41	5361.89	5395.47	5394.32	5401.6	5409.3	5400.17
162	PYRO-HI[120SEC.=]				3210.27	3260.37	3174.29	3309.58	3344.13
163	MR/Pc [MARKER	1.75/116	1.67/105	1.62/127	1.53/121	1.6/122	1.42/115	1.58/115	1.61/115
164	TR-OUT [Q>=120SEC]				217.623	222.217	215.486	229.464	244.349
165	FUEL D T[Q>=120SEC]				111.79	115.26	109.682	121.755	125.741
166	FUEL T IN [RND				106	107	106	108	119
167	PFVI[Q>=120SEC]				240.653	236.64	230.821	217.62	216.521
168	MMH T~ PFVI [V.P.]				390	388	386	382	382
169	q, BTU/SEC	13.9116	13.9991	13.3182	11.8991	12.1632	11.5812	12.2612	12.3877
170	MARKER 1								
171	MARKER 2								
172	MARKER 3								
173	MARKER 4			4					
174	MARKER 5						5		
175	MARKER 6								6
176	MR ERROR, %; F	-0.1228	-0.1763	-0.2417	-0.0522	-0.1205	-0.9251	-0.2461	-2.2459
177	TOL/TFL/2 VS R	59.7561	59.5827	59.3698	97.4829	99.1259	104.319	104.621	115.667
178	Dt [HOT]	0.82998	0.8305	0.82858	0.82802	0.82835	0.82777	0.82869	0.82892
179	C*[HOT] uM	5760	5801	5724	5752	5756	5756	5776	5770
180									

APPENDIX L

JOINT FAILURE ANALYSIS

GENCORP AEROJET

Propulsion Division

Materials Analysis

REPORT NO. MA-93-103

DATE 6 MAY 1993

WORK REQUESTED BY: D. M. JASSOWSKI	DEPT: 5267		PAGE 1 OF 5
SUBJECT: Metallurgical Failure Analysis of AJ10-221, S/N 001 C-103 Nozzle Extension			TABLES: 1
			FIGURES: 12
PROGRAM: AJ10-221	W.O. NO.: KGH34A22M8		ENCLOSURES: 2
PART NAME: Nozzle	PART NO.: 1206351-9	S/N: 001	MATERIAL: C-103 Cb

PURPOSE:

To determine the cause of brittle fracture of the C-103 nozzle extension at the Re/Cb transition joint after 6 hours of engine firing.

Summary:

Fracture of the nozzle was caused by severe embrittlement of the C-103 by oxygen diffusion from both the ID and OD uncoated nozzle surfaces during engine firing. Oxygen was introduced to the C-103 in the form of water vapor from both combustion gases (internally) and "wet" hydrogen cover gas (externally).

Numerous surface cracks, on both ID and OD surfaces of the uncoated C-103, were initiated during the firings. These surface cracks contributed to the fracture by acting as stress risers which lead to the failure of the embrittled C-103 at room temperature. These cracks were randomly distributed around the periphery of the nozzle joint and were caused by the C-103 degradation rather than material or design defects, or unusual structural loads.

DISTRIBUTION

L. Schoenman
Library (2)
File (3)

REPORT BY: M. MURPHY

REVIEWED BY:

APPROVED BY: J.P. BECK, MANAGER MATERIALS & PROCESSES

Background:

On 2/12/93 the C-103 nozzle extension completely separated from the AJ10-221 engine in the altitude testing facility during the installation of the LORAL heat shield. The engine had seen approximately 6 hours of firing, the last 2 of which were a continuous burn. According to the preliminary background report, Enclosure (1), the LORAL heat shield had just been installed when the personnel performing this work heard a noise which was found to be caused by the fracture of the nozzle at the nozzle/engine transition joint.

The AJ10-221 engine assembly is shown in Figure 1. The C-103 nozzle extension is normally a 286:1 exit ratio, however the subject nozzle was cut back to 47:1 to facilitate long duration altitude testing. The nozzle is joined to the rhenium chamber at the transition weld joint shown in Figure 2.

The altitude testing facility cannot completely eliminate oxygen from the cell during testing, therefore hydrogen gas was flowed around the exterior of the engine and nozzle to prevent oxidation. Most of the C-103 nozzle surface is coated with R512E silicide coating, however since there was a concern regarding contamination of the transition joint weld by the R512E, the end of the nozzle at the joint was left uncoated. This is the area of the fracture.

DETAILS OF ANALYSIS

Visual Inspection:

Examination of the fractured nozzle showed no obvious evidence of oxidation or other unusual surface anomalies, Figure 3. Closer examination of the OD surface at the fracture showed numerous secondary cracks running parallel to the primary fracture, Figure 4. This Figure also shows that cracking only occurred in the uncoated area of the nozzle. Macro-examination of the fracture surface shows a faceted surface indicative of brittle failure. Figures 5 and 6 show the similarity of the fracture appearance in two areas approximately 180° apart. Most of the fracture surface has a shiny appearance which is not indicative of high temperature fracture, i.e. not oxidized. There are also significant areas which are discolored, blue or grey, which are typical of light oxidation during high temperature exposure. These discolored areas are not continuous, and appear uniformly distributed around the fracture. These high temperature cracks originate from both the ID and OD surfaces.

It appears that multiple cracks formed at some time during the test program, and that these crack surfaces were exposed to elevated temperatures, however final fracture occurred at room temperature. The room temperature fracture was extremely brittle, and constituted at least 50% of the fracture surface.

Scanning Electron Microscope (SEM) Examination

Examination of the fracture surface in the SEM failed to reveal any new information. The discolored areas appeared to have a light film (probably oxide) however, this could not be verified by energy dispersive X-ray (EDX) analysis, due to the low atomic number of oxygen. No crack origin/s or propagation directions could be identified. No fatigue striations were observed.

SEM examination of the ID surface of the C-103 adjacent to the fracture revealed multiple thickness of the surface film, Figure 7. EDX analysis show only niobium. Further investigation of the surface film required X-ray diffraction analysis to identify low atomic number elements.

X-Ray Diffraction Analysis

Various sections of the fracture and ID surface film were analyzed by X-ray diffraction in order to identify low atomic number elements; oxygen, hydrogen, carbon, nitrogen, on the surface of the C-103. The results of this analysis are included in Enclosure (2). The uncoated ID surface of the C-103 was shown to be covered with an oxide film. Hydrides, nitrides, and carbides were not observed. The C-103 substrate below the oxide film was found to be C-103 with a high concentration of oxygen in solid solution. Again, no hydrogen, nitrogen, or carbon was observed.

Metallographic Examination

Five metallographic cross section samples were prepared from five equally spaced locations around the fracture. Each of the samples exhibited the same features. Figure 8 shows one of the sample cross-sections at low (50x) magnification. The normal C-103 microstructure shows distinctly etched grains, however the area adjacent to the fracture and to the uncoated C-103 surfaces shows that microstructural features are inhibited in an apparent diffusion zone. This diffusion zone corresponds exactly to the uncoated surfaces of the C-103. No diffusion zones are observed at locations of R512E coating cracks. Numerous secondary cracks are observed in the diffusion zone on both the ID and OD surfaces, primarily near the main fracture but with at least one OD crack relatively far from the fracture. Grain boundaries near the fracture are very distinct, indicating some type of grain boundary phase. Comparison of the ID and OD diffusion zones suggests equivalent diffusion rates (depth of penetration).

Closer examination of the C-103 microstructure near the fracture shows a continuous grain boundary phase, Figures 9 and 10. Some cracking is observed in this phase, Figure 10., Figure 10 also shows another phase on the grain boundary crack surface. It is presumed that the surface layer is NbO_2, and that the grain boundary phase is NbO. Both Figures show a local precipitate zone approximately 0.0015" deep in the C-103 grains at the fracture.

EDX Analysis of Metallographic Cross-Sections

The metallographic cross-section samples were analyzed by EDX to identify the grain boundary phase. Figure 11 shows an electron back scatter image of the grain boundary phases. Back scatter images reflect density differences. Low average density numbers produce a darker image than high average density. It can be seen from this Figure that the grain boundaries have a significantly lower average density than the grains, indicating a niobium compound rather than a hafnium compound. EDX analysis of the grain boundaries, and grains in unaffected C-103 showed identical analyses (primarily niobium with lesser amounts of hafnium) verifying this finding.

Microhardness Surveys

Microhardness measurements were made at various locations in the C-103 diffusion zone, Figure 12. The hardness data, presented in Table I, shows a severe increase in hardness in the diffusion zone compared to the unaffected C-103. Note that the hardness measurements adjacent to the ID and OD surfaces have the same approximate values as the measurements adjacent to the fracture. There is no measurable hardness gradient. These hardness results are identical to results obtained from C-103/combustion gas reaction tests performed at Aerojet in 1986 (reference 1).

DISCUSSION

All of the metallurgical evidence indicates that failure of the AJ10-221 nozzle was caused by gradual oxygen diffusion into the uncoated surfaces of the C-103 during engine firing, which resulted in severe C-103 embrittlement by oxygen solid solutioning. The diffusion occurred preferentially at grain boundaries, as indicated by the oxide film formation near the primary fracture. This preferential grain boundary embrittlement provided an intergrannular crack path for subsequent fracture. There is no evidence that preferential oxidation of the hafnium alloying element in the C-103 occurred. Furthermore, there is no metallographic or chemical evidence that hydrogen, nitrogen, or carbon reacted adversely with the C-103.

The failure mechanism was limited to the uncoated areas of the nozzle. The R512E coating was masked from the area of the transition weld joint to preclude inducing weld defects. It was anticipated that physical restriction would limit the accessibility of the combustion gases to the uncoated C-103, and that the hydrogen purge on the outside of the chamber and nozzle would prevent external oxidation.

It is now concluded that the external hydrogen cover gas reacted with air to form water vapor, which then reacted with the C-103 resulting in limited amounts of oxygen available for diffusion without significant gross oxidation of the unprotected C-103. Likewise, the internal combustion gases contain minimal free oxygen but significant amounts of water vapor. This hypothesis explains the equivalent diffusion rates from both the ID and OD surfaces of the C-103.

CONCLUSIONS:

1. Numerous cracks were initiated on both the ID and OD surfaces of the C-103 nozzle during engine testing, and were subjected to "wet" hydrogen and combustion gases at elevated temperature, however, final fracture occurred at room temperature.

2. The room temperature fracture occurred due to severe embrittlement of the C-103 by excessive oxygen in solid solution in the alloy, and the notch effect of the ID and OD cracks.

3. The source of oxygen which caused the embrittlement was the engine combustion gases and "wet" hydrogen cover gas on the exterior of the engine.

RECOMMENDATIONS:

1. Oxygen must be precluded from uncoated C-103, by precluding external oxygen, and by either an improved joint design, or by an uninterrupted R512E coating.

REFERENCES:

1. Aerojet Propulsion Division, Materials & Processes Dept. Report MA-86-103: Preliminary Evaluation of Uncoated Columbium Alloy in Elevated Temperature Oxidizing Atmospheres, J.A.Brown, 2/13/1986.

TABLE I

Microhardness Survey Results

	OD Surface	ID Surface	Fracture	C-103	
Surface	58 Rc	62 Rc	59 Rc	20 Rc	*
	58 Rc	60 Rc	58 Rc	71 Rb	
	59 Rc	57 Rc	59 Rc	73 Rb	
	59 Rc	57 Rc	59 Rc	76 Rb	

* Note: 20 Rc = 80 Rb (71 Rb equivalent to 11 Rc).

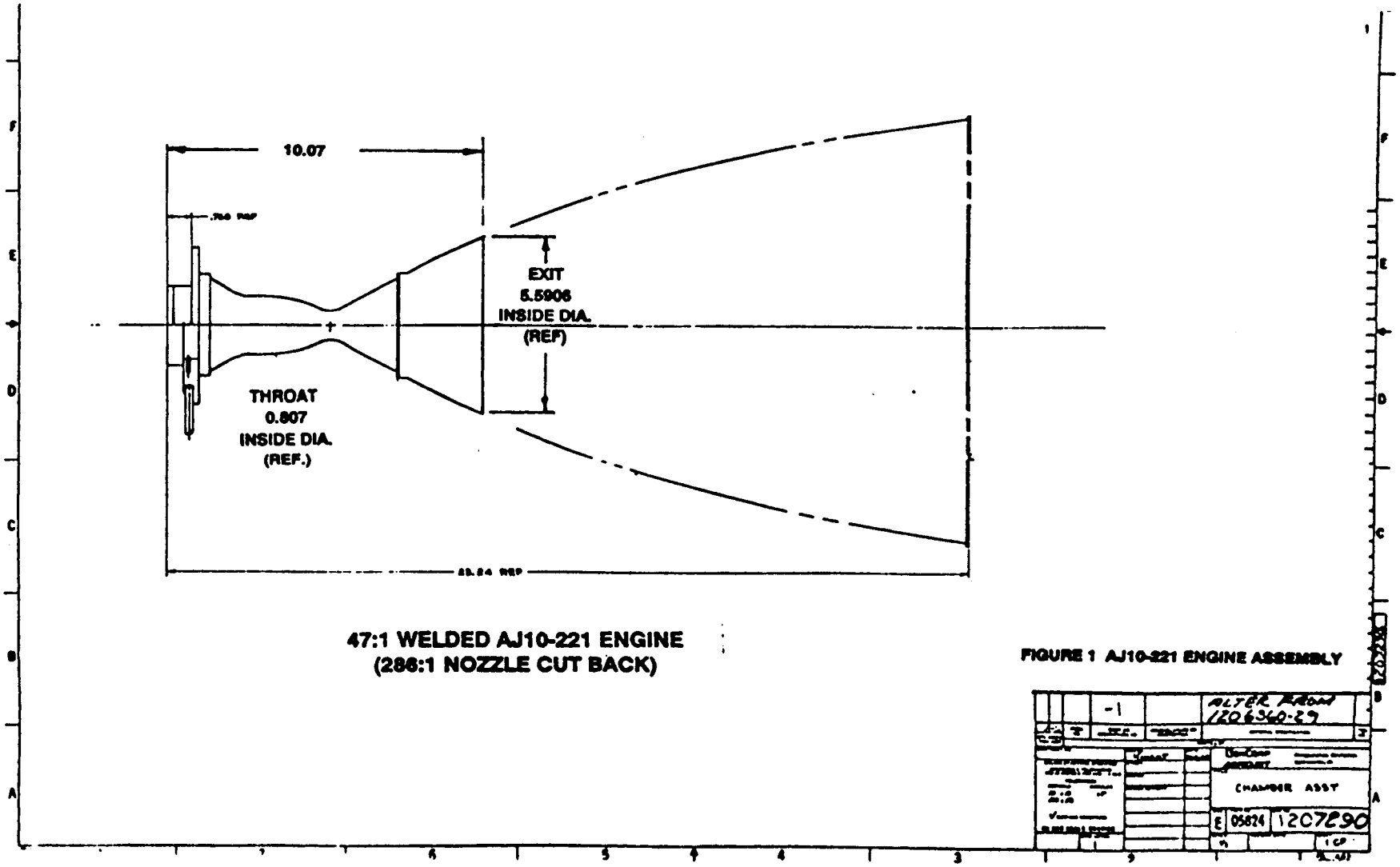

Figure 1

AJ10-221 Rhenium Chamber - C-103 Nozzle Engine Assembly

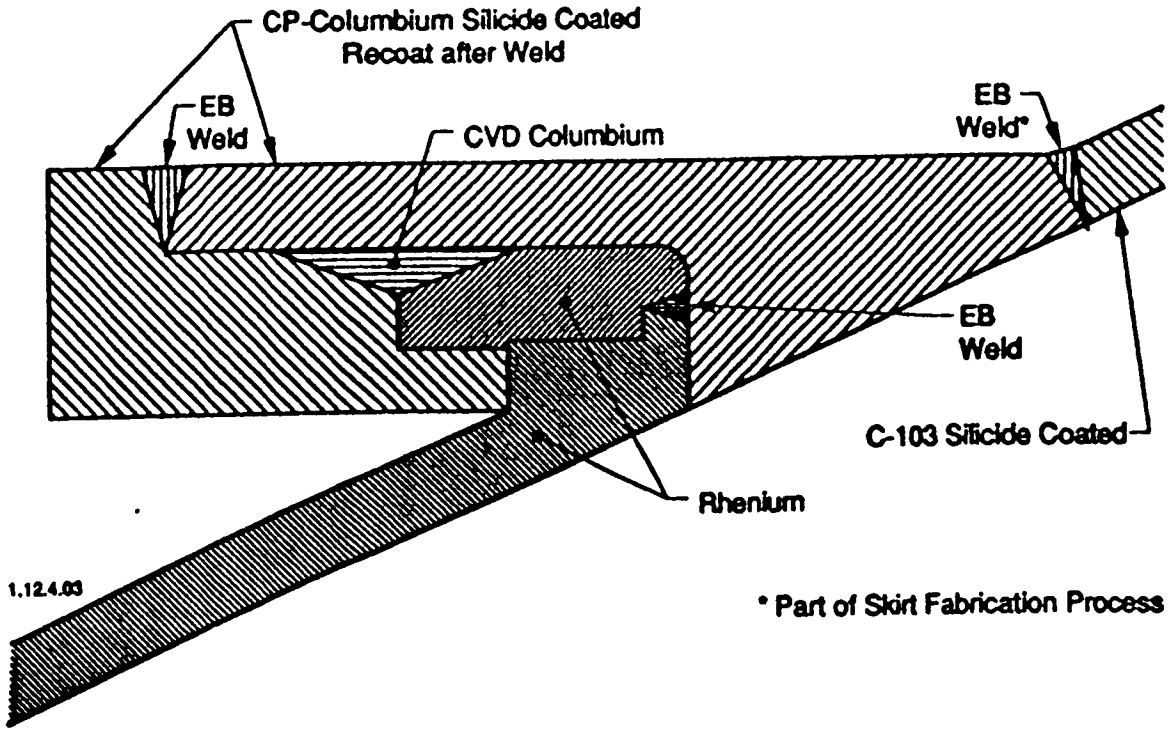

Figure 2

Details of Rhenium Chamber - C-103 Nozzle Transition Weld Joint

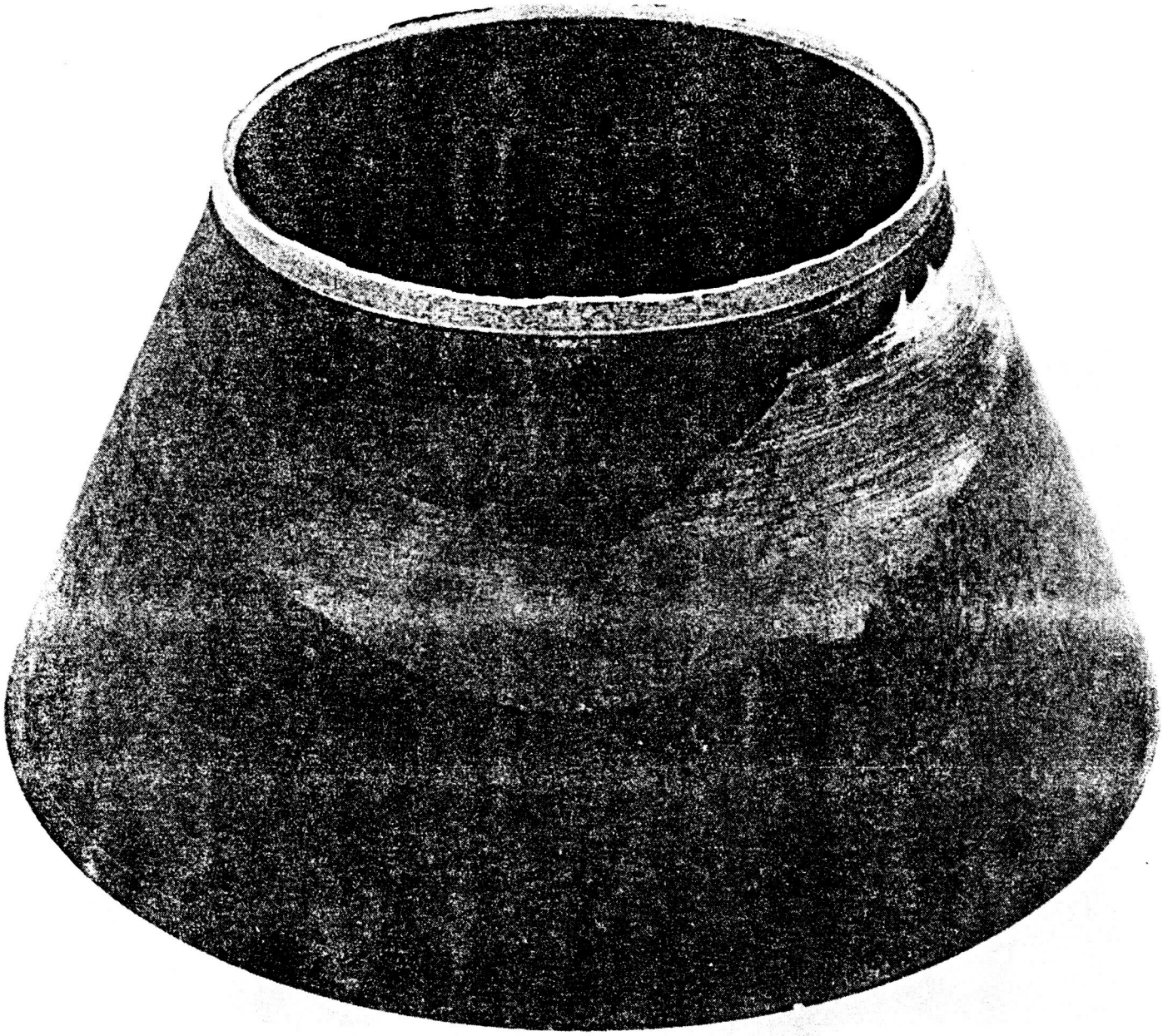

Figure 3

C-103 Nozzle After Separation from the AJ10-221 Chamber

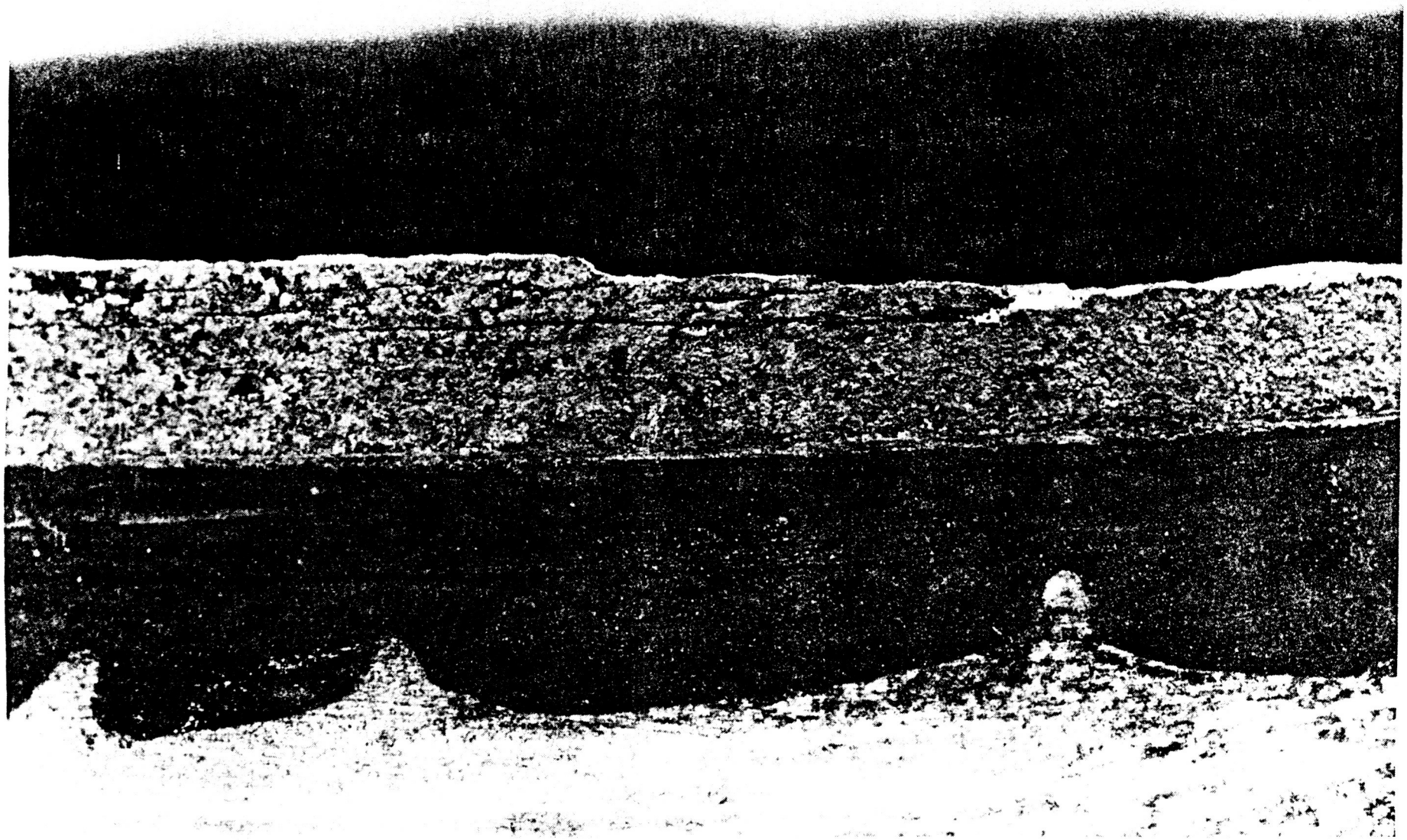

Figure 4

C-103 Nozzle OD Surface, Showing Uncoated Surface Adjacent to Fracture and Numerous Secondary Cracks Running Parallel to the Primary Fracture

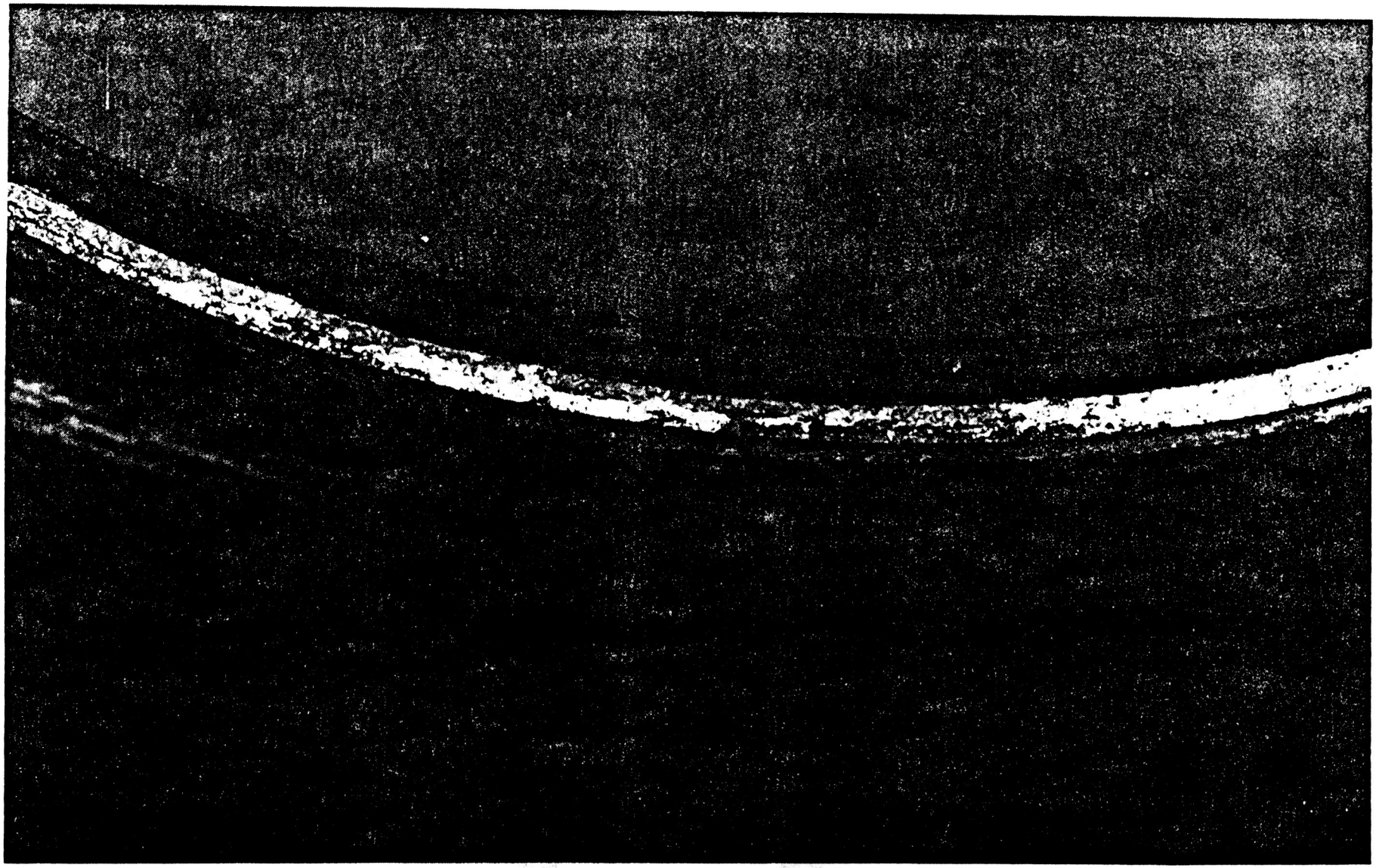

Figure 5

Fracture Surface of the C-103 Showing Darkened Fracture Surfaces (crack surfaces exposed to high temperature gases) Extending from both the OD and ID Nozzle Surfaces. Shiny Fracture Surface Shows Room Temperature Fracture.

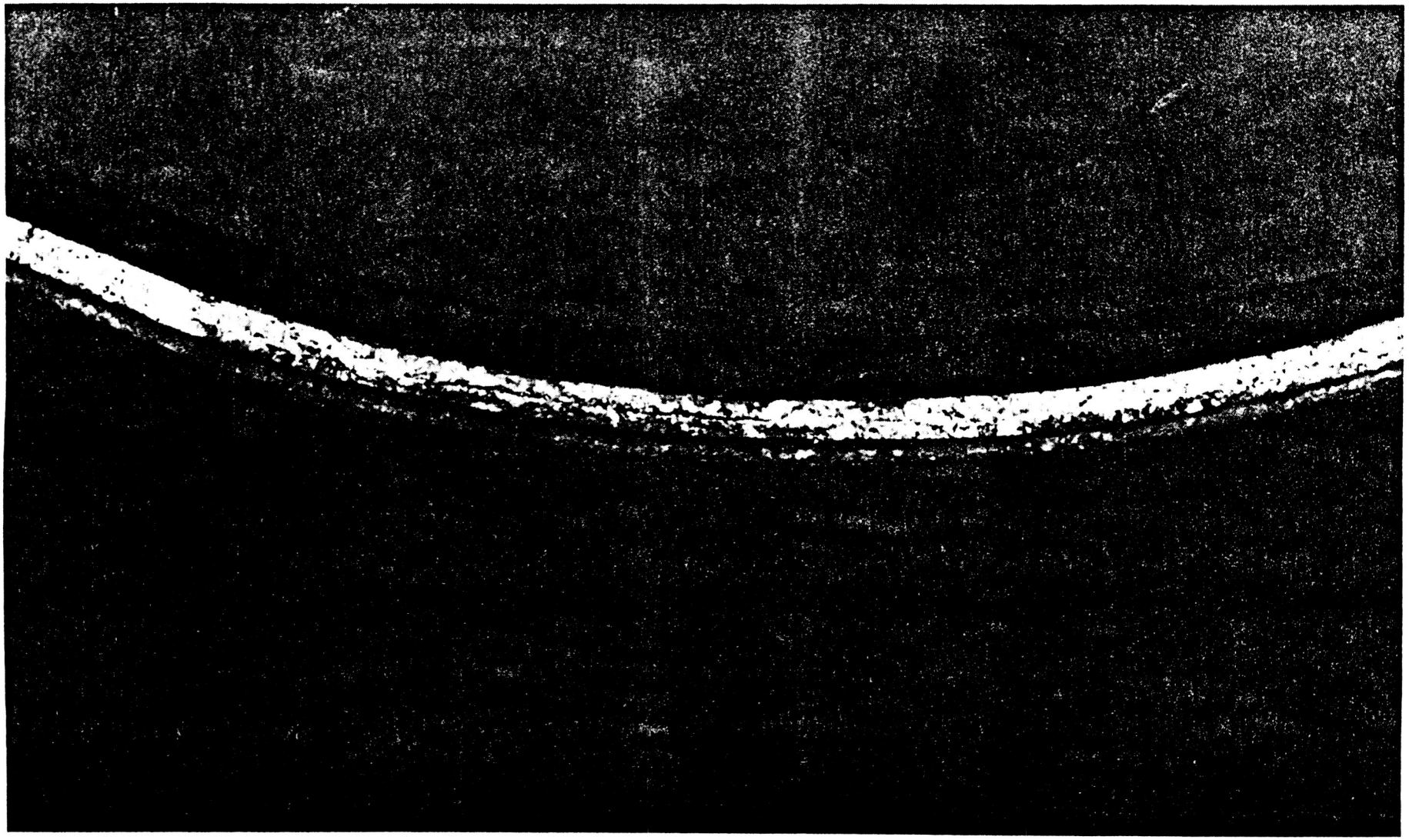

Figure 6

Fracture Surface of the C-103 Nozzle Approximately 180° from the Area Shown in Figure 5, Show Equivalent Features. There Does Not Appear to be a Single Failure Origin.

Figure 7

SEM examination of the C-103 nozzle surface showed multiple layers. These were identified by x-ray diffraction analysis as oxide layers. It is presumed that one layer formed with each engine firing.

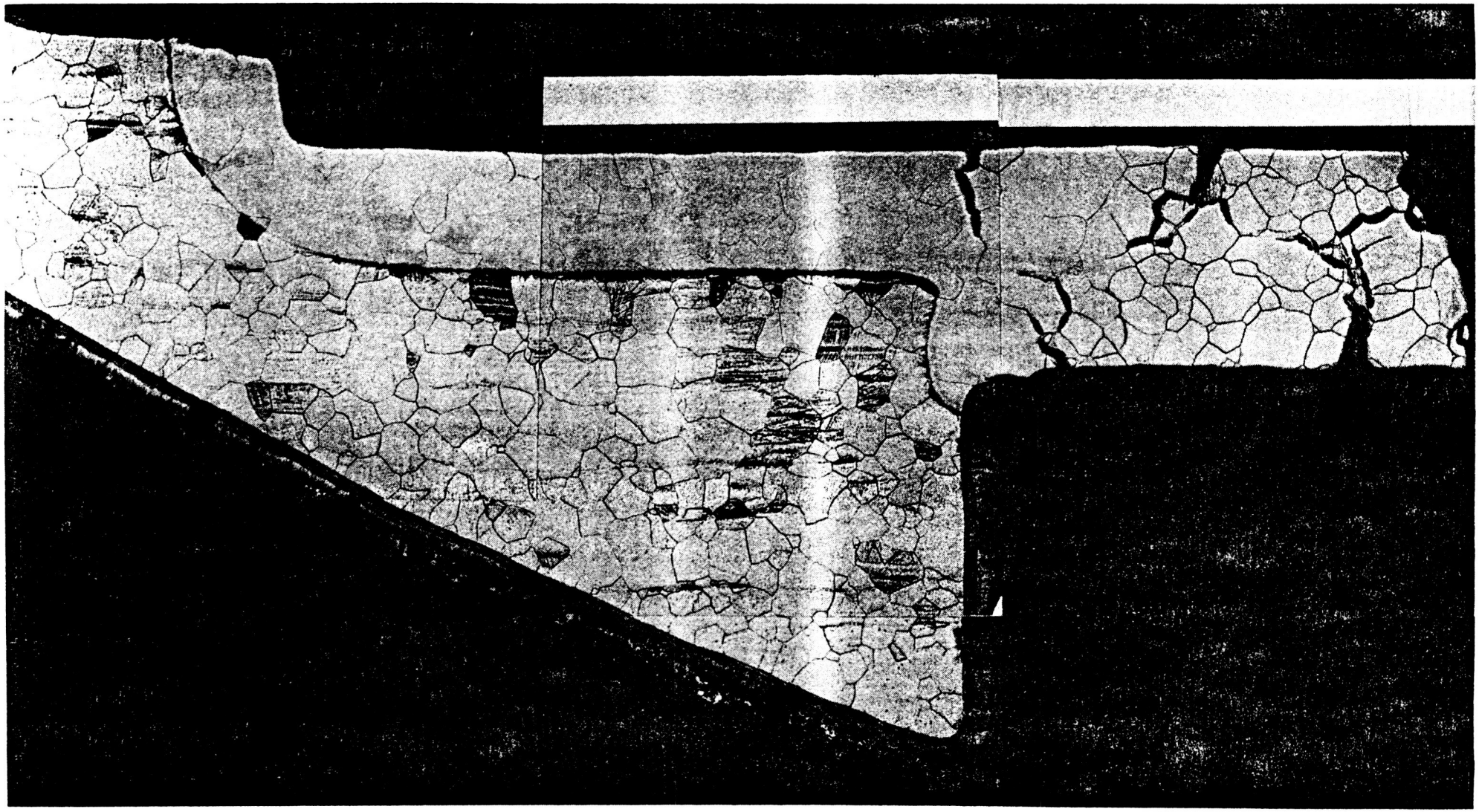

Figure 8

A metallographic cross-section thru the fractured end of the C--103 nozzle reveals the typical microstructure. A diffusion zone is seen to originate from uncoated C-103 surfaces. Multiple secondary cracks emanate from both the ID and OD surfaces. Grain boundaries near the fracture show an oxide phase.

Magnification: 50x

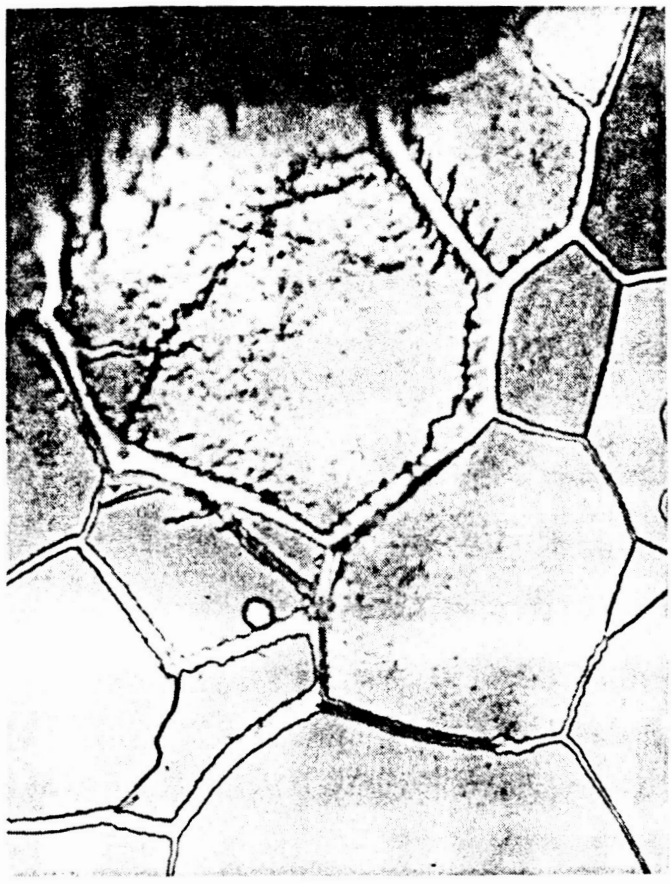

Figure 9

Grain boundaries near the fracture show thick, continuous grain boundary oxide layers. Some oxide precipitates are also seen in the grains close to the fracture surface.

Magnification: 500x

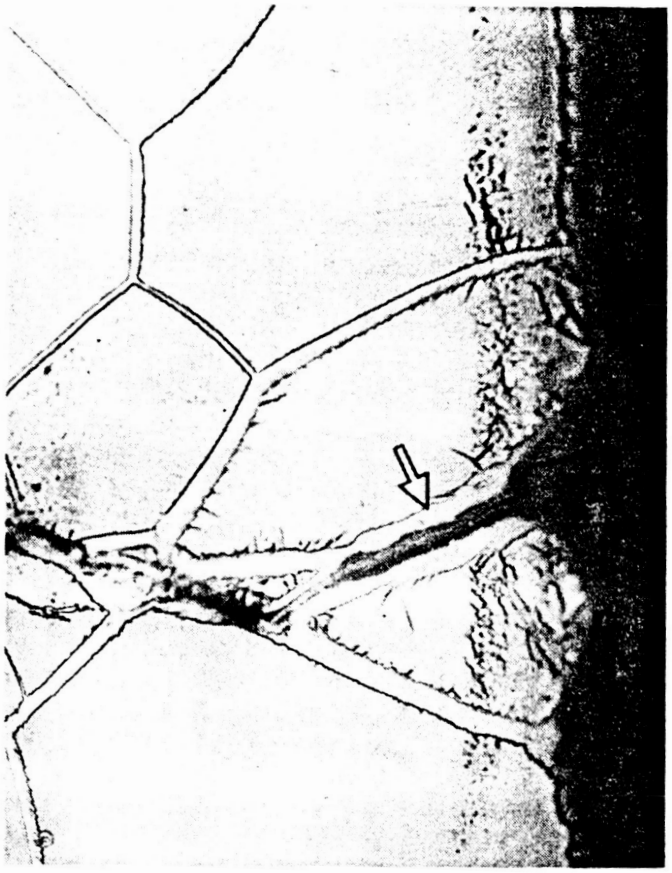

Figure 10

Grain boundaries near the nozzle ID surface appear very similar to those near the fracture in Figure 9. Fracture can be seen to occur along these grain boundaries, but not all grain boundaries fracture. A darker oxide can be seen at the crack in this photo (arrow). It is apparent that these represent two oxides, NbO in the grain boundaries and NbO_2 on exposed surfaces.

Magnification: 500x

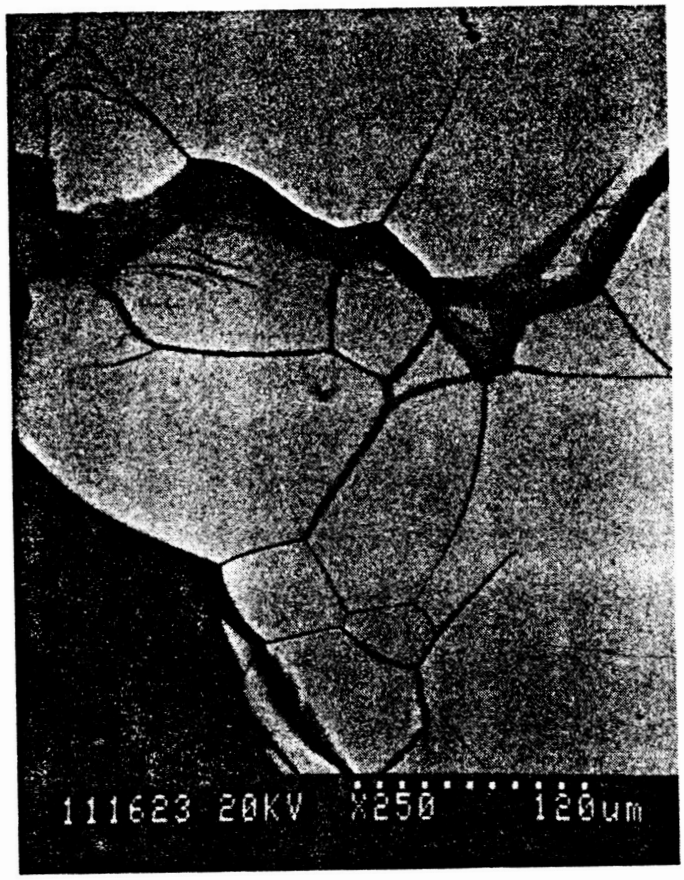

Figure 11

SEM back scatter images show the grain boundary phase to be a lower average atomic number and density, indicating NbO rather than HfO_2 HfO_2. HfO_2 and C-103 have approximately the same density and would therefore not be distinguishable in this type of image.

Figure 12

Microhardness traverses were taken from the ID, OD, and fracture surfaces, as well as in the unaffected C-103. Hardness in the diffusion zone was in the Rc 60 range, while the unaffected C-103 was in the Rb 75 range.

Enclosure (1)

Background Summary of AJ10-221 Testing, and Preliminary Description of the Circumstances of the Failure of the C-103 Nozzle.

D. M. Jassowski

HUGHES45

2-17-93

AJ10-221 S/N1 NOZZLE WELD JOINT FAILURE ANALYSIS BACKGROUND INFORMATION

FAILURE: On Friday, 12 February, at about 20:00 hrs, the nozzle C-103 skirt cleanly separated in a 360 deg location aft of the EB weld which attaches it to the C-103 to Re transition ring. The engine had just finished a 2-hr continuous burn and had been prepared for testing of the LORAL heat shield. Photographs of the engine were taken after the 2-hr test but prior to the shield installation.

Personnel performing the installation report that shield installation had been completed, they had stepped away from the stand, when they heard a noise. On inspection they found the nozzle skirt separated and resting between the diffuser and the engine. Photos were taken of this condition, the skirt was extracted by deflecting the shield forward and another set of photos taken. The engine/shield assembly was then tested successfully for 1200 sec. It is likely that some side loads were applied to the nozzle during shield installation; however, the clean break indicates that the joint area has inadequate structural properties.

BACKGROUND: The AJ10-221 engine assembly is shown in Figure 1. The C-103 nozzle skirt, P/N 1206351-9, is shown in Figure 2. It had been cut back from the 286:1 full skirt to 47:1 to facilitate long duration altitude testing. The transition from the CVD Ir-Re chamber to the silicide-coated C-103 nozzle skirt is shown in Figure 3. It utilzes a composite C-103 ring (Figure 3A) joined to a Re ring with CVD columbium. This ring is EB welded Re to Re at the aft end of the chamber exit. Figure 4 is one of a set of photos which document the appearance of the joint after assembly. Figure 5 shows the joint after 3.9 hrs of testing [photos of this area after 6 hrs of testing are being processed by Tech Pubs].

DESIGN: The AJ10-221 chamber is fabricated with CVD Ir-Re using a moly mandral. The full nozzle could be made integral with the chamber, but the very high temperature capability of Re is not required in this area, and this would result in a substantial cost and weight penalty. The approach chosen was to make a transition to silicide-coated C-103 at the location where the nozzle temperature is in a safe range for long-life operation of this material. The joint design provides a mechanical lock between the skirt and the chamber; the gas seal is provided by the CVD Cb, which is not intended to be the load path. The internal pressure at this point is about 0.8 psia; even with a failed CVD seal, leakage is not anticipated to be a problem for extended engine operation.

It should be noted that the C-103 in the area of the weld is intentially preloaded by the design/fabrication process. The parts are dimensioned so that the C-103 skirt bottoms on the end of the Re nozzle, leaving a gap of about 1 mil at the joint between the ring and the skirt. When the EB weld is made, the weld shrinkage on cooling preloads the part in tension. This is done to stiffen this joint for launch vibration loads.

DISCUSSION: The silicide coating is stopped at the inner and outer portions of the C-103 skirt joint to avoid contamination of the EB C-103 to C-103 weld. The black coating evident on the inside of the joint up to and in some places stepping beyond the break is beyond the area in which the part was silicide coated. The ring is spaced away from the Re to prevent migration of material between the parts. As can be seen in Figure 4, the actual EB weld area is relatively wide; the heat affected area visible in the photo is very close to where the part failed. The joint is exposed to combustion products on its backside (which can penetrate all the way up to the C-103 to C-103 EB weld. In addition, the engine exterior is flooded with hydrogen during firing and cool down, to protect the Re chamber from external oxidation. This joint design was tested in 15 deep thermal cycles

without apparent damage as the 22:1 Miniskirt chamber. That joint showed small amounts of leakage pre- and post-test from the backside of the C-103 retaining ring, indicative of leakage past either the Re-Re weld or [more likely] past the CVD Cb seal. The present joint was leak checked with 5 psig N2 after test -347; a very slight line fuzz leak was noted, at approximately the area at which the subsequent failure occurred. At the time of the leak check the joint had undergone 89 firings for a total duration of 3.9 hrs. To quantify leak rate, the joint was leak tested with helium at 5 psig. The measured leak rate was 6.5x10-3 cc/sec.

It appears that the leak that was detected after test -347 was a crack that had developed in the C-103 near the heat affected zone of the EB weld. Initial inspection of the separation surface shows some slightly darkened areas which could be the result of leakage during firing. It appears probable that the combination of weld affected area, exposure to reactive gas (hydrogen) and continued thermal/mechanical stress caused the material degradation and failure.

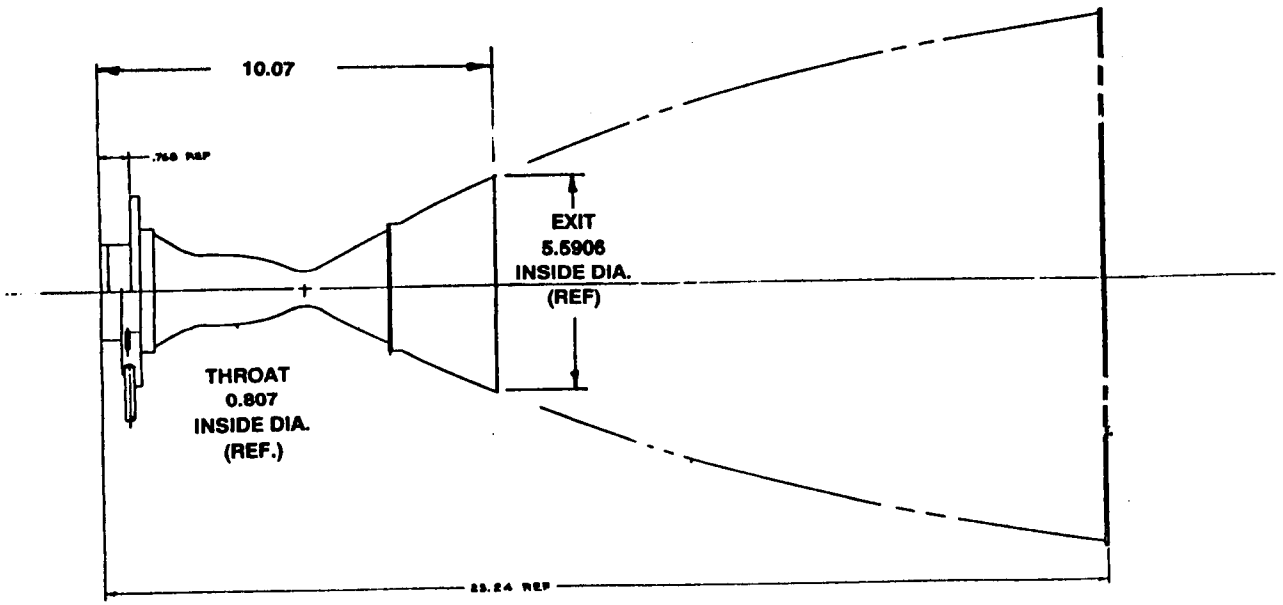

47:1 WELDED AJ10-221 ENGINE
(286:1 NOZZLE CUT BACK)

FIGURE 1 AJ10-221 ENGINE ASSEMBLY

-1
ALTER FROM 1206360-29
GenCorp Aerojet
CHAMBER ASSY
E 05824 1207290

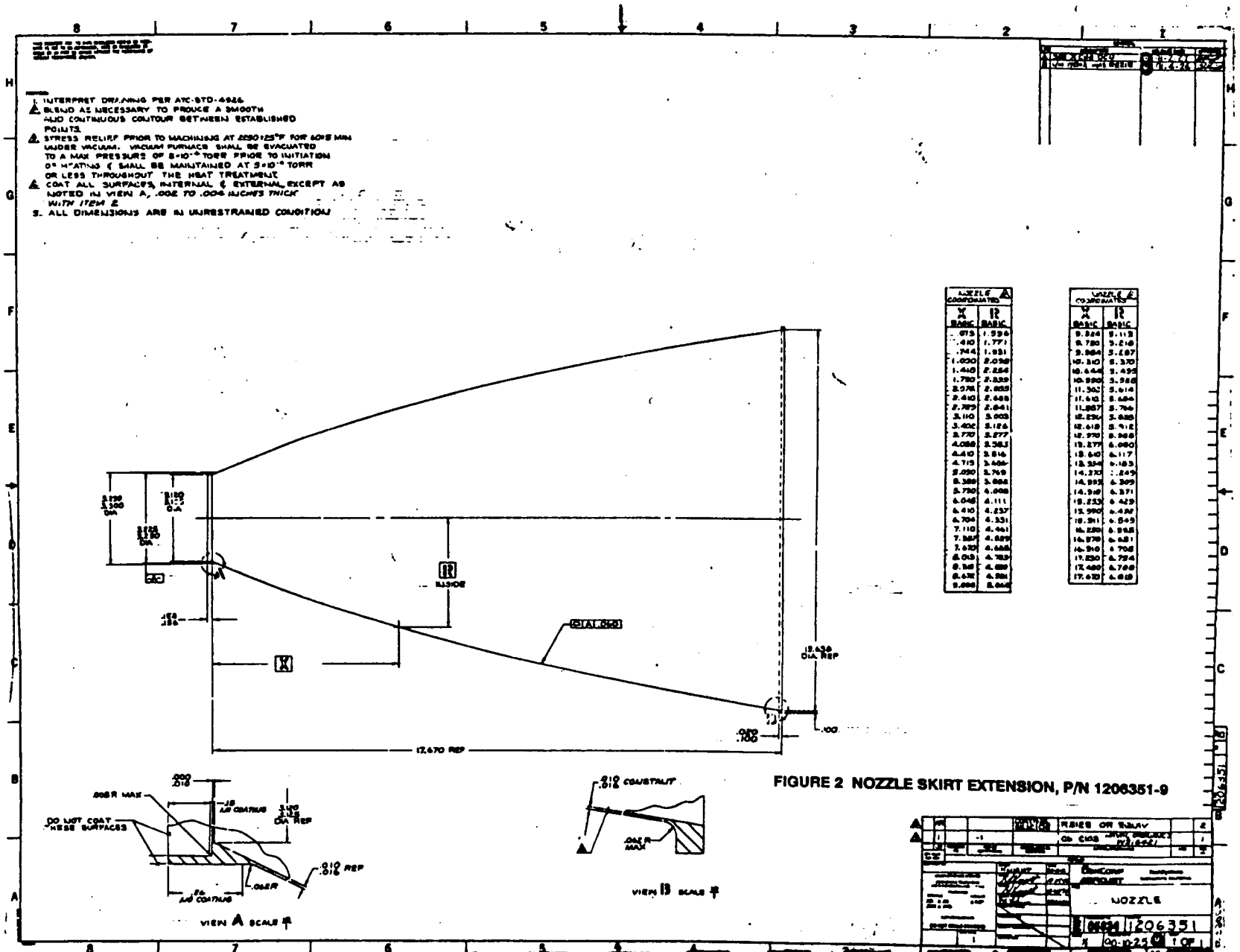

FIGURE 2 NOZZLE SKIRT EXTENSION, P/N 1206351-9

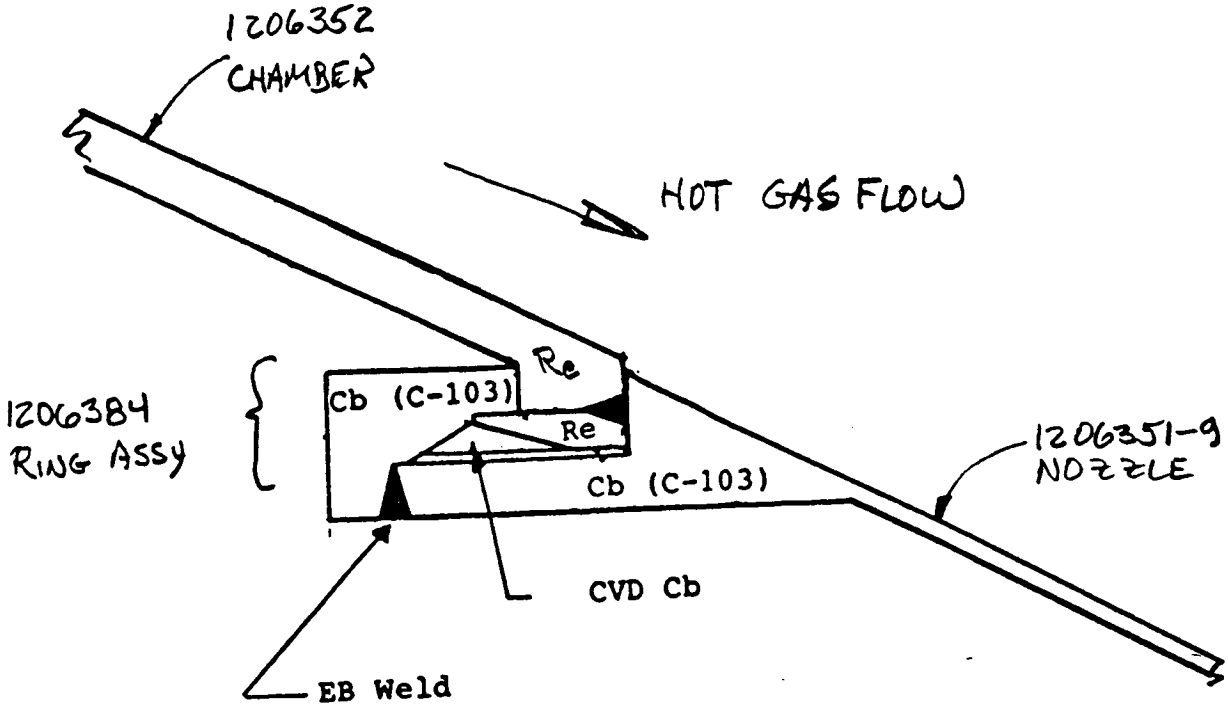

Approximately 10X

FIGURE 3 NOZZLE TRANSITION JOINT DETAILS

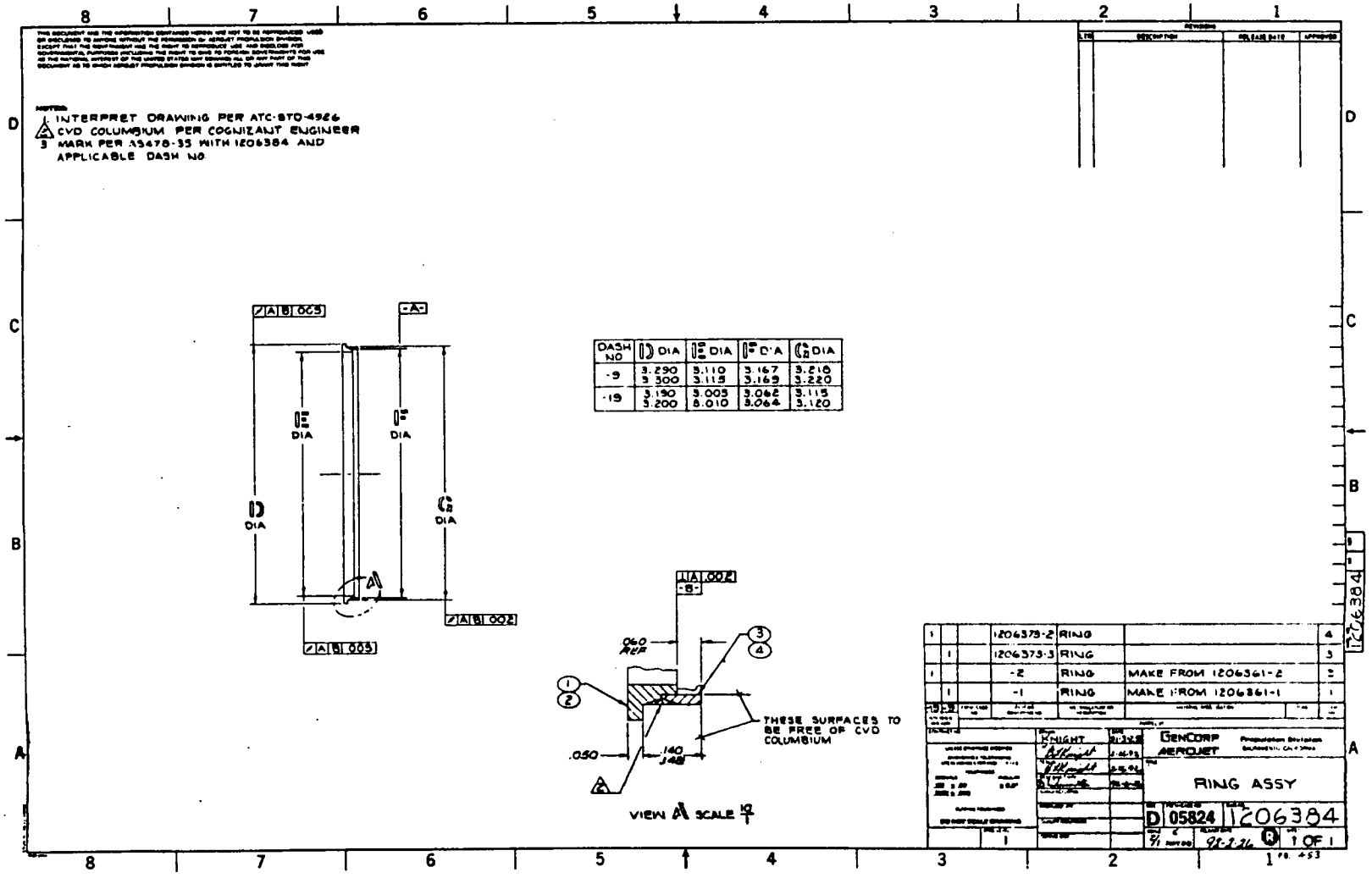

FIGURE 3A RING ASSEMBLY

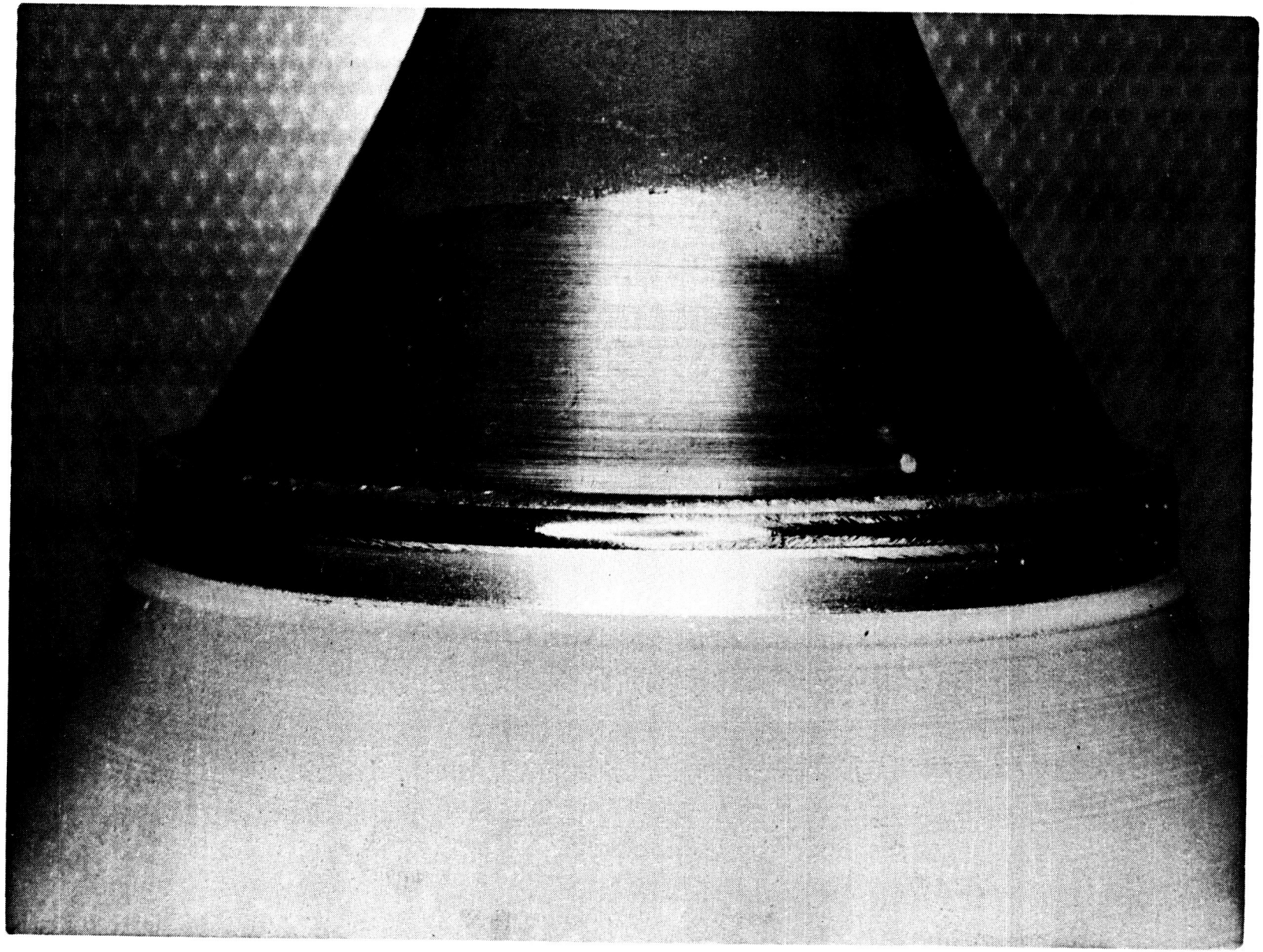

C0292 0672

Figure 4. C-103/C-103 EB Weld Joint Before Firing

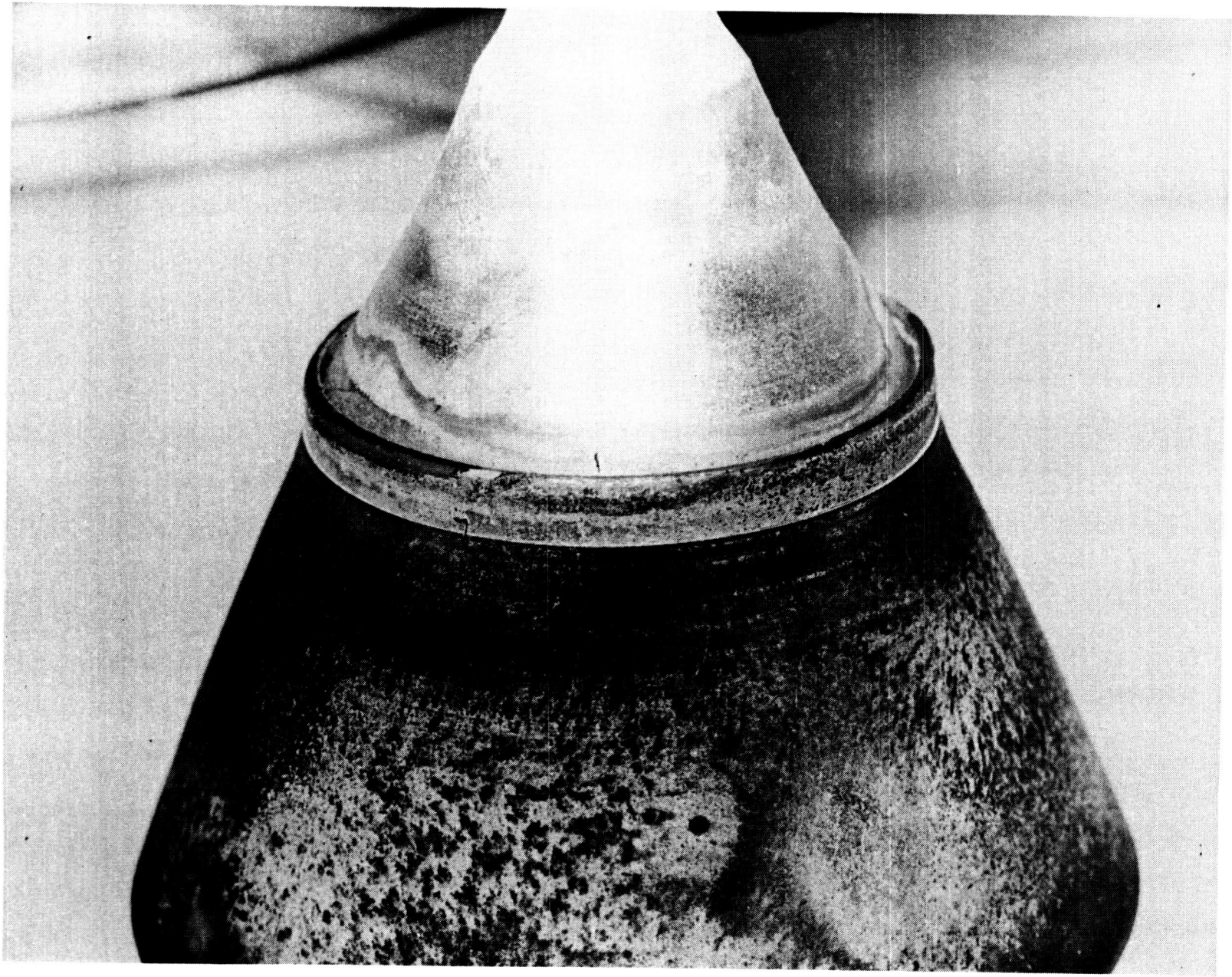

C0792 4644

Figure 5. C-103/C-103 EB Weld Joint After 3.9 Hours of Firing

Enclosure (2)

X-Ray Diffraction and Microprobe Results Report of the C-103 Nozzle Failure

A. M. Sheble

MATERIALS EVALUATION LABORATORY ANALYSIS

WORK ORDER:	DATE	DATE RECEIVED:
KGH 54A 22M8	03-15-93	03-05-93
REQUESTER:	EXTENSION	REFERENCE:
MURPHY, M. JASSOWSKI, D.	2849	
LWR NUMBER:	NR NUMBER	

ANALYSIS REQUESTED

SECTIONS FROM A FAILED TRANSITION JOINT OF A RHENIUM (Rh) C-103 ALLOY (Nb) COMPOSITE NOZZLE WERE RECEIVED IN THIS LABORATORY FOR DETERMINATION OF THE COMPOSITION OF A DIFFUSION LAYER SEEN IN THE CROSS-SECTION ON THE OUTSIDE SURFACE OF THE NOZZLE. A COPY OF AN SEM MONTAGE IMAGE OF THIS AREA IS SHOWN IN FIGURE 1. AND SHOWS WHERE ANALYSES WERE PERFORMED USING BOTH THE ELECTRON MICROPROBE (EMP) AND X-RAY DIFFRACTION (XRD) AND X-RAY FLUORESCENCE (XRF) ANALYSIS TECHNIQUES.

THE RESULTS OF THIS ANALYSIS ARE GIVEN IN TABLE I. AS CAN BE SEEN EMBRITTLEMENT OF THE C103 ALLOY HAS OCCURRED DUE TO DIFFUSION OF OXYGEN INTO THE OUTER SURFACES DURING FIRING. THE RESULTS SHOW AN OXYGEN CONCENTRATION IN THE MATRIX ON THE ORDER OF 500 ppm WITH A MUCH HIGHER CONCENTRATION AT THE GRAIN BOUNDARIES. THE RESULTS OF XRD AND XRF ON THE DIFFUSED SURFACE SHOW THE PRESENCE OF BOTH NIOBIUM OXIDE AND A NIOBIUM METAL LATTICE EXPANDED BY INTERSTITIAL OXYGEN DIFFUSION OF OXYGEN INTO THE NIOBIUM ALLOY OCCURS FIRST BY A GRAIN BOUNDARY MECHANISM AND THEN BY MATRIX DIFFUSION FOLLOWED ULTIMATELY BY GRAIN BOUNDARY COARSENING. IT APPEARS THAT OXYGEN OCCURS AS THE OXIDE IN THE GRAIN BOUNDARIES AND AS THE INTERSTITIAL IN THE MATRIX. THIS IS IN AGREEMENT WITH PREVIOUS WORK DONE ON A SIMILAR SYSTEM INVOLVING CVD Cb AND A C-103 ALLOY CONTAMINATED WITH OXYGEN (AEROJET IAL LAB NO. TS-035003, 03-11-85, COPY ATTACHED).

TABLE I

DESCRIPTION OF AREA ANALYSED (FIGURE 1.)	METHOD	RESULTS
MATRIX IN DIFFUSED LAYER (AREA A)	EMP	OXYGEN CONCENTRATION = 450-500 ppm
GRAIN BOUNDARY IN DIFFUSED LAYER (AREA B)	EMP	OXYGEN CONCENTRATION = 700-750 ppm
UN DIFFUSED MATRIX (AREA C)	EMP	OXYGEN NOT DETECTED = < 50 ppm
GRAIN BOUNDARY IN UN DIFFUSED AREA (AREA D)	EMP	OXYGEN CONCENTRATION = 500-600 ppm
ENLARGED G.B. IN DIFFUSED LAYER (AREA E)	EMP	OXYGEN CONCENTRATION = 1200-1500 ppm
SURFACE OF DIFFUSED LAYER (AREA F)	XRD/XRF	NIOBIUM OXIDE TANTALUM OXIDE NIOBIUM (metal) RHENIUM OXIDE

A. M. SHEBLE

R. S. RUFFIN

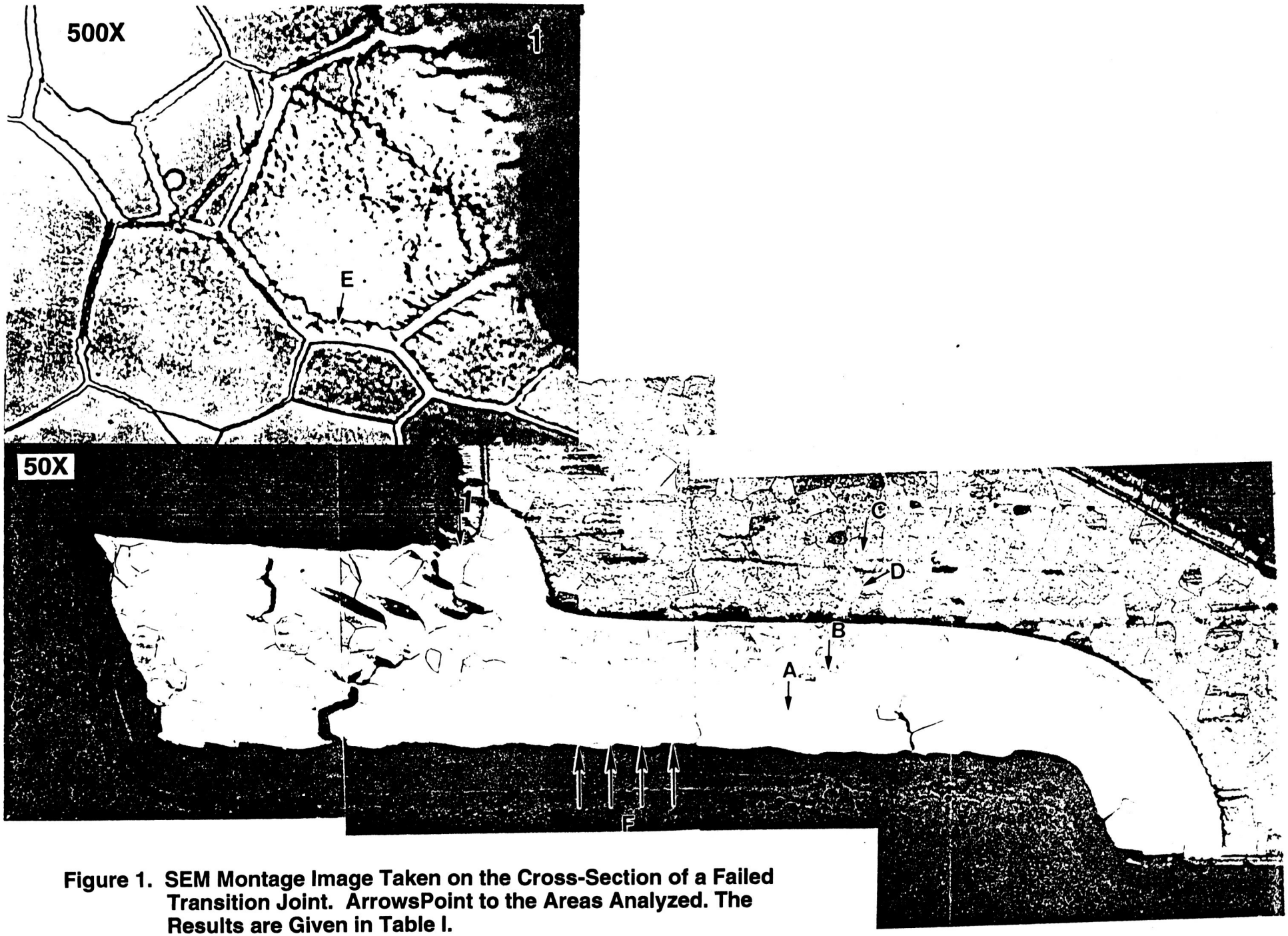

Figure 1. SEM Montage Image Taken on the Cross-Section of a Failed Transition Joint. ArrowsPoint to the Areas Analyzed. The Results are Given in Table I.

WORK REQUEST

3407

LAB NO.

SHADED AREAS TO BE COMPLETED BY LABORATORY COORDINATOR ONLY.

WORK ORDER	DATE REC'D	DATE REC'D	PRIORITY
1670 31 356T	3/11/85	3/7/85	
COGNIZANT ENGINEER	**EXT.**	**TIME IN**	**REC'D. BY**
V. Frick			
DESCRIPTION OF WORK		**DATE MAT'L REC'D.**	**TIME**

IAL #TS-035003

The results of an Electron Microprobe Analysis at the CVDCB/C103 alloy interface of sample C1B is given in Figure 1. As can be seen from Figure 1, the oxygen concentration in a 0.0043 in. band at the interface is approximately 560 ppm. Figure 2 shows an optical photomicrograph of the step scan area. It is apparent that oxygen has migrated into the C103 alloy by both bulk and grain boundary modes.

A. M. Sheble

ENGINEERING SIGNATURE

ENGINEERING SIGNATURE

EST. M/H TO COMPLETE	ASSIGNED TO NAME	DATE	TIME	FACILITIES MACHINE	EST. HOURS	COMPLETION DATE	TIME	M/H
EST. COMPLETE DATE								

DATE JOB CLOSED [redacted] SIGNATURE

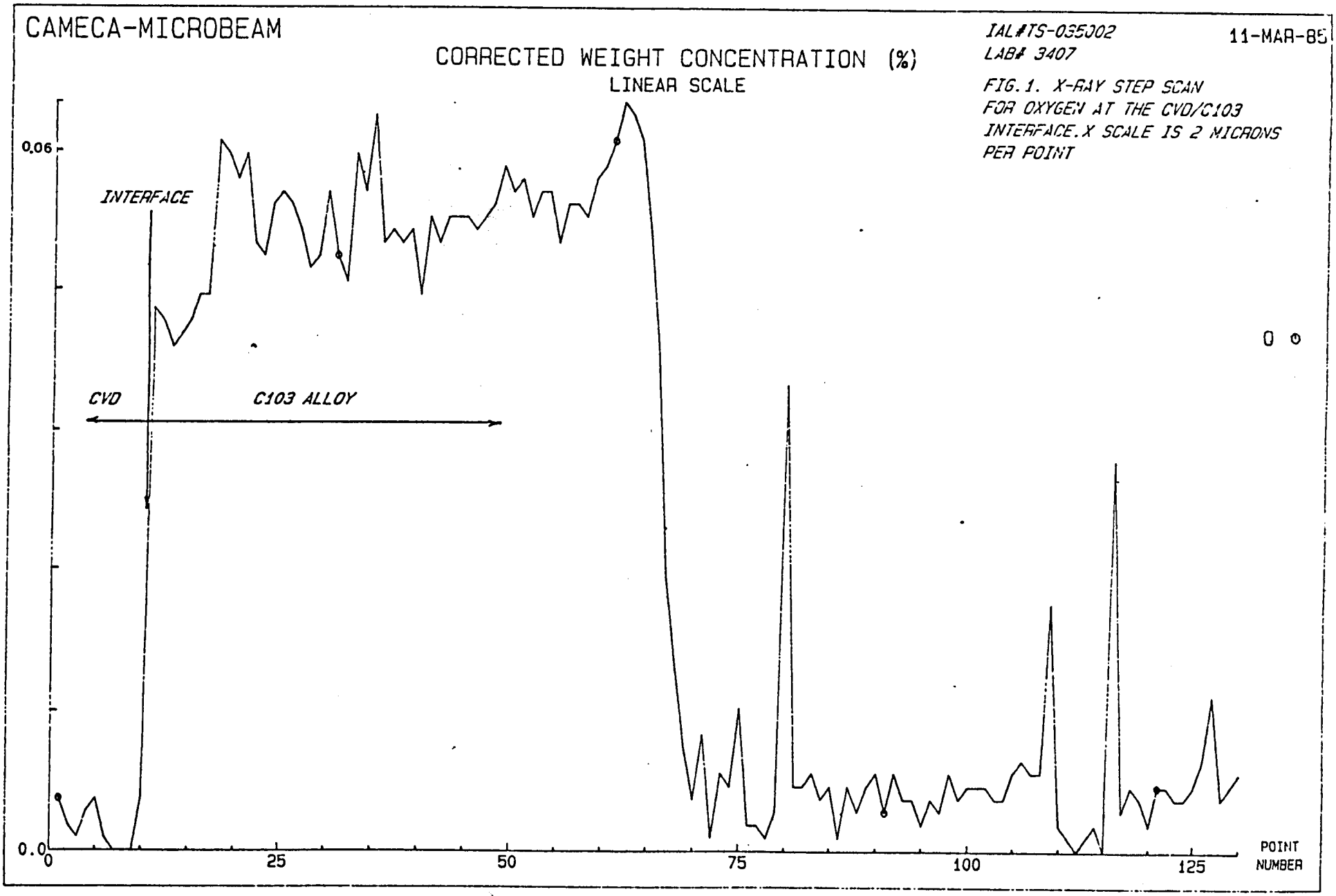
CAMECA-MICROBEAM
CORRECTED WEIGHT CONCENTRATION (%)
LINEAR SCALE
IAL#TS-035002
LAB# 3407
11-MAR-85
FIG. 1. X-RAY STEP SCAN FOR OXYGEN AT THE CVD/C103 INTERFACE. X SCALE IS 2 MICRONS PER POINT
0.06
0.0
INTERFACE
CVD
C103 ALLOY
0
25
50
75
100
125
POINT NUMBER

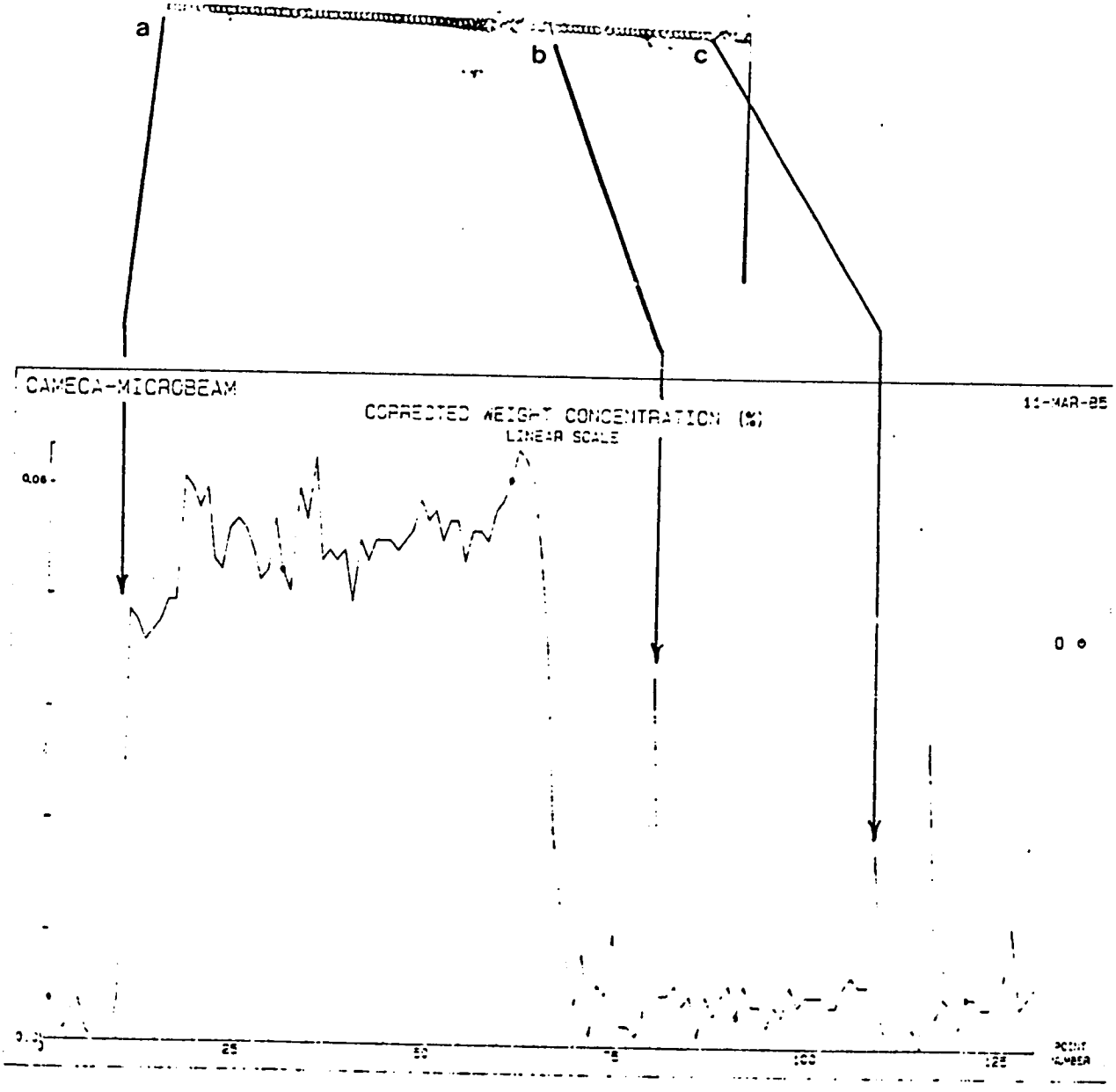

Figure 2. Optical Photomicrograph of Step Scan Area
Arrows pint to:
a) CVD Cb/C103 alloy interface
b) Grain boundary
c) Grain boundary

Average oxygen concentration between points 20 and 60 is 560 ppm.

APPENDIX M

POST TEST THRUSTER PHOTOS

An extensive set of photos was taken of the engine to document its post test appearance. Generally, three views of each area were taken to show all sides of the engine. A selected set of these photos is included in this appendix.

The engine assembly on the thrust mount, is shown in Figure M-1. This assembly includes the protective shroud gas shown in Figure M-2, which prevents oxidation of the rhenium during ground testing. The shroud gas manifold is shown disassembled in Figure M-3.

The engine assembly after removal of the shroud gas manifold, is shown in Figure M-4. Figure M-5 is a close-up of the rhenium chamber showing its crystal structure in the high temperature zone upstream of the throat.

The chamber-nozzle skirt joint is shown in Figure M-6. The Re nozzle-to-Re ring EB weld is clearly visible, as is the fracture zone in the oxidized C-103. The interior of the nozzle exit is shown in Figure M-7. The Ir coating is white in areas which have been heated to high temperature (approximately 3000°F); below this temperature it retains post Mo-etch appearance. A chip in the Ir coating is visible at about 5:00 near the white-to-gray transition. This could be a flaw in the coating or may be the result of impact damage from debris carried back into the nozzle by the shock wave that is directed at the nozzle when the diffuser unloads. The mark at about 10:00 (which has a slight wake downstream) is a discoloration on the surface which could be the result of a paint chip from the facility sticking on the hot surface.

The next four photos show interior surfaces of the thruster. Their locations are indicated in Figure M-8. Thereafter all the photos are at approximately 10X, taken through the throat using a low focus microscopic camera and a spot light source.

The first photo (Figure M-9) shows the high temperature Ir surface downstream of the cooled adapter. The granular appearance of the surface is typical throughout the interior.

The gap between the Ir-Re chamber and the cooled adapter is shown in Figure M-10. This photo also shows the rear face of the cooled adapter and some of its interior surface. The areas seen, starting at the top of the photo are: (1) radius of Ir/Re chamber, (2) gap, (3) downstream edge of cooled adapter, and (4) portion of inner cylindrical surface of the cooled adapter. The deposits which coat the cooled adapter

surface are believed to be iron compounds from the NTO, which is stored in steel and stainless steel systems and is generally near saturation, typically 4-5 ppm. Approximately 4800 lbm of NTO has flowed through the engine; at 4 ppm this is about 9 grams of ferric nitrate which forms ferric oxide on the hot surface. Since the decomposition temperature of iron oxide is 1538°C (2800°F) it is stable on the stainless steel cooled adapter but not on the Ir-Re chamber, which explains the absence of deposits in this area. Figure M-11 is a view farther into the cooled adapter, showing its interior downstream of the tip and the downstream face of the tip. Although somewhat out of focus it is evident that there is a clear, slivery zone which is the recirculation zone immediately downstream of the tip.

A portion of the center of the injector face, rows 1, 2, 3 and 4, is shown in Figure M-12, which has low contrast because of internal reflections from the white Ir surface. A deposit which has the appearance of iron oxide is present on the face, except at the elements themselves, which are clear.

Nothing seen in this examination of the thruster indicates any life-limiting areas or incipient failure mechanisms. However, no direct measurement of the thickness of the Ir coating is practical short of destructive measuring techniques, although quantitative NDE techniques for monitoring local variations in thickness are certainly feasible and absolute NDE measurement techniques could be developed.

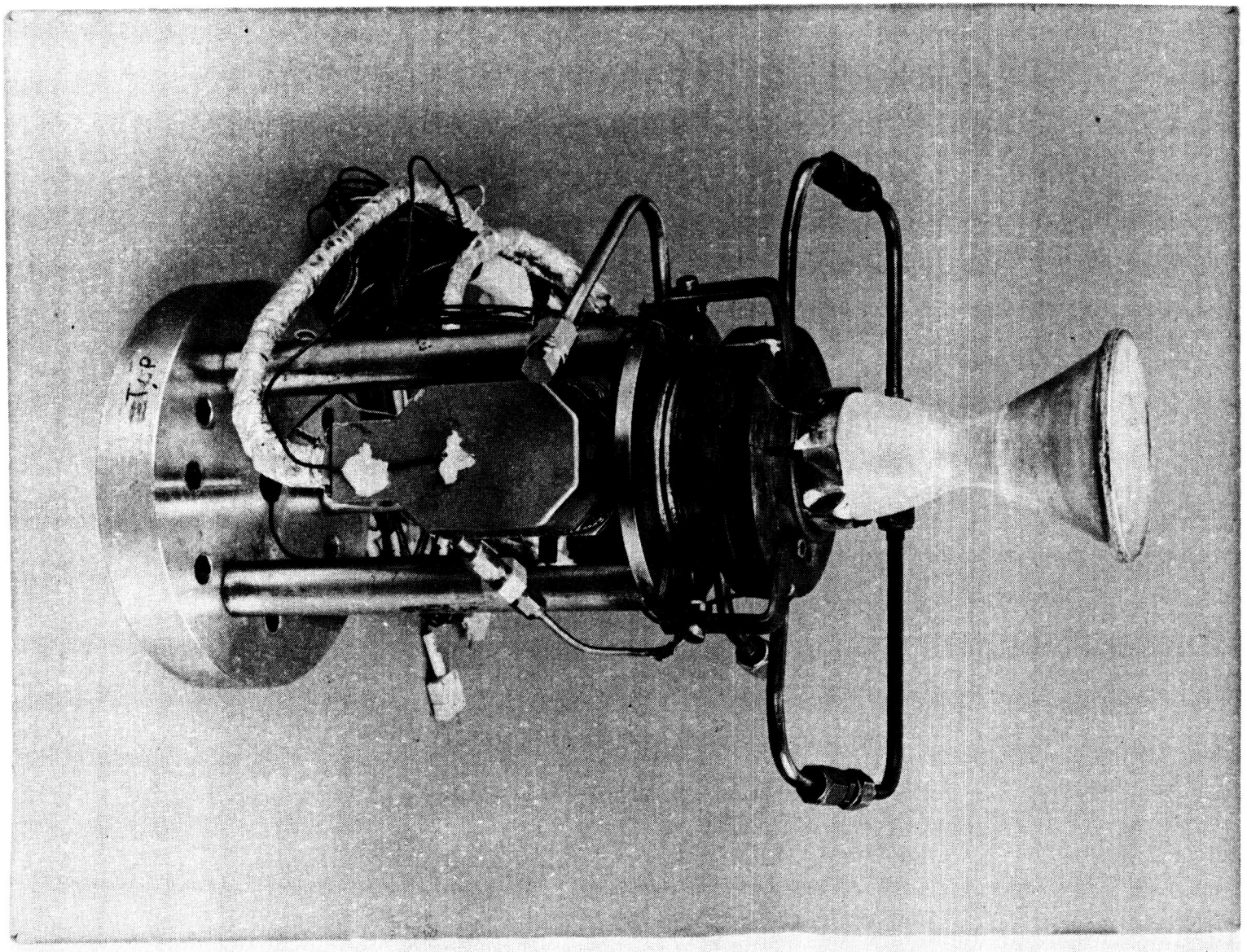

C0393 1425

Figure M-1. AJ10-221 Post Test - OM Thrust Mount

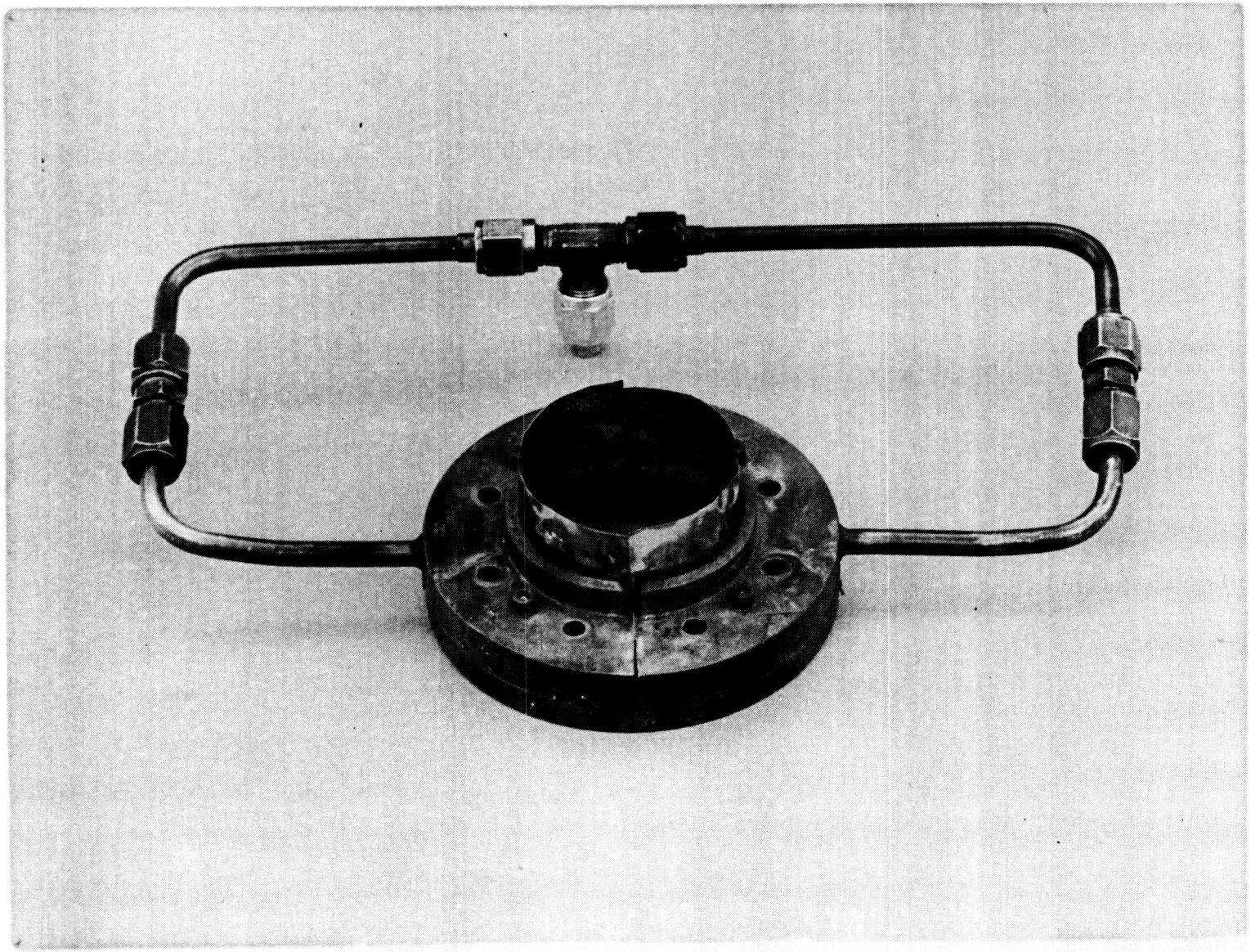

AJ10-221 ENGINE AFTER
6.2 HOURS OF FIRING

C0393 1441

Figure M-2. Protective Shroud Gas Manifold

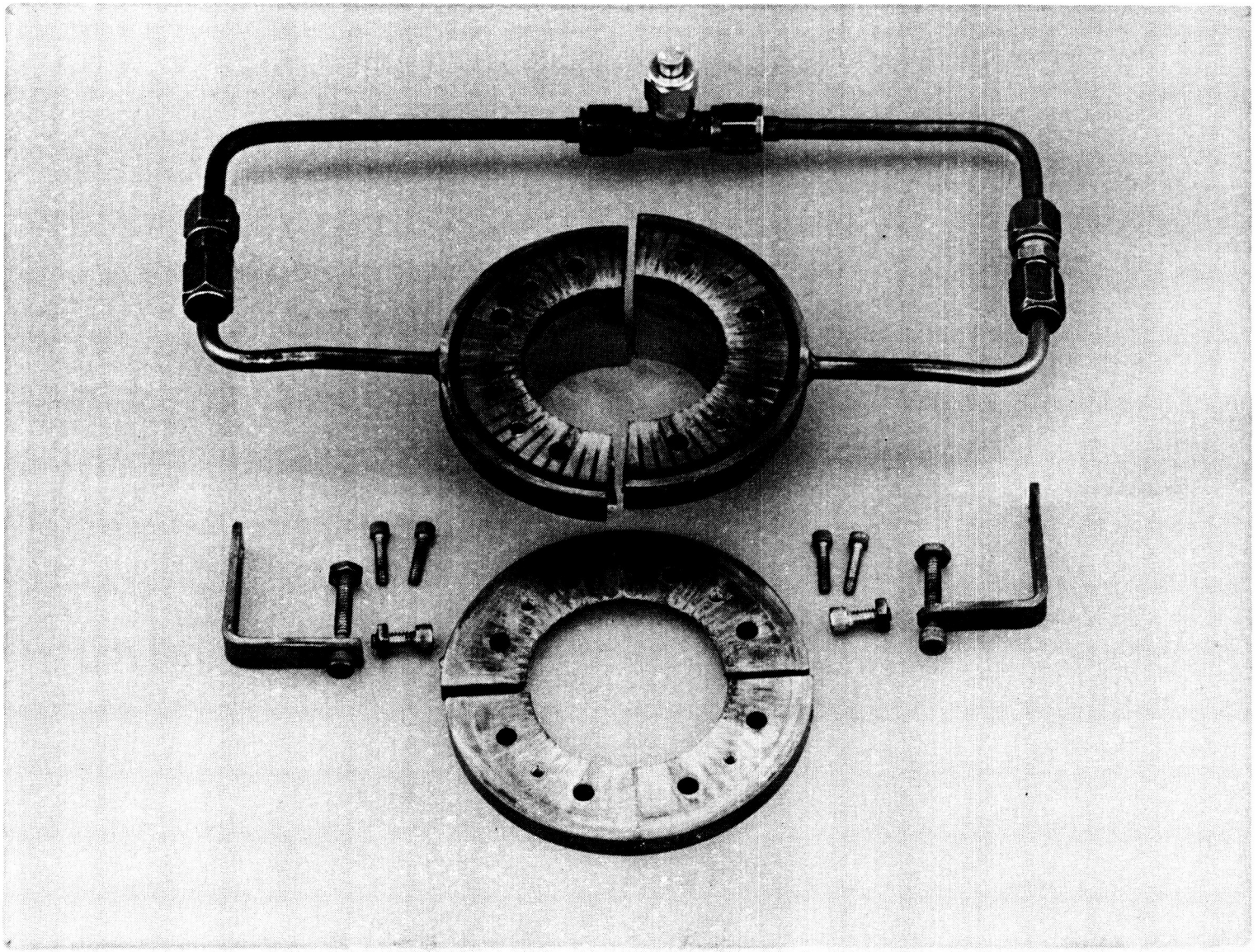

AJ10-221 ENGINE AFTER
6.2 HOURS OF FIRING

C0393 1443

Figure M-3. Shroud Gas Manifold Components

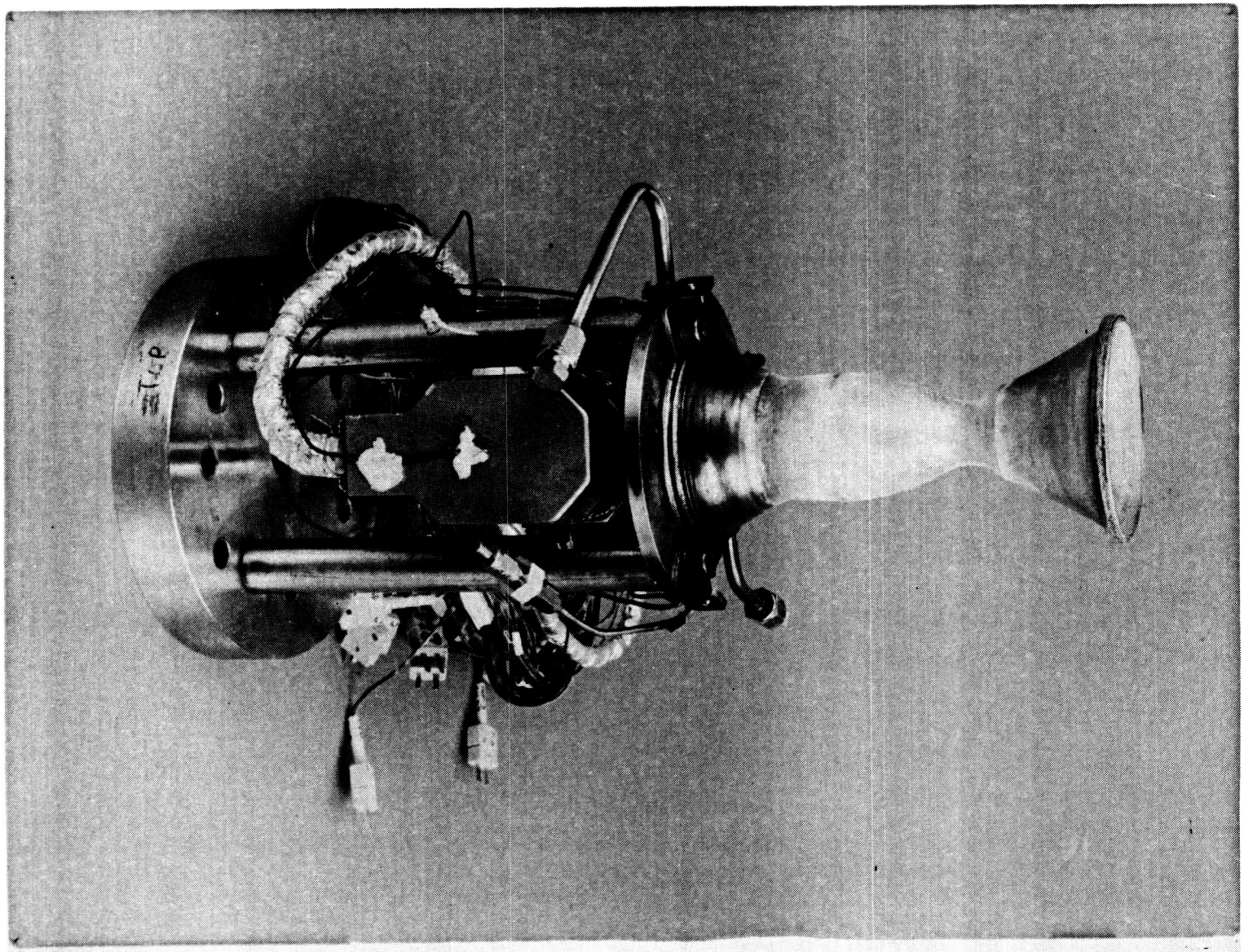

Figure M-4. AJ10-221 Engine Assembly

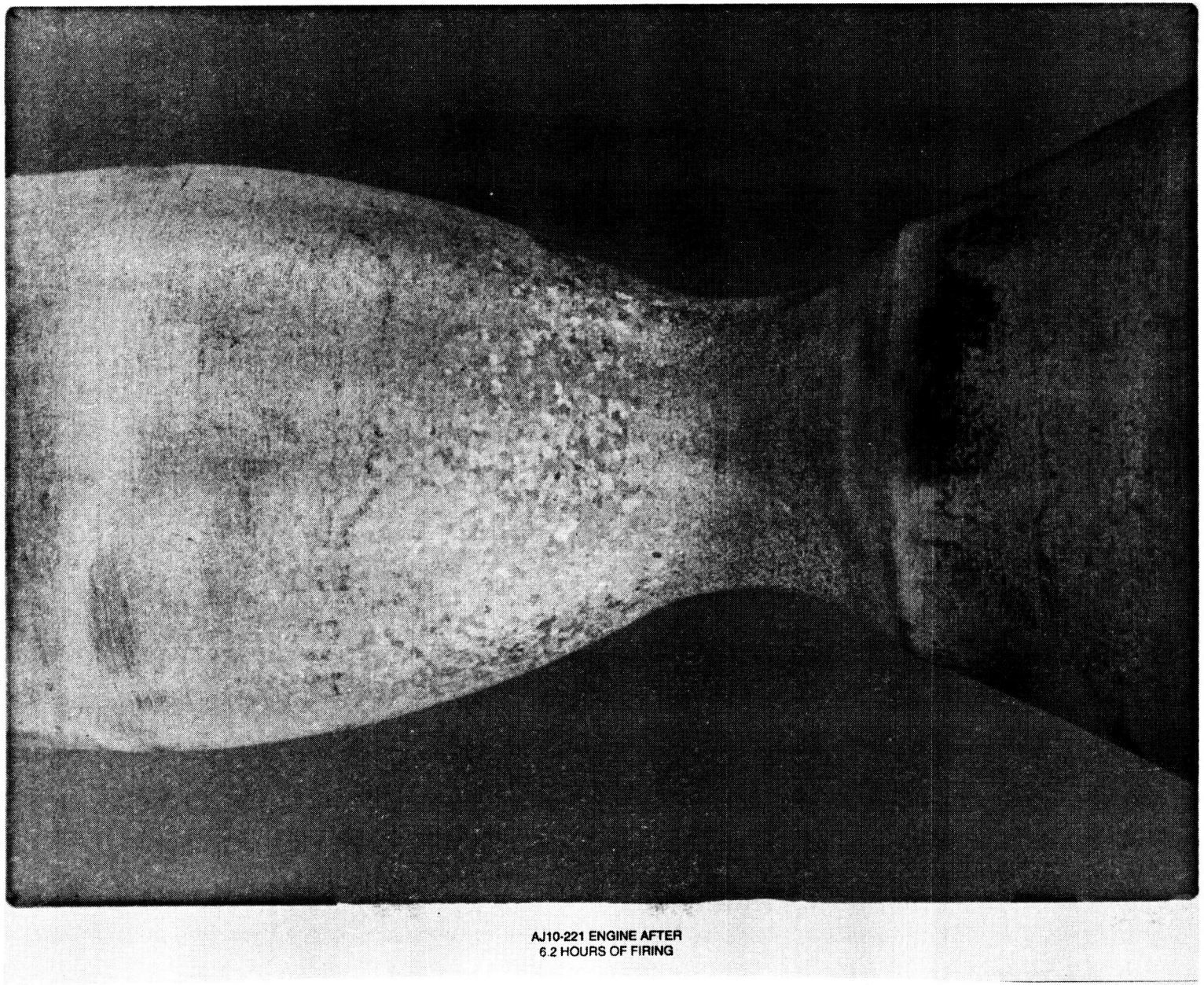

C0393 1448

Figure M-5. Close Up of Re Chamber Near Throat

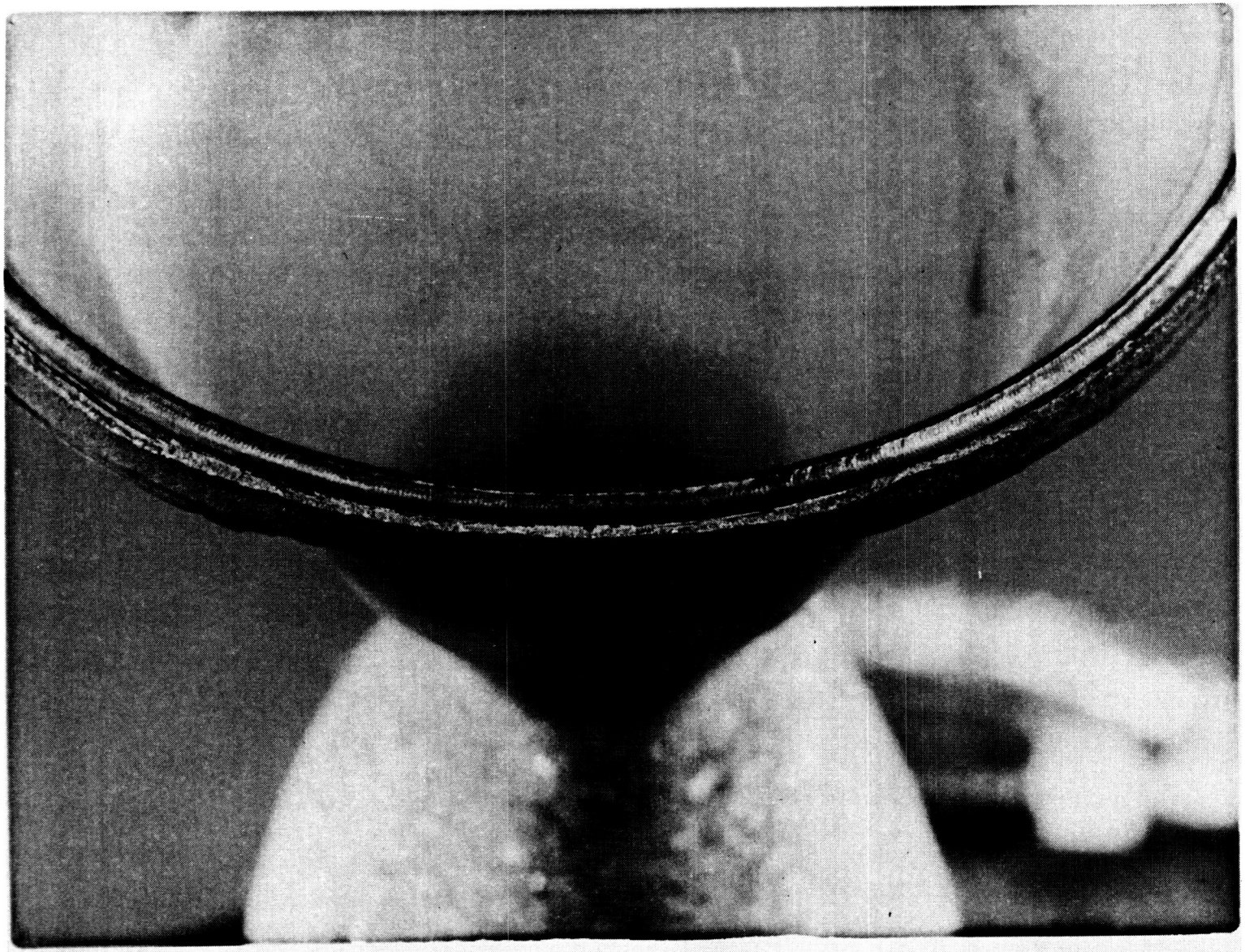

AJ10-221 ENGINE AFTER
6.2 HOURS OF FIRING

C0393 1437

Figure M-6. Re/C-103 Transition Zone

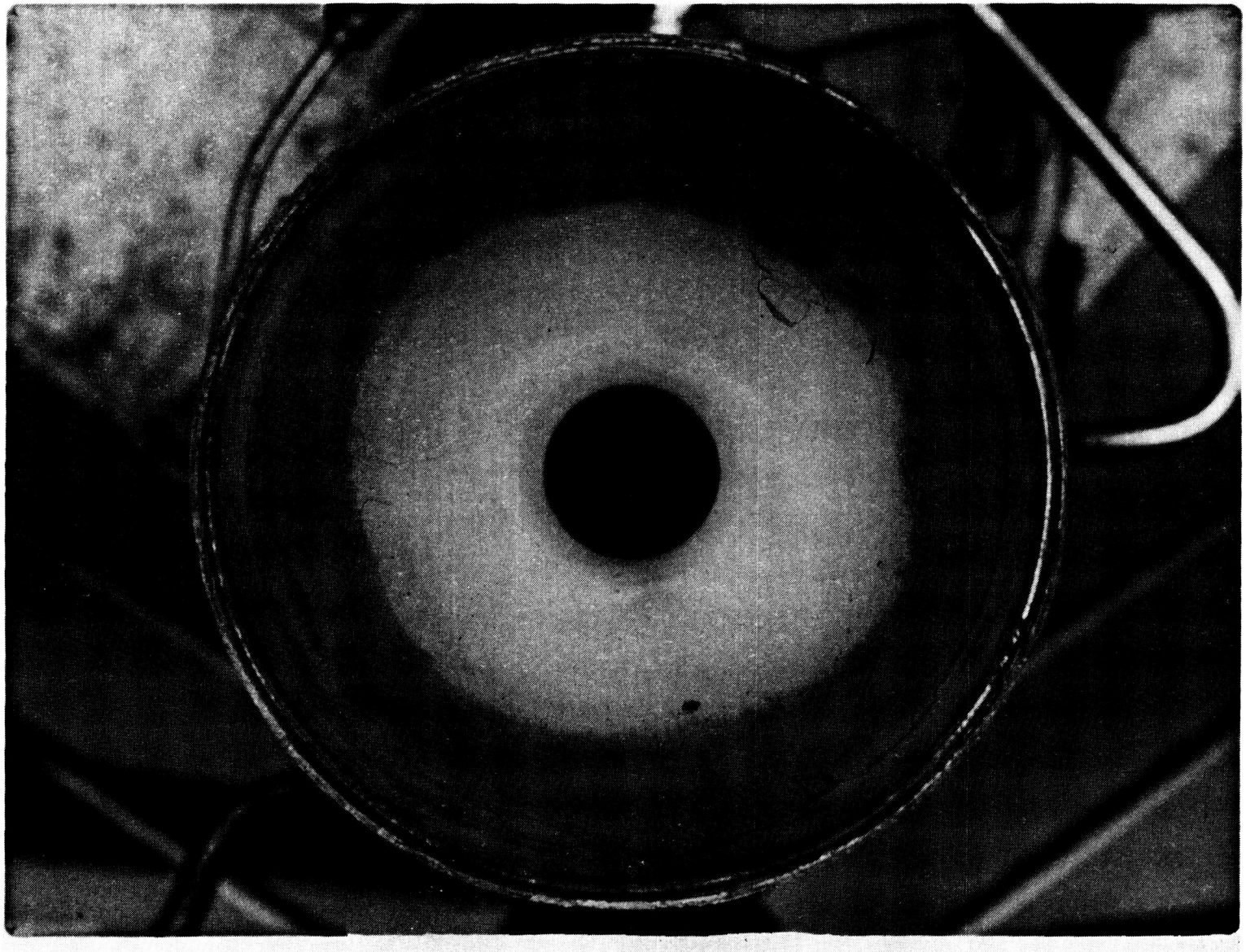

AJ10-221 ENGINE AFTER
6.2 HOURS OF FIRING

C0393 1439

Figure M-7. Interior of Nozzle Exit

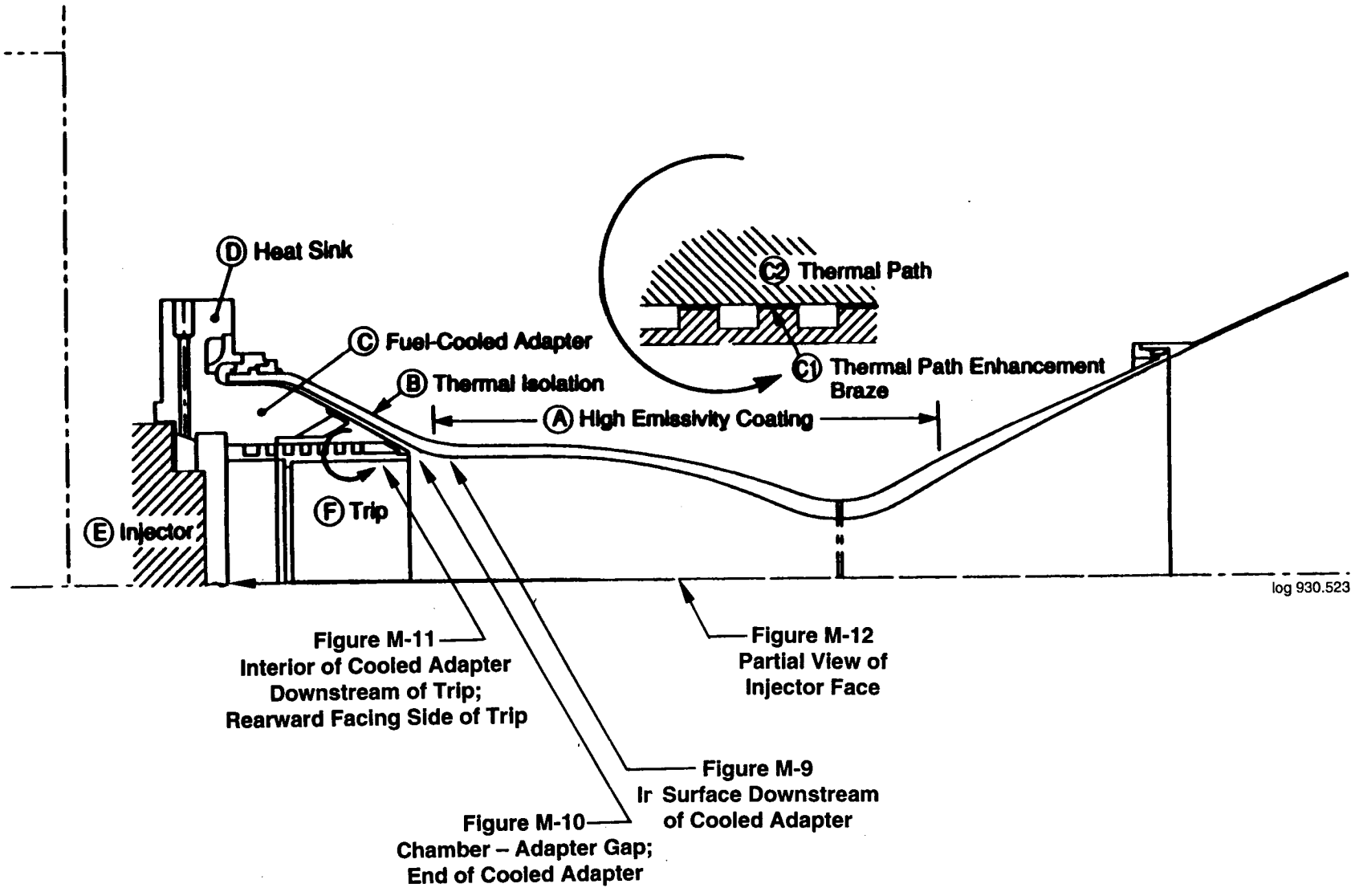

Figure M-8. Key to Internal Photos of Thruster

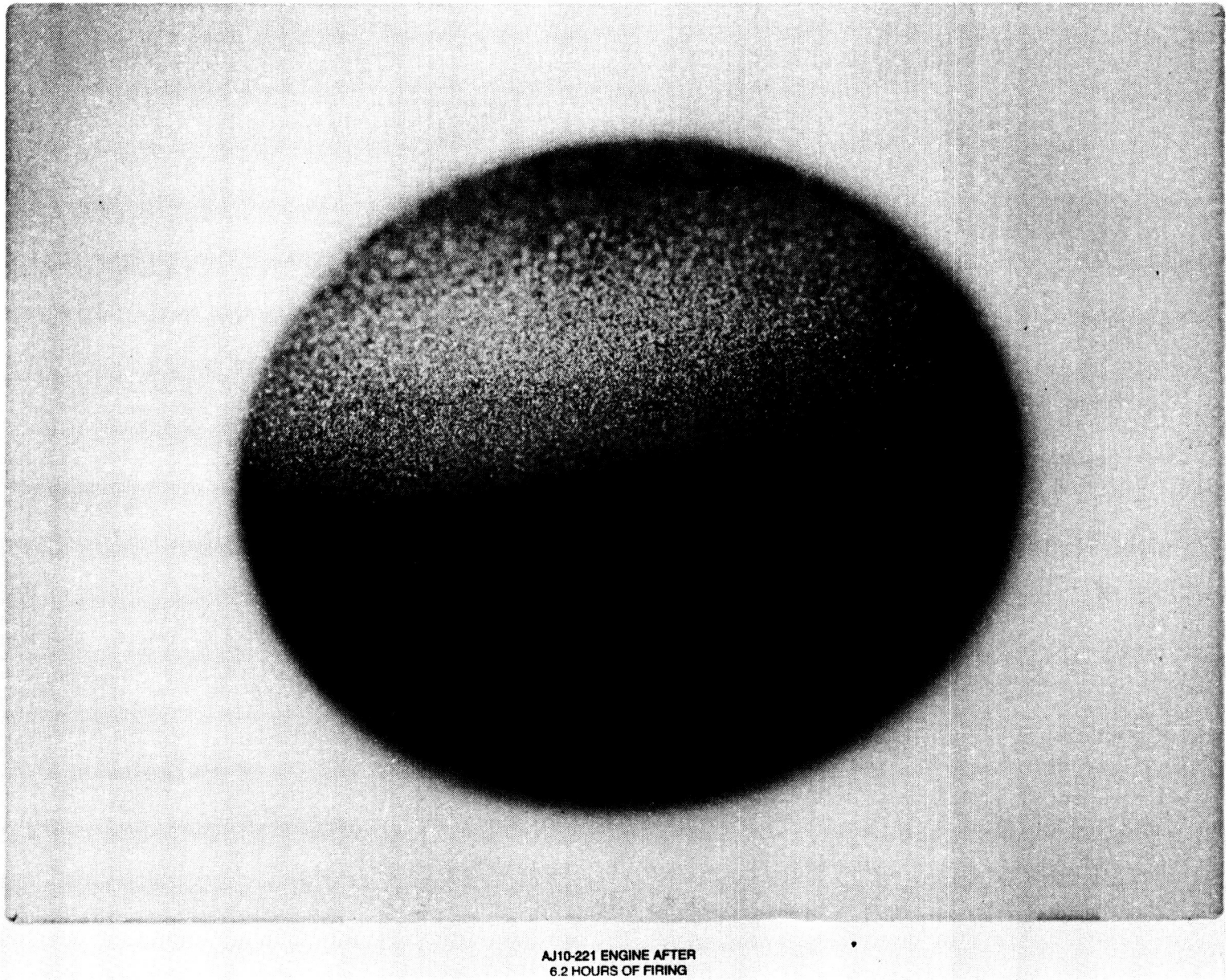

Figure M-9. Appearance of Ir Coating Downstream of Cooled Adapter

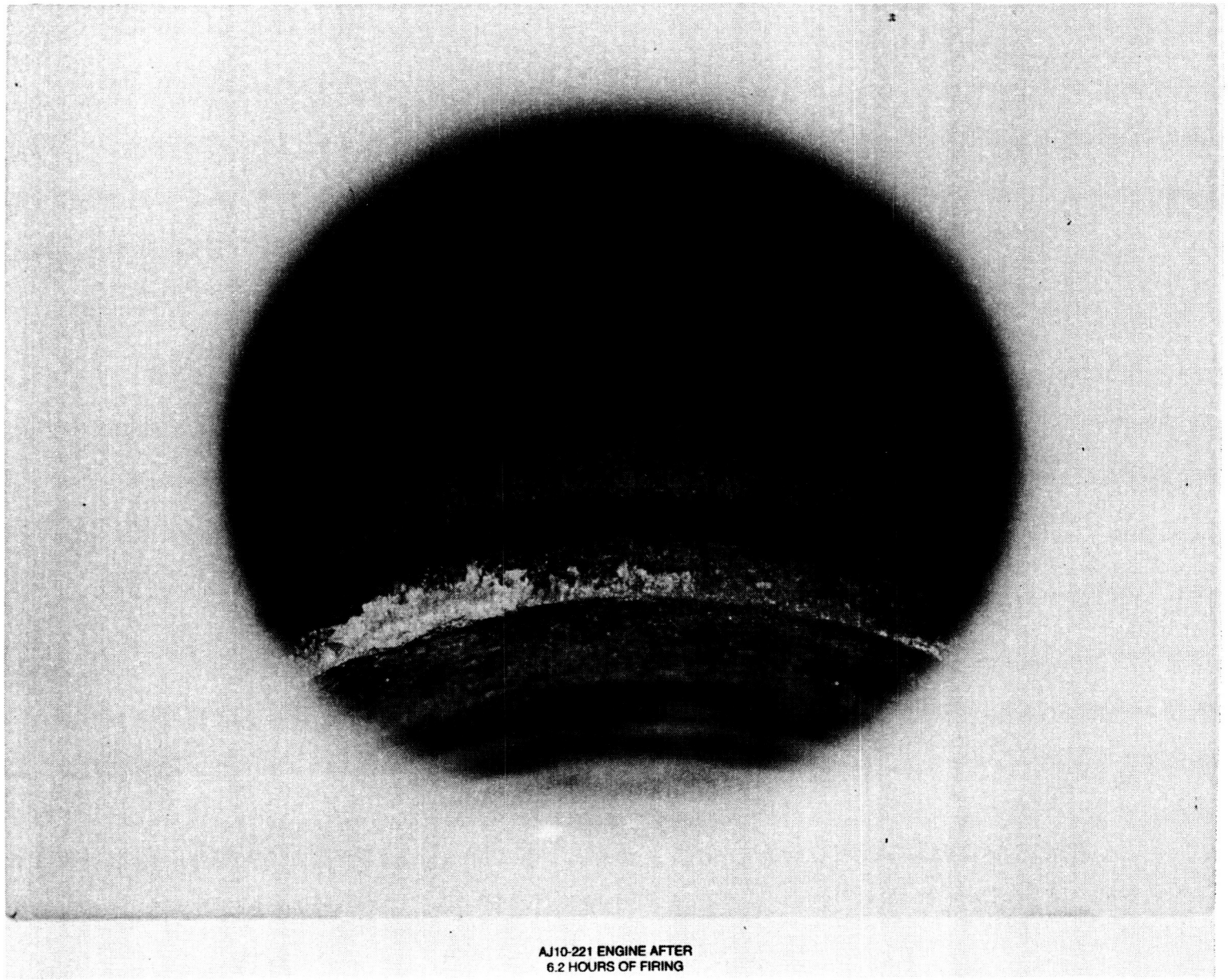

C0393 1446

Figure M-10. Chamber/Cooled Adapter Gap

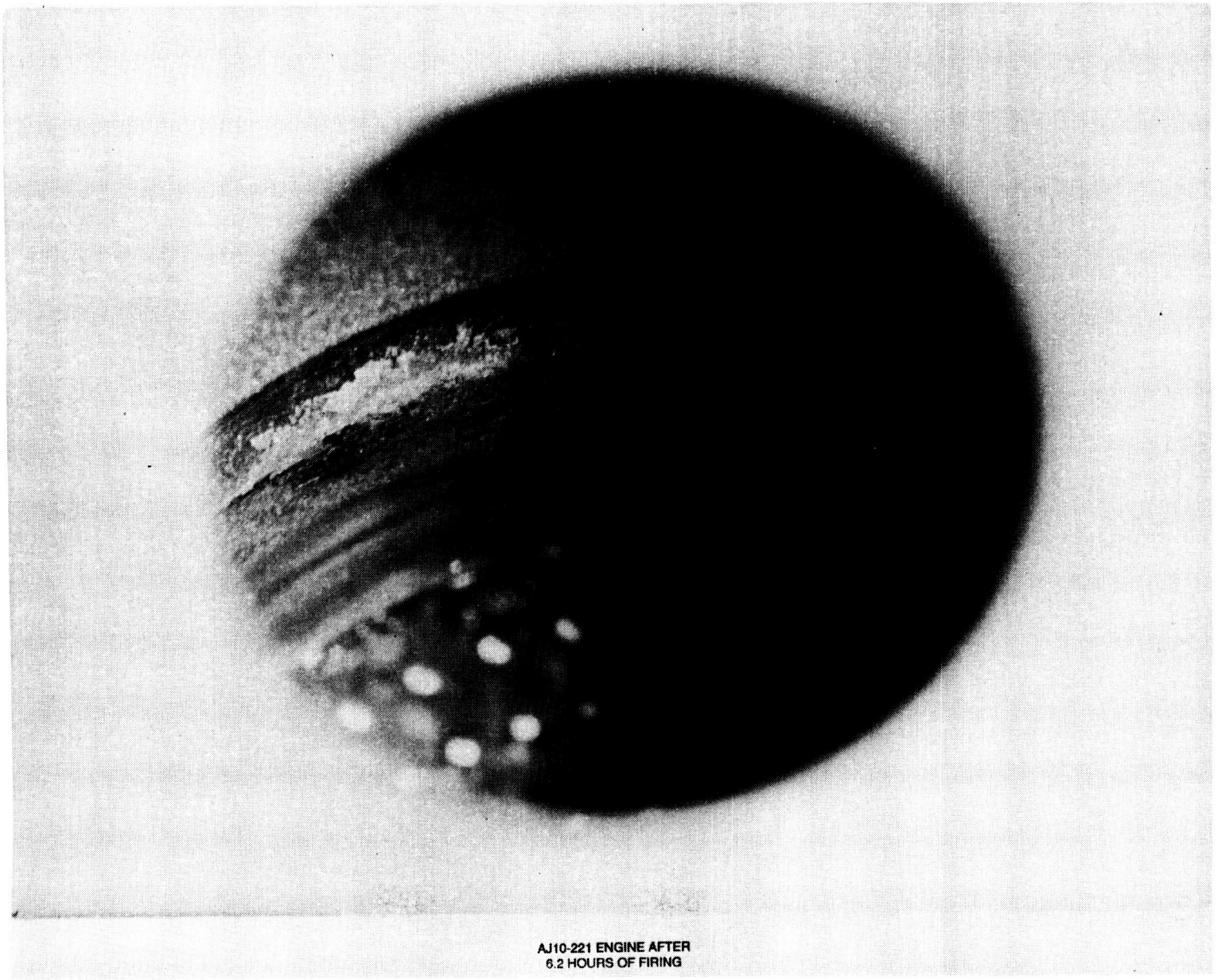

C0393 1452

Figure M-11. End and Interior Surface of Cooled Adapter

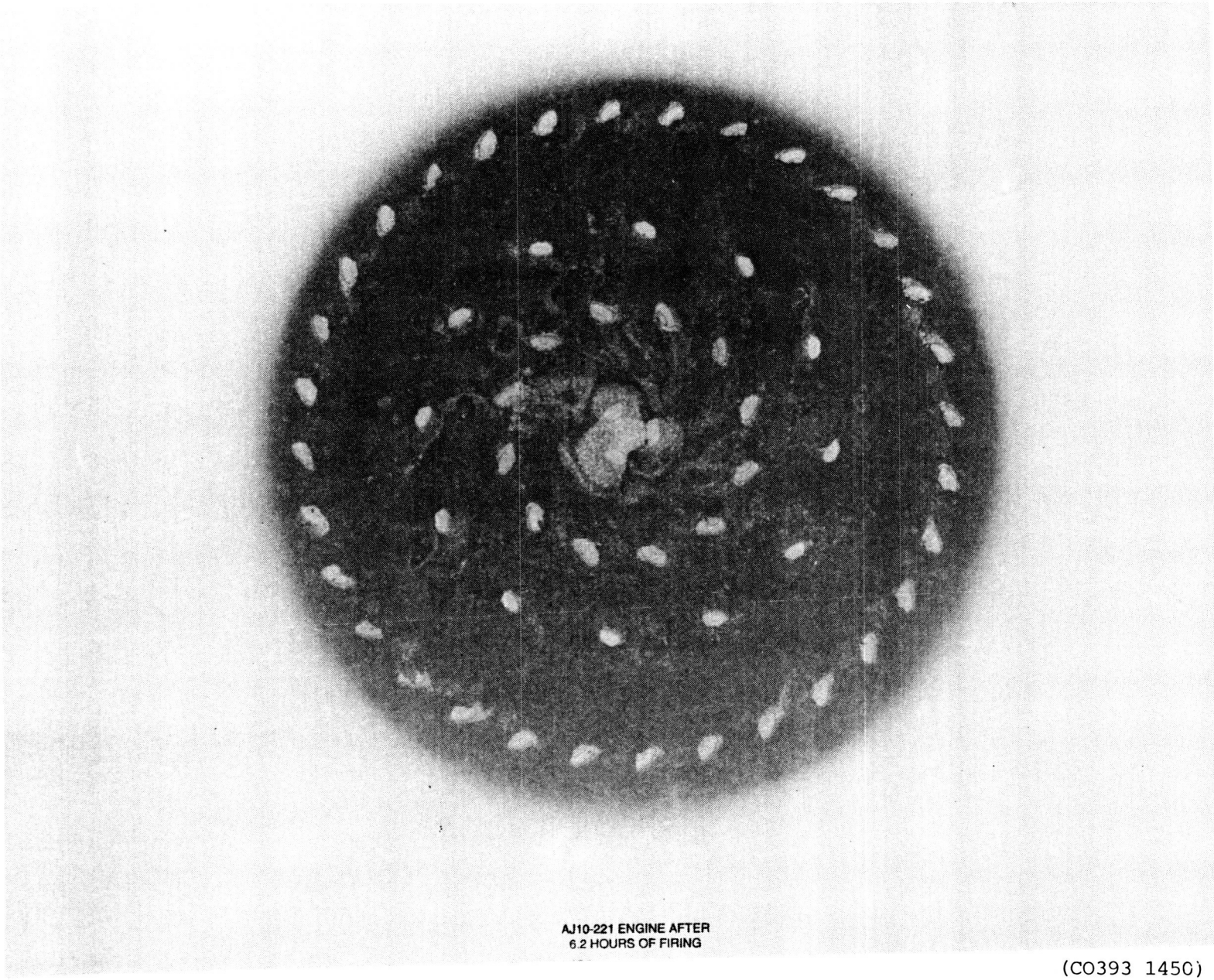

(CO393 1450)

Figure M-12. Portion of Injector Face

APPENDIX N

RHENIUM STRAINHARDENING EXPERIMENT

Rhenium Strain Hardening Experiment

Summary of Results

The following is a discussion of the data output from the testing of 2 rhenium specimens annealed to 3500 F. The specimen dimensions are shown in Figure N-1. A 0.20 inch long strain gage was laid on both sides of the specimen at the center. It was noted that Specimen 2B had a slight bend before the gages were applied.

The purpose of the test was to observe the stress-strain character of the material and then to submit the specimens to cyclic loading to determine if strain hardening occurs.

Figure N-2 shows maximum tension and compression stresses obtained as Specimen 1B was cycled through 1040 +/- load cycles. The final load-strain cycle was fairly linear and showed an increase in proportional limit from 9,710 psi to 38,860 psi.

Application of 1000 plus to minus displacement cycles resulted in a 4 times increase in proportional limit of the material.

Detailed Results

Figure N-3 through Figure N-22 show plots of load vs. strain for the tests of both specimens. It is noted that these data are not clean looking with smooth curves and well labeled load paths. The reason for the stepped appearance is that data were collected at discreet time points, which resulted in steps in the curves. There were also some noise signals which were not filtered out of the strain gage signal. The data are stored on floppy disk and could be further reduced to smooth curves. However, this would not add much value to the experiment as the goals of the test were obtained.

The following will lead the reader through the Figures to show the observed strain hardening:

1. Specimen 2B was first subjected to a slowly applied load to reach a value of 130 lbs. and a strain of 650 microinches (mi) and a stress of 7,430 psi. Figure N-3 shows a proportional limit of approximately 5000 psi stress. It was noted that as the load was applied slowly and held constant, the soft rhenium would relax easily. After reaching the maximum load, 10 cycles of +/- 0.001 inches of cross head displacement were

applied. Figure N-4 shows a similar result except that a strain of 350 mi was reached. This difference was attributed to the slight bend in the specimen observed before testing. No strain hardening was observed.

2. Since the slow load test on specimen 2B allowed relaxation and unloading it was decided to apply 10 cycles to of +/- 0.001 inch displacement to Specimen 1B. Figure N-5 shows these 10 cycles, where it can be seen that a maximum stress of 9,710 psi was reached. It is especially significant that the load-strain curve is linear. Thus, it is appears that rapidly load application results in a greater proportional limit. Cycles 11-20 are shown in Figure N-6.

3. Ten more cycles (21-30) were then applied with +/- 0.002 inch displacement at the cross head. The load increased to + 350 lbs tension and -320 lbs compression (Figure N-7). Note some small amount of buckling occurred and the compressive strain reached -1900 mi. The formation of this bend caused a bending moment and stress. Thus, the maximum compression stress is $-\frac{P}{A} + \frac{MC}{I}$ on Gage 1 and $\left(-\frac{P}{A} - \frac{MC}{I}\right)$ on Gage 2. Only Gage 1 for maximum tension is plotted.

4. Ten more cycles (31-40) were applied (Figure N-8) and the load increased to +390 lbs tension and -350 lbs compression. The strain cycled between -2150 mi and -0.5 mi. It is as if the grain structure was solidifying with applied cycles.

5. With some strain hardening observed from the first 40 cycles, it was decided to apply 1000 cycles at a rate of 0.1 cycles per second. This total plot is shown in Figure N-9. The load increased to +680 lbs tension and -400 lbs compression. The strain cycle ended at -150 mi and -0.85 mi. Note that this last cycle was fairly linear and covered a stress range of 61,720 psi.

6. Figures N-10 through N-14 show individual cycles at 11, 21, 140, 540 and 1040 cycles.

7. Figure N-15 shows a residual stress of 180 mi remained in the sample at gage 1 after removal from the machine.

8. Figures N-16 through N-21 show the data recorded from Gage 2. It is seen that this gage was on the compression side of the slightly buckled specimen as evidenced by the compressive strains as high as -4700 mi. It is also interesting to note in Figure N-16, that the hysterisis curve moved from left to right as the hardening process continued. Figure N-22 shows gage 2 retained -2340 mi. It was observed that the specimen had a slight bow after testing which confirmed the residual strain measurement.

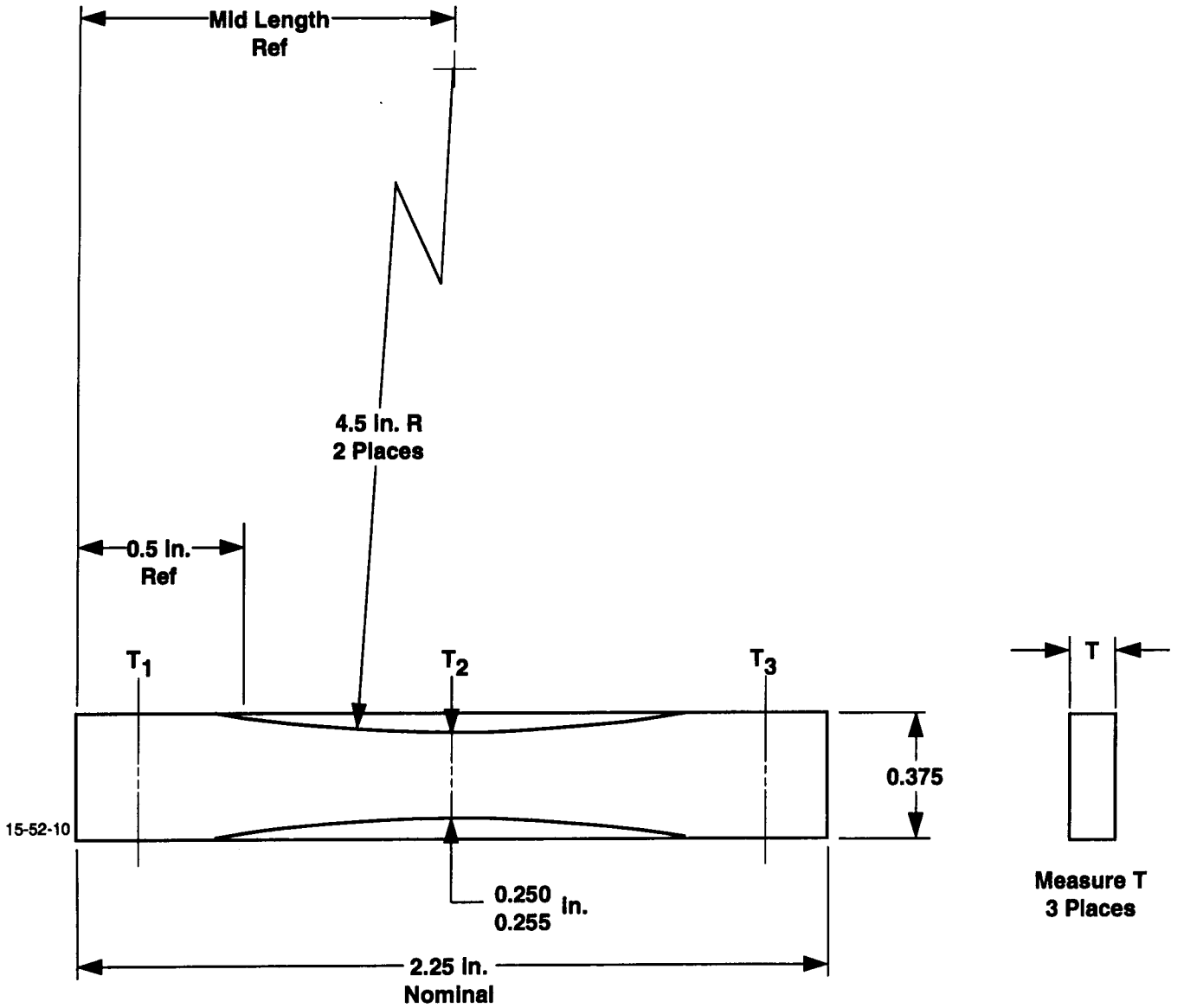

Figure N-1. Work Hardening Test Specimen Rhenium

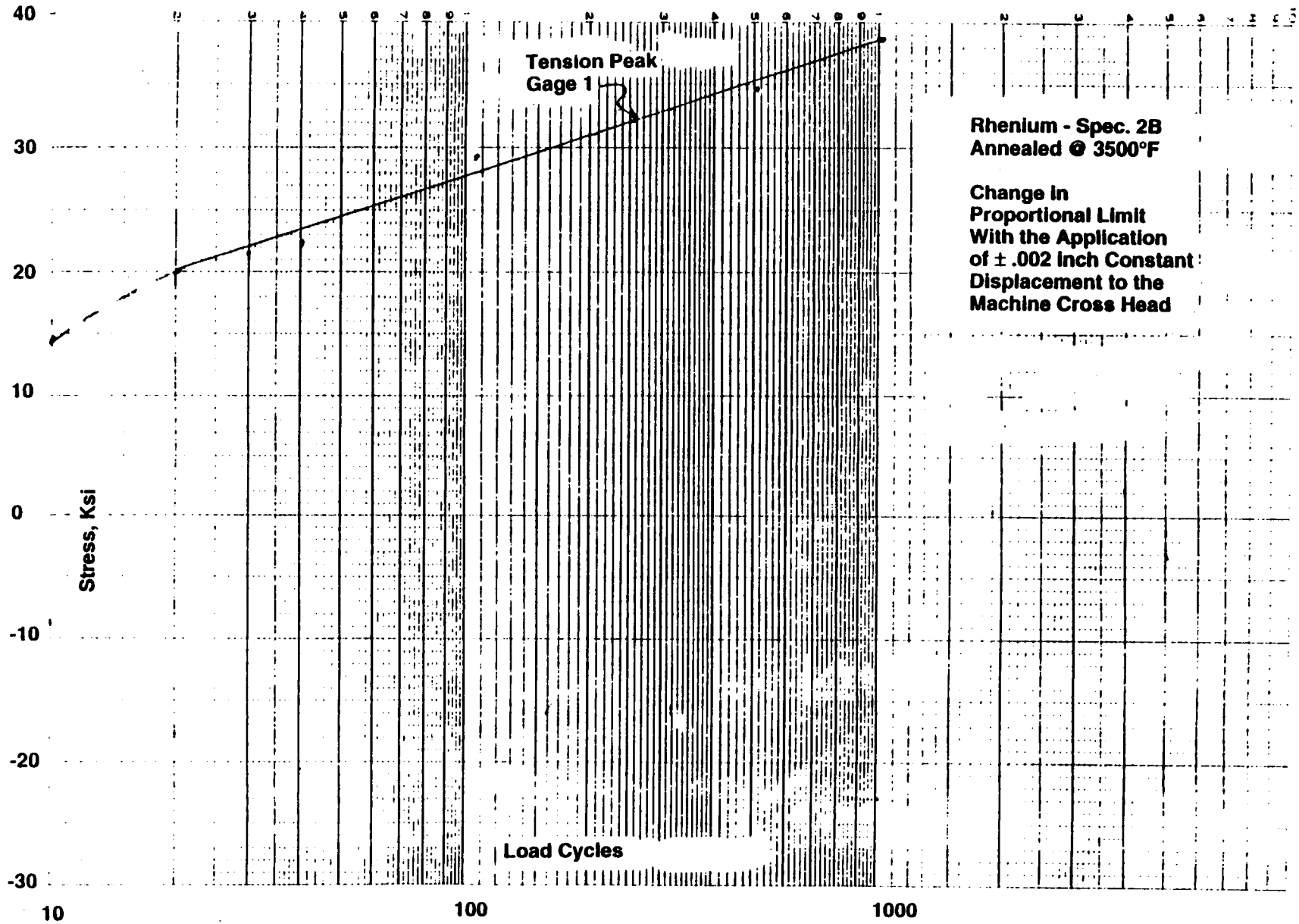

Figure N-2. Maximum Tension and Compression Stresses Obtained as Specimen1B Cycled Through 1040 ± Load Cycles

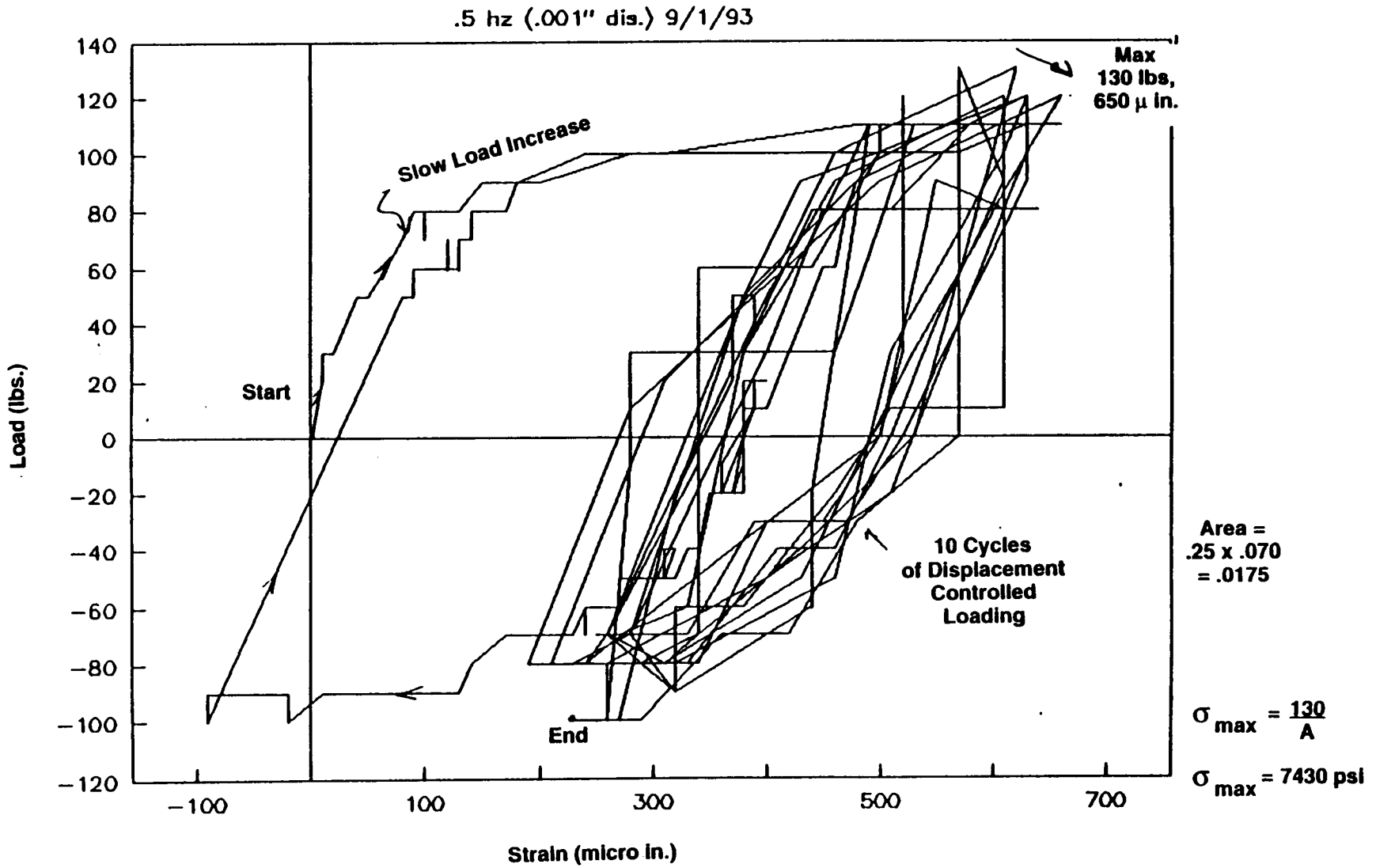

Figure N -3. Plot of Load vs. Strain - Specimen 2B, Gage 2

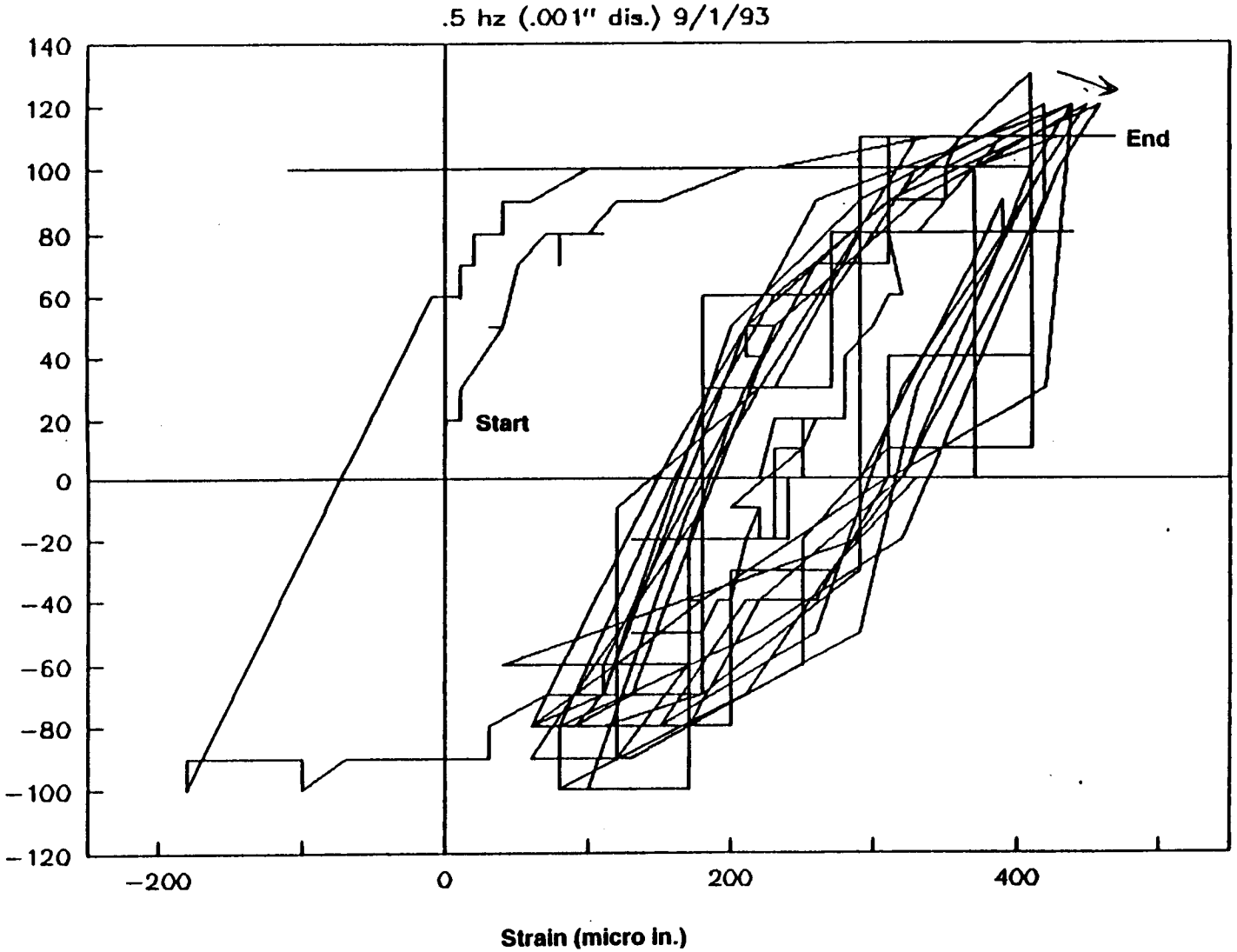

Figure N-4. Plot of Load vs. Strain - Specimen 2B, Gage 2

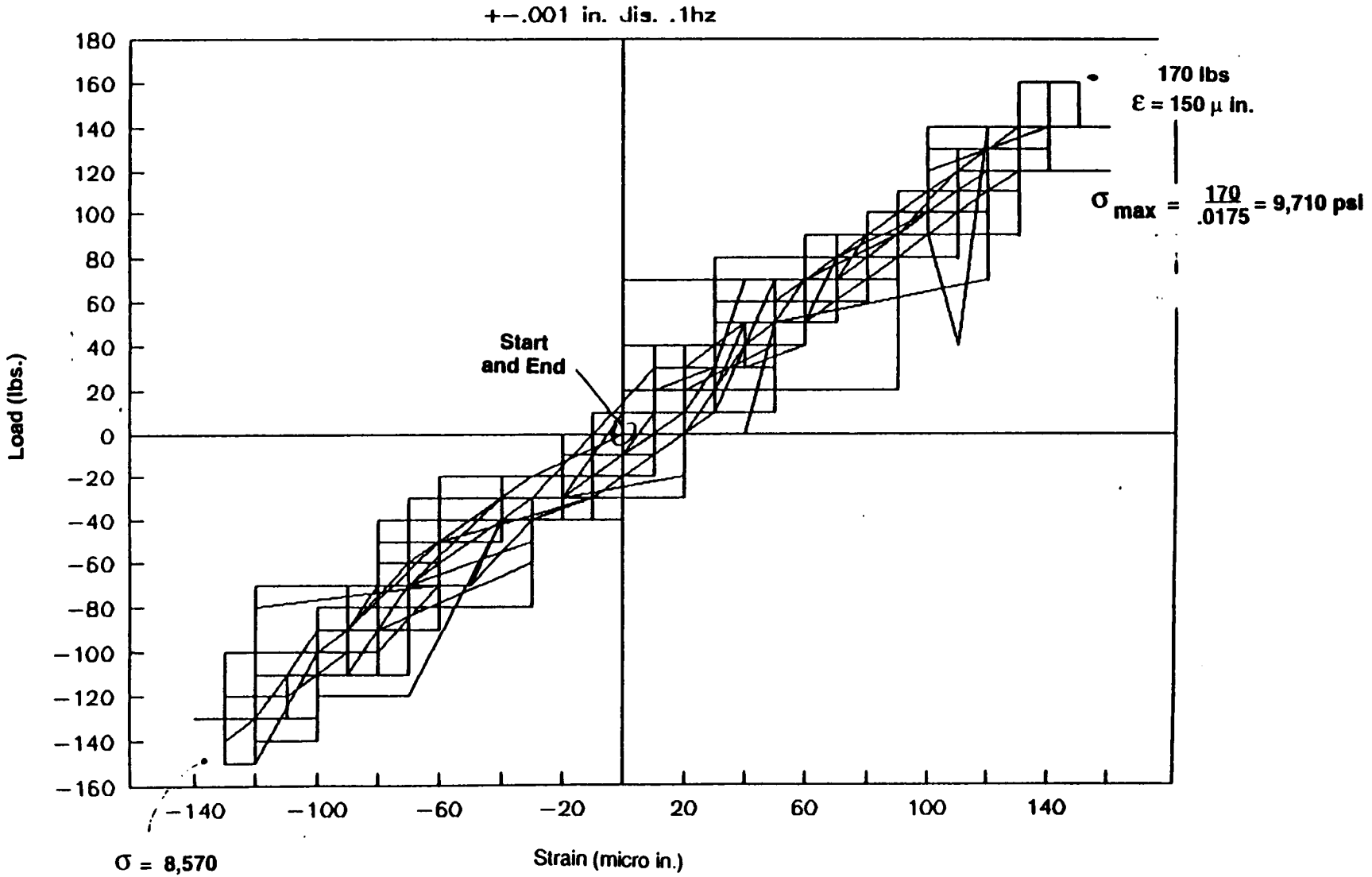

Figure N-5. Plot of Load vs. Strain - Specimen 1B, First 10 Cycles (Gage 1)

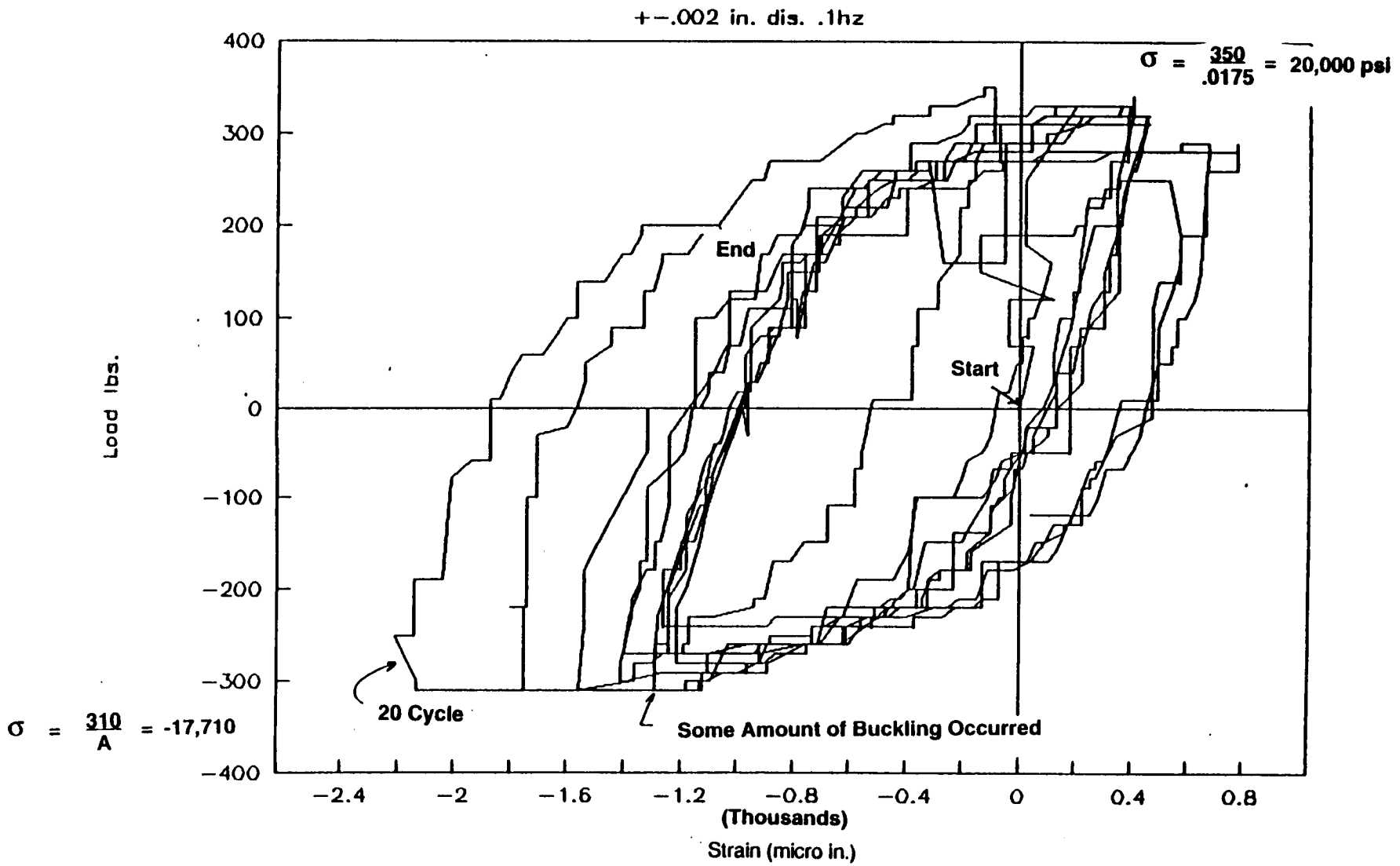

Figure N-6. Plot of Load vs. Strain - Specimen 1B, 20 Cycles (Gage 1)

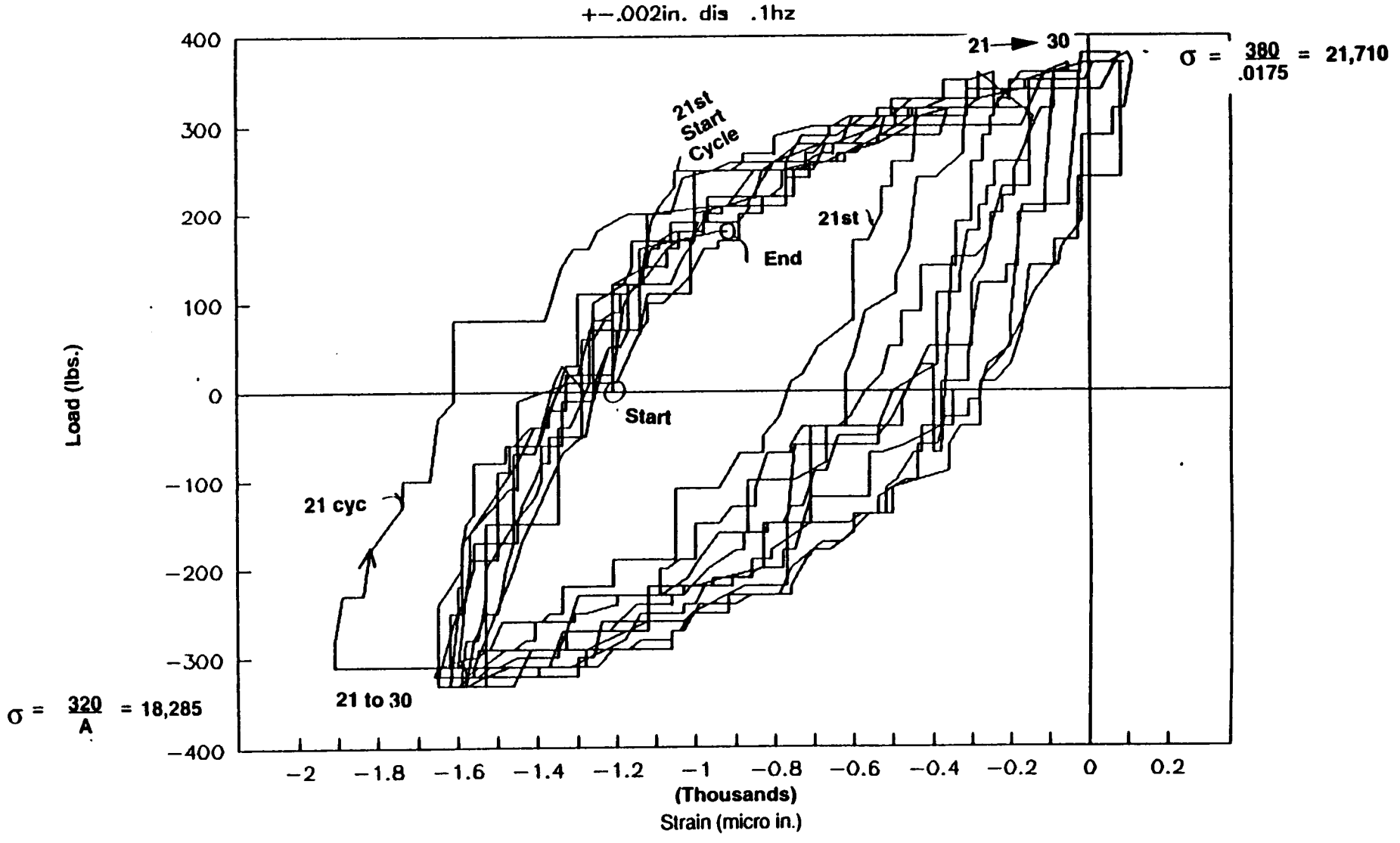

Figure N-7. Plot of Load vs. Strain - Specimen 1B, 21 to 30 Cycles (Gage 1)

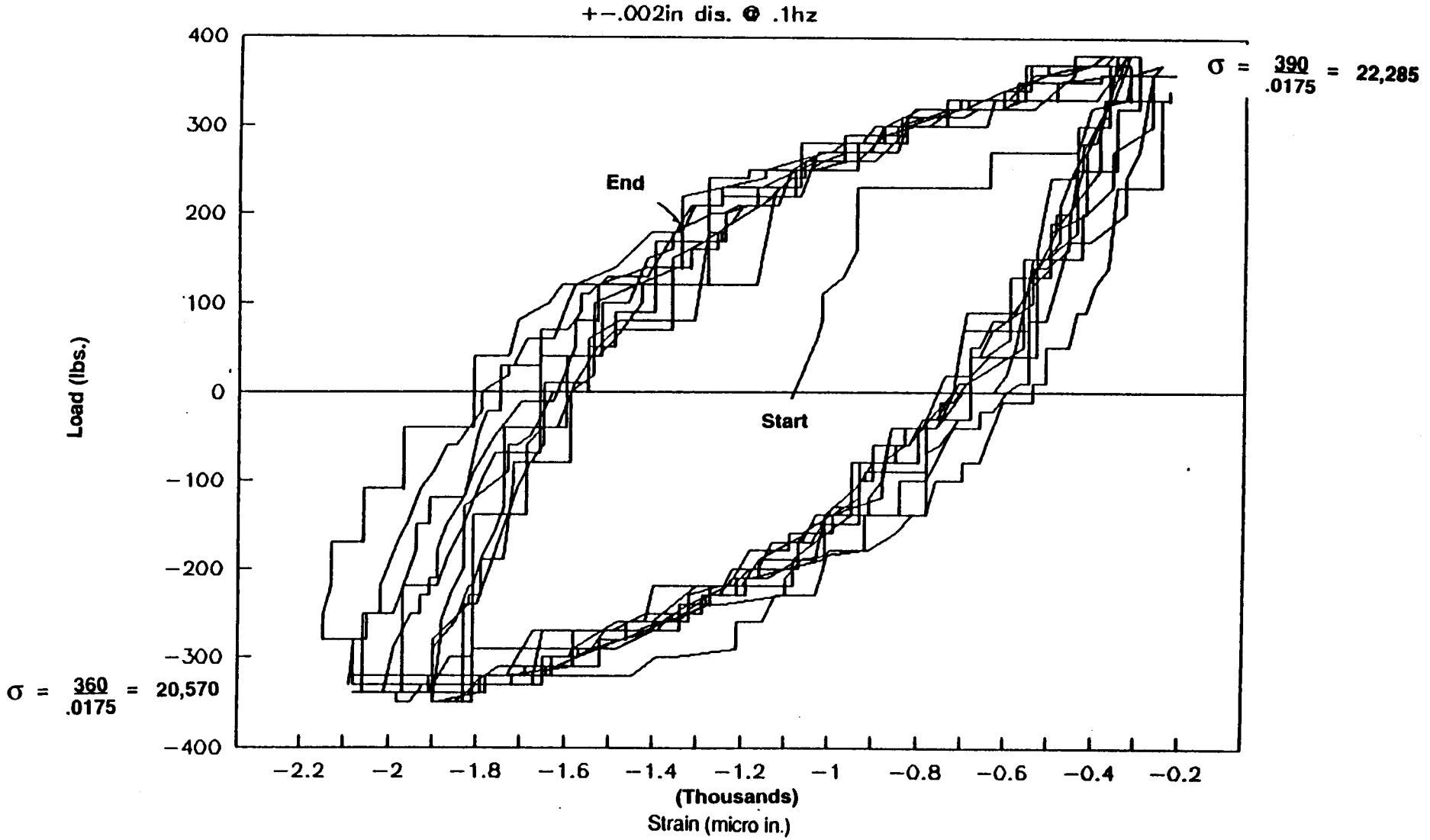

Figure N-8. Plot of Load vs. Strain - Specimen 1B, 31 to 40 Cycles (Gage 1)

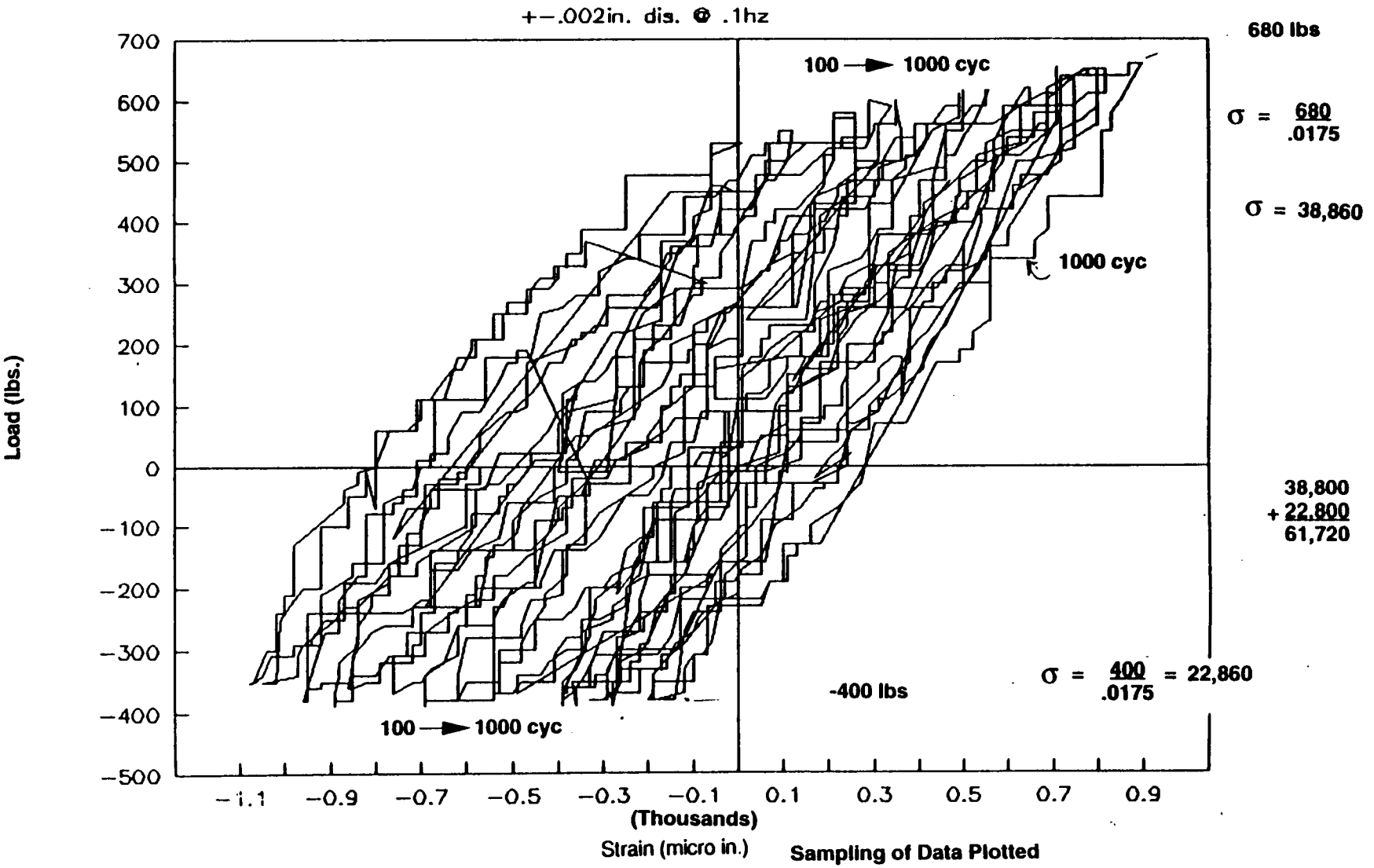

Figure N-9. Plot of Load vs. Strain - Specimen 1B, 100 to 1000 (+40) Cycles (Gage 1

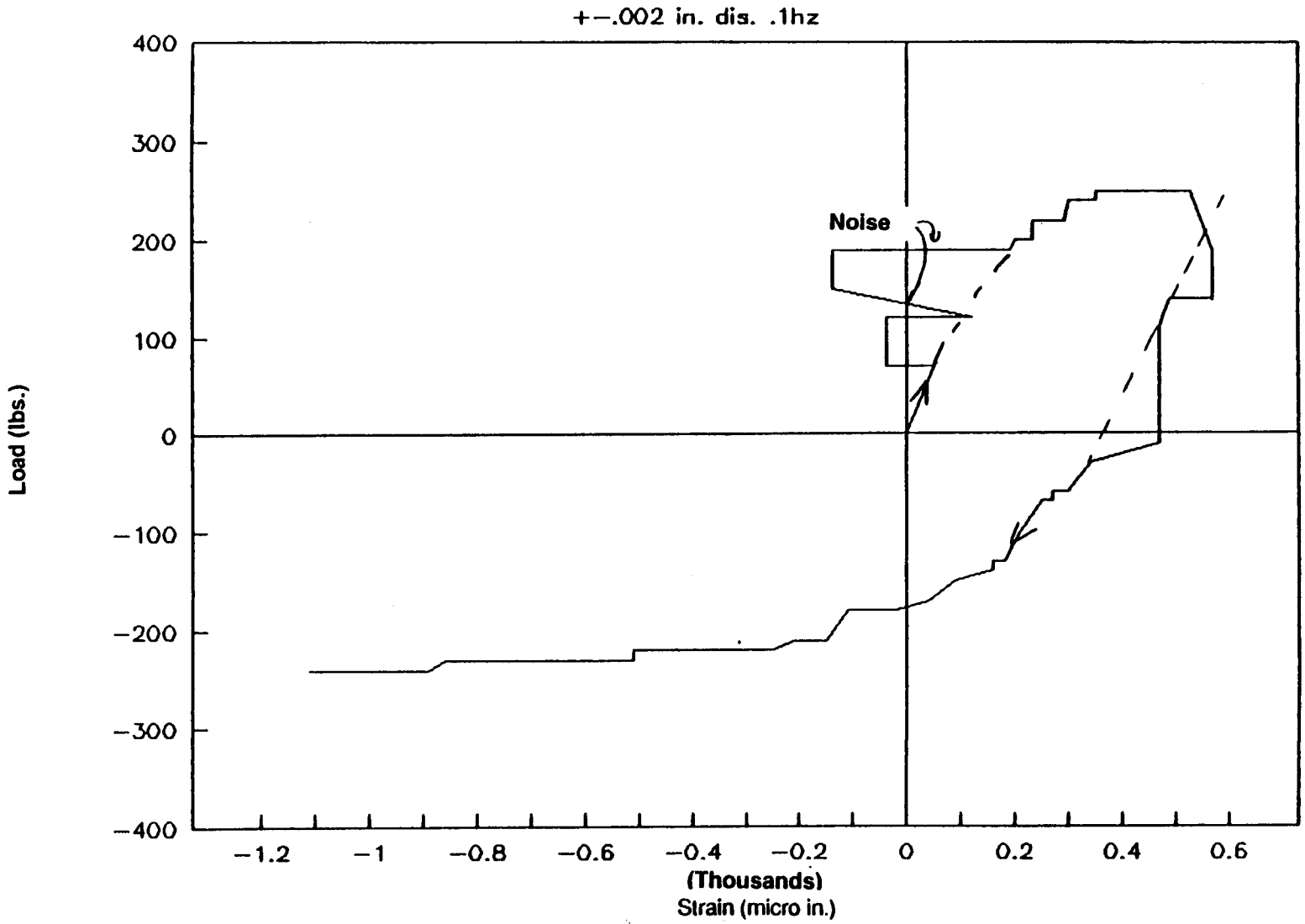

Figure N-10. Plot of Load vs. Strain - Specimen 1B, 11th Cycle (Gage 1)

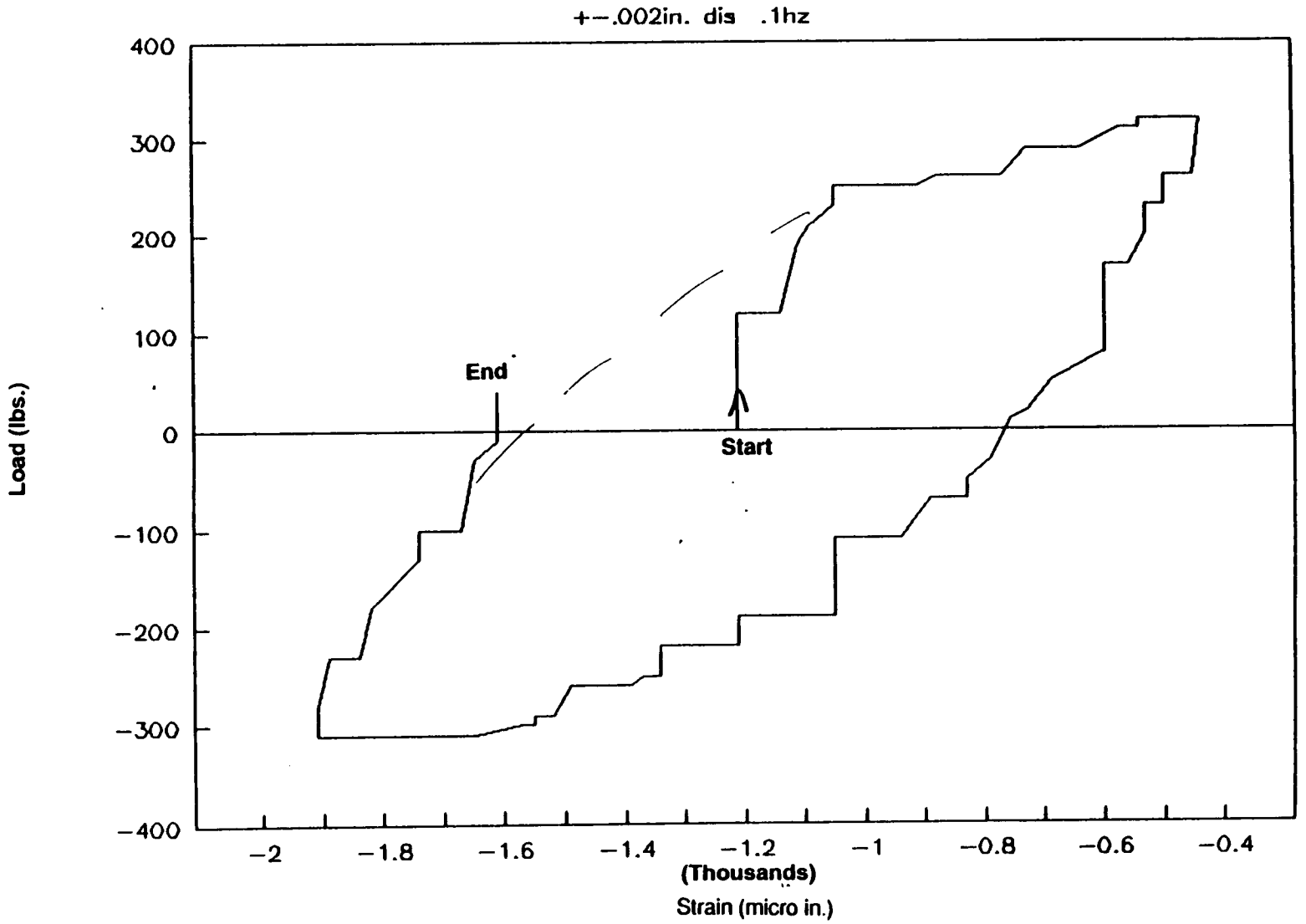

Figure N-11. Plot of Load vs. Strain - Specimen 1B, 21st Cycle (Gage 1)

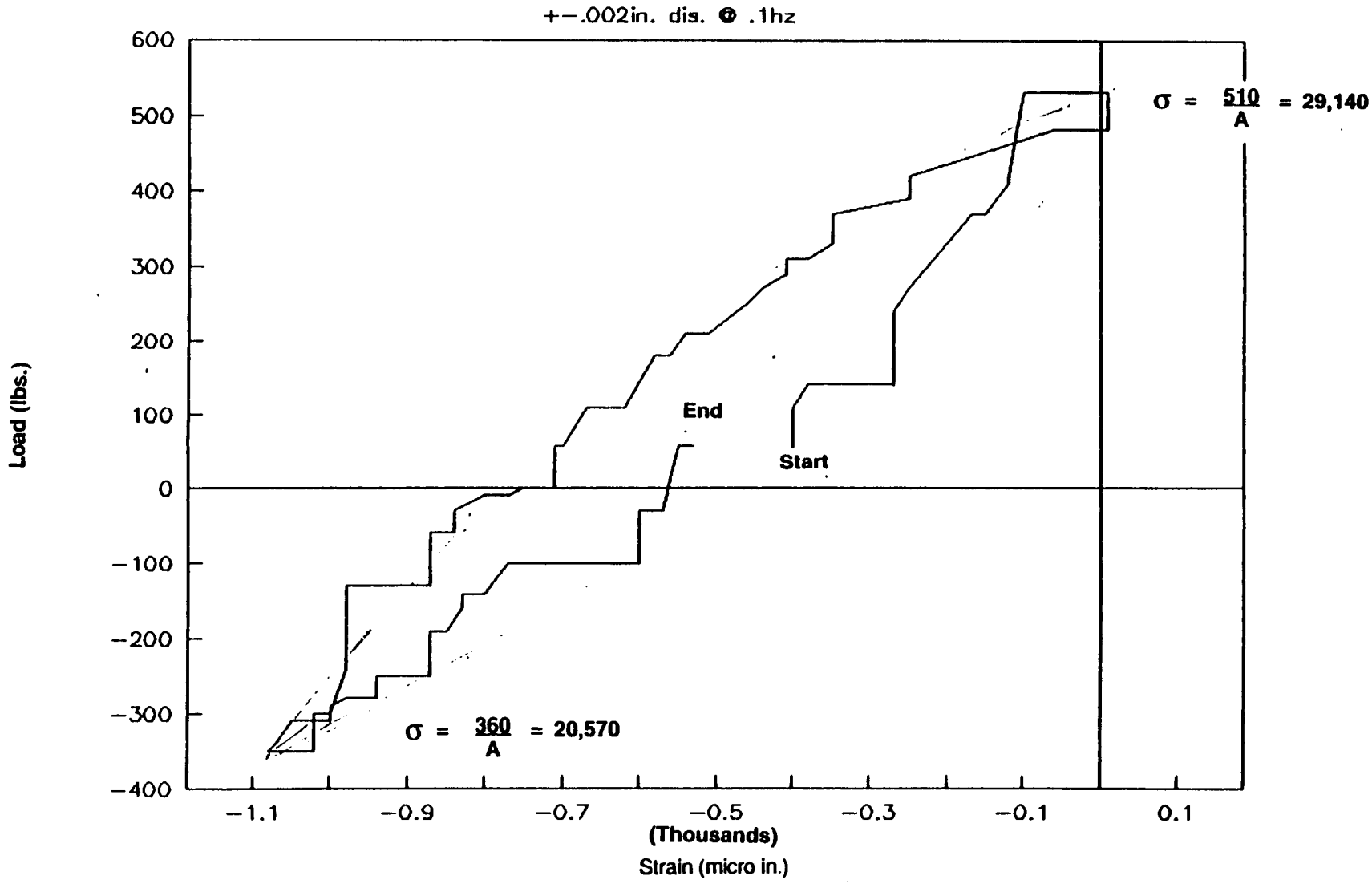

Figure N-12. Plot of Load vs. Strain - Specimen 1B, 100th Cycle (+40) (Gage 1)

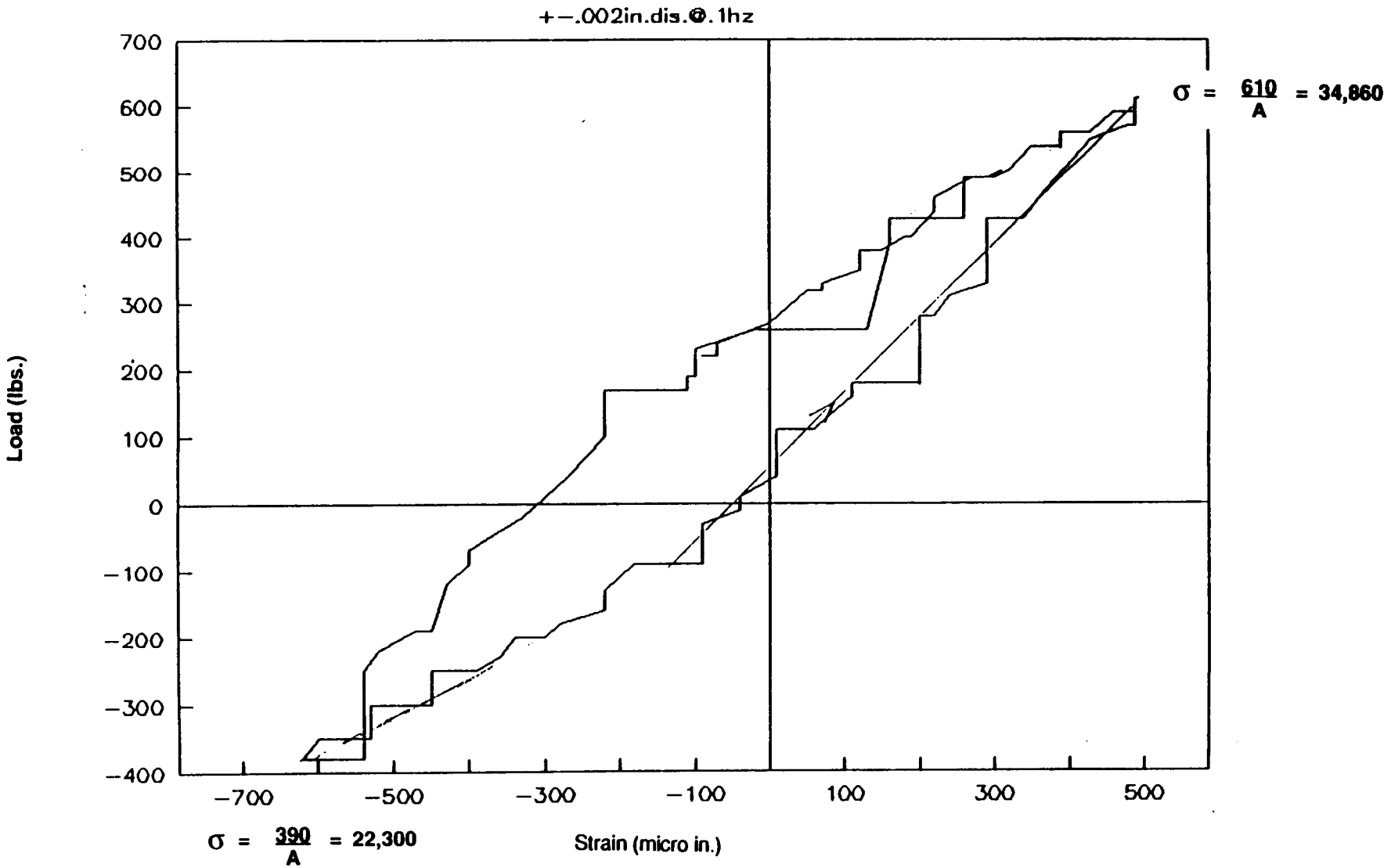

Figure N-13. Plot of Load vs. Strain - Specimen 1B, 100th Cycle (+40) (Gage 1)

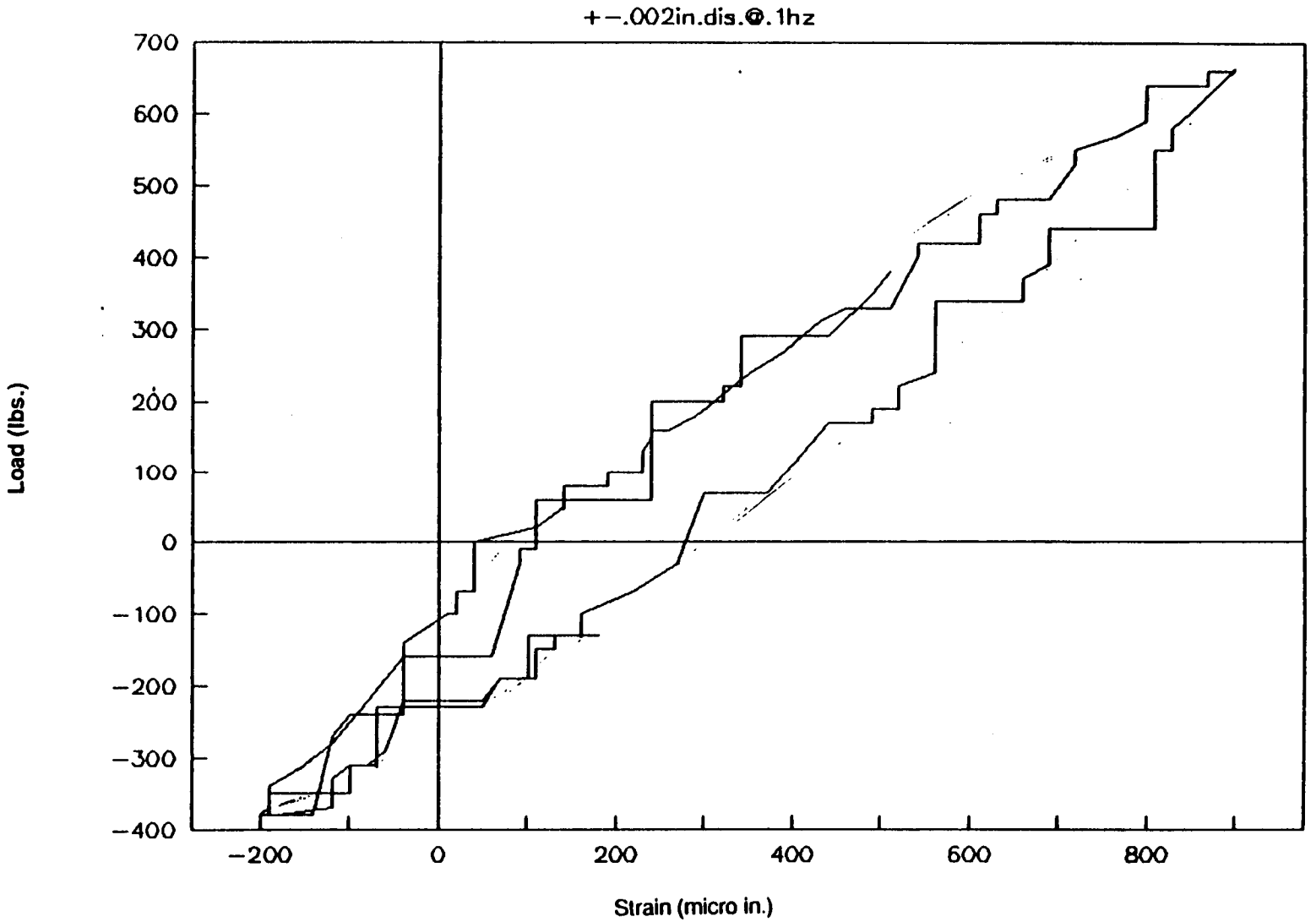

Figure N-14. Plot of Load vs. Strain - Specimen 1B, 1000th Cycle (+40) (Gage 1)

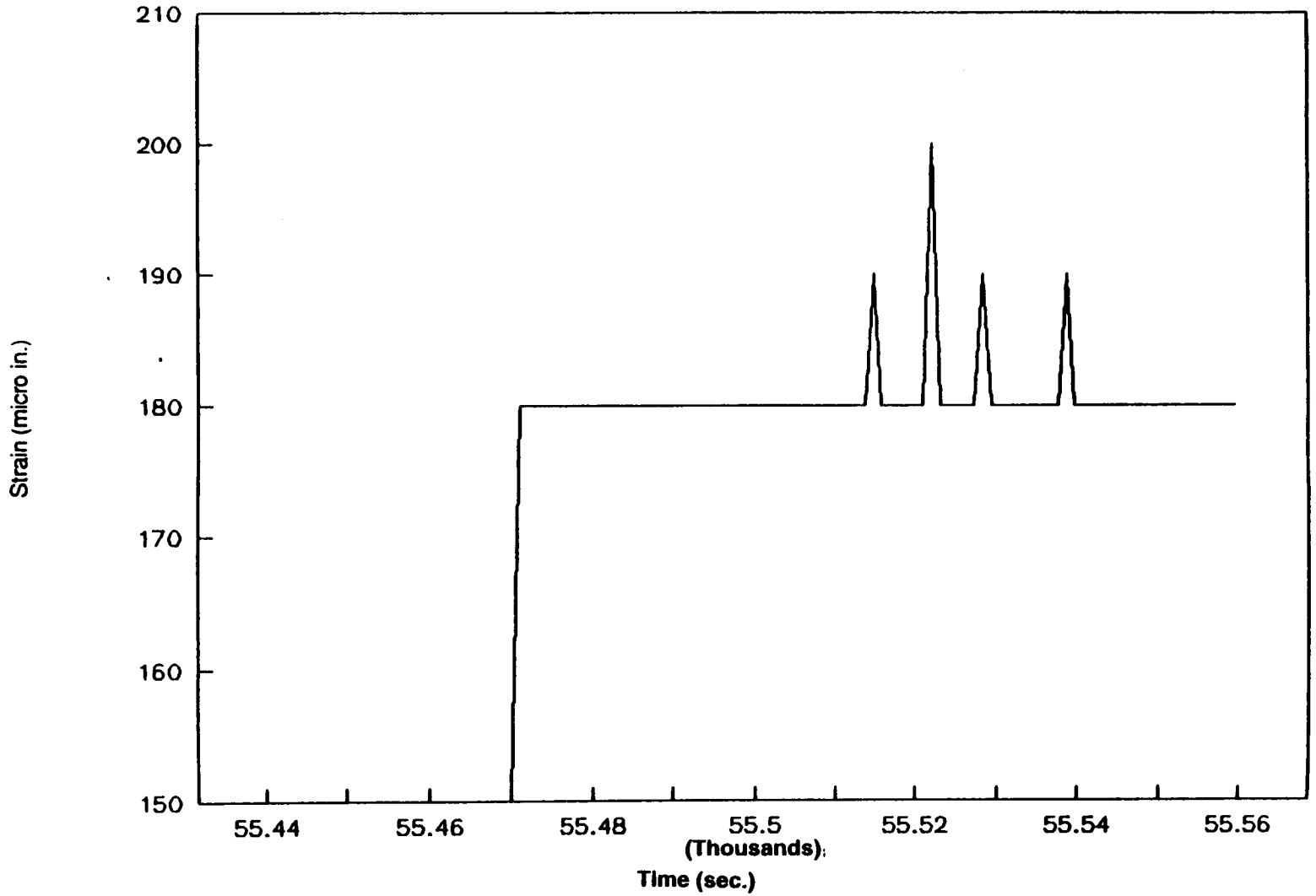

Figure N-15. Plot of Load vs. Strain - Removing Sample 1B (Gage 1)

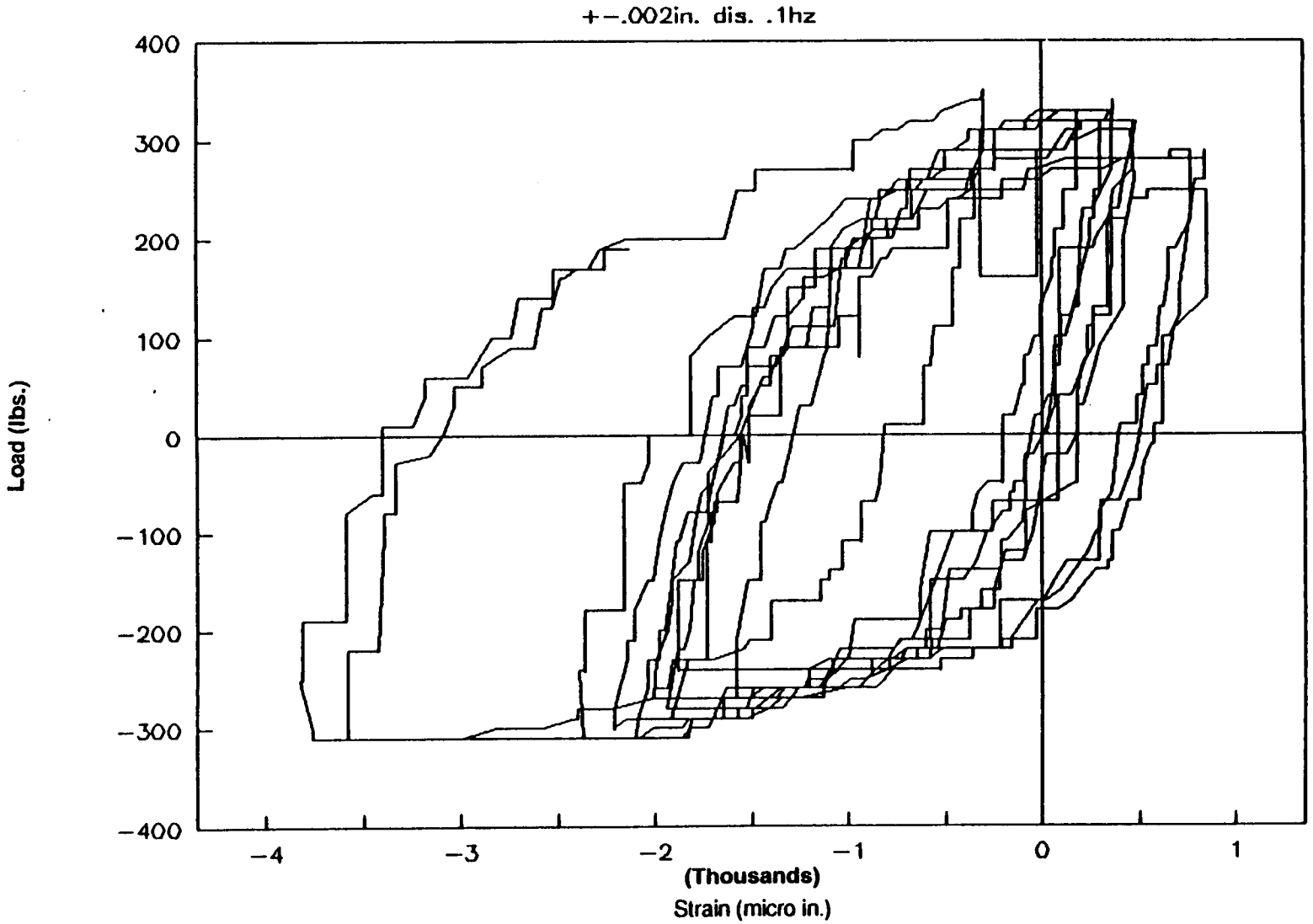

Figure N-16. Plot of Load vs. Strain - Specimen 1B, 11 to 20 Cycles (Gage 2)

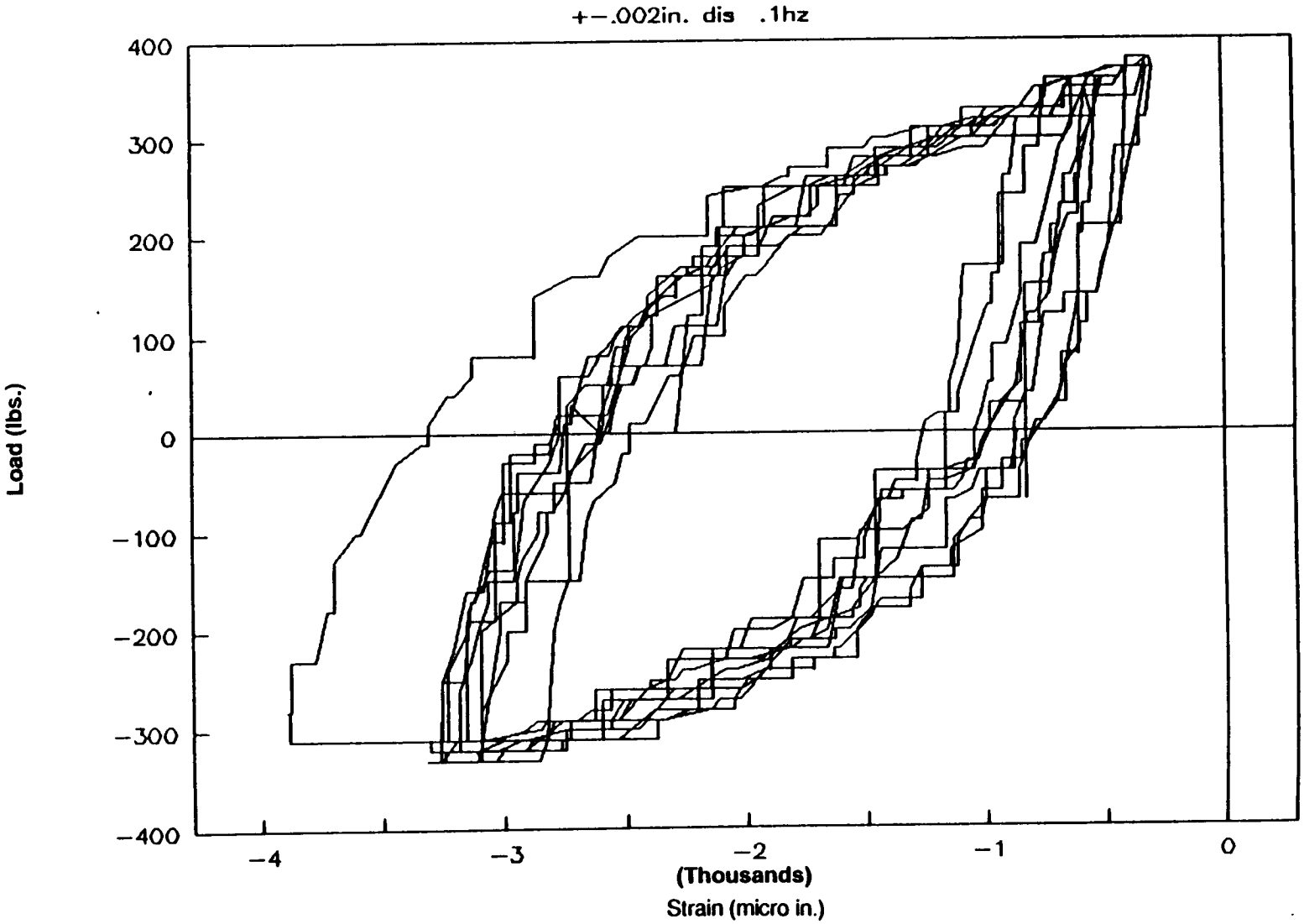

Figure N-17. Plot of Load vs. Strain - Specimen 1B, 21 to 30 Cycles (Gage 2)

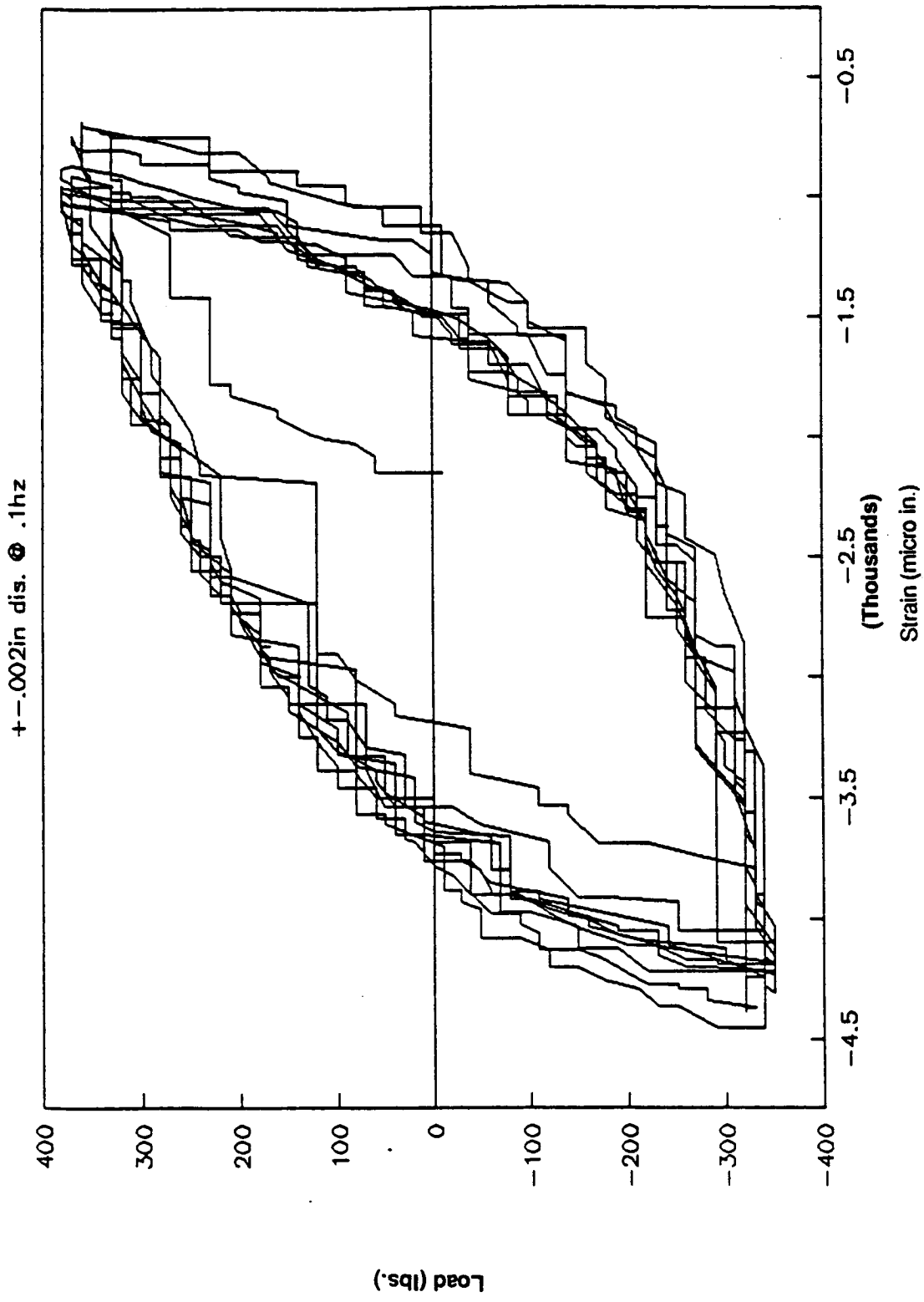

Figure N-18. Plot of Load vs. Strain - Specimen 1B, 31 to 40 Cycles (Gage 2)

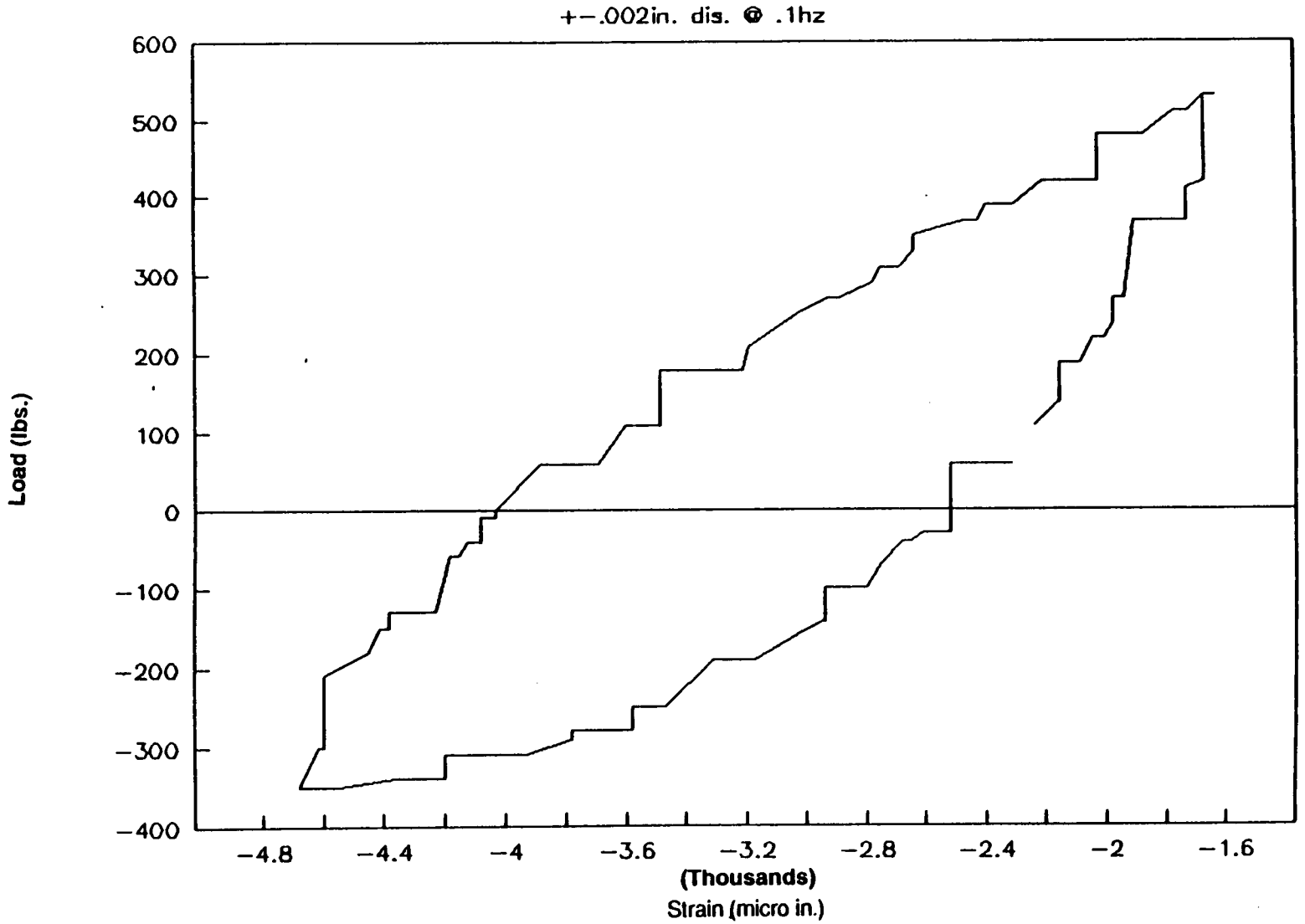

Figure N-19. Plot of Load vs. Strain - Specimen 1B, 100th Cycle (+40) (Gage 2)

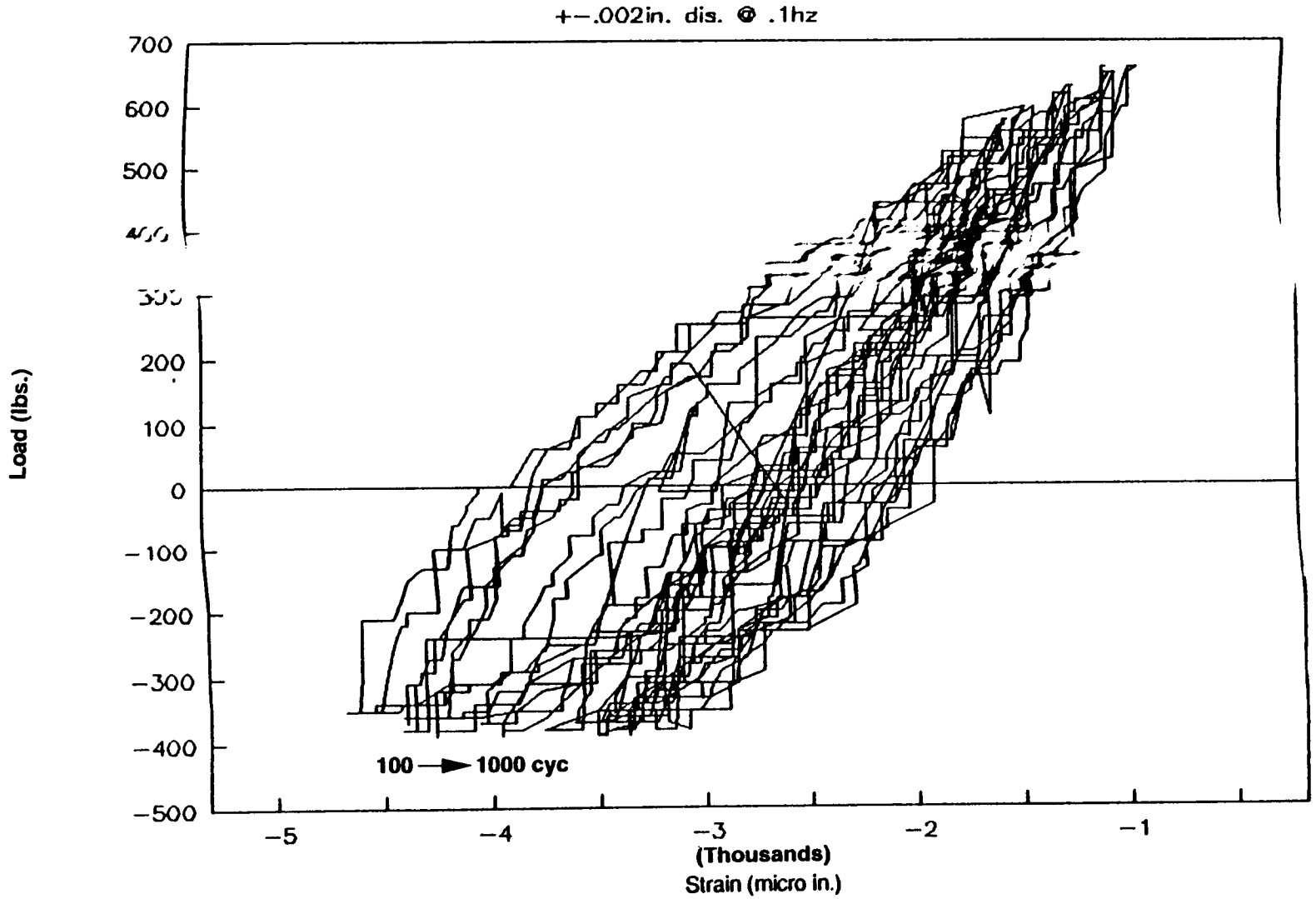

Figure N-20. Plot of Load vs. Strain - Specimen 1B, 100 to 1000 Cycles (+40) (Gage 2)

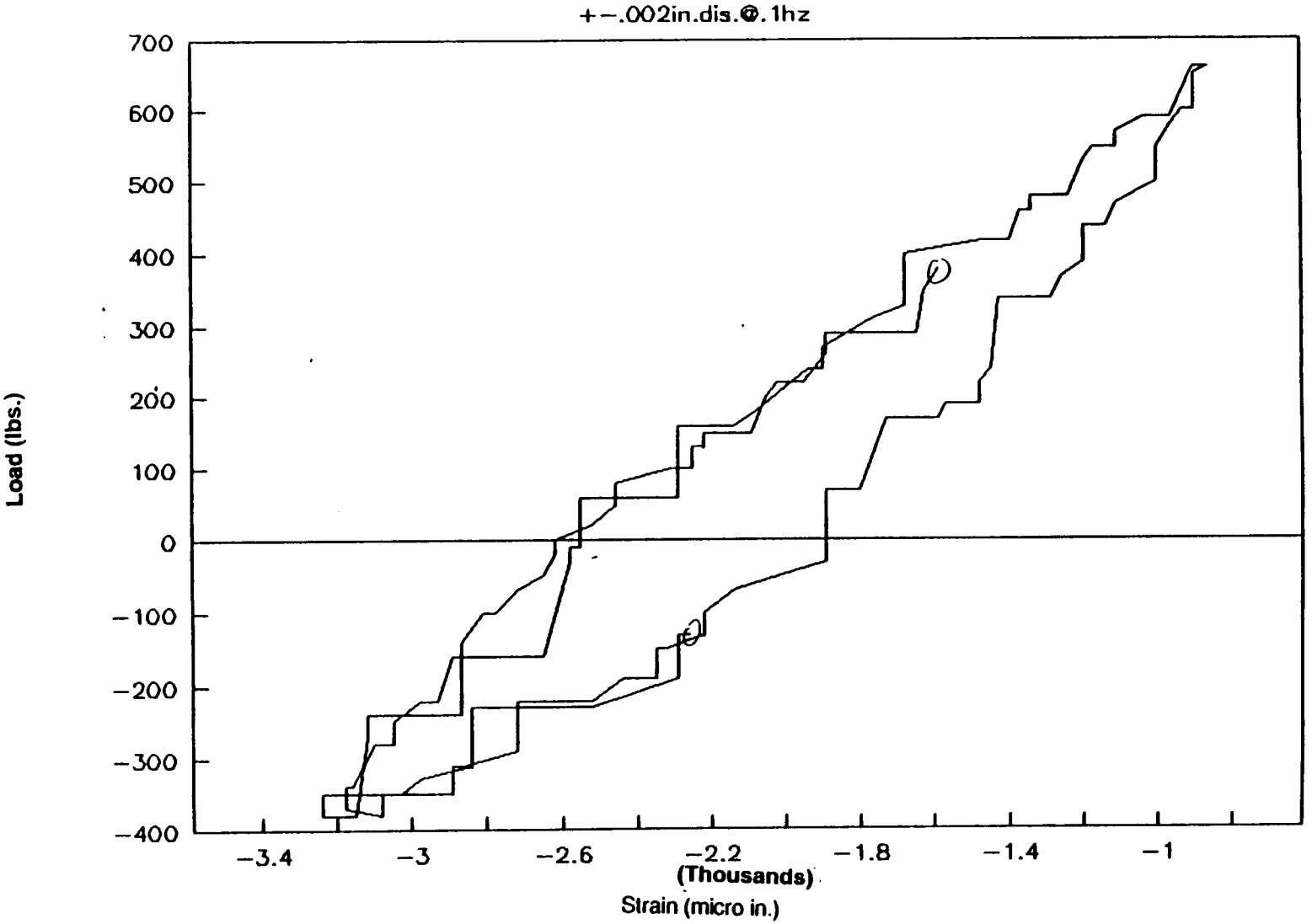

Figure N-21. Plot of Load vs. Strain - Specimen 1B, 1000th Cycle (+40) (Gage 2)

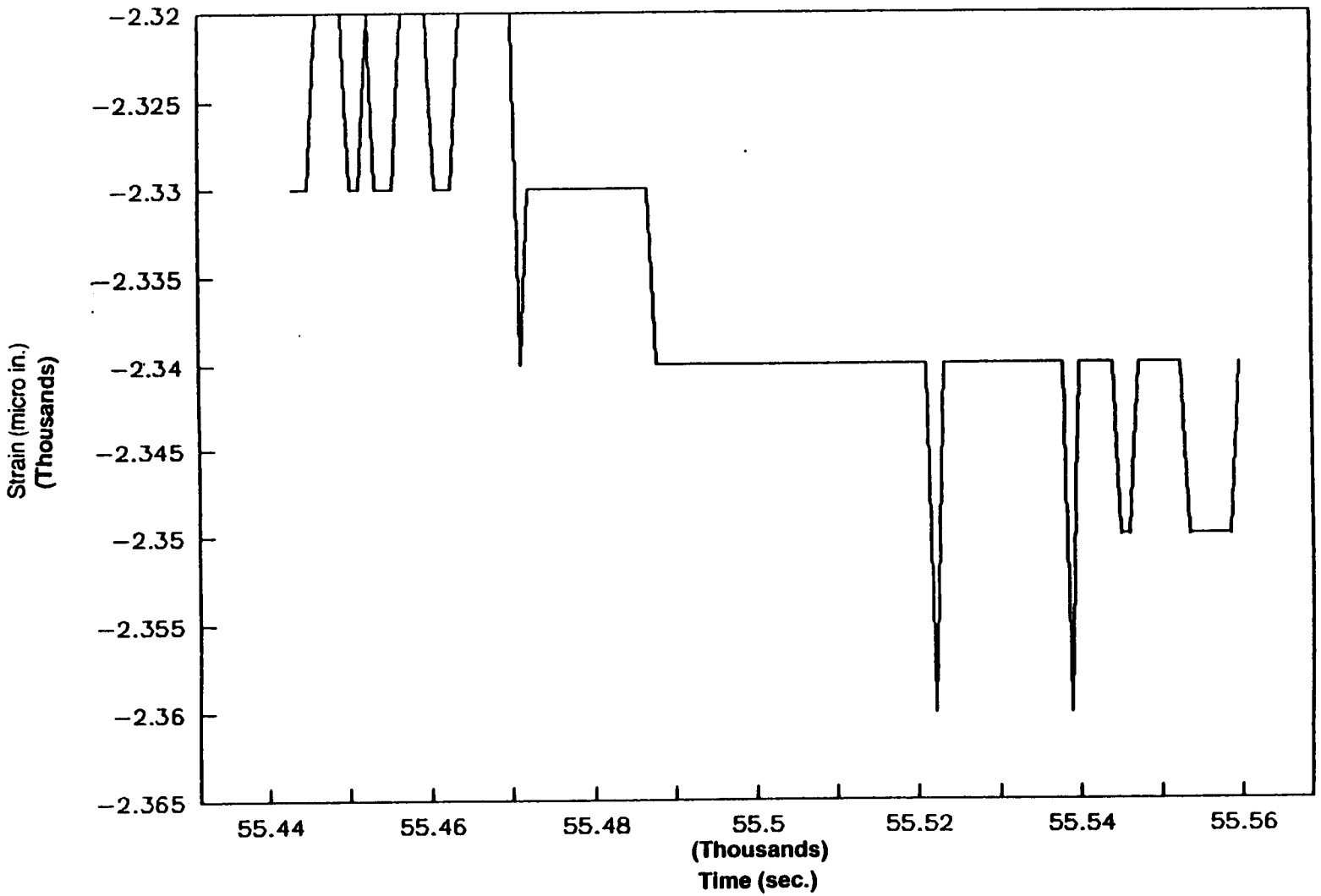

Figure N-22. Plot of Load vs. Strain - Removing Sample 1B (Gage 2)